

**Visualization  
of  
the Volterra Defects  
and of  
the Space around a Black Hole**

Inaugural-Dissertation

zur Erlangung des Doktorgrades  
der Mathematisch-Naturwissenschaftlichen Fakultät  
der Universität zu Köln

vorgelegt von

**Jürgen Karl Weidmann**  
aus Sindelfingen

**Köln 1998**

Berichterstatter: Prof. Dr. F.W. Hehl  
Prof. Dr. D. Stauffer

Tag der mündlichen Prüfung: 15. Juni 1998

# Überblick

Die vorliegende Dissertation zeigt, wie die Visualisierung numerisch gewonnener Daten dabei helfen kann, neue physikalische Ansichten und mathematische Erkenntnisse zu gewinnen. Visualisierungsprogramme ermöglichen eine Veranschaulichung selbst sehr umfangreicher mathematischer Formeln. Es ist heute nicht mehr nötig über ein ausgezeichnetes mathematisches Verständnis zu verfügen, um sich den Verlauf komplizierter mathematischer Funktionen vorstellen zu können. Computer-Algebra Systeme wie „Axiom“, „Macsyma“, „Maple“, „Mathematica“ oder „Reduce“ sind pädagogisch sehr wertvoll. Sie können die Scheu vor der höheren Mathematik nehmen und kreativen Kanälen die Tore öffnen. Ich möchte anhand zweier Beispiele anführen, wie mir diese modernen Werkzeuge geholfen haben, mein Verständnis der Elastizitätstheorie und der Relativitätstheorie zu vertiefen. Die vorgestellten Bilder entstanden mit Hilfe des „Advanced Visualization System“, kurz AVS, und dem Computer-Algebra System „Reduce“.

Die Arbeit beinhaltet zwei Abhandlungen, die unabhängig voneinander verstanden werden können. Die deutsche Zusammenfassung befindet sich daher jeweils am Anfang dieser beiden Schriftstücke. Im ersten, ausführlichen Teil „New Solution Algorithm for the Volterra Defects“ werden Verformungen von 3-dimensionalen Festkörpern betrachtet, wobei neue Lösungen für die Volterra Defekte vorgestellt werden. Eine Auswahl der erstellten Computer-Algebra- und C/C<sup>++</sup>-Programme befindet sich im Anhang. Im zweiten, kürzeren Teil „The Space around a Black Hole“ wird ab Seite 133 die Verformung des flachen Raumes durch die Anwesenheit von Materie, insbesondere eines schwarzen Loches, veranschaulicht. Einige ausgewählte Farbtafeln befinden sich aus technischen Gründen am Ende der Dissertation.



## Part I

# New Solution Algorithm for the Volterra Defects

## Zusammenfassung

Die Elastizitätstheorie behandelt die Wirkung von Kräften auf einen Festkörper, wobei der Zusammenhang der auftretenden Spannungen mit den erzeugten Verformungen von besonderem Interesse ist. Die lineare Elastizitätstheorie geht näherungsweise von einer Proportionalität zwischen Spannung und Verformung aus und basiert auf dem verallgemeinertem Hookschen Gesetz. Bereits im Jahre 1638 beschäftigte sich Galileo Galilei mit der Verbiegung eines Holzbalkens und den dazu nötigen Kräften [1]. Im Jahre 1822 stellte Cauchy die wesentlichen Weichen zur modernen Elastizitätstheorie mit zwei material abhängigen Parametern im isotropen Fall. Er stellte die wichtigen Gleichgewichtsbedingungen auf, die die mathematische Verbindung der Spannungskomponenten mit den Kräften herstellen, die auf einen Körper wirken. Das Problem der Bestimmung des Dehnungs- und Spannungszustandes des betrachteten Körpers konnte so auf ein mathematisch analytisches Problem reduziert werden. Die Suche galt nun den mathematischen Funktionen, die die jeweilige Deformation des Körpers möglichst genau beschreiben konnten. Diese Funktionen müssen die Gleichgewichts- und spezifische Randbedingungen erfüllen. Viele Anstrengungen z.B. von Euler, Green, Laplace, Navier, Poisson, Stokes, und Young wurden unternommen, um Funktionen zu finden, die insbesondere die biharmonischen Differentialgleichungen der Gleichgewichtsbedingungen erfüllen [2]. Die zur Integration dieser partiellen Differentialgleichungen verwandten Methoden lassen sich in zwei Klassen einteilen. Einerseits die Konstruktion einer Greensche Funktion mit Hilfe der Potentialtheorie, und andererseits die Suche nach Lösungen im Bereich der Kugelfunktionen oder der trigonometrischen Funktionen, und deren Modifikation entsprechend der Randbedingungen [3]. Der hier vorgestellte Algorithmus hat einen völlig anderen physikalisch motivierten Ansatz. Ich verwende zur Lösung der Gleichgewichtsbedingungen und zur Anpassung an die jeweiligen Randwerte das Vektorfeld der Divergenz des Dehnungstensors. Ich möchte meinen Algorithmus anhand der Volterra Defekte bzw. der Volterra Versetzungen erläutern, da diese eine Beschreibungsmöglichkeit für viele physikalische Phänomene bieten. E. Orowan [4] und M. Polanyi [5] konnten z.B. 1934 sowie G.I. Taylor [6] 1943, die plastische Verformung von Metall mittels Versetzungen erklären. Die Manifestation einer Versetzung kann nur von einem atomistischen Blickpunkt heraus verstanden werden. Die Summe aller Versetzungen resultiert aber in einer makroskopisch sichtbaren Verformung des Körpers. Diese Erkenntnis half viele Rätsel der Festkörperphysik zu lösen [7]. Es konnten z.B. der kristalline Aufbau, bestimmte Schmelzvorgänge [8] und einige optische Eigenschaften erklärt werden. V. Volterra untersuchte am Anfang unseres Jahrhunderts 3-dimensionale mehrfach zusammenhängende elastische Körper, insbesondere eindeutig definierte Deformationen von Hohlzylindern (zweifach zusammenhängend). Sein Interesse galt der gesamten, durch eine Versetzung verursachten Verformung des Körpers und den damit verbundenen Spannungen. Seine Untersuchungen wurden anhand von Zylindern aus Gummi dargestellt [20]. Zur weiteren Untermauerung seiner mathematischen Resultate verwendete er die Photoelastizitätsmethode an transparenten Zylindern aus Gelatine [21], [22]. Nach dem Kirchhoffschen Eindeutigkeitsatz sind in mehrfach zusammenhängenden Körpern die Spannungen nicht eindeutig durch die äußeren Kräfte festgelegt [7]. Mehrfach zusammenhängende Körper sind somit von besonderem Interesse, da für sie Gleichgewichtszustände existieren, die es für einfach zusammenhängende Körper nicht gibt. Der Spannungstensor ist hier nicht eindeutig bestimmt. Ein verformter zweifach zusammenhängender Körper kann den Gleich-

gewichtszustand erreichen, obwohl in ihm Spannungen auftreten. Derartige Spannungen werden als Eigenspannungen bezeichnet. Sie werden durch die Verformung des Körpers und nicht durch äußere Kräfte verursacht. Eine Versetzung ist die elementare Quelle der Eigenspannungen. Diese Art von Verformung wurde von V. Volterra als Distorsion bezeichnet. Eine Distorsion im Sinne von Volterra besteht aus einer regulären Verformung, die durch die Summe der folgenden Prozesse erzeugt wird [21]

- Zerschneidung des Körpers
- Bewegung der beiden Schnittflächen
- Wegnahme bzw. Einfügung von evtl. überschüssigem bzw. fehlendem Material
- Verbindung der beiden verformten Schnittebenen.

In dieser Arbeit wird anstelle von Distorsion die modernere Bezeichnung Defekt im Sinne von deWit [23], [24] verwendet. In einem Kristall kann ein Defekt durch einen Hohlzylinder um die Versetzungslinie angenähert werden. Die Versetzungslinie verläuft entlang der erweiterten Schnittfläche durch den Zylinder. Bei den unten dargestellten Volterra Defekten ist die Versetzungslinie jeweils die z-Achse. Jeder Defekt ist durch eine Schraubbewegung der Schnittflächen und somit durch drei Translationen oder drei Rotationen eindeutig festgelegt. Diese sechs Elementarversetzungen sind die Volterra Defekte, mit welchen jede mögliche Verformung angenähert werden kann.



a) X-Stufen Dislokation



b) Y-Stufen Dislokation



c) Schrauben Dislokation



d) X-Twist Disklination



e) Y-Twist Disklination



f) Keil Disklination

**Fig. 1.** Die sechs Volterra Defekte

Entstand der Defekt aus nur einer Translation, so nannte Volterra diesen eine Dislokation (a,b,c), entstand der Defekt aus nur einer Rotation, so wurde dieser als eine Disklination bezeichnet (d,e,f). Der Burger Vektor gibt an, wie die Schnittflächen bei den Dislokationen verschoben werden. Der axiale Frank Vektor gibt die Rotationsachse an, um welche die Schnittflächen bei den Disklinationen gedreht werden.

Lange Zeit wurden Disklinationen nicht als charakteristische Defekte in einem Kristall angesehen [25]. F.R.N. Nabarro [26] und F.C. Frank [27] gelang es aber Hinweise auf Disklinationen in kondensierter Materie zu finden [28]. Heute gibt es eine Vielzahl von Anwendungen der sogenannten Disklinationstheorie und ihrer Basis, den Volterra Defekten. Neben M. Klemm und Y. Bouligand mit ihrer Arbeit über flüssige Kristalle [9], [10], Magnetismus [9],[11] und biologische Objekte [10], [12], findet die Disklinationstheorie auch eine Anwendung bei der Analyse von Polarisations Effekten, der Beugung von elektromagnetischen Wellen [13], der Versetzung der Erdkruste [15], bei Phasenübergängen [14], bei der Wirbelstruktur in Halbleitern [16] oder in superflüssigem Helium [17], [8]. Darüberhinaus wiesen Tod [18] sowie Puntigam und Soleng [19] auf Analogien von bestimmten kosmischen Strings zu zwei Arten von kristallinen Defekten hin.

Heutzutage sind einige der Dehnungs- und Spannungstensoren der sechs Volterra Defekte bekannt, die als Analogon zu einer kristallinen Versetzung oder zu einem verformten Hohlzylinder aufgefaßt werden können. So fanden z.B. Volterra [20], Koehler [29] und Leibfried [30] einige Lösungen für die Dislokationen und vor allem deWit [23] fand Lösungen für die Disklinationen. Alle bisher bekannten Lösungen benötigen einen zusätzlichen Parameter, um ein Versetzungsfeld mit den richtigen Dimensionen zu erhalten. Ein derartiger Parameter ist hier, mit Ausnahme der Keil Disklination, nicht mehr nötig. Eine reguläre Versetzung und ihre erste und zweite Ableitung muß im Sinne von Volterra eindeutig, endlich und stetig sein [21]. Der von Volterra festgelegte Begriff entspricht somit der heutigen mathematischen Bedeutung und wird synonym für analytisch oder holomorph angewendet. Ein physikalisch verwendbares Versetzungsfeld muß zusätzlich noch die Gleichgewichtsbedingungen erfüllen. Das bedeutet, daß die Divergenz des Spannungstensors verschwindet, falls vorausgesetzt wird, daß keine äußeren Kräfte wirken. Desweiteren muß der Dehnungstensor die St. Venantschen Kompatibilitätsbedingungen erfüllen und der Spannungsvektor an der Oberfläche verschwinden. Das Ziel ist es, ein solches *realistisches* Versetzungsfeld zu finden, welches die gesamte elastische Verformung des Körpers beschreiben kann.

Wie Volterra werden wir mit einem einfachen Versetzungsfeld beginnen, welches den Defekt beschreibt, und dessen zugehöriger Dehnungstensor die St. Venantschen Bedingungen erfüllt. Dieses wird als *initiales* Versetzungsfeld  $\vec{u}_0$  bezeichnet. Der zugehörige Spannungstensor wird i.Allg. nicht divergenzfrei sein. Das Versetzungsfeld muß durch ein *additives* Vektorfeld  $\vec{u}_1$  erweitert werden um als *realistisch* zu gelten. Das *additive* Vektorfeld  $\vec{u}_1$  wird aus dem Produkt der Divergenz des Dehnungstensors mit einer noch zu bestimmenden Funktion bestehen. Diese Funktion wird durch das Lösen eines linearen partiellen Differentialgleichungssystems zweiter Ordnung gefunden werden. Durch dieses Vorgehen wird das *initiale* Versetzungsfeld in einer für den jeweiligen Defekt charakteristischen Art verändert. In Abschnitt 2.2 wird nach einer kurzen Wiederholung der wichtigsten Aspekte der linearen Elastizitätstheorie die Methode zum Auffinden eines Versetzungsfeldes mit divergenzfreiem Spannungstensor vorgestellt. In den folgenden Abschnitten werden die sechs Volterra Defekte berechnet und derart modifiziert, daß sie als analog zu einem



Kristall oder einem Hohlzylinder angesehen werden können.

In Abschnitt 3.1 wird die X-Stufen Dislokation analog zu einem Kristall vorgestellt. Der zugehörige Spannungsvektor wird an der Versetzungs- oder Dislokationslinie im Zentrum des Zylinders singulär und verschwindet annähernd an der Oberfläche des Kristalls. Hierfür gibt es bereits zwei gleichwertige Lösungen. Die eine wurde 1941 von Koehler [29] gefunden, die zweite entdeckte Kröner [7] 1958. Beide verwendeten die Spannungsfunktionsmethode. Die Existenz verschiedener Lösungen steht aber nicht im Widerspruch zum Eindeutigkeitsatz [31], [32], weil die Randbedingungen in allen Fällen nur näherungsweise erfüllt sind. Im Jahre 1957 berechnete Bullough [33] die Intensitätsverteilung von linear und von zirkular polarisiertem Licht einer einzelnen X-Stufen Dislokation in Silikon. Dies wurde später von Bond und Andrus [34], Nikitenko und Dedukh [35], sowie von Kosevich [36] verifiziert. Im Abschnitt 3.1.1 wird eine kurze Einführung in die Photoelastizitätsmethode gegeben, und die Übereinstimmung der Messungen mit den hier vorgestellten Berechnungen gezeigt. Desweiteren wird eine Übereinstimmung der Intensitätsverteilung des zirkular polarisierten Lichtes und der zur Verformung des ursprünglichen Körpers nötigen spezifischen Energie gezeigt. In Abschnitt 3.2 wird das Versetzungsfeld einer X-Stufen Dislokation in einem Kristall auf das eines Hohlzylinders erweitert. In diesem Fall verschwindet der Spannungsvektor näherungsweise auch am inneren Radius des Zylinders. Leibfried und Lücke [30] haben dies bereits im Jahre 1949 vorgenommen, sie präsentierten eine Lösung, die auf dem Versetzungsfeld von Koehler basiert.

Im 4. Kapitel wird das Gleiche für die Y-Stufen Dislokation durchgeführt. V. Volterra inspizierte im Jahre 1914 die photoelastischen Aufnahmen der Y-Stufen Dislokation eines Hohlzylinders [21], [22]. Seine mathematischen Untersuchung stimmen mit den hier vorgestellten Ergebnissen überein. Die Übereinstimmung mit den Fotos ist im Fall der Keil Disklination besser. Alle berechneten Bilder der Y-Stufen Dislokation entsprechen denen der X-Stufen Dislokation, wenn diese um  $\pi/2$  um die z-Achse gedreht werden.

Die wohlbekannte Schrauben Dislokation wird aufgrund ihrer Besonderheit in Kapitel 5 behandelt. Das bereits bekannte Versetzungsfeld kann als analog zu einem Kristall und zu einem Hohlzylinder aufgefaßt werden, da der Spannungsvektor überall orthogonal zum radialen Normalvektor ist (Fig 3.2). Dies ist ein Hinweis auf die besondere Rolle dieser Versetzung.

Die beiden Twist Disklinationen sind das Thema der Kapitel 6 und 7. In diesen Fällen führt der vorgestellte Algorithmus zu einem Versetzungsfeld mit einem zugehörigen Spannungstensor, dessen Divergenz in z-Richtung nicht verschwindet. Die erhaltenen Versetzungsfelder werden mit Hilfe der bekannten Differentialgleichungen der Gleichgewichtsbedingungen erweitert. Diese Gleichungen können in den betrachteten Fällen auf eine Gleichung reduziert werden, da nur noch die z-Komponente zu modifizieren ist. Der Spannungsvektor wurde hier bezüglich des unverformten Körpers berechnet. Dies kann für den vorausgesetzten linearen Fall durchgeführt werden, weil dieser nur für kleine Verformungen gültig ist. Die Bestimmung der exakten Spannungsvektoren war mit dem Computer-Algebra System „Reduce“ nicht möglich. Dies ist ein Hinweis auf sehr umfangreiche mathematische Ausdrücke. Die Näherungen der Twist Disklinationen analog zu einem Kristall oder einem Hohlzylinder sind nicht so gut wie die für die Stufen Dislokationen, weil der Spannungsvektor an den Stellen einen konstanten Wert annimmt, an denen er verschwinden sollte. Mit Berücksichtigung der durchgeführten Näherungen denke ich, daß es gerechtfertigt ist, die vorgestellten Versetzungsfelder als *realistisch*

zu bezeichnen. In Kapitel 8 wird schließlich die Keil Disklination behandelt. Diese ist mathematisch wesentlich komplizierter als die anderen Defekte. Die Keil Disklination ist der zur trivial gelösten Schrauben Dislokation korrespondierende Defekt. Beide Defekte zeigen eine Axialsymmetrie und sind für kosmische Strings oder die Wirbelstrukturen in superflüssigem Helium von Interesse [19]. Der Spannungsvektor ist bei der Keil Disklination überall parallel zu dem radialen Normalvektor (Fig 5.2). V.Volterra stellte im Jahre 1906 ein Versetzungsfeld vor, welches näherungsweise die Keil Disklination beschreibt [20]. Dieses wurde von Volterra und deWit [23], [24] derart modifiziert, daß zwar die Gleichgewichtsbedingungen erfüllt wurden, aber der Spannungsvektor vom Zentrum aus nach außen zunahm. Volterra [20] publizierte für einen Hohlzylinder eine gute Approximation eines Spannungstensor, der die notwendigen Gleichgewichtsbedingungen erfüllt, und dessen Spannungsvektor an der Oberfläche näherungsweise verschwindet. Experimentell verifizierte er seine Angabe wieder mittels photoelastischer Aufnahmen [21], [22]. Der vorgestellte Spannungstensor hängt aber nicht über das Hookesche Gesetz mit dem Dehnungstensor zusammen, der sich aus dem angegebenen Versetzungsfeld ergibt. A.E. Romanov and V.I. Vladimirov [28] versuchten 1992 das von deWit eingeführte Versetzungsfeld zu verändern. Meine Überprüfung ergab einen nicht divergenzfreien Spannungstensor. Ich habe es ebenfalls nicht geschafft, ein Versetzungsfeld zu finden, welches die Keil Disklination exakt beschreiben kann. Aus diesem Grund wird hier weiterhin die von Volterra eingeführte Näherung verwendet. Diese wird in den Abschnitten 8.1 und 8.2 mit Hilfe der vorgestellten Methode so erweitert, daß die erhaltenen Versetzungsfelder als analog zu einem Kristall oder einem Hohlzylinder angesehen werden können. Im Gegensatz zu Volterra verschwindet hier der entsprechende Spannungsvektor an der Oberfläche des Zylinders. Dies zeigt, wie effektiv der vorgestellte Algorithmus angewendet werden kann, selbst wenn der erste Teil nicht zum Erfolg führt.

# Contents

|          |  |            |
|----------|--|------------|
| <b>1</b> | <b>Introduction</b>                                      | <b>2</b>   |
| <b>2</b> | <b>Method to find divergence-free stress tensors</b>     | <b>7</b>   |
| 2.1      | The linear elasticity theory . . . . .                   | 7          |
| 2.2      | The new method . . . . .                                 | 9          |
| <b>3</b> | <b>The x-edge dislocation</b>                            | <b>11</b>  |
| 3.1      | The x-edge dislocation in a crystal . . . . .            | 13         |
| 3.1.1    | The photo-elasticity method . . . . .                    | 18         |
| 3.2      | The x-edge dislocation of a tubular cylinder . . . . .   | 22         |
| <b>4</b> | <b>The y-edge dislocation</b>                            | <b>33</b>  |
| 4.1      | The y-edge dislocation in a crystal . . . . .            | 35         |
| 4.2      | The y-edge dislocation of a tubular cylinder . . . . .   | 42         |
| <b>5</b> | <b>The screw dislocation</b>                             | <b>51</b>  |
| <b>6</b> | <b>The x-twist disclination</b>                          | <b>57</b>  |
| 6.1      | The x-twist disclination in a crystal . . . . .          | 60         |
| 6.2      | The x-twist disclination of a tubular cylinder . . . . . | 65         |
| <b>7</b> | <b>The y-twist disclination</b>                          | <b>73</b>  |
| 7.1      | The y-twist disclination in a crystal . . . . .          | 76         |
| 7.2      | The y-twist disclination of a tubular cylinder . . . . . | 81         |
| <b>8</b> | <b>The wedge disclination</b>                            | <b>89</b>  |
| 8.1      | The wedge disclination in a crystal . . . . .            | 92         |
| 8.2      | The wedge disclination of a tubular cylinder . . . . .   | 99         |
| <b>9</b> | <b>Conclusions</b>                                       | <b>105</b> |
| 9.1      | Summary . . . . .  | 105        |
| 9.2      | The new Volterra defects . . . . .                       | 106        |
|          | <b>References</b>  | <b>109</b> |
| <b>A</b> | <b>The divergence of the stress tensor</b>               | <b>113</b> |
| <b>B</b> | <b>Reduce-Programm für die Elastizitätstheorie</b>       | <b>116</b> |
| <b>C</b> | <b>C++-Programm zur Visualisierung</b>                   | <b>126</b> |

## 1 Introduction

The mathematical elasticity theory is occupied with an attempt to calculate the states of strain and stress within a solid body, which is subjected to given forces acting through its volume and to given traction across its surface. Its effort is to obtain results that shall be practically applicable to architecture, engineering, and all other useful arts where the material of construction is solid. The resistance of solids to rupture already occupied Galileo Galilei in 1638. He considered the deformation of a beam with one end built in a wall [1]. In 1822 Cauchy investigated most of the elements of the elasticity theory. His researches leads in the isotropic case to two material-dependent constants. He determined the equilibrium equations by which the stress components are connected with the forces distributed through the volume. The problem of determining the states of strain and stress within a solid body was now reducible to the analytical problem of finding the mathematical functions to represent the components of the displacement. These functions must satisfy the differential equations of equilibrium and certain special conditions at the surface of the body. A lot of efforts were made since that time, e.g. by Euler, Navier, Stokes, Poisson, Laplace, Green, Young, and others, to solve these equations. The methods devised for integrating these equations fall into two classes. The Green's function methods are based on his theory of the potential and constitute of determining the solution with the help of definite integrals. The second class is based on the search of special solutions and their modifications to satisfy the boundary conditions. These methods may be regarded as constituting an extension of the methods of expansion in the spherical harmonics and in the trigonometrical series [3]. The introduced algorithm has a completely different, physically motivated ansatz. We use the divergence of the strain tensor to solve the equilibrium equations and also to modify the solutions to fit for different boundary conditions.

We want to apply our algorithm to the Volterra defects, because they are helpful for the description of a variety of physical phenomena. G.I. Taylor [6], E. Orowan [4], and M. Polanyi [5] e.g. found out in 1934, that the plastic deformation of metal is produced by defects. The manifestation of one defect can only be understood by an atomic point of view, but the sum of all defects results in the macroscopic viewable deformation of the body. This approach helped to solve a lot of riddles in solid states physics [7] e.g. for the crystalline structure, melting processes [8] or optical properties. Nowadays, there exist many applications for the so called disclination theory, with its kernel, the Volterra defects. Beside M. Kleman and Y. Bouligand with their work on liquid crystals [9], [10], magnetics [9], [11] and biological objects [10], [12], the disclination theory is also useful by analyzing polarization effects and the diffraction of electro-magnetic waves [13], phase transitions [14], earth crust displacements [15], and the vortex structures in superconductors [16], and in superfluid helium [17], [8]. Moreover, Tod [18], and Puntigam and Soleng [19] pointed out analogies between certain cosmic strings and two kinds of defects in a crystal.

Vito Volterra, one of the founders of the disclination theory, examined at the beginning of our century 3-dimensional multiply connected elastic bodies, especially certain deformations of tubular cylinders (twice connected). He was interested in the tensions and the whole deformation of the body caused by the defect. Volterra's researches were illustrated by means of rubber-made cylinders [20]. Furthermore he used the photo-elasticity method on cylinders made of transparent gelatine to prove his mathematical results [21],

[22]. Multiply connected bodies are from special interest, because the tensions are not determined definitively by the outer forces like in simple connected ones (Kirchhoffscher Eindeutigkeitssatz) [7]. For multiple connected bodies exists therefore states of equilibrium, which does not exist for simple connected ones. The stress tensor is not definite. A deformed twice connected body can reach a state of equilibrium although there act some tensions. These tensions are called self tensions and are caused by the deformation instead of outer forces. A defect is therefore the elementary source of a self tension. Vito Volterra named such defects distortions. He defined a distortion as the sum of the following processes to attain a regular deformation ([21] page 142)

- cut the body
- move both cutting planes
- if necessary take off or fill in material
- connect the deformed planes.

We will use the modern nomination defect in the sense of deWit [23], [24] instead of distortion. Each defect is determined by a screw motion of the cutting planes, and so by six elements, three translations and three rotations. These six elementary displacements build up the six Volterra defects and can be used to approximate any kind of deformation.

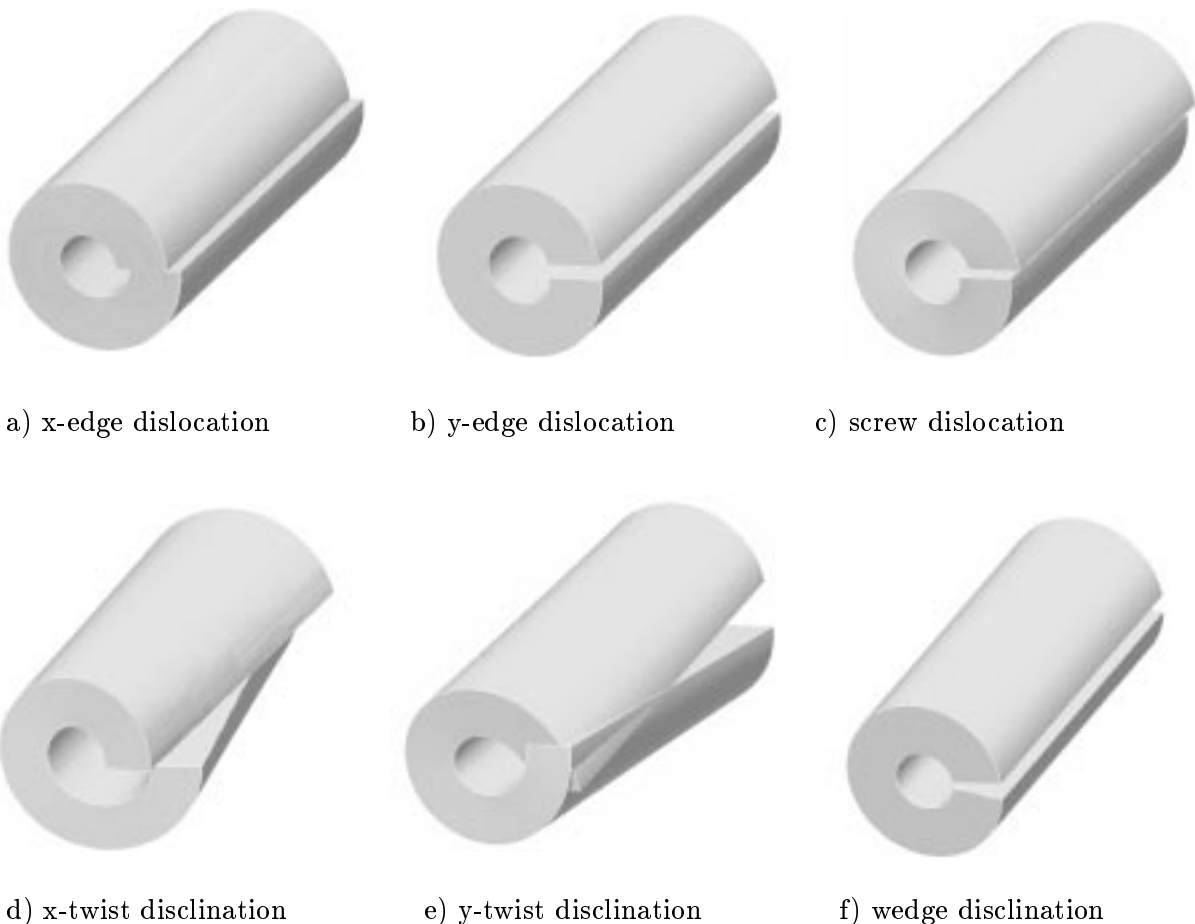


**Fig. 1.** The six Volterra defects

If the defect consists only of a translation, Volterra called it a dislocation (a,b,c), if it consists only of a rotation, he called it a disclination (d,e,f).

A defect can be regarded as a crystalline displacement with a related Burger's vector. In a crystal it can be approximated by a cylinder around the dislocation- or disclination line, which is here the z-axis. For a long time disclinations were not considered as defects characteristic of crystalline solids [25]. F.R.N. Nabarro [26] and F.C. Frank [27] made important progresses in applying the disclinations to condensed matter physics [28]. Nowadays, some strain and stress tensors of these six defects are known in the case of a crystal defect or a tubular cylinder. Volterra [20], Koehler [29], and Leibfried [30], e.g., found some solutions for the dislocations and, especially deWit [23], for the disclinations. A regular deformation and its derivatives of the first and the second order had in the sense of Volterra to be definite, finite and continual [21]. A correct displacement field has moreover to fulfill the equilibrium conditions, i.e., a divergence-free stress tensor in the case of no external forces. In addition, the corresponding strain tensor has to fulfill St. Venant's compatibility conditions, and the stress vector field has to vanish at the surface of the body, as far as it is not orthogonal to the normal vector of the surface. Our aim is to find such a *realistic* displacement field to describe the entire elastic deformation of the body.

Like Volterra we will start with a simple displacement characterizing the defect and fulfilling the St. Venant compatibility conditions. We will call this the *initial* displacement field  $\vec{u}^0$ . The corresponding stress tensor generally is not divergence-free. The displacement needs to be supplemented by an *additional* displacement field  $\vec{u}^1$  in order to become *realistic*. We will add as  $\vec{u}^1$  the divergence vector field of the strain tensor multiplied by a function. We will derive this functions by solving a system of linear second order partial differential equations. Thereby the displacement will be improved in a way specific for the defect.

In section 2.2, after reminding ourselves of some general aspects of the linear elasticity theory, we will formulate our method for finding a displacement field with a divergence-free stress tensor. In the following sections we will calculate the six Volterra defects and modify them in a way that they can be looked at as analogous to a crystal or to a tubular cylinder.

In section 3.1 the x-edge dislocation will be presented in analogy to a crystal defect. We will calculate a stress vector field that becomes singular at the dislocation line in the center and vanishes approximately at the outer surface of the crystal. The singularity at the center of the crystal can be approximated by a tubular cylinder around the disclination line. Two similar solutions for this were already given by Koehler [29] in 1941 and by Kröner [7] in 1958. They used the stress function method to find their results, where an additional parameter is necessary to get a displacement field with the correct dimensions. In our case is such a parameter not necessary, nevertheless, our result is nearly the same. The existence of different solutions is not in contradiction to the uniqueness statements [31], [32], because the boundary conditions are only fulfilled approximately. In 1957, Bulough [33] calculated the intensity distribution of linear and circular polarized light of a single x-edge dislocation in silicon. This was later verified by Bond and Andrus [34], Nikitenko and Dedukh [35], and by Kosevich [36]. In section 3.1.1 we will give a short introduction into the photo-elasticity method and will show agreement with our computations. We will find a similarity between the fringe pattern of circular polarized light and the specific energy for changing the shape of the origin body. In 3.2 the solution for the

x-edge dislocation in a crystal will be extended to a tubular cylinder, with approximately vanishing stress vectors at the inner and the outer envelope of the cylinder. This was already done in 1949 by Leibfried and Lücke [30], who presented a displacement field, based on Koehler's solution.

In chapter 4 we will do the same for the y-edge dislocation. V. Volterra inspected in 1914 the fringe patterns of the y-edge dislocation in a tubular cylinder [21], [22]. His mathematical examinations of the photographs will coincide with our calculations. The agreement with the photographs will be better for the wedge disclination. Our calculated fringe patterns of the y-edge dislocation will be similar to the patterns of the x-edge dislocation, if they will be rotated around the z-axis about an angular of  $\pi/2$ .

In chapter 5 we will examine the very well known screw dislocation, because of its curiosity. The known displacement field can be interpreted as analogous to a crystal and to a tubular cylinder. The stress vector field is everywhere orthogonal to the radial normal vector (Fig. 3.2.). This is a hint for the special role of this displacement.

The two twist disclinations will be the subjects of the chapters 6 and 7. In these cases our algorithm will lead to a displacement field with a remaining divergence of the stress tensor in z-direction. The further modification of this displacement field will be done by using the known equilibrium equations. The calculations of the eigenvalues of the strain and the stress tensor were in the cases of the twist disclinations hard to handle. We found no experimental researches about these cases and disclaimed therefore the calculations of the fringe patterns, which are based on the eigenvalues. The stress vector fields will be related in the case of the twist disclinations to the normal vector fields of the origin undeformed body. This can be done in the presumed linear and elastic case, because it is only useful for small defects. The calculations of the exact vector fields were not possible with the computer algebra system "Reduce". This indicates huge expressions. The approximations of the twist disclinations as analogous to a crystal or a tubular cylinder will not be as well as for the edge-dislocations, because the resulting stress vector field will only reach a constant amount where it should vanish. We think the interpretation of the introduced displacement fields as approximately *realistic* will be justifiable with retrospect to the done approximations.

In chapter 8 we will consider the wedge disclination. It is mathematically much more complicated than the other defects. The wedge disclination is the corresponding defect to the trivial solved screw dislocation. Both defects show a cylindrical symmetry and are of interest for cosmic strings or vortex structures in superfluid Helium [19]. The stress vector is here everywhere parallel to the radial normal vector (Fig. 5.2). Volterra gave in 1906 an approximation of the initial displacement field that may describe this disclination [20]. Volterra and deWit [23], [24] modified this approximation of the initial displacement field in a way that the equilibrium conditions were fulfilled, but the amount of the belonging stress vector rises from the center to the envelope of the cylinder. For a tubular cylinder Vito Volterra gave in his publication " Sur l'équilibre des corps élastiques " [20] (page 447) a good approximation for a stress tensor which satisfies the necessary conditions. The equilibrium conditions are fulfilled and the stress vector field vanishes approximately at the lateral areas of the cylinder. Volterra gave an experimental verification by a photo-elastic picture shown in [21] and in [22]. The presented stress tensor is not related by Hooke's law to the strain tensor belonging to the displacement field given by Volterra. A.E. Romanov and V.I. Vladimirov tried in 1992 to modify the displacement field from deWit in a way that the according stress vector field fulfills the necessary conditions for

a tubular cylinder [28]. Our check yields no divergence-free stress tensors. We do not succeed in solving the partial differential equations for getting a displacement field of the wedge disclination with a divergence-free stress tensor. This is the reason why we will take Volterra's approximation and will modify it by means of our algorithm in section 8.1 for a crystal and in 8.2 for a tubular cylinder. Different to Volterra we will get vanishing stress vectors at the envelopes of the cylinder. This shows how boundary problems can be effectively solved with the second part of our algorithm, even if the first part fails.

We will work with the approximation of a plane state of strain, so the displacement in z-direction is neglectable, and of a plane state of stress, which enables us to take the z-component of the stress vector out of account. Physically this can be pictured as a cylinder with infinite elongation in z-direction. The calculations are done in the sense of a linearized theory for small static displacements of an isotropic elastic body. If not mentioned otherwise, all expressions are given in terms of Cartesian coordinates, furthermore the summation convention is adopted in the whole article. All plots will be done for a Young's modulus of  $E = 10^6 \text{Pa}$  and a Poisson's ratio of  $\nu = 0.45$  (rubber).



## 2 Method to find divergence-free stress tensors

We first want to remind ourselves of some important rules in linear elasticity theory.

### 2.1 The linear elasticity theory

The displacement vector field at any point  $P$  is defined as the difference between the place of  $P$  afterwards the displacement  $\vec{x}'(P)$  and before,

$$\vec{u}(P) := \vec{x}'(P) - \vec{x}(P) \quad . \quad (1)$$

The linear approximation for small displacements yields the following symmetric strain tensor:

$$\boldsymbol{\varepsilon}_{ij} \approx \frac{1}{2}(u_{i,j} + u_{j,i}) = u_{(i,j)} \quad . \quad (2)$$

The strain tensor has to fulfill the compatibility conditions (Kröner [7], page 127)

$$\boldsymbol{\varepsilon}^{hij} \boldsymbol{\varepsilon}^{klm} \boldsymbol{\varepsilon}_{jl,ik} = 0 \quad , \quad (3)$$

with the totally antisymmetric Levi-Civita tensor  $\boldsymbol{\varepsilon}^{hij}$ .

This can be reduced to the six St. Venant equations (Sokolnikoff [37], page 28)

$$\begin{aligned} \boldsymbol{\varepsilon}_{11,23} &= -\boldsymbol{\varepsilon}_{23,11} + \boldsymbol{\varepsilon}_{31,21} + \boldsymbol{\varepsilon}_{12,31} \quad , \\ \boldsymbol{\varepsilon}_{22,31} &= \boldsymbol{\varepsilon}_{23,12} - \boldsymbol{\varepsilon}_{31,22} + \boldsymbol{\varepsilon}_{12,32} \quad , \\ \boldsymbol{\varepsilon}_{33,12} &= \boldsymbol{\varepsilon}_{23,13} + \boldsymbol{\varepsilon}_{31,23} - \boldsymbol{\varepsilon}_{12,33} \quad , \\ 2\boldsymbol{\varepsilon}_{12,12} &= \boldsymbol{\varepsilon}_{11,22} + \boldsymbol{\varepsilon}_{22,11} \quad , \\ 2\boldsymbol{\varepsilon}_{23,23} &= \boldsymbol{\varepsilon}_{22,33} + \boldsymbol{\varepsilon}_{33,22} \quad , \\ 2\boldsymbol{\varepsilon}_{13,13} &= \boldsymbol{\varepsilon}_{33,11} + \boldsymbol{\varepsilon}_{11,33} \quad . \end{aligned} \quad (4)$$

The relation between the strain tensor and the stress tensor can be formulated by means of the generalized Hooke law:

$$\boldsymbol{\sigma}^{ij} = \mathbf{E}^{ijkl} \boldsymbol{\varepsilon}_{kl} \quad , \quad (5)$$

which is valid for the elastic case and for small displacements.

The elastic moduli  $\mathbf{E}^{ijkl}$  for isotropic media are (Kröner [7], page 52)

$$\mathbf{E}^{ijkl} = \frac{E}{2(1+\nu)} \left( \frac{2\nu}{1-2\nu} \mathbf{g}^{ij} \mathbf{g}^{kl} + \mathbf{g}^{ik} \mathbf{g}^{jl} + \mathbf{g}^{il} \mathbf{g}^{jk} \right) \quad , \quad (6)$$

with Young's modulus  $E$  and Poisson's ratio  $\nu$ .

In Cartesian coordinates, with  $\mathbf{g}^{ij} = \boldsymbol{\delta}^{ij}$ , Hooke's law turns out to be (Klingbeil [38], page 139)

$$\boldsymbol{\sigma}^{ij} = \frac{E}{(1+\nu)} \left( \boldsymbol{\varepsilon}^{ij} + \frac{\nu}{1-2\nu} \boldsymbol{\delta}^{ij} \boldsymbol{\varepsilon}_k^k \right) \quad . \quad (7)$$

The stress vector  $\vec{f}_A$  is defined by the force  $d\vec{F}_A$ , acting on a plane  $dA$ , which is necessary to preserve the deformation at this point,

$$d\vec{F}_A := \vec{f}_A dA \quad . \quad (8)$$

The stress vector is the scalar product of the stress tensor with the outer normal vector  $\vec{n}_A$  of the plane,

$$\vec{f}_A = \vec{n}_A \cdot \boldsymbol{\sigma} \quad . \quad (9)$$

A body is in equilibrium, if the vector  $\vec{F}_V$ , representing the volume density of the forces acting from outside, is compensated by the divergence of the stress tensor,

$$F_V^i = -\boldsymbol{\sigma}^{ij}{}_{,j} \quad . \quad (10)$$

These three coupled partial differential equations determine together with Hooke's law the six free components of the stress tensor. It is very difficult to deform a body mathematically into a body that satisfied the equilibrium conditions. In many cases is only the origin body before the deformation required to be in equilibrium. This is called the theory of first order. Here we work with the theory of second order, where the deformed body had to fulfill the equilibrium conditions too. The divergence of the stress tensor writes with the generalized Hooke's law of eq.(7) [2]

$$\boldsymbol{\sigma}^{ij}{}_{,j} = \frac{E\nu}{(1+\nu)(1-2\nu)} \sum_l \frac{\partial \varepsilon_{ll}}{\partial x_i} + \frac{E}{1+\nu} \boldsymbol{\varepsilon}^{ij}{}_{,j} \quad .$$

If we substitute the strain tensor of (eq. (2)) by the displacement vector, we get the equilibrium equations of eq. (10) as

$$\begin{aligned} \boldsymbol{\sigma}^{ij}{}_{,j} &= \frac{E\nu}{(1+\nu)(1-2\nu)} \sum_l \frac{\partial^2 u_l}{\partial x_l \partial x_i} + \frac{E}{2(1+\nu)} \sum_j \left( \frac{\partial^2 u_j}{\partial x_i \partial x_j} + \frac{\partial^2 u_i}{\partial x_j^2} \right) \\ &= -F_V^i \quad . \end{aligned} \quad (11)$$

Sorting the summands leads to

$$\frac{E}{2(1+\nu)} \sum_j \left( \frac{1}{(1-2\nu)} \frac{\partial^2 u_j}{\partial x_i \partial x_j} + \frac{\partial^2 u_i}{\partial x_j^2} \right) = -F_V^i \quad . \quad (12)$$

External forces are assumed to be absent. Hence the equilibrium conditions for the static case can be written as

$$\boldsymbol{\sigma}^{ij}{}_{,j} = 0 \quad . \quad (13)$$

In the inspected linear, elastic and isothermal case the outer work required for the displacement  $\vec{u}$  of the isotropic body with the volume  $V$  is stored as the inner energy  $U$  given by [39] [20]

$$U = \frac{1}{2} \int_V \boldsymbol{\varepsilon}_{ij} \boldsymbol{\sigma}^{ij} dV \quad . \quad (14)$$

If we examine only an infinitesimal volume element this leads to the specific inner energy, the free elastic energy [7], [2], or the strain-energy density [40]. This expression was first introduced by George Green in 1839 [37], [41],

$$\tilde{U} = \frac{1}{2} \boldsymbol{\varepsilon}_{ij} \boldsymbol{\sigma}^{ij} = \frac{1}{2} E^{ijkl} \boldsymbol{\varepsilon}_{ij} \boldsymbol{\varepsilon}_{kl} \quad . \quad (15)$$

It represents the energy accumulated in each volume element caused by the elastic deformation. It can be divided into two parts. The specific energies which are necessary for changing the volume  $\tilde{U}_V$ , and for changing the shape of the origin body  $\tilde{U}_F$  [39],

$$\tilde{U} = \tilde{U}_V + \tilde{U}_F \quad , \quad (16)$$

with

$$\tilde{U}_V = \frac{1}{6} \boldsymbol{\varepsilon}_k^k \boldsymbol{\sigma}_k^k \quad . \quad (17)$$

## 2.2 The new method

We want a *realistic* displacement field  $\vec{u}^r$ , with a strain tensor that accomplishes the St. Venant compatibility conditions, a divergence-free stress tensor and vanishing stress vectors at the surface of the body. Furthermore it should describe the entire deformation of the body. The idea was to search for intrinsic attributes of elasticity theory to describe the *reactive* deformation of the body, caused by the defect. We took an *initial* displacement field  $\vec{u}^0$ , which characterizes the defect, and inspected some of its characteristic attributes. We remarked a similar structure of the stress vector field and the divergence vector fields of the strain and the stress tensor ( $\vec{f}_A^0 \sim \boldsymbol{\varepsilon}^{ij}_{,j} \sim \boldsymbol{\sigma}^{ij}_{,j}$ ). From a physical point of view each of them may describe the *reactive* deformation.

We looked for an *additional* displacement  $\vec{u}^1$  that leads, together with  $\vec{u}^0$ , to a *realistic* displacement field  $\vec{u}^r$ ,

$$\vec{u}^r = \vec{u}^0 + \vec{u}^1 \quad . \quad (18)$$

We first chose as  $\vec{u}^1$  the stress vector field  $\vec{f}_A^0$  belonging to  $\vec{u}^0$ ,

$$\vec{u}^1 \propto \vec{f}_A^0 \quad . \quad (19)$$

By deforming the body into the direction of  $\vec{f}_A^0$ , we hoped to be able to construct a *realistic* displacement field with vanishing stress vectors at the surface. This failed, because we obtained rising components of the divergence of the stress tensor and the stress vector field.

Next we tried the divergence of the stress tensor

$$\vec{u}^1 \propto \boldsymbol{\sigma}^{ij}_{,j} \quad . \quad (20)$$

The similarity between the divergences of the strain and the stress tensor, the comparison with the known results, and some more calculations lead us to the ansatz

$${}^1u_k = {}^1w \mathcal{W} \mathbf{\varepsilon}_{km}^0,{}^m \quad (21)$$

with the divergence of the strain tensor of the *initial* displacement field, the constant  ${}^1w$  and the function  $\mathcal{W} = \mathcal{W}(x, y, z)$ . The function  $\mathcal{W}$  is necessary in order to create a vector field, which leads, together with the *initial* displacement  $\vec{u}^0$ , to equilibrium. The product of the constant  ${}^1w$  and the function  $\mathcal{W}$  has the dimension

$$\dim[{}^1w\mathcal{W}] = (\text{length})^2 \quad . \quad (22)$$

The strain tensor of the new displacement field is given by

$$\boldsymbol{\varepsilon}_{kl} = \mathbf{\varepsilon}_{kl}^0 + \mathbf{\varepsilon}_{kl}^1 \quad , \quad (23)$$

with the strain tensor of the *initial* displacement field

$$\mathbf{\varepsilon}_{kl}^0 = u_{(k,l)}^0 \quad , \quad (24)$$

and the strain tensor of the *additional* displacement

$$\mathbf{\varepsilon}_{kl}^1 = u_{(k,l)}^1 \quad . \quad (25)$$

With our ansatz for the displacement field (21), the last can be written as

$$\mathbf{\varepsilon}_{kl}^1 = {}^1w \left( \mathcal{W} \mathbf{\varepsilon}_{(k|m}^0,{}^m)_{,|l)} \right) \quad . \quad (26)$$

With Hooke's law (7) follows for the divergence of the stress tensor:

$$\boldsymbol{\sigma}^{ij}{}_{,j} = \frac{E}{1+\nu} \left[ \boldsymbol{\varepsilon}^{ij}{}_{,j} + \frac{\nu}{1-2\nu} \boldsymbol{\varepsilon}_k{}^{k,i} \right] \quad . \quad (27)$$

With (23) and (26), and since  $(-1 < \nu < 0.5)$ , it turns out to be zero, if

$$\mathbf{\varepsilon}_{ij}^0{}_{,j} + {}^1w \left( \mathcal{W} \mathbf{\varepsilon}_{(i|m}^0,{}^m)_{,|j)} \right)_{,j} + \frac{\nu}{1-2\nu} \left[ \boldsymbol{\varepsilon}_k{}^{k,i} + {}^1w \left( \mathcal{W} \mathbf{\varepsilon}_{km}^0,{}^m \right)^{k,i} \right] = 0 \quad . \quad (28)$$

These equations for the determination of the function  $\mathcal{W}$  and the constant  ${}^1w$  are the mathematical corner stone of our method to derive divergence-free stress tensors.

### 3 The x-edge dislocation



**Fig. 1.1:** The x-edge dislocation

In the case of dislocations, the displacement vector  $\vec{u}$  has to undergo a certain finite increment  $\vec{b}$  after passage around any closed contour  $s$  that encircles the dislocation line (A. M. Kosevich [36] page 39) and is called a Burgers circuit [42]. This condition can be formulated as

$$\oint u_k ds_k = \oint u_k(s_k(t)) \frac{\partial s_k(t)}{\partial t} dt = b_k \quad , \quad (29)$$

if we parameterize the contour with  $t$ .

The components of the considered Burgers vector  $\vec{b}$  are

$$\vec{b} = (b_1, 0, 0) \quad . \quad (30)$$

We choose in all calculations

$$\vec{s}(t) = \left( \cos t, \sin t, 0 \right) \quad . \quad (31)$$

A simple displacement field, which characterizes the x-edge dislocation and fulfills the St. Venant conditions and equation (29), is given by

$$\begin{aligned} u_x^0 &= \frac{b_1}{2\pi} \arctan\left(\frac{y}{x}\right) \quad , \\ u_y^0 &= 0 \quad , \\ u_z^0 &= 0 \quad . \end{aligned} \quad (32)$$

We call this the *initial* displacement of the x-edge dislocation. It is shown in fig. 1.1 For the strain tensor of this displacement field (32) we find

$$\begin{aligned}
\mathbf{\varepsilon}_{xx}^0 &= -\frac{b_1}{2\pi} \frac{y}{(x^2 + y^2)} \quad , \\
\mathbf{\varepsilon}_{xy}^0 &= \frac{b_1}{4\pi} \frac{x}{(x^2 + y^2)} \quad , \\
\mathbf{\varepsilon}_{xz}^0 &= 0 \quad , \\
\mathbf{\varepsilon}_{yy}^0 &= 0 \quad , \\
\mathbf{\varepsilon}_{yz}^0 &= 0 \quad , \\
\mathbf{\varepsilon}_{zz}^0 &= 0 \quad ,
\end{aligned} \tag{33}$$

with a divergence of

$$\begin{aligned}
\mathbf{\varepsilon}_{xj}^0{}_{,j} &= \frac{b_1}{2\pi} \frac{xy}{(x^2 + y^2)^2} \quad , \\
\mathbf{\varepsilon}_{yj}^0{}_{,j} &= -\frac{b_1}{4\pi} \frac{(x^2 - y^2)}{(x^2 + y^2)^2} \quad , \\
\mathbf{\varepsilon}_{zj}^0{}_{,j} &= 0 \quad .
\end{aligned} \tag{34}$$

The divergence of the stress tensor turns out to be proportional to the divergence of the strain tensor,

$$\mathbf{\sigma}^0{}_{ij}{}_{,j} = \frac{E}{(1 + \nu)(1 - 2\nu)} \mathbf{\varepsilon}^0{}_{ij}{}_{,j} \quad . \tag{35}$$

The displacement (32) has no divergence-free stress tensor. It needs to be extended by an *additional* displacement field  $\overset{1}{\vec{u}}$ . This can be calculated with our ansatz (21). To determine the function  $\overset{1}{\mathcal{W}}$  and the constant  $\overset{1}{w}$ , we solve the partial differential equation (28). We start with the x-component of the divergence of the stress tensor  $\mathbf{\sigma}^0{}_{xj}{}_{,j}$ , which vanishes if (see Appendix eq.(293))

$$\begin{aligned}
\overset{1}{w} &\left( (1 - \nu)(\overset{1}{\mathcal{W}}\mathbf{\varepsilon}^0{}_{xm}{}_{,m})_{,x,x} + \left(\frac{1}{2} - \nu\right)\left((\overset{1}{\mathcal{W}}\mathbf{\varepsilon}^0{}_{xm}{}_{,m})_{,y,y} + (\overset{1}{\mathcal{W}}\mathbf{\varepsilon}^0{}_{xm}{}_{,m})_{,z,z}\right) \right. \\
&\quad \left. + \frac{1}{2}\left((\overset{1}{\mathcal{W}}\mathbf{\varepsilon}^0{}_{ym}{}_{,m})_{,x,y} + (\overset{1}{\mathcal{W}}\mathbf{\varepsilon}^0{}_{zm}{}_{,m})_{,x,z}\right) \right) \\
&+ (1 - \nu)\mathbf{\varepsilon}^0{}_{xx}{}_{,x} + (1 - 2\nu)\left(\mathbf{\varepsilon}^0{}_{xy}{}_{,y} + \mathbf{\varepsilon}^0{}_{xz}{}_{,z}\right) + \nu\left(\mathbf{\varepsilon}^0{}_{yy}{}_{,x} + \mathbf{\varepsilon}^0{}_{zz}{}_{,x}\right) = 0 \quad .
\end{aligned} \tag{36}$$

We know from our ansatz (21), that for the divergence of the strain tensor considered (eq. (34)), the function  $\overset{1}{\mathcal{W}}$  has to have the dimension of [length]<sup>2</sup>. If we choose

$$\overset{1}{\mathcal{W}} = x^2 + y^2 \quad , \tag{37}$$

we find that the first component of the divergence of the stress tensor vanishes if the constant

$${}^1w = -\frac{1}{4\nu - 3} . \quad (38)$$

This is one solution for the y-component too (see appendix). The *additional* displacement reads with (37) and (38)

$$\begin{aligned} {}^1u_x &= -\frac{b_1}{2\pi} \frac{1}{(4\nu - 3)} \frac{xy}{(x^2 + y^2)} , \\ {}^1u_y &= \frac{b_1}{4\pi} \frac{1}{(4\nu - 3)} \frac{(x^2 - y^2)}{(x^2 + y^2)} , \\ {}^1u_z &= 0 . \end{aligned} \quad (39)$$

As shown in the next section, its addition to the *initial* displacement (32) leads to a divergence-free stress tensor (see eq.(51), eq.(52), and appendix).

### 3.1 The x-edge dislocation in a crystal

The stress vector field of a crystal defect diverges at the disclination line and vanishes at the surface of the crystal. The defect can be approximated by a cylinder around the disclination line.

We take the *initial* displacement  $\vec{u}^0$  of the x-edge dislocation, see eq.(32), and add the calculated *additional* displacement field  $\vec{u}^1$  of (39). We get as result the *realistic* displacement vector field which describes the x-edge dislocation in a crystal

$$\vec{u}^c = \vec{u}^0 + \vec{u}^1 , \quad (40)$$

with

$$\begin{aligned} {}^c u_x &= \frac{b_1}{2\pi} \left( \arctan\left(\frac{y}{x}\right) - \frac{1}{(4\nu - 3)} \frac{xy}{(x^2 + y^2)} \right) , \\ {}^c u_y &= \frac{b_1}{4\pi} \frac{1}{(4\nu - 3)} \frac{(x^2 - y^2)}{(x^2 + y^2)} , \\ {}^c u_z &= 0 . \end{aligned} \quad (41)$$

As will be shown below, the corresponding stress vector (55) vanishes for large outer radii and gets singular at the center of the cylinder.

The integral (29) along the contour-line  $\vec{s}(t)$  of equation (31) has the components

$$\begin{aligned} \oint u_x \frac{\partial s_x}{\partial t} dt &= \frac{b_1}{6\pi(4\nu - 3)} \left( 3(4\nu - 3)[t \cos(t) - \sin(t)] + \sin^3(t) \right) \Big|_0^{2\pi} = b_1 , \\ \oint u_y \frac{\partial s_y}{\partial t} dt &= \frac{-b_1}{12\pi(4\nu - 3)} \left( (2 \sin^2(t) - 3) \sin(t) \right) \Big|_0^{2\pi} = 0 , \\ \oint u_z \frac{\partial s_z}{\partial t} dt &= 0 . \end{aligned} \quad (42)$$

We calculate the strain tensor of this displacement field and obtain

$$\begin{aligned}
\epsilon_{xx} &= \frac{b_1}{\pi} \frac{1}{(4\nu - 3)} \frac{y(2\nu(x^2 + y^2) - 2x^2 - y^2)}{(x^2 + y^2)^2} , \\
\epsilon_{xy} &= \frac{b_1}{\pi} \frac{1}{(4\nu - 3)} \frac{x(\nu(x^2 + y^2) - x^2)}{(x^2 + y^2)^2} , \\
\epsilon_{xz} &= 0 , \\
\epsilon_{yy} &= -\frac{b_1}{\pi} \frac{1}{(4\nu - 3)} \frac{x^2 y}{(x^2 + y^2)^2} , \\
\epsilon_{yz} &= 0 , \\
\epsilon_{zz} &= 0 .
\end{aligned} \tag{43}$$

Its trace is given by

$$\epsilon_k^k = -\frac{b_1}{\pi} \frac{2\nu - 1}{(4\nu - 3)} \frac{y}{x^2 + y^2} . \tag{44}$$

The divergence of the strain tensor reads

$$\begin{aligned}
\epsilon_{xj}{}^{,j} &= \frac{b_1}{\pi} \frac{2\nu}{(4\nu - 3)} \frac{xy}{(x^2 + y^2)^2} , \\
\epsilon_{yj}{}^{,j} &= -\frac{b_1}{\pi} \frac{\nu}{(4\nu - 3)} \frac{(x^2 - y^2)}{(x^2 + y^2)^2} , \\
\epsilon_{zj}{}^{,j} &= 0 .
\end{aligned} \tag{45}$$

We compare this with the divergence of the strain tensor of the *initial* displacement and find the proportional relation

$$\epsilon_{xj}{}^{,j} = \frac{4\nu}{4\nu - 3} \mathbf{0} \epsilon_{xj}{}^{,j} , \tag{46}$$

that will be helpful in section 3.2.

Diagonalisation yields the principal strains

$$\begin{aligned}
\hat{\epsilon}_{11} &= -\frac{b_1}{2\pi} \frac{1}{(4\nu - 3)} \frac{\mathcal{A} + (2\nu - 1)y}{(x^2 + y^2)} , \\
\hat{\epsilon}_{22} &= \frac{b_1}{2\pi} \frac{1}{(4\nu - 3)} \frac{\mathcal{A} - (2\nu - 1)y}{(x^2 + y^2)} , \\
\hat{\epsilon}_{33} &= 0 .
\end{aligned} \tag{47}$$

For convenience we introduced the function

$$\mathcal{A} := \sqrt{(4\nu^2 - 8\nu + 4)x^2 + (4\nu^2 - 4\nu + 1)y^2} . \tag{48}$$



By Hooke's law the stress tensor turns out to be

$$\begin{aligned}
\sigma^{xx} &= -\frac{b_1}{\pi} \frac{E}{(4\nu-3)(\nu+1)} \frac{y(\nu(x^2+y^2)-2x^2-y^2)}{(x^2+y^2)^2} , \\
\sigma^{xy} &= \frac{b_1}{\pi} \frac{E}{(4\nu-3)(\nu+1)} \frac{x(\nu(x^2+y^2)-x^2)}{(x^2+y^2)^2} , \\
\sigma^{xz} &= 0 , \\
\sigma^{yy} &= \frac{b_1}{\pi} \frac{E}{(4\nu-3)(\nu+1)} \frac{y(\nu(x^2+y^2)-x^2)}{(x^2+y^2)^2} , \\
\sigma^{yz} &= 0 , \\
\sigma^{zz} &= \frac{b_1}{\pi} \frac{E\nu}{(4\nu-3)(\nu+1)} \frac{y}{(x^2+y^2)} , 
\end{aligned} \tag{49}$$

with the trace

$$\sigma_k^k = \frac{b_1}{\pi} \frac{E}{(4\nu-3)} \frac{y}{x^2+y^2} = -\frac{E}{(2\nu-1)} \epsilon_k^k . \tag{50}$$

The stress tensor is divergence-free. The x-component of the divergence of the stress tensor vanishes according to

$$\sigma^{x1}_{,1} = -\sigma^{x2}_{,2} = \frac{b_1}{\pi} \frac{E}{(4\nu-3)(\nu+1)} \frac{2xy(\nu(x^2+y^2)-2x^2)}{(x^2+y^2)^3} , \tag{51}$$

and the y-component according to

$$\sigma^{y1}_{,1} = -\sigma^{y2}_{,2} = -\frac{b_1}{\pi} \frac{E}{(4\nu-3)(\nu+1)} \frac{\nu(x^4-y^4)-x^4+3x^2y^2}{(x^2+y^2)^3} . \tag{52}$$

Diagonalisation yields the principal stresses

$$\begin{aligned}
\dot{\sigma}^{11} &= -\frac{b_1}{2\pi} \frac{E}{(4\nu-3)(\nu+1)} \frac{\mathcal{A}-y}{(x^2+y^2)} , \\
\dot{\sigma}^{22} &= \frac{b_1}{2\pi} \frac{E}{(4\nu-3)(\nu+1)} \frac{\mathcal{A}+y}{(x^2+y^2)} , \\
\dot{\sigma}^{33} &= \frac{b_1}{2\pi} \frac{2E\nu}{(4\nu-3)(\nu+1)} \frac{y}{(x^2+y^2)} , 
\end{aligned} \tag{53}$$

with function  $\mathcal{A}$  from eq. (48).

In cylindrical coordinates the stress tensor reads

$$\begin{aligned}
\sigma^{rr} &= \frac{b_1}{\pi} \frac{E\nu}{(4\nu-3)(\nu+1)} \frac{\sin(\varphi)}{r} , \\
\sigma^{r\varphi} &= \frac{b_1}{\pi} \frac{E(\nu-1)}{(4\nu-3)(\nu+1)} \frac{\cos(\varphi)}{r} , \\
\sigma^{rz} &= 0 , \\
\sigma^{\varphi\varphi} &= -\frac{b_1}{\pi} \frac{E(\nu-1)}{(4\nu-3)(\nu+1)} \frac{\sin(\varphi)}{r} , \\
\sigma^{\varphi z} &= 0 , \\
\sigma^{zz} &= \frac{b_1}{\pi} \frac{E\nu}{(4\nu-3)(\nu+1)} \frac{\sin(\varphi)}{r} .
\end{aligned} \tag{54}$$

These components are proportional to them given by Weertman [43] for Kröner's solution [7].

We always will work here with the stress vector fields which belongs first to the interior normal vector field of the envelope of the cylinder pointing into the center and second to the normal vector field which belongs to the top respectively the bottom of the cylinder and is parallel to the z-axis. In the case of the x-edge dislocation in a crystal, the whole stress vector field reads in cylindrical coordinates

$$\begin{aligned}
f_r &= -\frac{b_1}{\pi} \frac{E}{(4\nu-3)(\nu+1)} \frac{1}{r} \\
&\times \left( -b_1(3\nu-2) \sin^2(\varphi) \nu(4\nu-3) \pi r \sin(\varphi) - 2b_1(\nu-1)^2 \right) \\
&\times \left( b_1^2 \left( (4\nu-3) \sin^2(\varphi) + 4\nu^2 - 4(2\nu-1) \right) \right. \\
&\quad \left. - 2(4\nu-3)(2\nu-1) b_1 \pi r \sin(\varphi) + (4\nu-3)^2 \pi^2 r^2 \right)^{-1/2} , \\
f_\varphi &= \frac{b_1}{\pi} \frac{E}{(4\nu-3)(\nu+1)} \frac{\cos(\varphi)}{r} \left( (\nu-1) \left( b_1 \sin(\varphi) - (4\nu-3) \pi r \right) \right) \\
&\times \left( b_1^2 \left( (4\nu-3) \sin^2(\varphi) + 4\nu^2 - 4(2\nu-1) \right) \right. \\
&\quad \left. - 2(4\nu-3)(2\nu-1) b_1 \pi r \sin(\varphi) + (4\nu-3)^2 \pi^2 r^2 \right)^{-1/2} , \\
f_z &= \frac{b_1}{\pi} \frac{E\nu}{(4\nu-3)(\nu+1)} \frac{y}{x^2+y^2} .
\end{aligned} \tag{55}$$

We neglect the z-component of this vector field with the assumption of a plane state of stress. The resulting vectors are plotted in fig. 1.2a, the isolines of their amount can be seen in fig. 1.2b.

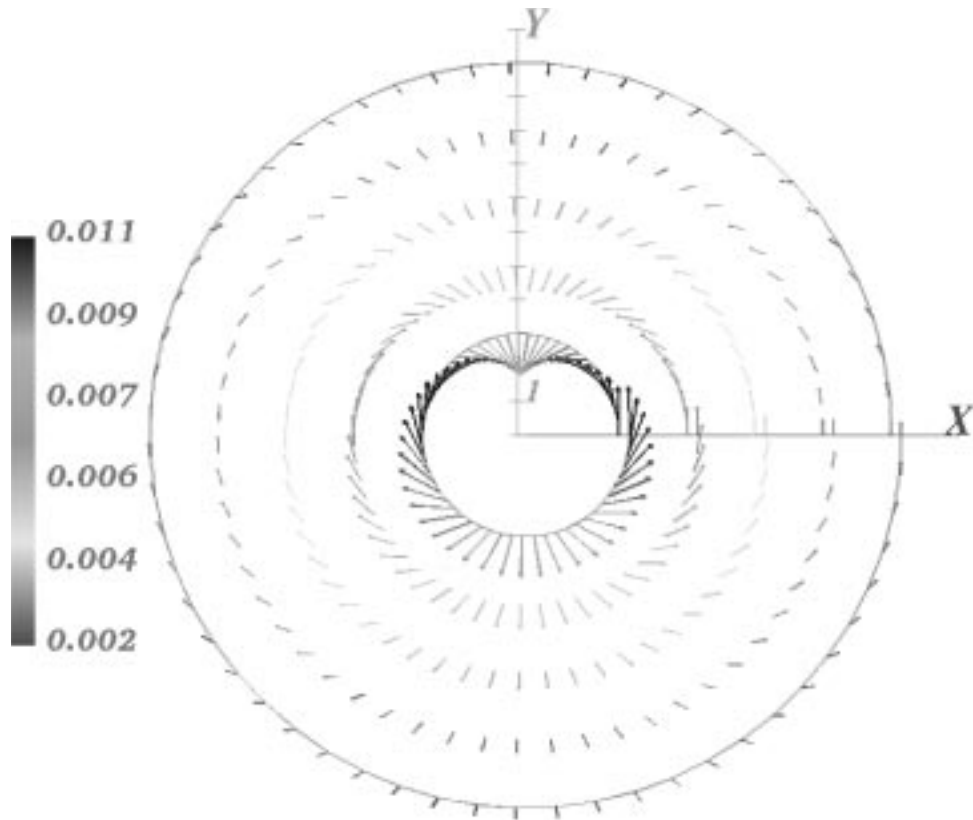


Fig. 1.2a. Stress vector field around an x-edge dislocation in a crystal with  $b_1 = 0.1\pi$  [length]. See also colour plate I

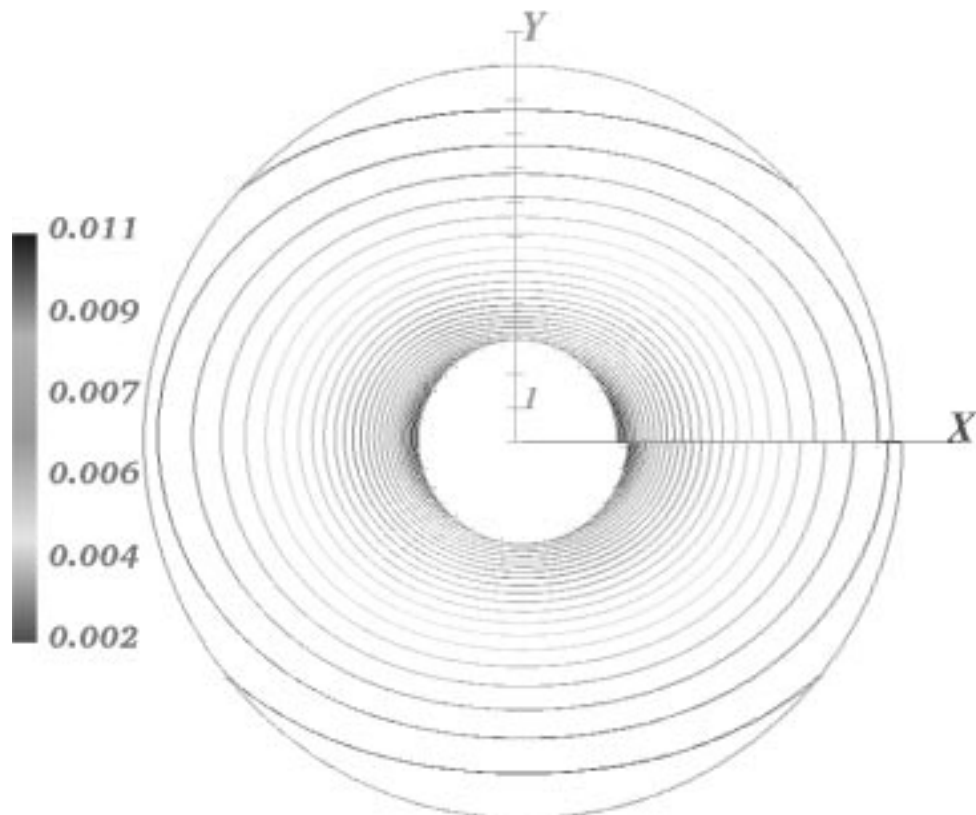


Fig. 1.2b. Isolines of the amount (in units of MPa) of the stress vector field around an x-edge dislocation in a crystal with  $b_1 = 0.1\pi$  [length]

For convenience we examine analytically the amount of the stress vector. We depict the angles  $\varphi = 0$  and  $\varphi = \pi/2$ . The amount calculates for  $\varphi = 0$  to

$$|\vec{f}| \Big|_{(\varphi=0)} = \frac{b_1}{\pi} \frac{E(\nu-1)}{(4\nu-3)(\nu+1)} \frac{1}{r} \quad . \quad (56)$$

This is similar to  $1/r$ . The same for  $\varphi = \pi/2$ , where we get

$$|\vec{f}| \Big|_{(\varphi=\pi/2)} = \frac{b_1}{\pi} \frac{E\nu}{(4\nu-3)(\nu+1)} \frac{1}{r} \quad . \quad (57)$$

The amount of the stress vector field gets singular for very small radii ( $r \rightarrow 0$ ) and vanishes for large outer radii ( $r \rightarrow \infty$ ). The displacement field presented can be interpreted as analogous to a crystal defect.

### 3.1.1 The photo-elasticity method

The photo-elasticity method is well established to examine the stresses in deformed bodies. It works with transparent materials which become optical anisotropic under tension. The object, a crystal plate, e.g., is placed in between crossed polarizer and analyzer. In absence of the doubly refracting plate no light is transmitted by the system.

In the case of plane polarized light, the intensity  $I$  of the transmitted light can be calculated by

$$I = I_0^2 \sin^2\left(\frac{\delta}{2}\right) \sin^2(2\gamma) \quad . \quad (58)$$

Here  $I_0$  is the amplitude of the incident plane polarized light,  $\gamma$  is the angle between the oscillation direction in one of the crossed Nicols and one principal direction. They are related to the slip direction. This is in all the cases considered the x-axis. The phase difference  $\delta$  of the beams when traveling through the crystal of thickness  $t$  is determined by the difference of the principal stresses  $\dot{\sigma}^{11}$  and  $\dot{\sigma}^{22}$  acting in the wave front plane,

$$\delta = \frac{2\pi t O}{\lambda} (\dot{\sigma}^{11} - \dot{\sigma}^{22}) \quad . \quad (59)$$

The incident light has the wavelength  $\lambda$  and the stress-optic coefficient  $O$ . The dimensions of  $O$  are those of the reciprocal of a stress [44]. For more details see R.Bullough [33] and V.I.Nikitenko [35]. The intensity distribution of the transmitted plane polarized light

computes with the Computer Algebra System “Reduce” to

$$\begin{aligned}
I = & -\frac{I_0^2}{(x^2 + y^2)} \sin^2 \left( \frac{b_1}{2\pi(4\nu - 3)} \frac{\mathcal{A}}{(x^2 + y^2)} \right) \\
& \times \left( \left[ \left( \mathcal{B} \sin(\beta)x + \left[ \nu(x^2 + y^2) - x^2 \right] \left[ \mathcal{A} + 2\nu y - y \right] \cos(\beta) \right)^2 \right. \right. \\
& \quad \left. \left. - \mathcal{B}^2 x^2 - \left( \nu(x^2 + y^2) - x^2 \right)^2 \left( \mathcal{A} + 2\nu y - y \right)^2 \right] \right. \\
& \quad \left. \times \left[ \mathcal{B} \sin(\beta)x + \left( \nu(x^2 + y^2) - x^2 \right) \left( \mathcal{A} + 2\nu y - y \right) \cos(\beta) \right]^2 \right) \\
& \times \left( \mathcal{K} y \left( (3x^2 + y^2)\nu^2 - 2\nu^3(x^2 + y^2) - x^2 \right) \right. \\
& \quad \left. - (24x^4 + 17x^2 y^2 + y^4)\nu^2 + 2\nu(8x^2 + 3y^2)x^2 \right. \\
& \quad \left. + 4\nu^3(4x^2 + y^2)(x^2 + y^2) - 4(x^2 + y^2)^2\nu^4 - 4x^4 - x^2 y^2 \right)^{-2} . \tag{60}
\end{aligned}$$

Here we have introduced the function

$$\mathcal{B} := 2\nu(2x^2 + y^2) - 2\nu^2(x^2 + y^2) - \mathcal{A}y - 2x^2 - y^2 \quad , \tag{61}$$

with  $\mathcal{A}$  from eq.(48).

The dimensionless constant  $\nu$ , is defined by

$$\nu := \frac{2\pi t O}{\lambda} \frac{E}{(\nu + 1)} \quad . \tag{62}$$

We normalize for all photo-elastic diagrams,

$$\nu := 1 \quad . \tag{63}$$

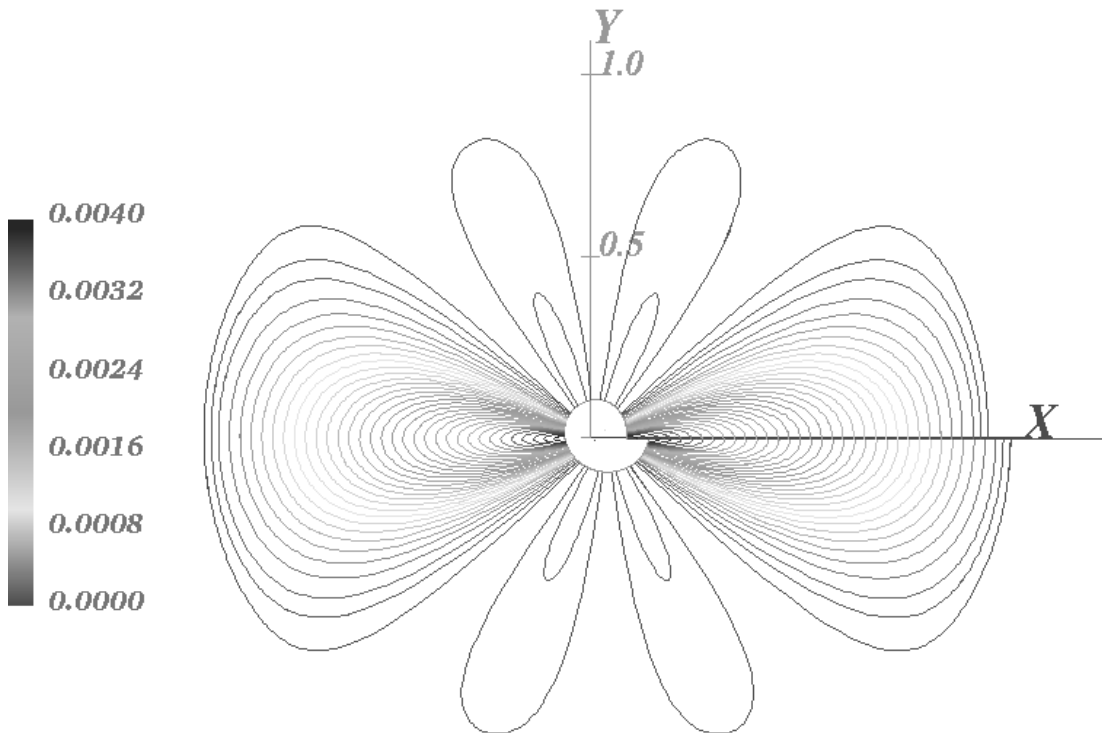


Fig. 1.3a.

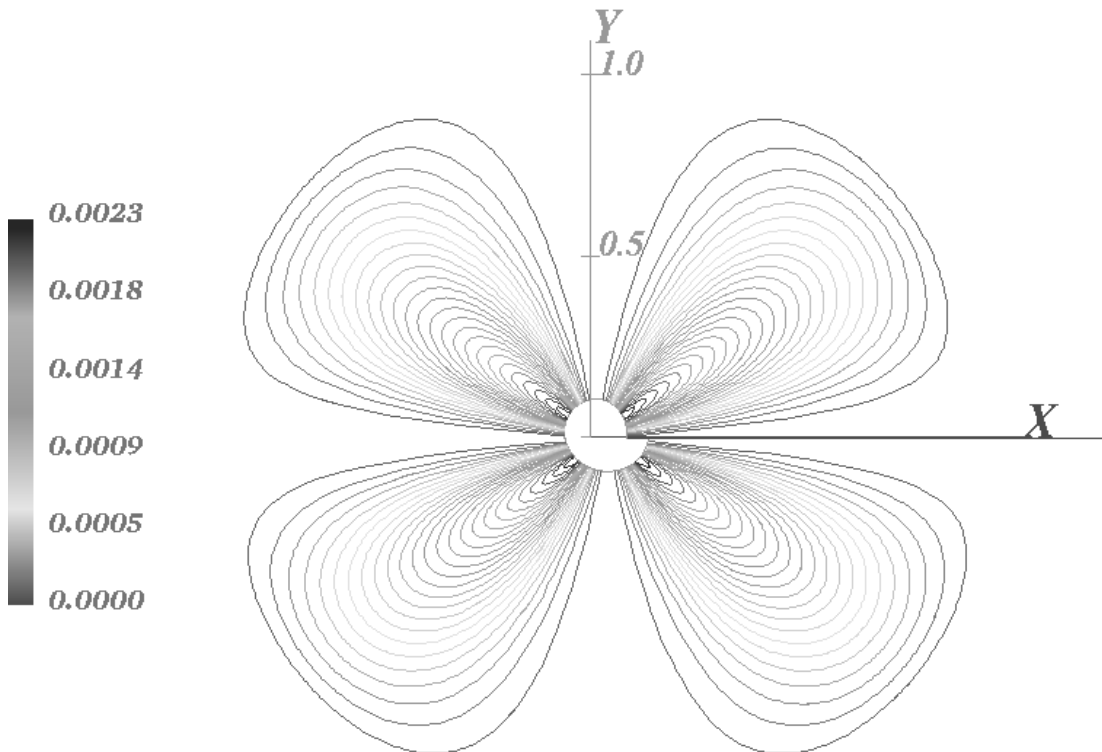


Fig. 1.3b.

**Fig. 1.3.** Intensity distribution of plane polarized light for double refraction fields caused by the stresses around an x-edge dislocation in a crystal (in units of  $I_0^2$ ), for a)  $\beta = 0$ , and b)  $\beta = \pi/4$ . We choose  $b_1 = 0.02\pi$  [length]. See also colour plate II.

The intensity depends on  $\beta$ , the angle between the polarizer and the slip direction. Our intensity distribution contains much more terms as the corresponding approximation given by Bullough [33], but the isolines show an analogous course. Figure 1.3a shows the intensity distribution for  $\beta = 0$  and fig. 1.3b for  $\beta = \pi/4$ . The presented figures are similar to the fringe pattern photos taken by Bond et. al. [34] and by Nikitenko et al. [35].

For circular polarized light the intensity distribution of the transmitted light is given by

$$I = I_0^2 \sin^2\left(\frac{\delta}{2}\right) \quad . \quad (64)$$

This leads in our cases with  $\mathcal{A}$  of eq.(48) to

$$\begin{aligned} I &= I_0^2 \sin^2\left(\frac{b_1}{2\pi(4\nu-3)} \frac{\mathcal{A}}{x^2+y^2}\right) \\ &= I_0^2 \sin^2\left(\frac{b_1}{2\pi(4\nu-3)} \frac{\sqrt{(4\nu^2-8\nu+4)x^2+(4\nu^2-4\nu+1)y^2}}{x^2+y^2}\right) \quad , \end{aligned} \quad (65)$$

and is shown in fig. 1.4.

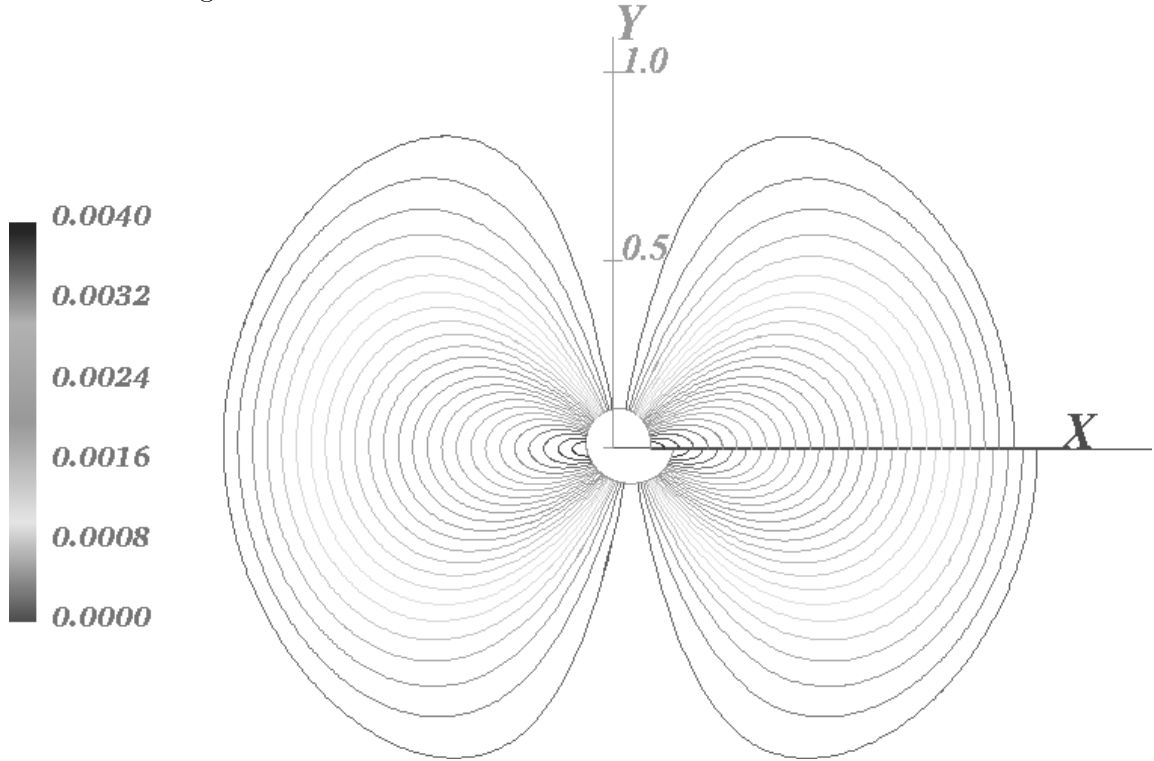


**Fig. 1.4.** Intensity distribution of circular polarized light for double refraction fields due to the stress field around an x-edge dislocation in a crystal (in units of  $I_0^2$ ,  $b_1 = 0.02\pi$  [length])

The isolines of our calculations show again an analogous course as Bullough's [33]. We think it is remarkable that fig. 1.4 is nearly the same as we get for the specific energy

for changing the shape of the origin body,

$$\tilde{U}_F = \frac{b_1^2}{3\pi^2} \frac{E}{(4\nu - 3)^2(\nu + 1)} \frac{(3\nu^2 - 6\nu + 3)x^2 + (4\nu^2 - 4\nu + 1)y^2}{(x^2 + y^2)^2} . \quad (66)$$

Mathematically this can be understood, if we approximate in eq.(65) the sinus-function

$$\sin x \approx \sum_{n=0}^{\infty} \frac{(-1)^n}{(2n+1)!} x^{2n+1} = x - \frac{1}{6}x^3 + \frac{1}{120}x^5 - \dots ,$$

by its argument

$$I \approx I_0^2 \left( \frac{b_1^2}{4\pi^2} \frac{(4\nu^2 - 8\nu + 4)x^2 + (4\nu^2 - 4\nu + 1)y^2}{(x^2 + y^2)^2} \right) . \quad (67)$$

This scalar field is approximately proportional to  $\tilde{U}_F$ . The course of the isolines only differs in a constant factor of  $x^2$  in the numerator.

### 3.2 The x-edge dislocation of a tubular cylinder

The stress vector field of a tubular cylinder has to vanish at the inner radius  $r_1$  and at the outer radius  $r_2$ , providing the stress vector is not orthogonal to the normal vector of the surface. We are looking for an *additional* displacement which leads, together with the *realistic* displacement in a crystal  $\overset{c}{\vec{u}}$  (eq.(41)), to such a stress vector field,

$$\begin{aligned} \overset{t}{\vec{u}} &= \overset{0}{\vec{u}} + \overset{1}{\vec{u}} + \overset{2}{\vec{u}} \\ &= \overset{c}{\vec{u}} + \overset{2}{\vec{u}} . \end{aligned} \quad (68)$$

The stress tensor belonging to  $\overset{c}{\vec{u}}$  is already divergence-free. Hence, the *additional* vector field  $\overset{2}{\vec{u}}$  has to have a divergence-free stress tensor itself, otherwise the addition to  $\overset{c}{\vec{u}}$  would not lead to a state of equilibrium. We could use this time the divergence of the strain tensor  $\epsilon^{im},_m$  of equation (45). We showed in equation (46) that it is as well possible to use the divergence of the strain tensor of the *initial* displacement field. We make the ansatz

$$\overset{2}{u}_i = \overset{2}{w} \mathcal{W} \overset{0}{\epsilon}{}^{im},_m . \quad (69)$$

We find that this displacement fulfills the differential equation (28) if we choose

$$\overset{2}{\mathcal{W}} = 1 . \quad (70)$$

The corresponding stress tensor is in this case divergence-free for every constant  $\overset{2}{w}$  (dimension of [length]<sup>2</sup>). Hence the constant  $\overset{2}{w}$  enables us to fit our solution to the proposed boundary condition. The displacement field of an x-edge dislocation of a tubular cylinder



reads with  $\vec{u}^c$  of eq.(41) , eq.(68), and the ansatz (69) with eq.(70)

$$\begin{aligned} u_x^t &= \frac{b_1}{2\pi} \left( \arctan\left(\frac{y}{x}\right) - \frac{1}{(4\nu-3)} \frac{xy}{(x^2+y^2)} \left(1 - \frac{\overset{2}{w}}{(x^2+y^2)}\right) \right) , \\ u_y^t &= \frac{b_1}{4\pi} \frac{1}{(4\nu-3)} \frac{x^2-y^2}{(x^2+y^2)} \left(1 - \frac{\overset{2}{w}}{(x^2+y^2)}\right) , \\ u_z^t &= 0 . \end{aligned} \quad (71)$$

The integral (29) along the contour-line  $\vec{s}(t)$  of equation (31) has the components

$$\begin{aligned} \oint u_x \frac{\partial s_x}{\partial t} dt &= - \frac{b_1}{6\pi(4\nu-3)} \left( \left(\overset{2}{w}-1\right) \sin^3(t) - 3 \left(t \cos(t) - \sin(t)\right) (4\nu-3) \right) \Big|_0^{2\pi} = b_1 , \\ \oint u_y \frac{\partial s_y}{\partial t} dt &= \frac{b_1}{12\pi(4\nu-3)} \left(\overset{2}{w}-1\right) \left(2 \sin^2(t) - 3\right) \sin(t) \Big|_0^{2\pi} = 0 , \\ \oint u_z \frac{\partial s_z}{\partial t} dt &= 0 . \end{aligned} \quad (72)$$

They are independent of  $\overset{2}{w}$ . The passage around the closed contour  $s(t)$  leads for any constant  $\overset{2}{w}$  to the increment  $b_1$  .

We are going to determine the constant  $\overset{2}{w}$  in retrospect to the stress vector field in cylindrical coordinates. The stress vector field, belonging to  $\vec{u}^c$ , already vanishes for large outer radii  $r_2$ . In the case of a tubular cylinder it should also vanish at the inner radius  $r_1$ . We only found vanishing stress vectors at the entire inner radius, if  $\overset{2}{w}$  is a function of the polar angle  $\varphi$ , but  $\overset{2}{w}$  has to be constant, else the equilibrium conditions are no longer fulfilled. We approximated the stress vector field by relating it to the normal vector field of the origin, not deformed body. This can be done in the linearized theory, which only works for small displacements. Now we were able to determine  $\overset{2}{w}$  as a constant. We get the same result by niliating the  $\sigma^{rr}$ -component of the stress tensor in cylindrical coordinates. Leibfried and Lücke [30] choose this way for their approximation. The stress tensor in cylindrical coordinates is given by

$$\begin{aligned} \sigma^{rr} &= - \frac{b_1}{2\pi} \frac{E}{(4\nu-3)(\nu+1)} \left(\overset{2}{w}-2\nu r^2\right) \frac{\sin(\varphi)}{r^3} , \\ \sigma^{r\varphi} &= \frac{b_1}{2\pi} \frac{E}{(\nu+1)} \left((4\nu-3)\overset{2}{w} + 2(\nu-1)r^2\right) \frac{\cos(\varphi)}{r^3} , \\ \sigma^{rz} &= 0 , \\ \sigma^{\varphi\varphi} &= \frac{b_1}{2\pi} \frac{E}{(\nu+1)} \left((4\nu-3)\overset{2}{w} - 2(\nu-1)r^2\right) \frac{\sin(\varphi)}{r^3} , \\ \sigma^{\varphi z} &= 0 , \\ \sigma^{zz} &= \frac{b_1}{\pi} \frac{E\nu}{(4\nu-3)(\nu+1)} \frac{\sin(\varphi)}{r} . \end{aligned} \quad (73)$$

It is not possible to choose  $\overset{2}{w}$  the way that both,  $\sigma^{rr}$  and  $\sigma^{r\varphi}$ , vanish. We take

$$\overset{2}{w} = 2\nu r_1^2 , \quad (74)$$

so  $\sigma^{rr}$  becomes zero for  $r = r_1$ . This constant leads to the following approximation for a *realistic* displacement field of a tubular cylinder

$$\begin{aligned} u_x^t &= \frac{b_1}{2\pi} \left( \arctan\left(\frac{y}{x}\right) - \frac{1}{(4\nu - 3)} \frac{xy}{(x^2 + y^2)} \left(1 - \frac{2\nu r_1^2}{(x^2 + y^2)}\right) \right) , \\ u_y^t &= \frac{b_1}{2\pi} \frac{1}{2(4\nu - 3)} \frac{x^2 - y^2}{(x^2 + y^2)} \left(1 - \frac{2\nu r_1^2}{(x^2 + y^2)}\right) , \\ u_z^t &= 0 . \end{aligned} \tag{75}$$

The strain tensor

$$\begin{aligned} \epsilon_{xx} &= -\frac{b_1}{\pi} \frac{y}{(4\nu - 3)} \frac{\nu \left( r_1^2 (3x^2 - y^2) + 2(x^2 + y^2)^2 \right) - 2x^4 - 3x^2y^2 - y^4}{(x^2 + y^2)^3} , \\ \epsilon_{xy} &= \frac{b_1}{\pi} \frac{x}{(4\nu - 3)} \frac{\nu \left( r_1^2 (x^2 - 3y^2) + (x^2 + y^2)^2 \right) - x^4 - x^2y^2}{(x^2 + y^2)^3} , \\ \epsilon_{xz} &= 0 , \\ \epsilon_{yy} &= \frac{b_1}{\pi} \frac{y}{(4\nu - 3)} \frac{r_1^2 \nu (3x^2 - y^2) - x^4 - x^2y^2}{(x^2 + y^2)^3} , \\ \epsilon_{yz} &= 0 , \\ \epsilon_{zz} &= 0 , \end{aligned} \tag{76}$$

has the trace

$$\epsilon_k^k = \frac{b_1}{\pi} \frac{(2\nu - 1)}{(4\nu - 3)} \frac{y}{(x^2 + y^2)} . \tag{77}$$

The divergence of the strain tensor is the same as in eq.(45) for a crystal.

The stress tensor of the x-edge dislocation of a tubular cylinder

$$\begin{aligned}
\sigma^{xx} &= -\frac{b_1}{\pi} \frac{E}{(4\nu-3)(\nu+1)} \frac{y}{(x^2+y^2)^3} \\
&\quad \times \left( \nu \left( r_1^2(3x^2-y^2) + (x^2+y^2)^2 \right) - 2x^4 - 3x^2y^2 - y^4 \right) , \\
\sigma^{xy} &= \frac{b_1}{\pi} \frac{E}{(4\nu-3)(\nu+1)} \frac{x}{(x^2+y^2)^3} \\
&\quad \times \left( \nu \left( r_1^2(x^2-3y^2) + (x^2+y^2)^2 \right) - x^4 - x^2y^2 \right) , \\
\sigma^{xz} &= 0 , \\
\sigma^{yy} &= \frac{b_1}{\pi} \frac{E}{(4\nu-3)(\nu+1)} \frac{y}{(x^2+y^2)^3} \\
&\quad \times \left( \nu \left( r_1^2(3x^2-y^2) + (x^2+y^2)^2 \right) - x^4 - x^2y^2 \right) , \\
\sigma^{yz} &= 0 , \\
\sigma^{zz} &= \frac{b_1}{\pi} \frac{E\nu}{(4\nu-3)(\nu+1)} \frac{y}{(x^2+y^2)} , \tag{78}
\end{aligned}$$

has the same trace as before (eq.(50)).

The stress tensor is divergence-free. The x-component of the divergence of the stress tensor vanishes according to

$$\begin{aligned}
\sigma^{x1}_{,1} = -\sigma^{x2}_{,2} &= \frac{b_1}{\pi} \frac{2E}{(4\nu-3)(\nu+1)} \frac{xy}{(x^2+y^2)^4} \\
&\quad \times \left( \nu \left( 6r_1^2(x^2-y^2) + (x^2+y^2)^2 \right) - 2(x^4+x^2y^2) \right) , \tag{79}
\end{aligned}$$

and the y-component according to

$$\begin{aligned}
\sigma^{y1}_{,1} = -\sigma^{y2}_{,2} &= -\frac{b_1}{\pi} \frac{E}{(4\nu-3)(\nu+1)} \frac{1}{(x^2+y^2)^4} \\
&\quad \times \left( \nu \left( 3r_1^2(x^4-6x^2y^2+y^4) + x^6 + x^4y^2 - x^2y^4 - y^6 \right) \right. \\
&\quad \left. - x^6 + 2x^4y^2 + 3x^2y^4 \right) . \tag{80}
\end{aligned}$$

The eigenvalues of the stress tensor are

$$\begin{aligned}
\dot{\sigma}^{11} &= \frac{b_1}{2\pi} \frac{E}{(4\nu-3)(\nu+1)} \frac{1}{(x^2+y^2)^2} \left( (x^2+y^2)y - \mathcal{C} \right) , \\
\dot{\sigma}^{22} &= \frac{b_1}{2\pi} \frac{E}{(4\nu-3)(\nu+1)} \frac{1}{(x^2+y^2)^2} \left( (x^2+y^2)y + \mathcal{C} \right) , \\
\dot{\sigma}^{33} &= \frac{b_1}{2\pi} \frac{2E\nu}{(4\nu-3)(\nu+1)} \frac{y}{(x^2+y^2)} , \tag{81}
\end{aligned}$$

with the function

$$\begin{aligned} \mathcal{C} := & \left( -4\nu \left( r_1^2(2x^2 - y^2) + 2x^4 + 3x^2y^2 + y^4 \right) (x^2 + y^2) \right. \\ & + 4x^6 + 9x^4y^2 + 6x^2y^4 + y^6 \\ & \left. + 4\nu^2(x^2 + y^2) \left( r_1^2 + 2r_1y + x^2 + y^2 \right) \left( r_1^2 - 2r_1y + x^2 + y^2 \right) \right)^{1/2}. \end{aligned} \quad (82)$$

In cylindrical coordinates the stress tensor reads

$$\begin{aligned} \sigma^{rr} &= -\frac{b_1}{\pi} \frac{E\nu}{(4\nu - 3)(\nu + 1)} \left( r_1^2 - r^2 \right) \frac{\sin(\varphi)}{r^3}, \\ \sigma^{r\varphi} &= \frac{b_1}{\pi} \frac{E}{(4\nu - 3)(\nu + 1)} \left( \nu r_1^2 + (\nu - 1)r^2 \right) \frac{\cos(\varphi)}{r^3}, \\ \sigma^{rz} &= 0, \\ \sigma^{\varphi\varphi} &= \frac{b_1}{\pi} \frac{E}{(4\nu - 3)(\nu + 1)} \left( \nu r_1^2 - (\nu - 1)r^2 \right) \frac{\sin(\varphi)}{r^3}, \\ \sigma^{\varphi z} &= 0, \\ \sigma^{zz} &= \frac{b_1}{\pi} \frac{E\nu}{(4\nu - 3)(\nu + 1)} \frac{\sin(\varphi)}{r}. \end{aligned} \quad (83)$$

We found the following stress vector field, belonging to the interior normal vector field of the cylinder and the normal vector field in the direction of the z-axis

$$\begin{aligned}
f_r &= -\frac{b_1}{\pi} \frac{E}{(4\nu - 3)(\nu + 1)} \frac{1}{r^3} \\
&\times \left( (2\nu r_1^2 - r^2)(3\nu - 2) \sin^2(\varphi) b_1 r^2 - \nu(4\nu - 3)(r_1^2 - r^2) \sin(\varphi) \pi r^3 \right. \\
&\quad \left. - b_1(\nu r_1^2 + 2(\nu - 1)2r^2)(\nu r_1^2 + \nu - 1)r^2 \right) \\
&\times \left( b_1^2 \left( - (2\nu r_1^2 - r^2)(4\nu - 3) \sin^2(\varphi) r^2 + \nu^2(r_1^2 - 2r^2)^2 - 4\nu(r_1^2 + 2r^2)r^2 + 4r^4 \right) \right. \\
&\quad \left. + 2b_1 \pi r^3 (4\nu - 3) \left( \nu r_1^2 - (2\nu - 1)r^2 \right) \sin(\varphi) + (4\nu - 3)^2 \pi^2 r^6 \right)^{-1/2}, \\
f_\varphi &= \frac{b_1}{\pi} \frac{E}{(4\nu - 3)(\nu + 1)} \frac{\cos(\varphi)}{r} \\
&\times \left( - \left( - 2\nu^2 r_1^2 + \nu(r_1^2 - (\nu - 1)r^2) \right) b_1 \sin(\varphi) \right. \\
&\quad \left. - \nu(4\nu - 3) \pi r r_1^2 - (\nu - 1)(4\nu - 3) \pi r^3 \right) \\
&\times \left( b_1^2 \left( - (2\nu r_1^2 - r^2)(4\nu - 3) \sin^2(\varphi) r^2 + \nu^2(r_1^2 - 2r^2)^2 - 4\nu(r_1^2 + 2r^2)r^2 + 4r^4 \right) \right. \\
&\quad \left. + 2b_1 \pi r^3 (4\nu - 3) \left( \nu r_1^2 - (2\nu - 1)r^2 \right) \sin(\varphi) + (4\nu - 3)^2 \pi^2 r^6 \right)^{-1/2}, \\
f_z &= \frac{b_1}{\pi} \frac{E\nu}{(4\nu - 3)(\nu + 1)} \frac{y}{x^2 + y^2}. \tag{84}
\end{aligned}$$

We neglect again the z-component. The resulting stress vector field is plotted in fig. 1.5a, the amount in fig 1.5b (see also fig. 2.5. at page 46). We choose in all plots of the tubular cylinders for the inner radius  $r_1 = 3$  [length], for the outer radius  $r_2 = 11$  [length], and  $b_1 = 0.1\pi$ [length]. The vector field above turns for small inner radii ( $r_1 \rightarrow 0$ ) into the stress vector field analogous to a crystal (eq. (55)).

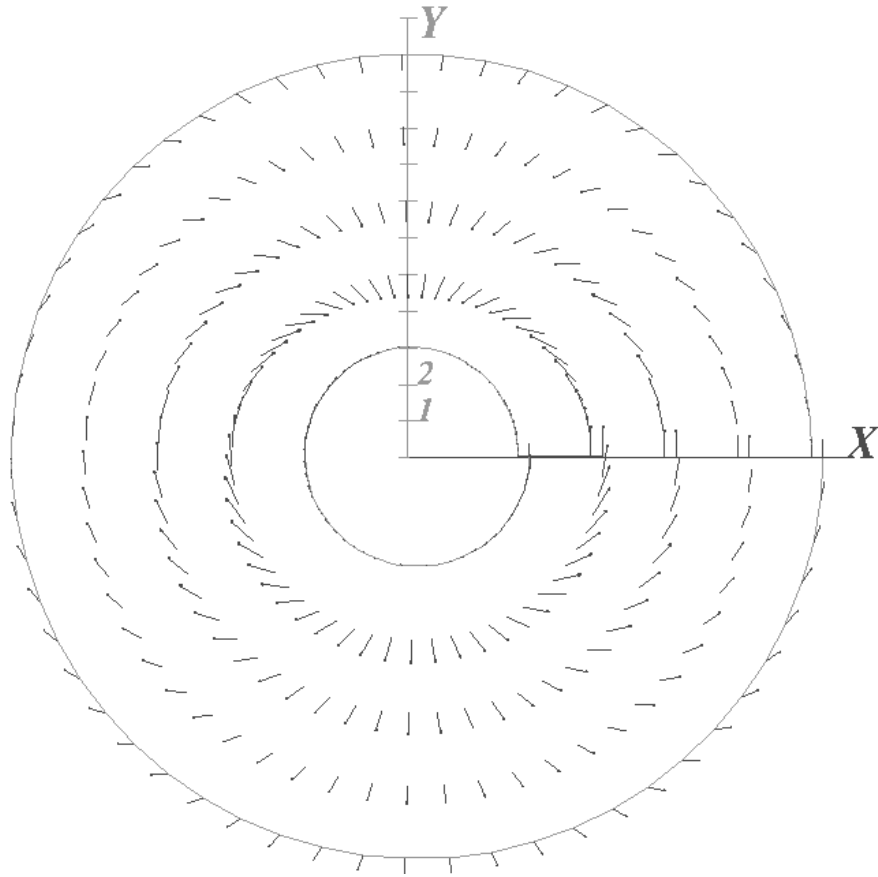


Fig. 1.5a. Stress vector field of the x-edge dislocation of a tubular cylinder

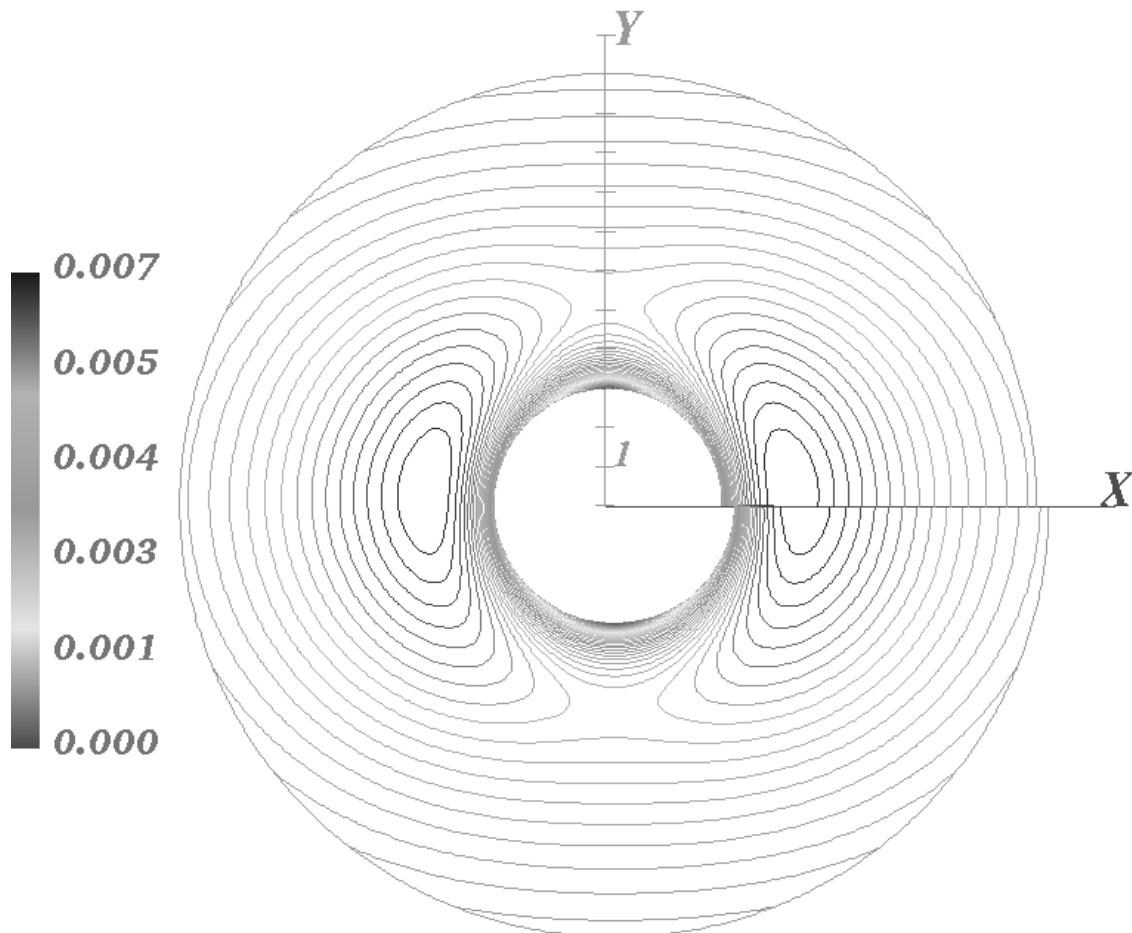


Fig. 1.5b. Amount of the stress vector field of the x-edge dislocation (in units of MPa). See also colour plate III

To get more information about the stress vector field of eq.(84), we examine the amount, shown in fig. 1.5b. We depict the angles  $\varphi = 0$  , and  $\varphi = \pi/2$ .

For  $\varphi = 0$  we obtain

$$|\vec{f}| \Big|_{(\varphi=0)} = \frac{b_1}{\pi} \frac{E}{(4\nu - 3)(\nu + 1)} \frac{\nu(r_1^2 + r^2) - r^2}{r^3} \quad , \quad (85)$$

which is similar to  $1/r$ . For  $\varphi = 0$  the amount reaches its maximum at  $r = \sqrt{3\nu/(1 - \nu)}r_1$ , since ( $0 < \nu < 0.5$ ). At the inner radius  $r_1$  it reads

$$|\vec{f}| \Big|_{(r=r_1)(\varphi=0)} = \frac{b_1}{\pi} \frac{(2\nu - 1)E}{(4\nu - 3)(\nu + 1)} \frac{1}{r_1} \quad . \quad (86)$$

This is proportional to  $1/r_1$ .

If  $\varphi = \pi/2$ , the amount turns to

$$|\vec{f}| \Big|_{(\varphi=\pi/2)} = \frac{b_1}{\pi} \frac{E\nu}{(4\nu - 3)(\nu + 1)} \frac{(r_1^2 - r^2)}{r^3} \quad . \quad (87)$$

This is again similar to  $1/r$ . For  $\varphi = \pi/2$  the amount of the stress vector field reaches its maximum at  $r = \sqrt{3}r_1$  and vanishes at the inner radius  $r_1$ ,

$$|\vec{f}| \Big|_{(r=r_1)(\varphi=\pi/2)} = 0 \quad . \quad (88)$$

Figure 1.5a shows that the stress vector field is at the inner radius more or less orthogonal to the interior normal vector field. The scalar product of the stress vector and the interior normal vector reads at the inner radius and for  $\varphi = 0$

$$(\vec{f} \cdot \vec{n}) \Big|_{(r=r_1)(\varphi=0)} = -b_1^2 \frac{E(2\nu - 1)(3\nu - 2)}{(\nu + 1)} \frac{2}{(4\nu - 3)^2 \pi^2 r_1^2 + (3\nu - 2)^2 b_1^2} \quad . \quad (89)$$

This is similar to  $1/r_1^2$ . The stress vector field at the inner radius  $r_1$ , and at  $\varphi = 0$  is proportional to  $1/r_1$ , but for small inner radii it is approximately orthogonal to the interior normal vector. If  $\varphi = \pi/2$  it vanishes exactly at  $r_1$ . The amount of the stress vectors vanishes at the outer radius with  $1/r_2$ . The displacement field presented (eq.(75)) can be interpreted as analogous to a tubular cylinder.

The intensity distribution of the transmitted plane polarized light computes to (see section 3.1.1)

$$I = 4 I_0^2 \sin^2 \left( \frac{b_1}{2\pi(4\nu - 3)} \frac{\mathcal{C}}{(x^2 + y^2)^2} \right) \times \left( \frac{\mathcal{D} \sin(\beta) + \mathcal{E} \cos(\beta)x}{\mathcal{D}^2 + \mathcal{E}^2 x^2} - 1 \right) \frac{\mathcal{D} \sin(\beta) + \mathcal{E} \cos(\beta)x}{\mathcal{D}^2 + \mathcal{E}^2 x^2} \quad . \quad (90)$$

The fringe patterns can be seen in fig. 1.6a for  $\beta = 0$  and in fig. 1.6b for  $\beta = \pi/4$  (see also fig. 2.6 at page 48).

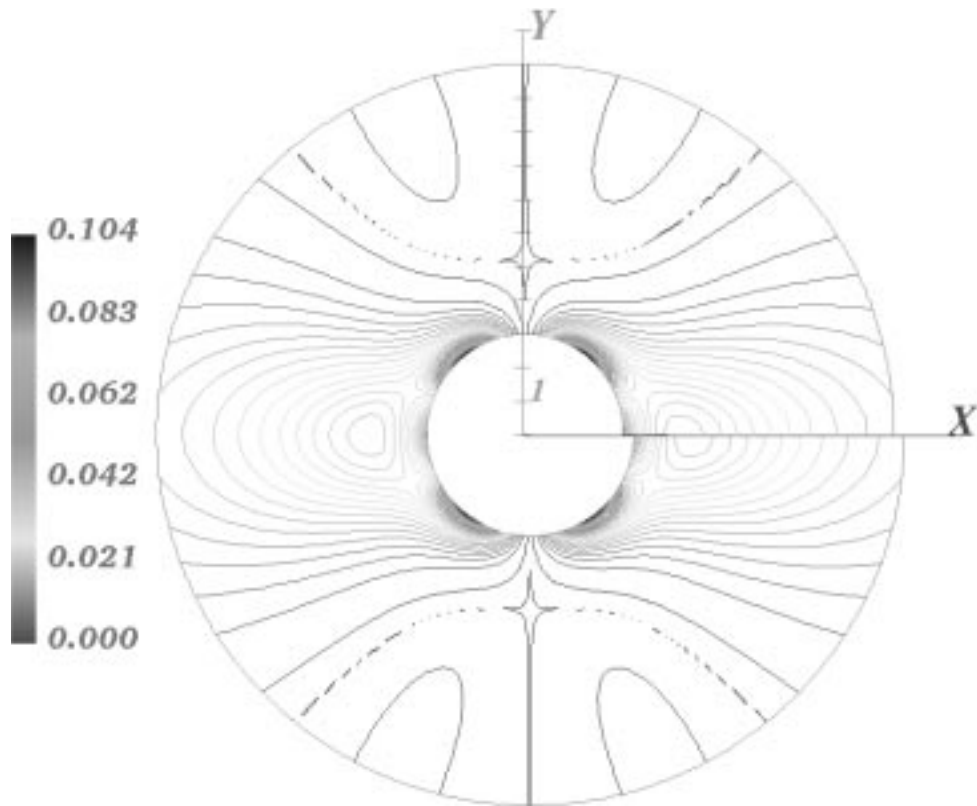
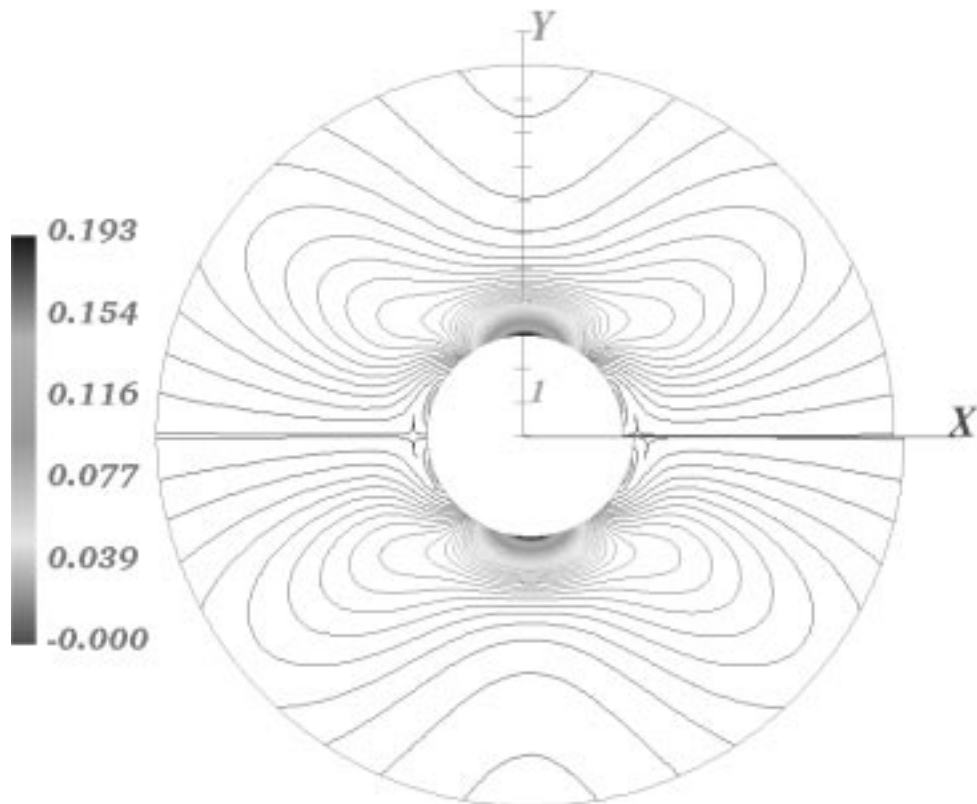


Fig. 1.6a.



**Fig. 1.6.** Intensity distribution  $[10^{-3}I_0^2]$  of plane polarized light for double refraction fields in a tubular cylinder due to the stress field caused by an x-edge dislocation with  $b_1 = 0.1\pi$  [length]. The angle between the polarizer and the slip direction is a)  $\beta = 0$ , b)  $\beta = \pi/4$ . See also colour plate IV.



To keep the overview, we introduced the following functions:

$$\begin{aligned} \mathcal{D} := & \nu(x^2 + y^2) \left( (4x^4 - x^2y^2 - y^4)r_1^2 + 4x^6 + 6x^4y^2 + 2x^2y^4 \right) \\ & - 2\nu^2(x^2 + y^2) \left( (2x^4 - 3x^2y^2 - y^4)r_1^2 + (x^2 + y^2)r_1^4 + x^6 + 2x^4y^2 + x^2y^4 \right) \\ & + \left( (3x^2 + y^2)\nu r_1^2 - x^4 - x^2y^2 \right) \mathcal{C}y - 2x^8 - 5x^6y^2 - 4x^4y^4 - x^2y^6 \end{aligned} \quad (91)$$

$$\begin{aligned} \mathcal{E} := & \left( 2\nu(x^2 + y^2)y + \mathcal{C} - x^2y - y^3 \right) \\ & \times \left( \left( (x^2 - 3y^2)r_1^2 + x^4 + 2x^2y^2 + y^4 \right) \nu - x^4 - x^2y^2 \right) . \end{aligned} \quad (92)$$

For circular polarized light we get

$$\begin{aligned} I = & I_0^2 \sin^2 \left( \frac{b_1}{2\pi(4\nu - 3)} \frac{\mathcal{C}}{(x^2 + y^2)^2} \right) \\ = & I_0^2 \sin^2 \left( \frac{b_1}{2\pi(4\nu - 3)} \frac{1}{(x^2 + y^2)^2} \right. \\ & \times \left[ 4\nu^2 \left( (r_1^4x^2 + 2r_1^2x^4 + x^6) + 3(x^4y^2 + x^2y^4) + (r_1^4y^2 - 2r_1^2y^4 + y^6) \right) \right. \\ & + 4\nu \left( (-2r_1^2x^4 - 2x^6) + (-r_1^2x^2y^2 - 5x^4y^2 - 4x^2y^4) + (r_1^2y^4 - y^6) \right) \\ & \left. \left. + 4x^6 + 9x^4y^2 + 6x^2y^4 + y^6 \right]^{1/2} \right) . \end{aligned} \quad (93)$$

This intensity distribution is plotted in fig. 1.7. It is for  $r_1 = 0$  (crystal) identical with the intensity distribution of circular polarized light given in eq.(65).

The specific energy for changing the shape of the origin body

$$\begin{aligned} \tilde{U}_F = & \frac{b_1^2}{\pi^2} \frac{E}{(4\nu - 3)^2(\nu + 1)} \frac{1}{3(x^2 + y^2)^2} \\ & \times \left( \nu^2 \left( 3(r_1^4x^2 + 2r_1^2x^4 + x^6) + 10x^4y^2 + 11x^2y^4 + (3r_1^4y^2 - 6r_1^2y^4 + 4y^6) \right) \right. \\ & - \nu \left( (-6r_1^2x^4 - 6x^6) + (-3r_1^2x^2y^2 - 16x^4y^2 - 14x^2y^4) + (3r_1^2y^4 - 4y^6) \right) \\ & \left. + 3x^6 + 7x^4y^2 + 5x^2y^4 + y^6 \right) , \end{aligned} \quad (94)$$

shows again a similar course as the isolines of the fringe pattern for circular polarized light appearing in eq.(93). For  $y = 0$  both are zero at  $x = \pm\sqrt{\nu/(1-\nu)}r_1$  (outside the tubular cylinder) and reach their maximum at  $x = \pm\sqrt{3\nu/(1-\nu)}r_1$ . The amount of the stress vector field (85) is along the x-axis at the same places maximal. The isolines of the amount of the stress vector field follows approximately a similar course as the specific energy, but the intensity distribution is different. The specific energy for changing the shape of the

origin body is maximal where the amount of the stress vector has its minimum.

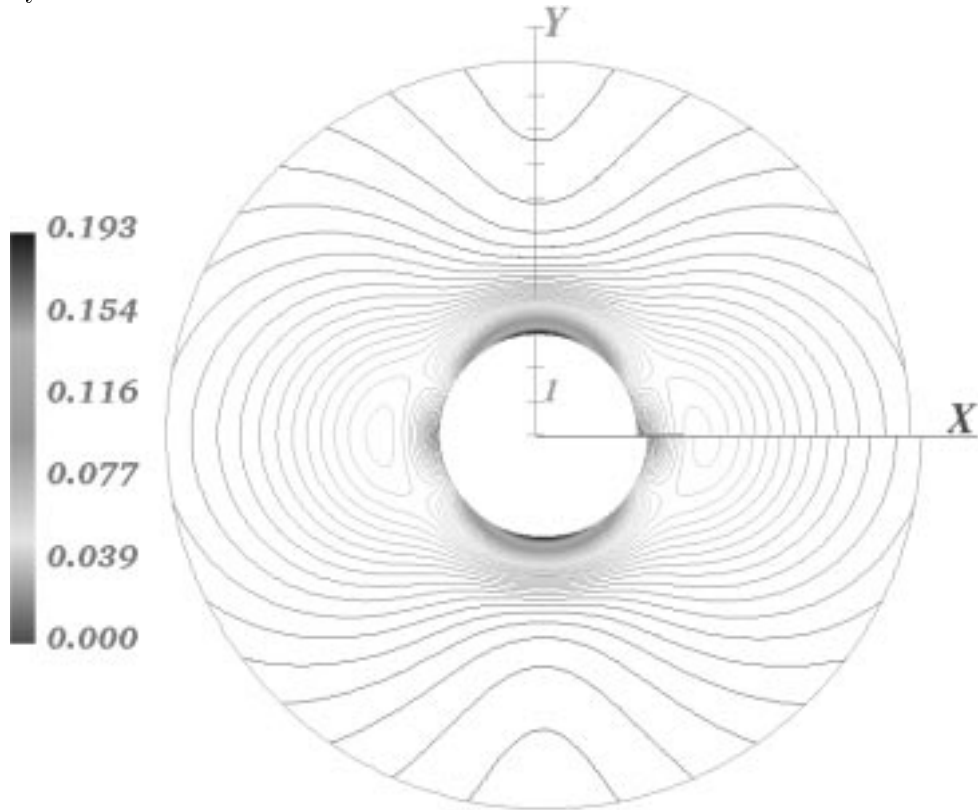


**Fig. 1.7.** Intensity distribution of circular polarized light for double refraction fields in a tubular cylinder (in units of  $10^{-3} I_0^2$ ) due to the stress field caused by an x-edge dislocation with  $b_1 = 0.1\pi$

## 4 The y-edge dislocation

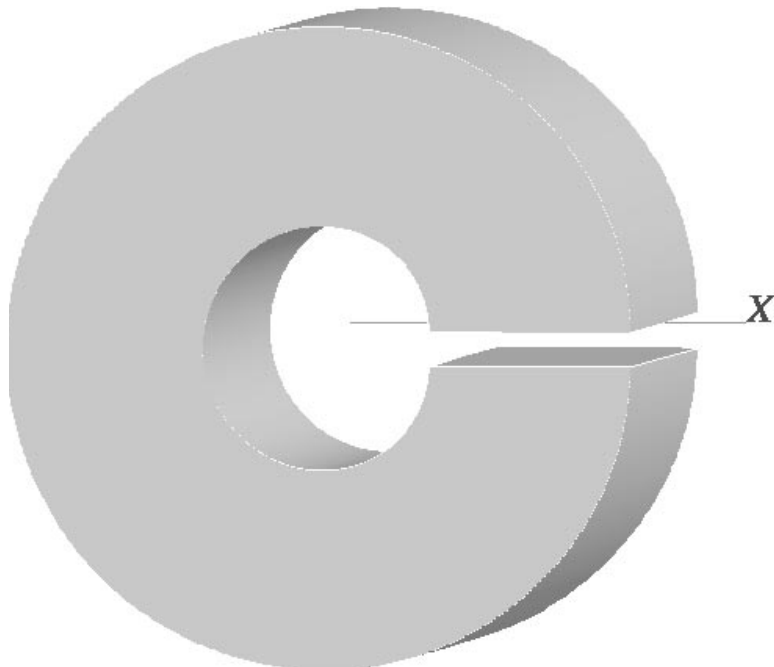


**Fig. 2.1:** The y-edge dislocation

The y-edge dislocation is similar to the x-edge dislocation. We get all expressions the same way as before. The calculated images coincides with them of the x-edge dislocation, rotated about  $\pi/2$  around the z-axis. The Burger vector  $\vec{b}$  has here only a y-component,

$$\vec{b} = (0, b_2, 0) \quad . \quad (95)$$

The initial displacement field, which characterizes the y-edge dislocation is given by

$$\begin{aligned} u_x^0 &= 0 \quad , \\ u_y^0 &= \frac{b_2}{2\pi} \arctan\left(\frac{y}{x}\right) \quad , \\ u_z^0 &= 0 \quad . \end{aligned} \quad (96)$$

It is shown in fig. 2.1.

The integral (29) along the contour-line  $s(t)$  of eq. (31) has the components

$$\begin{aligned} \oint u_x \frac{\partial s_x}{\partial t} dt &= 0 \quad , \\ \oint u_y \frac{\partial s_y}{\partial t} dt &= \frac{b_2}{2\pi} \left( t \sin(t) + \cos(t) \right) \Big|_{-\pi/2}^{3\pi/2} = b_2 \quad , \\ \oint u_z \frac{\partial s_z}{\partial t} dt &= 0 \quad . \end{aligned} \quad (97)$$

The strain tensor of this displacement field (96) calculates to

$$\begin{aligned}
\overset{0}{\boldsymbol{\varepsilon}}_{xx} &= 0 \quad , \\
\overset{0}{\boldsymbol{\varepsilon}}_{xy} &= -\frac{b_2}{4\pi} \frac{y}{(x^2 + y^2)} \quad , \\
\overset{0}{\boldsymbol{\varepsilon}}_{xz} &= 0 \quad , \\
\overset{0}{\boldsymbol{\varepsilon}}_{yy} &= \frac{b_2}{2\pi} \frac{x}{(x^2 + y^2)} \quad , \\
\overset{0}{\boldsymbol{\varepsilon}}_{yz} &= 0 \quad , \\
\overset{0}{\boldsymbol{\varepsilon}}_{zz} &= 0 \quad .
\end{aligned} \tag{98}$$

As the divergence vector field of the strain tensor we have

$$\begin{aligned}
\overset{0}{\boldsymbol{\varepsilon}}_{xj}{}^{,j} &= -\frac{b_2}{4\pi} \frac{(x^2 - y^2)}{(x^2 + y^2)^2} \quad , \\
\overset{0}{\boldsymbol{\varepsilon}}_{yj}{}^{,j} &= -\frac{b_2}{2\pi} \frac{xy}{(x^2 + y^2)^2} \quad , \\
\overset{0}{\boldsymbol{\varepsilon}}_{zj}{}^{,j} &= 0 \quad .
\end{aligned} \tag{99}$$

The divergence vector fields of the stress tensor again turns out to

$$\overset{0}{\boldsymbol{\sigma}}{}^{ij}{}_{,j} = \frac{E}{(1 + \nu)(1 - 2\nu)} \overset{0}{\boldsymbol{\varepsilon}}{}^{ij}{}^{,j} \quad . \tag{100}$$

The displacement field (96) has no divergence-free stress tensor. It needs to be extended by an additional displacement field  $\overset{1}{\vec{u}}$ . This can be calculated with our ansatz (21). We find, that the partial differential equation (28) is solved by the same function

$$\overset{1}{\mathcal{W}} = x^2 + y^2 \quad , \tag{37}$$

and the same constant

$$\overset{1}{w} = \frac{-1}{4\nu - 3} \quad , \tag{38}$$

as in the case of the x-edge dislocation. As the additional displacement field we find

$$\begin{aligned}
\overset{1}{u}_x &= \frac{b_2}{4\pi} \frac{1}{(4\nu - 3)} \frac{(x^2 - y^2)}{(x^2 + y^2)} \quad , \\
\overset{1}{u}_y &= \frac{b_2}{2\pi} \frac{1}{(4\nu - 3)} \frac{xy}{(x^2 + y^2)} \quad , \\
\overset{1}{u}_z &= 0 \quad .
\end{aligned} \tag{101}$$

Its addition to the initial displacement (96) leads to a divergence-free stress tensor. As shown in the next section, the calculated displacement field fulfills already the boundary conditions of a crystal.

## 4.1 The y-edge dislocation in a crystal

We take the initial displacement of the y-edge dislocation  $\vec{u}^0$  eq.(96) and add the calculated additional displacement field  $\vec{u}^1$  eq.(101). As result we get the realistic displacement vector field, which describes the y-dislocation in a crystal

$$\vec{u}^c = \vec{u}^0 + \vec{u}^1 \quad , \quad (102)$$

with

$$\begin{aligned} u_x^c &= \frac{b_2}{4\pi} \frac{1}{(4\nu - 3)} \frac{(x^2 - y^2)}{(x^2 + y^2)} \quad , \\ u_y^c &= \frac{b_2}{2\pi} \left( \arctan\left(\frac{y}{x}\right) + \frac{1}{(4\nu - 3)} \frac{xy}{(x^2 + y^2)} \right) \quad , \\ u_z^c &= 0 \quad . \end{aligned} \quad (103)$$

As shown later on, the belonging stress vector (117) vanishes for large outer radii and gets singular at the center of the cylinder.

The integral (29) along the contour-line  $s(t)$  of eq. (31) has the components

$$\begin{aligned} \oint u_x \frac{\partial s_x}{\partial t} dt &= \frac{-b_2}{12\pi(4\nu - 3)} \left( (2 \sin^2(t) + 1) \cos(t) - 1 \right) \Big|_{-\pi/2}^{3\pi/2} = 0 \quad , \\ \oint u_y \frac{\partial s_y}{\partial t} dt &= \frac{b_2}{6\pi(4\nu - 3)} \left( 3(4\nu - 3)t \sin(t) + (12\nu - 10 + \sin^2(t)) \cos(t) + 1 \right) \Big|_{-\pi/2}^{3\pi/2} \\ &= b_2 \quad , \\ \oint u_z \frac{\partial s_z}{\partial t} dt &= 0 \quad . \end{aligned} \quad (104)$$

The strain tensor of this displacement field calculates to

$$\begin{aligned} \epsilon_{xx} &= \frac{b_2}{\pi} \frac{1}{(4\nu - 3)} \frac{xy^2}{(x^2 + y^2)^2} \quad , \\ \epsilon_{xy} &= -\frac{b_2}{\pi} \frac{1}{(4\nu - 3)} \frac{y(\nu(x^2 + y^2) - y^2)}{(x^2 + y^2)^2} \quad , \\ \epsilon_{xz} &= 0 \quad , \\ \epsilon_{yy} &= \frac{b_2}{\pi} \frac{1}{(4\nu - 3)} \frac{x(2\nu(x^2 + y^2) - x^2 - 2y^2)}{(x^2 + y^2)^2} \quad , \\ \epsilon_{yz} &= 0 \quad , \\ \epsilon_{zz} &= 0 \quad , \end{aligned} \quad (105)$$

with the trace

$$\epsilon_k^k = \frac{b_2}{\pi} \frac{2\nu - 1}{(4\nu - 3)} \frac{x}{x^2 + y^2} \quad . \quad (106)$$

Its divergence is given by

$$\begin{aligned}\boldsymbol{\varepsilon}_{xj}{}^{,j} &= -\frac{b_2}{\pi} \frac{\nu}{(4\nu-3)} \frac{(x^2-y^2)}{(x^2+y^2)^2} \quad , \\ \boldsymbol{\varepsilon}_{yj}{}^{,j} &= \frac{b_2}{\pi} \frac{2\nu}{(4\nu-3)} \frac{xy}{(x^2+y^2)^2} \quad , \\ \boldsymbol{\varepsilon}_{zj}{}^{,j} &= 0 \quad .\end{aligned}\tag{107}$$

We find again the proportionality relation with the divergence of the strain tensor of the initial displacement field:

$$\boldsymbol{\varepsilon}_{xj}{}^{,j} = \frac{4\nu}{(4\nu-3)} \mathbf{0}_{xj}{}^{,j} \quad .\tag{108}$$

The eigenvalues of the strain tensor are

$$\begin{aligned}\dot{\varepsilon}_{11} &= \frac{b_2}{2\pi} \frac{1}{(4\nu-3)} \frac{\mathcal{G} + (2\nu-1)x}{(x^2+y^2)} \quad , \\ \dot{\varepsilon}_{22} &= -\frac{b_2}{2\pi} \frac{1}{(4\nu-3)} \frac{\mathcal{G} - (2\nu-1)x}{(x^2+y^2)} \quad , \\ \dot{\varepsilon}_{33} &= 0 \quad .\end{aligned}\tag{109}$$

We've introduced here the function

$$\mathcal{G} = \sqrt{-4\nu(x^2+2y^2) + 4\nu^2(x^2+y^2) + x^2 + 4y^2} \quad .\tag{110}$$

We calculate the stress tensor by means of Hooke's law

$$\begin{aligned}\boldsymbol{\sigma}^{xx} &= -\frac{b_2}{\pi} \frac{E}{(4\nu-3)(\nu+1)} \frac{x(\nu(x^2+y^2)-y^2)}{(x^2+y^2)^2} \quad , \\ \boldsymbol{\sigma}^{xy} &= -\frac{b_2}{\pi} \frac{E}{(4\nu-3)(\nu+1)} \frac{y(\nu(x^2+y^2)-y^2)}{(x^2+y^2)^2} \quad , \\ \boldsymbol{\sigma}^{xz} &= 0 \quad , \\ \boldsymbol{\sigma}^{yy} &= \frac{b_2}{\pi} \frac{E}{(4\nu-3)(\nu+1)} \frac{x(\nu(x^2+y^2)-x^2-2y^2)}{(x^2+y^2)^2} \quad , \\ \boldsymbol{\sigma}^{yz} &= 0 \quad , \\ \boldsymbol{\sigma}^{zz} &= -\frac{b_2}{\pi} \frac{E\nu}{(4\nu-3)(\nu+1)} \frac{x}{(x^2+y^2)} \quad ,\end{aligned}\tag{111}$$

with the trace

$$\boldsymbol{\sigma}_k{}^k = -\frac{b_2}{\pi} \frac{E}{(4\nu-3)} \frac{x}{x^2+y^2} = -\frac{E}{(2\nu-1)} \boldsymbol{\varepsilon}_k{}^k \quad .\tag{112}$$

The stress tensor is divergence-free. The x-component of the divergence of the stress tensor vanishes according to

$$\boldsymbol{\sigma}^{x1}{}_{,1} = -\boldsymbol{\sigma}^{x2}{}_{,2} = \frac{b_2}{\pi} \frac{E}{(4\nu-3)(\nu+1)} \frac{\nu(x^4-y^4) - 3x^2y^2 + y^4}{(x^2+y^2)^3} \quad ,\tag{113}$$

and the y-component according to

$$\sigma^{y^1}_{,1} = -\sigma^{y^2}_{,2} = \frac{b_2}{\pi} \frac{E}{(4\nu - 3)(\nu + 1)} \frac{2xy(\nu(x^2 + y^2) - 2y^2)}{(x^2 + y^2)^3} . \quad (114)$$

In cylindrical coordinates the stress tensor writes

$$\begin{aligned} \sigma^{rr} &= -\frac{b_2}{\pi} \frac{E\nu}{(4\nu - 3)(\nu + 1)} \frac{\cos(\varphi)}{r} , \\ \sigma^{r\varphi} &= \frac{b_2}{\pi} \frac{E(\nu - 1)}{(4\nu - 3)(\nu + 1)} \frac{\sin(\varphi)}{r} , \\ \sigma^{rz} &= 0 , \\ \sigma^{\varphi\varphi} &= \frac{b_2}{\pi} \frac{E(\nu - 1)}{(4\nu - 3)(\nu + 1)} \frac{\cos(\varphi)}{r} , \\ \sigma^{\varphi z} &= 0 , \\ \sigma^{zz} &= -\frac{b_2}{\pi} \frac{E\nu}{(4\nu - 3)(\nu + 1)} \frac{\cos(\varphi)}{r} . \end{aligned} \quad (115)$$

Diagonalisation yields the principal stresses

$$\begin{aligned} \dot{\sigma}^{11} &= -\frac{b_2}{2\pi} \frac{E}{(4\nu - 3)(\nu + 1)} \frac{\mathcal{G} + x}{(x^2 + y^2)} , \\ \dot{\sigma}^{22} &= \frac{b_2}{2\pi} \frac{E}{(4\nu - 3)(\nu + 1)} \frac{\mathcal{G} - x}{(x^2 + y^2)} , \\ \dot{\sigma}^{33} &= -\frac{b_2}{\pi} \frac{E\nu}{(4\nu - 3)(\nu + 1)} \frac{x}{(x^2 + y^2)} , \end{aligned} \quad (116)$$

with the function  $\mathcal{G}$  from equation (110).

The sum of the stress vector fields, which belongs to the normal vector of the envelope of the cylinder pointing into its center, and to the normal vector in the direction of the z-axis, is in the case of the y-edge dislocation in a crystal given by

(cylindrical coordinates)

$$\begin{aligned}
f_r &= -\frac{b_2}{\pi} \frac{E}{(4\nu-3)(\nu+1)} \frac{1}{r} \\
&\times \left( \left[ b_2 \left( (2\nu-1) \sin^2(\varphi) - 2\nu^2 + 2\nu - 1 \right) - (4\nu-3) \cos(\varphi) \pi r \right] \sin^2(\varphi) \right. \\
&\quad \left. + \left( (4\nu-3) \pi r + b_2 (2\nu-1) \cos(\varphi) \right) (\sin^2(\varphi) - \nu) \cos(\varphi) \right) \\
&\times \left( -b_2^2 \left( (4\nu-3) \sin^2(\varphi) - 4\nu^2 + 4\nu - 1 \right) \right. \\
&\quad \left. + (4\nu-3)^2 \pi^2 r^2 + 2(4\nu-3)(2\nu-1) b_2 \pi r \cos(\varphi) \right)^{-1/2}, \\
f_\varphi &= \frac{b_2}{\pi} \frac{E}{(4\nu-3)(\nu+1)} \frac{1}{r} \\
&\times \left( (\nu-1) \left( b_2 \cos(\varphi) + (4\nu-3) \pi r \right) \sin(\varphi) \right) \\
&\times \left( -b_2^2 \left( (4\nu-3) \sin^2(\varphi) - 4\nu^2 + 4\nu - 1 \right) \right. \\
&\quad \left. + (4\nu-3)^2 \pi^2 r^2 + 2(4\nu-3)(2\nu-1) b_2 \pi r \cos(\varphi) \right)^{-1/2}, \\
f_z &= -\frac{b_2}{\pi} \frac{E\nu}{(4\nu-3)(\nu+1)} \frac{x}{x^2 + y^2}. \tag{117}
\end{aligned}$$

We neglect again the z-component of this vector field with the assumption of an infinite elongation of the crystal in z-direction. The resulting vectors are plotted in fig. 2.2. We get a similar figure as in the case of the x-edge dislocation rotated about an angular of  $\pi/2$  around the z-axis.

For convenience we examine the amounts of this vector field. We depict the angles  $\varphi = 0$  and  $\varphi = \pi/2$ .

For  $\varphi = 0$  the amount

$$|\vec{f}| \Big|_{(\varphi=0)} = \frac{b_2}{\pi} \frac{E\nu}{(4\nu-3)(\nu+1)} \frac{1}{r}, \tag{118}$$

is proportional to  $1/r$ .

The same for  $\varphi = \pi/2$ , with

$$|\vec{f}| \Big|_{(\varphi=\pi/2)} = \frac{b_2}{\pi} \frac{E(\nu-1)}{(4\nu-3)(\nu+1)} \frac{1}{r}. \tag{119}$$

The amount of the stress vector field gets singular for very small radii ( $r \rightarrow 0$ ) and vanishes for large outer radii ( $r \rightarrow \infty$ ). The displacement field presented can be interpreted as analogous to a crystal defect.



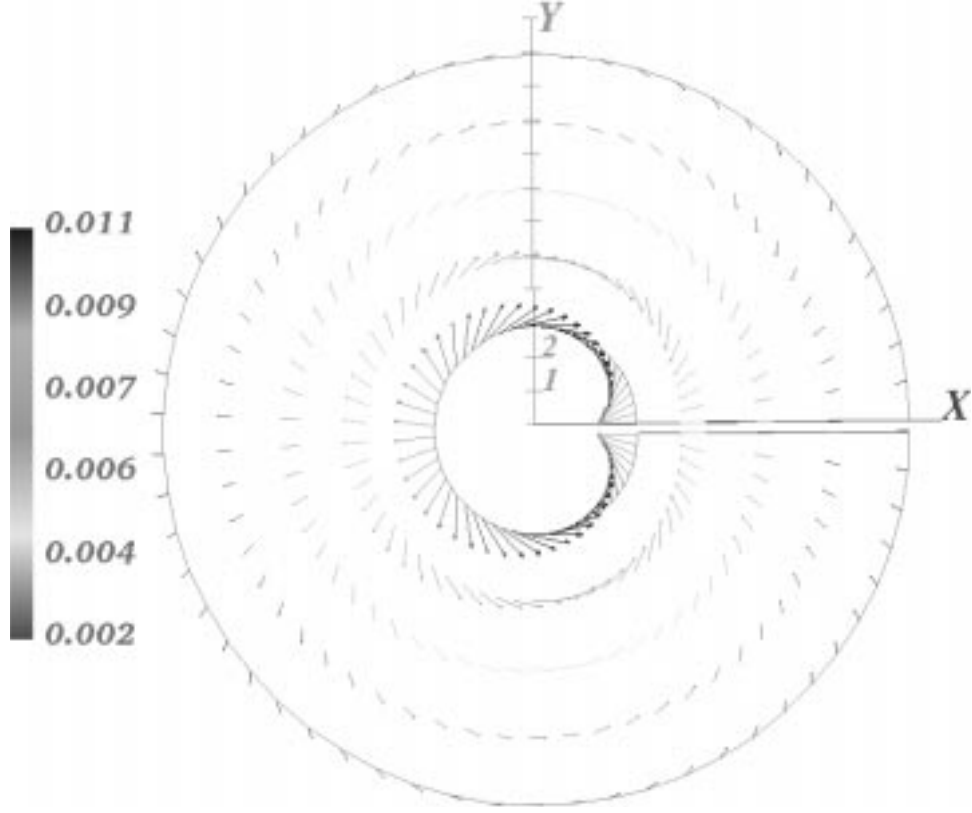


**Fig. 2.2.** Stress vector field around an  $y$ -edge dislocation in a crystal with  $b_2 = -0.1\pi$  [length]

The intensity distribution of the transmitted plane polarized light computes to

$$\begin{aligned}
 I &= I_0^2 \sin^2 \left( \frac{b_2}{2\pi} \frac{\mathcal{G}}{4\nu - 3x^2 + y^2} \right) \\
 &\times \sin^2 \left( 2 \left[ \arccos \left( \frac{(\mathcal{G}\mathcal{H} + \mathcal{I}) \sin(\beta) - \mathcal{J}(\mathcal{G} + (2\nu - 1)x)y \cos(\beta)}{\sqrt{(\mathcal{G}\mathcal{H} + \mathcal{I})^2 + (\mathcal{J}(\mathcal{G} + (2\nu - 1)x))^2 y^2}} \right) - \pi \right] \right),
 \end{aligned} \tag{120}$$

with  $\mathcal{G}$  from eq. (110) and the functions

$$\begin{aligned}
 \mathcal{H} &:= \left( 2\nu(x^2 + y^2) - x^2 - 2y^2 \right) x \\
 \mathcal{I} &:= 2\nu \left( \nu(x^2 + y^2) - x^2 - 2y^2 \right) (2x^2 + y^2) + x^4 + 4x^2 y^2 + 2y^4 \\
 \mathcal{J} &:= \nu(x^2 + y^2) - y^2
 \end{aligned} \tag{121}$$

The constant  $\beta$  is defined in equation (62). Figure 2.3a shows the intensity distribution for  $\beta = 0$  and figure 2.3b for  $\beta = \pi/4$ .

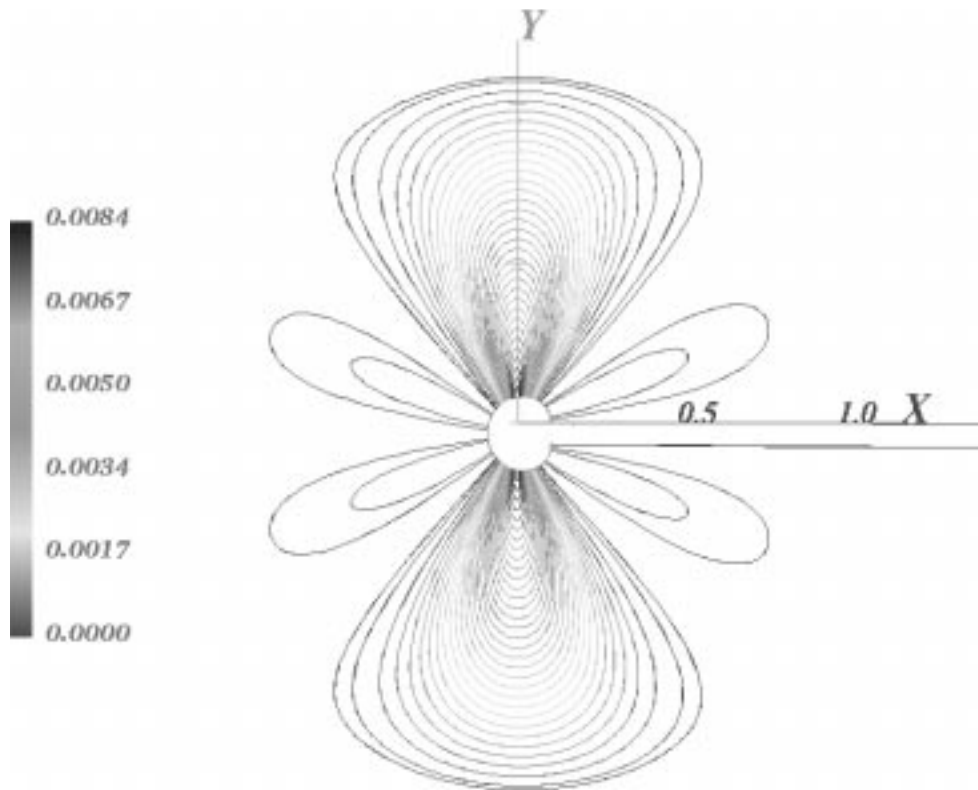


Fig. 2.3a.

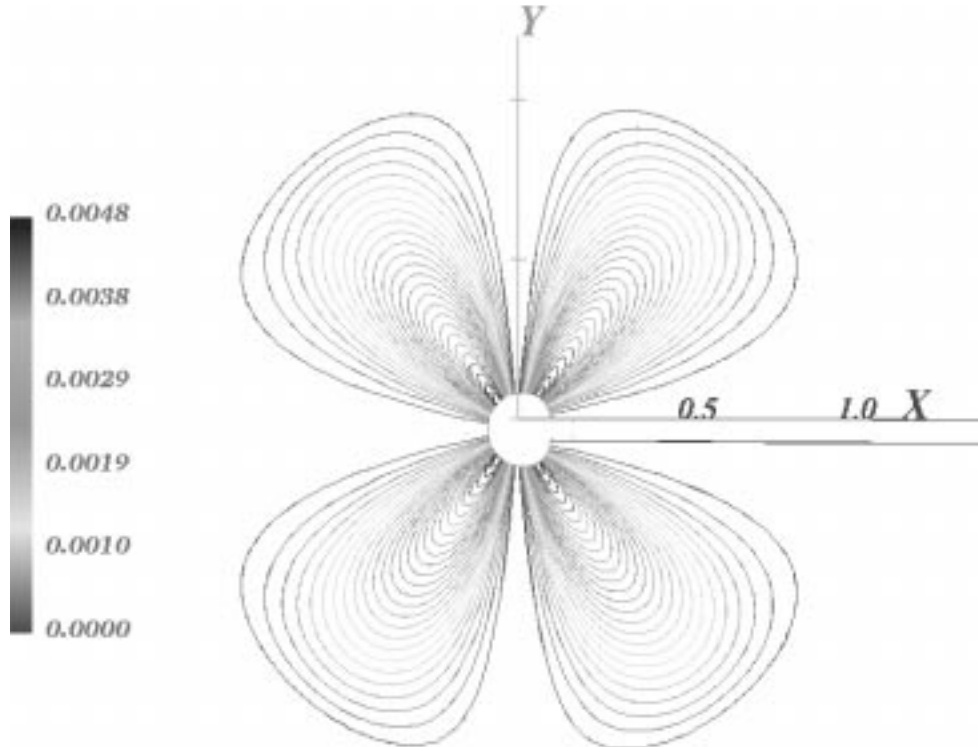


Fig. 2.3b.

**Fig. 2.3.** Isolines of the intensity distribution for double refraction fields due to the stress field around an y-edge dislocation for a)  $\beta = 0$ , and b)  $\beta = \pi/4$  (in units of  $I_0^2$ ). We choose  $b_2 = 0.1\pi$  [length]

For circular polarized light the intensity distribution of the transmitted light is given by

$$I = I_0^2 \sin^2 \left( \frac{b_2}{2\pi(4\nu - 3)} \frac{\mathcal{G}}{x^2 + y^2} \right) . \quad (122)$$

This is shown in fig. 2.4.

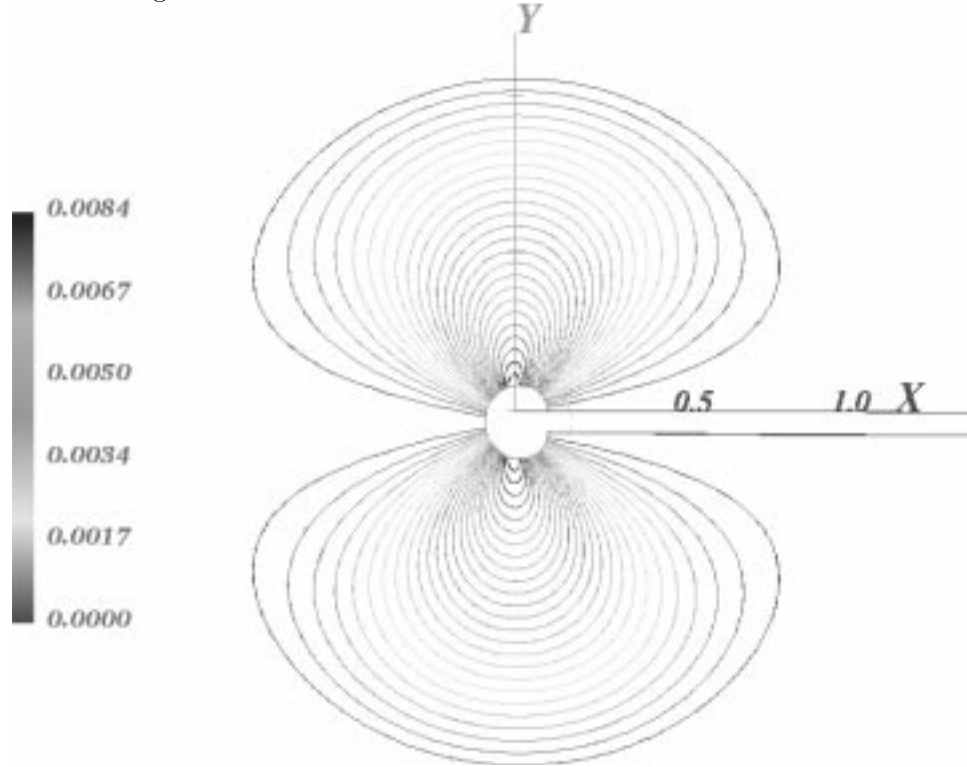


**Fig 2.4** Intensity distribution (isolines) of circular polarized light for double refraction fields due to the stress field around an  $y$ -edge dislocation in a crystal (in units of  $I_0^2$ ). We choose  $b_2 = 0.1\pi$  [length]

Figure 2.4 is the same image as we get for the specific energy for changing the shape of the origin body:

$$\tilde{U}_F = \frac{b_2^2}{3\pi^2} \frac{E}{(4\nu - 3)^2(\nu + 1)} \frac{(4\nu^2 - 4\nu + 1)x^2 + (3\nu^2 - 6\nu + 3)y^2}{(x^2 + y^2)^2} . \quad (123)$$

The intensity distribution of circular polarized light is approximately proportional to  $\tilde{U}_F$ . The course of the isolines only differs in a constant factor of  $y^2$  in the numerator.

## 4.2 The y-edge dislocation of a tubular cylinder

The stress vector field of a tubular cylinder has to vanish at the inner radius  $r_1$  and the outer radius  $r_2$ . We proceed in the same way like in the case of the x-edge dislocation. We are looking for an additional displacement field that leads, together with the realistic displacement in a crystal  $\vec{u}^c$  eq.(103), to such a stress vector field. We calculate the following ansatz for the displacement field of an y-edge dislocation

$$\begin{aligned} u_x^t &= \frac{b_2}{4\pi} \frac{1}{(4\nu - 3)} \frac{x^2 - y^2}{(x^2 + y^2)} \left(1 - \frac{\overset{2}{w}}{(x^2 + y^2)}\right) \quad , \\ u_y^t &= \frac{b_2}{2\pi} \left[ \arctan\left(\frac{y}{x}\right) + \frac{1}{(4\nu - 3)} \frac{xy}{(x^2 + y^2)} \left(1 - \frac{\overset{2}{w}}{(x^2 + y^2)}\right) \right] \quad , \\ u_z^t &= 0 \quad . \end{aligned} \tag{124}$$

The integral (29) along the contour-line  $\vec{s}(t)$  of equation (31) has the components

$$\begin{aligned} \oint u_x \frac{\partial s_x}{\partial t} dt &= \frac{b_2}{12\pi(4\nu - 3)} \left( (\overset{2}{w} - 1) (2 \sin^2(t) + 1) \cos(t) - 1 \right) \Big|_{-\pi/2}^{3\pi/2} = 0 \quad , \\ \oint u_y \frac{\partial s_y}{\partial t} dt &= \frac{b_2}{6\pi(4\nu - 3)} \left( 3(4\nu - 3)t \sin(t) + (12\nu - 10 + \sin^2(t)) \cos(t) \right. \\ &\quad \left. + 1 + \overset{2}{w} (\cos^3(t) - 1) \right) \Big|_{-\pi/2}^{3\pi/2} = b_2 \quad , \\ \oint u_z \frac{\partial s_z}{\partial t} dt &= 0 \quad . \end{aligned} \tag{125}$$

They are independent of  $\overset{2}{w}$ . The passage round the closed contour-line  $\vec{s}(t)$  leads for every constant  $\overset{2}{w}$  to the increment  $b_2$ .

We determine the constant  $\overset{2}{w}$  again in retrospect to the  $\sigma^{rr}$ -component of the stress tensor in cylindrical coordinates

$$\begin{aligned} \sigma^{rr} &= \frac{b_2}{2\pi} \frac{E}{(4\nu - 3)(\nu + 1)} \left( \overset{2}{w} - 2\nu r^2 \right) \frac{\cos(\varphi)}{r^3} \quad , \\ \sigma^{r\varphi} &= \frac{b_2}{2\pi} \frac{E}{(4\nu - 3)(\nu + 1)} \left( \overset{2}{w} + 2(\nu - 1)r^2 \right) \frac{\sin(\varphi)}{r^3} \quad , \\ \sigma^{rz} &= 0 \quad , \\ \sigma^{\varphi\varphi} &= -\frac{b_2}{2\pi} \frac{E}{(4\nu - 3)(\nu + 1)} \left( \overset{2}{w} - 2(\nu - 1)r^2 \right) \frac{\cos(\varphi)}{r^3} \quad , \\ \sigma^{\varphi z} &= 0 \quad , \\ \sigma^{zz} &= -\frac{b_2}{\pi} \frac{E\nu}{(4\nu - 3)(\nu + 1)} \frac{\cos(\varphi)}{r} \quad . \end{aligned} \tag{126}$$

Like before it is not possible to choose  $\overset{2}{w}$  the way, that both,  $\sigma^{rr}$  and  $\sigma^{r\varphi}$  vanishes. We take again

$$\overset{2}{w} = 2\nu r_1^2 \quad , \tag{127}$$

so  $\sigma^{rr}$  becomes zero for  $r = r_1$  and the displacement of a tubular cylinder of eq. (124) becomes

$$\begin{aligned} {}^t u_x &= \frac{b_2}{4\pi} \frac{1}{(4\nu - 3)} \frac{x^2 - y^2}{(x^2 + y^2)} \left( 1 - \frac{2\nu r_1^2}{(x^2 + y^2)} \right) , \\ {}^t u_y &= \frac{b_2}{2\pi} \left( \arctan\left(\frac{y}{x}\right) - \frac{1}{(4\nu - 3)} \frac{xy}{(x^2 + y^2)} \left( 1 - \frac{2\nu r_1^2}{(x^2 + y^2)} \right) \right) , \\ {}^t u_z &= 0 . \end{aligned} \quad (128)$$

The strain tensor

$$\begin{aligned} \epsilon_{xx} &= \frac{b_2}{\pi} \frac{x}{(4\nu - 3)} \frac{\nu r_1^2 (x^2 - 3y^2) + x^2 y^2 + y^4}{(x^2 + y^2)^3} , \\ \epsilon_{xy} &= \frac{b_2}{\pi} \frac{y}{(4\nu - 3)} \frac{\nu (r_1^2 (3x^2 - y^2) - (x^2 + y^2)^2) + x^2 y^2 + y^4}{(x^2 + y^2)^3} , \\ \epsilon_{xz} &= 0 , \\ \epsilon_{yy} &= -\frac{b_2}{\pi} \frac{x}{(4\nu - 3)} \frac{\nu (r_1^2 (x^2 - 3y^2) - 2(x^2 + y^2)^2) + x^4 + 3x^2 y^2 + 2y^4}{(x^2 + y^2)^3} , \\ \epsilon_{yz} &= 0 , \\ \epsilon_{zz} &= 0 , \end{aligned} \quad (129)$$

has the same trace as in the case analogous to a crystal (eq.(106)). Equally the divergence of the strain tensor is the same as in eq.(107). The stress tensor of the y-edge dislocation of a tubular cylinder follows by means of Hooke's law

$$\begin{aligned} \sigma^{xx} &= \frac{b_2}{\pi} \frac{E}{(4\nu - 3)(\nu + 1)} \frac{x}{(x^2 + y^2)^3} \\ &\quad \times \left( \nu (r_1^2 (x^2 - 3y^2) - (x^2 + y^2)^2) + x^2 y^2 + y^4 \right) , \\ \sigma^{xy} &= \frac{b_2}{\pi} \frac{E}{(4\nu - 3)(\nu + 1)} \frac{y}{(x^2 + y^2)^3} \\ &\quad \times \left( \nu (r_1^2 (3x^2 - y^2) - (x^2 + y^2)^2) + x^2 y^2 + y^4 \right) , \\ \sigma^{xz} &= 0 , \\ \sigma^{yy} &= -\frac{b_2}{\pi} \frac{E}{(4\nu - 3)(\nu + 1)} \frac{x}{(x^2 + y^2)^3} \\ &\quad \times \left( \nu (r_1^2 (x^2 - 3y^2) - (x^2 + y^2)^2) + x^4 + 3x^2 y^2 + 2y^4 \right) , \\ \sigma^{yz} &= 0 , \\ \sigma^{zz} &= -\frac{b_2}{\pi} \frac{E\nu}{(4\nu - 3)(\nu + 1)} \frac{x}{(x^2 + y^2)} . \end{aligned} \quad (130)$$

Its trace is again the same as in the case of the displacement analogous to a crystal (eq. (112)).

The stress tensor is divergence-free. The x-component of the divergence of the stress tensor vanishes according to

$$\begin{aligned} \sigma^{x1}_{,1} = -\sigma^{x2}_{,2} = & -\frac{b_2}{\pi} \frac{E}{(4\nu-3)(\nu+1)} \frac{1}{(x^2+y^2)^4} \\ & \times \left( \nu \left( 3r_1^2(x^4 - 6x^2y^2 + y^4) - x^6 + -x^4y^2 + x^2y^4 + y^6 \right) \right. \\ & \left. + 3x^4y^2 + 2x^2y^4 - y^6 \right) . \end{aligned} \quad (131)$$

The y-component according to

$$\begin{aligned} \sigma^{y1}_{,1} = -\sigma^{y2}_{,2} = & -\frac{b_2}{\pi} \frac{2E}{(4\nu-3)(\nu+1)} \frac{xy}{(x^2+y^2)^4} \\ & \times \left( \nu \left( 6r_1^2(x^2 - y^2) - (x^2 + y^2)^2 \right) + 2x^2y^2 + 2y^4 \right) . \end{aligned} \quad (132)$$

In cylindrical coordinates the stress tensor of the y-edge dislocation of a tubular cylinder writes

$$\begin{aligned} \sigma^{rr} &= \frac{b_2}{\pi} \frac{E\nu}{(4\nu-3)(\nu+1)} \left( r_1^2 - r^2 \right) \frac{\cos(\varphi)}{r^3} , \\ \sigma^{r\varphi} &= \frac{b_2}{\pi} \frac{E}{(4\nu-3)(\nu+1)} \left( \nu r_1^2 + (\nu-1)r^2 \right) \frac{\sin(\varphi)}{r^3} , \\ \sigma^{rz} &= 0 , \\ \sigma^{\varphi\varphi} &= -\frac{b_2}{\pi} \frac{E}{(4\nu-3)(\nu+1)} \left( \nu r_1^2 - (\nu-1)r^2 \right) \frac{\cos(\varphi)}{r^3} , \\ \sigma^{\varphi z} &= 0 , \\ \sigma^{zz} &= -\frac{b_2}{\pi} \frac{E\nu}{(4\nu-3)(\nu+1)} \frac{\cos(\varphi)}{r} . \end{aligned} \quad (133)$$

The eigenvalues calculates to

$$\begin{aligned} \dot{\sigma}^{11} &= -\frac{b_2}{2\pi} \frac{E}{(4\nu-3)(\nu+1)} \frac{1}{(x^2+y^2)^2} \left( \mathcal{K} + x(x^2+y^2) \right) , \\ \dot{\sigma}^{22} &= \frac{b_2}{2\pi} \frac{E}{(4\nu-3)(\nu+1)} \frac{1}{(x^2+y^2)^2} \left( \mathcal{K} - x(x^2+y^2) \right) , \\ \dot{\sigma}^{33} &= -\frac{b_2}{\pi} \frac{E\nu}{(4\nu-3)(\nu+1)} \frac{x}{(x^2+y^2)} , \end{aligned} \quad (134)$$

with the function

$$\begin{aligned} \mathcal{K} := & \left( 4\nu(x^2 + y^2) \left( r_1^2(x^2 - 2y^2) - x^4 - 3x^2y^2 - 2y^4 \right) \right. \\ & - 4\nu^2(x^2 + y^2) \left( 2r_1^2(x^2 - y^2) - r_1^4 - (x^2 + y^2)^2 \right) \\ & \left. + x^6 + 6x^4y^2 + 9x^2y^4 + 4y^6 \right)^{1/2}. \end{aligned} \quad (135)$$

We found the following sum of the stress vector fields in cylindrical coordinates which belongs to the interior normal vector field of the cylinder and the normal vector field in the direction of the  $z$ -axis

$$\begin{aligned} f_r = & -\frac{b_2}{\pi} \frac{E}{(4\nu - 3)(\nu + 1)} \frac{1}{r^3} \\ & \times \left( \pi \cos(\varphi) \nu r^3 (4\nu - 3)(r_1^2 - r^2) \right. \\ & \quad + b \sin^2(\varphi) r^2 \left( r_1^2(4\nu - 6\nu^2) + r^2(3\nu - 2) \right) \\ & \quad \left. + b\nu \left( \nu \left[ r_1^2(3r^2 - r_1^2) - 2r^4 + \nu^2 \right] - r_1^2 r^2 + r^4 \right) \right) \\ & \times \left( b_2^2 \left( (4\nu - 3)(2\nu r_1^2 - r^2) r^2 \sin^2(\varphi) + \nu^2 (r_1^2 - 2r^2)^2 + 2\nu r^2 (r_1^2 - 2r^2) + r^4 \right) \right. \\ & \quad \left. - 2b_2 \pi \cos(\varphi) r^3 (4\nu - 3) \left( \nu (r_1^2 - 2r^2) + r^2 \right) + (4\nu - 3)^2 \pi^2 r^6 \right)^{-1/2}, \\ f_\varphi = & -\frac{b_2}{\pi} \frac{E}{(4\nu - 3)(\nu + 1)} \frac{\sin(\varphi)}{r} \\ & \times b_2 \cos(\varphi) \left( \nu [(2\nu - 1)r_1^2 + r^2] - r^2 \right) + 4\nu^2 \pi (r_1^2 r + r^3) - 3\nu \pi r_1^2 r + \pi r^3 (3 - 7\nu) \\ & \times \left( \pi \cos(\varphi) \nu r^3 (4\nu - 3)(r_1^2 - r^2) \right. \\ & \quad + b \sin^2(\varphi) r^2 \left( r_1^2(4\nu - 6\nu^2) + r^2(3\nu - 2) \right) \\ & \quad \left. + b\nu \left( \nu \left[ r_1^2(3r^2 - r_1^2) - 2r^4 + \nu^2 \right] - r_1^2 r^2 \right) \right) \\ & \times \left( b_2^2 \left( (4\nu - 3)(2\nu r_1^2 - r^2) r^2 \sin^2(\varphi) + \nu^2 (r_1^2 - 2r^2)^2 + 2\nu r^2 (r_1^2 - 2r^2) + r^4 \right) \right. \\ & \quad \left. - 2b_2 \pi \cos(\varphi) r^3 (4\nu - 3) \left( \nu (r_1^2 - 2r^2) + r^2 \right) + (4\nu - 3)^2 \pi^2 r^6 \right)^{-1/2}, \\ f_z = & -\frac{b_2}{\pi} \frac{E\nu}{(4\nu - 3)(\nu + 1)} \frac{x}{x^2 + y^2}. \end{aligned} \quad (136)$$

We neglect again the  $z$ -component of this vector field. The resulting vectors are plotted in fig. 2.5a. The isolines of the amount of the stress vector field is depicted in fig. 2.5b.

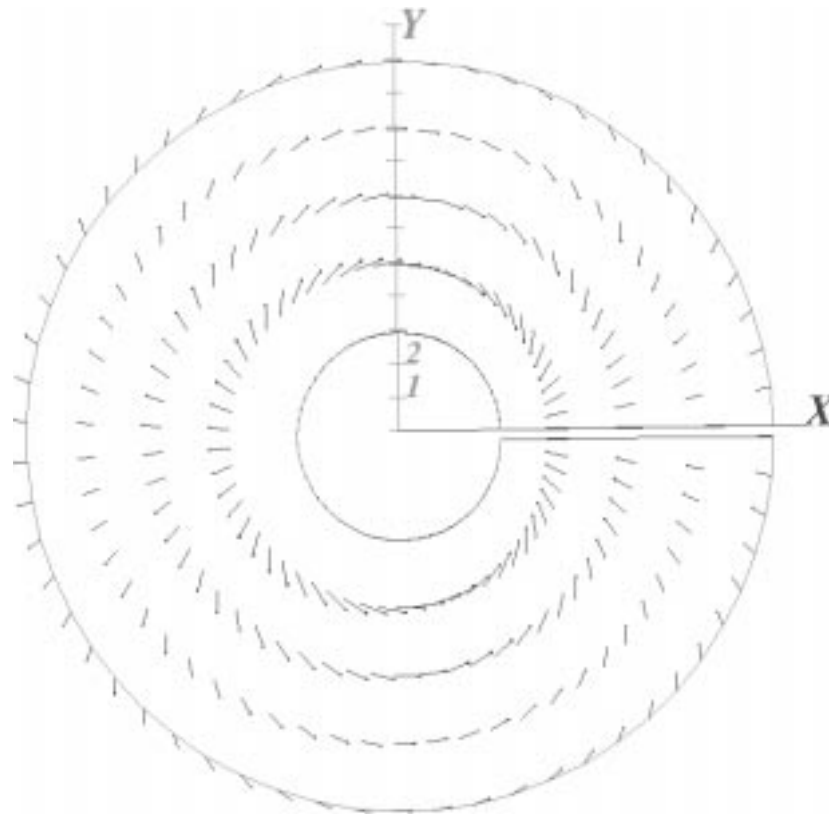


**Fig. 2.5a.** Stress vector field of the y-edge dislocation of a tubular cylinder with  $b_1 = 0.1\pi$  [length]

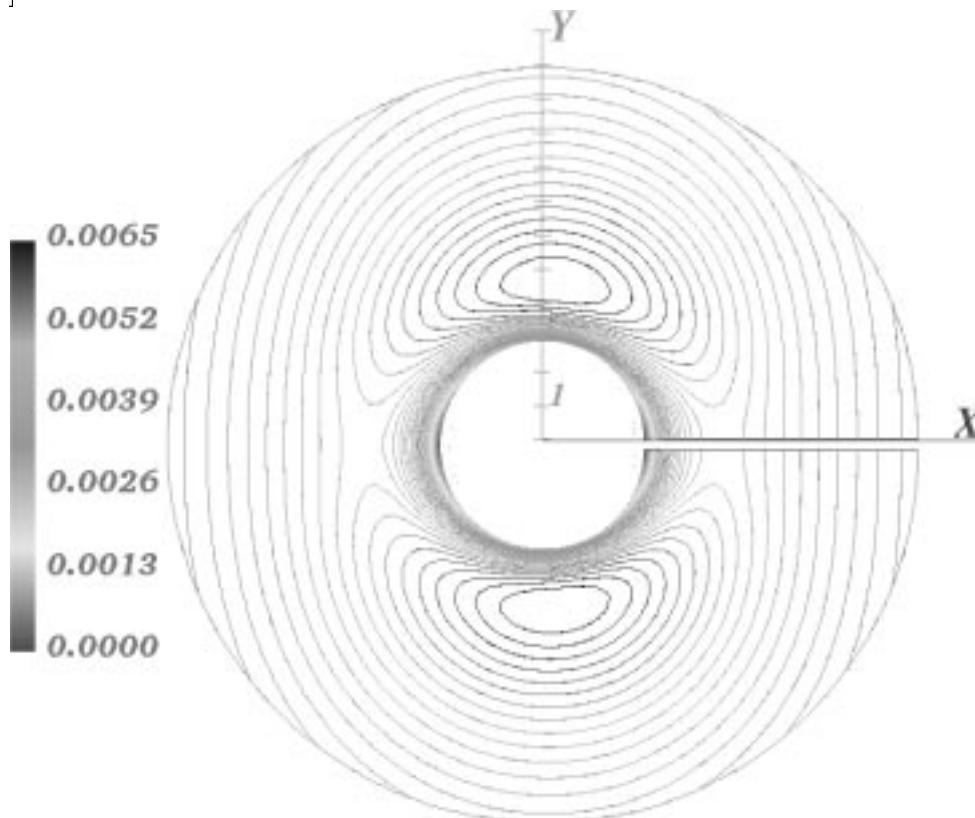


**Fig. 2.5b.** Isolines of the amount of the stress vector field of the x-edge dislocation of a tubular cylinder with  $b_1 = 0.1\pi$  [length] (in units of MPa)



To get more information about the stress vector field of eq.(136), we examine the amount, shown in fig. 2.5b. We depict the angles  $\varphi = 0$ , and  $\varphi = \pi/2$ .

For  $\varphi = 0$  we obtain

$$|\vec{f}| \Big|_{(\varphi=0)} = \frac{b_2}{\pi} \frac{E\nu}{(4\nu-3)(\nu+1)} \frac{(r_1^2 - r^2)}{r^3} . \quad (137)$$

This is similar to  $1/r$ .

If  $\varphi = \pi/2$ , the amount turns to

$$|\vec{f}| \Big|_{(\varphi=\frac{\pi}{2})} = \frac{b_2}{\pi} \frac{E}{(4\nu-3)(\nu+1)} \frac{\nu(r_1^2 + r^2) - r^2}{r^3} , \quad (138)$$

which is also similar to  $1/r$ . The amount shows the same behavior as in the corresponding case of the x-edge dislocation, rotated about  $\pi/2$  around the z-axis (see fig 1.5 at page 28). The displacement field presented (eq.(128)) can be interpreted as analogous to a tubular cylinder.

The intensity distribution of the transmitted plane polarized light computes to

$$I = I_0^2 \sin^2 \left( \frac{b_2}{2\pi} \frac{\mathcal{K}}{(4\nu-3)(x^2+y^2)^2} \right) \times \sin^2 \left( 2 \left[ \arccos \left( \frac{\mathcal{K}\mathcal{L} \sin(\beta) - (\mathcal{M}\mathcal{N} - \mathcal{J} + x^3 + xy^2)y \cos(\beta)}{\sqrt{\mathcal{K}^2\mathcal{L}^2 + \mathcal{M}^2(\mathcal{N} + \mathcal{K} - x^3 - xy^2)^2 y^2}} \right) - \pi \right] \right) . \quad (139)$$

The fringe patterns can be seen in fig. 2.6a for  $\beta = 0$  and in fig. 2.6b for  $\beta = \pi/4$ . We get the same figures as in the case of the edge dislocation, rotated about  $\pi/2$  around the z-axis (see fig 1.6 at page 30). To keep the overview we adopted beside the function  $\mathcal{K}$  of eq.(135) the following three functions

$$\begin{aligned} \mathcal{L} &:= x \left( \nu \left( r_1^2(x^2 - 3y^2) - 2x^4 - 4x^2y^2 - 2y^4 \right) + x^4 + 3x^2y^2 + 2y^4 \right) \\ &\quad + 2\nu^2(x^2 + y^2) \left( r_1^2(3x^4 - 3x^2y^2 - 2y^4) - r_1^4(x^2 + y^2) - 2x^6 - 5x^4y^2 - 4x^2y^4 - y^6 \right) \\ &\quad - \nu(x^2 + y^2) \left( r_1^2(3x^4 - 5x^2y^2 - 4y^4) - 4x^6 - 14x^4y^2 - 14x^2y^4 - 4y^6 \right) \\ &\quad - x^8 - 6x^6y^2 - 11x^4y^4 - 8x^2y^6 - 2y^8 \\ \mathcal{M} &:= \nu \left( r_1^2(3x^2 - y^2) - x^4 - 2x^2y^2 - y^4 \right) + x^2y^2 + y^4 \\ \mathcal{N} &:= 2\nu x(x^2 + y^2) . \end{aligned} \quad (140)$$

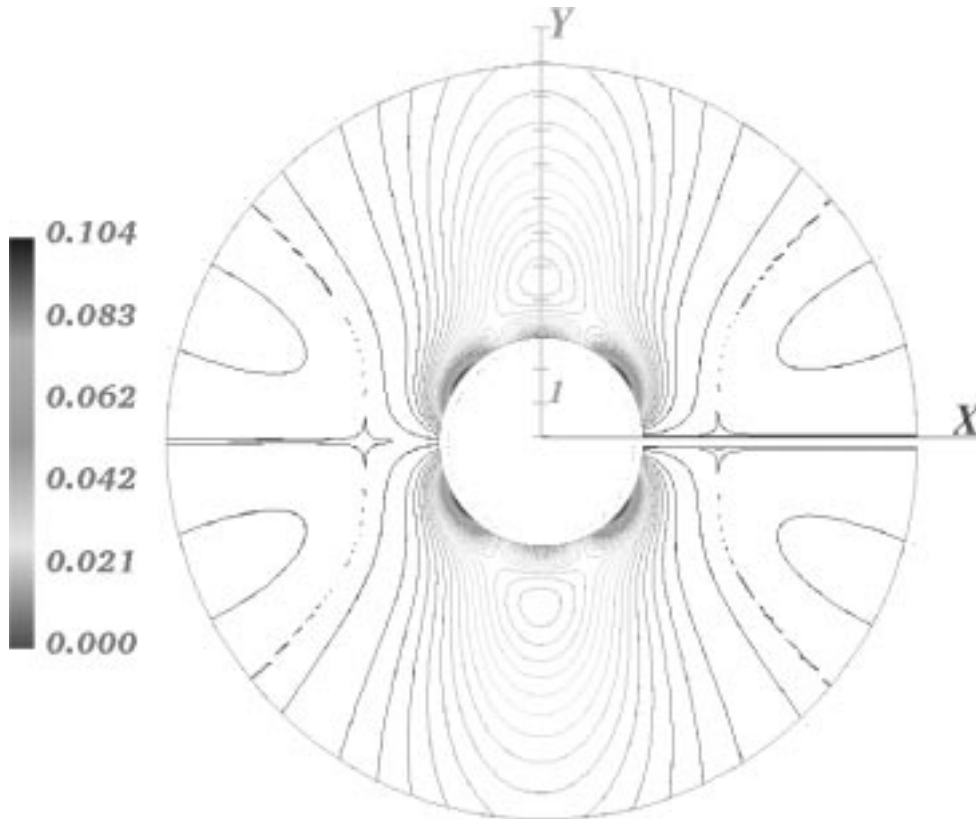


Fig. 2.6a.

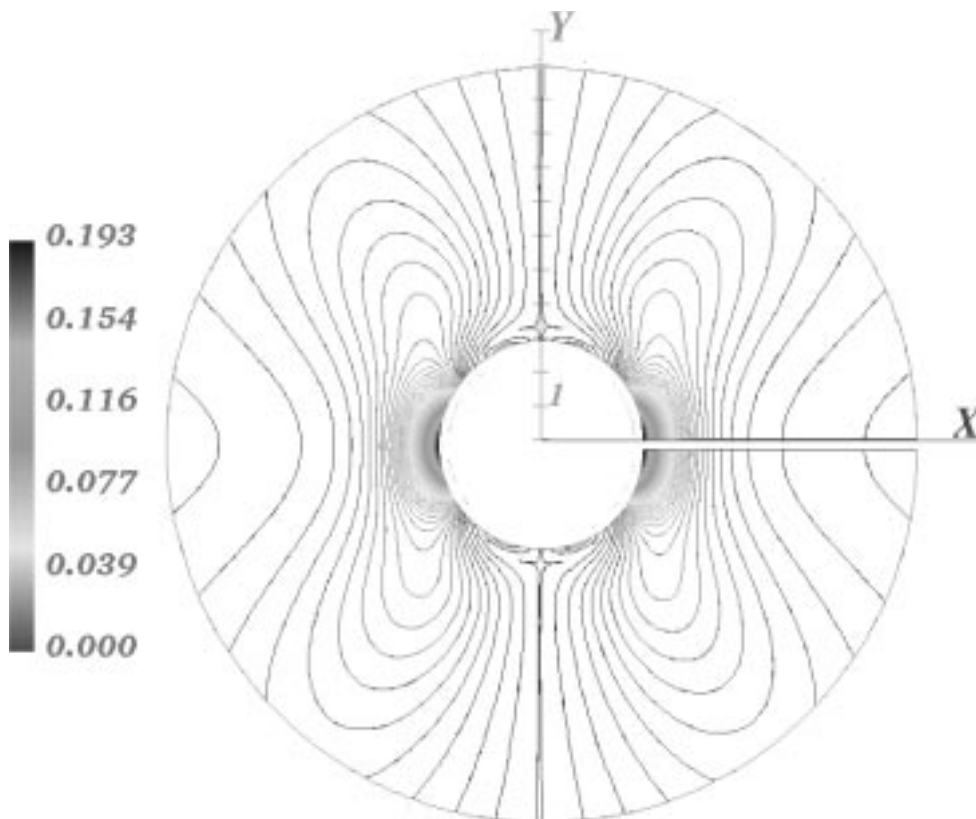


Fig. 2.6. Intensity distribution [ $10^{-3}I_0^2$ ] of plane polarized light for double refraction fields in a tubular cylinder due to the stress field caused by an y-edge dislocation. The angle between the polarizer and the slip direction is a)  $\beta = 0$  and b)  $\beta = \pi/4$

Volterra presented the experimental photographs in “Drei Vorlesungen über neuere Fortschritte der mathematischen Physik” [21] page 147f. Volterra’s mathematical approach coincide very well with our calculations. The agreement with the photographs is much better in the case of the wedge disclination.

For circular polarized light we get:

$$I = I_0^2 \sin^2 \left( \frac{b_2}{2\pi(4\nu-3)} \frac{\mathcal{K}}{(x^2+y^2)^2} \right) . \quad (141)$$

This is plotted in fig. 2.7. It is for  $r_1 = 0$  identical with the intensity of a crystal (122).

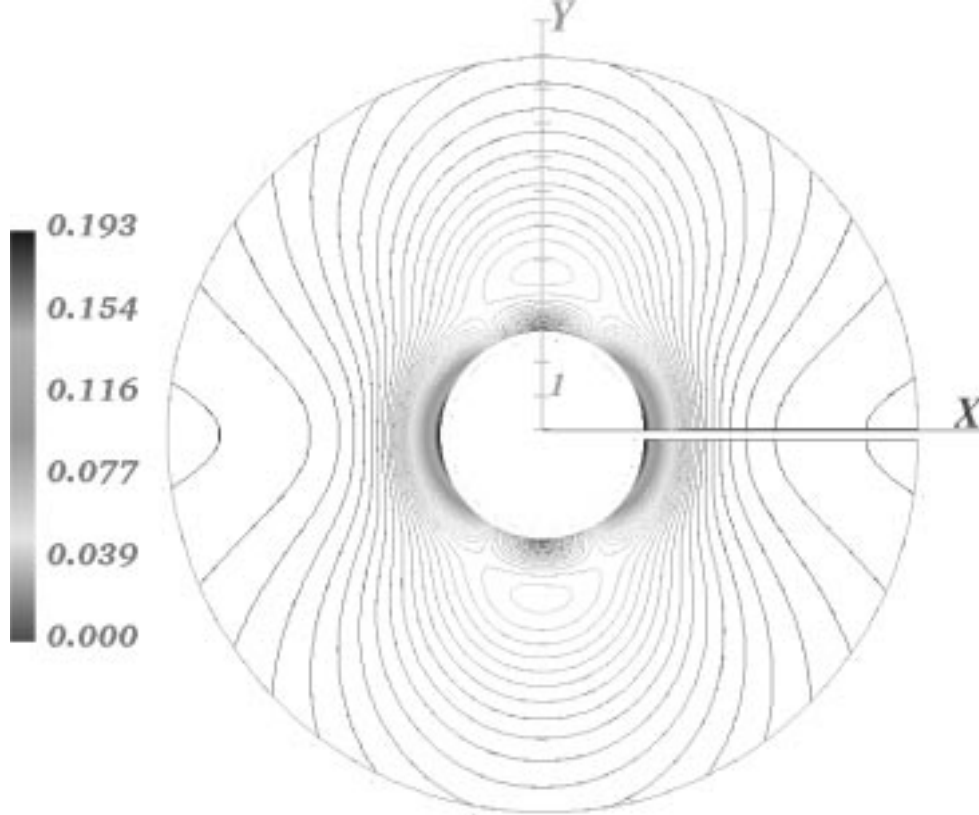


**Fig. 2.7.** Intensity distribution of circular polarized light for double refraction fields in a tubular cylinder (in units of the quadratic amplitude of the incident polarized light  $10^{-3}I_0^2$ ) due to the stress field caused by an y-edge dislocation with  $b_2 = 0.1\pi$

The specific energy for changing the shape of the origin body,

$$\begin{aligned} \tilde{U}_F = & \frac{b_1^2}{\pi^2} \frac{E}{(4\nu-3)^2(\nu+1)} \frac{1}{3(x^2+y^2)^3} \\ & \times \left( -\nu^2 \left( 6r_1^2(x^2-y^2) - 3r_1^4 - 4x^4 - 7x^2y^2 - 3y^4 \right) \right. \\ & \left. + \nu \left( 3r_1^2(x^2-2y^2) - 4x^4 - 10x^2y^2 - 6y^4 \right) + x^4 + 4x^2y^2 + 3y^4 \right) , \end{aligned} \quad (142)$$

leads again to a similar image. For  $x = 0$  both are zero at  $y = \pm\sqrt{\nu/(1-\nu)}r_1$  (outside the tubular cylinder) and reach their maximum at  $y = \pm\sqrt{3\nu/(1-\nu)}r_1$ . The amount of

the stress vector of equation (137) is along the y-axis at the same places maximal and shows approximately an analogous course, but its minimum coincides with the maximum of the specific energy.

## 5 The screw dislocation

The screw dislocation is the splendid defect, because the initial displacement field may already be interpreted as analogous to a crystal and a tubular cylinder.

The Burger vector  $b_k$  has in the case of the screw dislocation only a z-component

$$\vec{b} = (0, 0, b_3) \quad . \quad (143)$$

The initial displacement field, which characterizes the screw dislocation is given by

$$\begin{aligned} u_x^0 &= 0 \quad , \\ u_y^0 &= 0 \\ u_z^0 &= \frac{b_3}{2\pi} \arctan\left(\frac{y}{x}\right) \quad . \end{aligned} \quad (144)$$

It is shown in fig. 3.1.

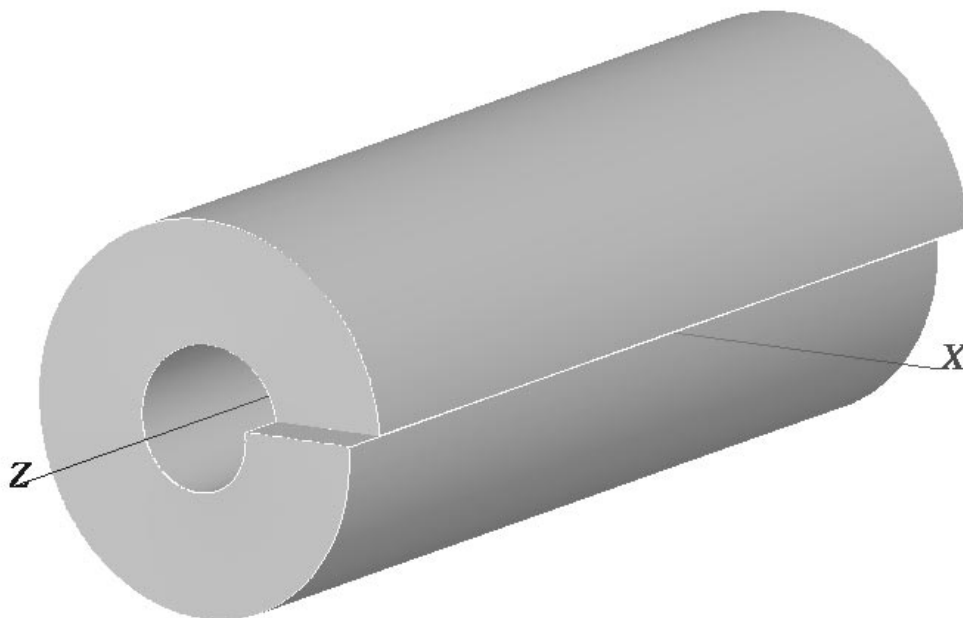


**Fig. 3.1.** The screw dislocation

The strain tensor of this displacement field calculates to

$$\begin{aligned} \epsilon_{xx}^0 &= 0 \quad , \\ \epsilon_{xy}^0 &= 0 \quad , \\ \epsilon_{xz}^0 &= \frac{b_2}{2\pi} \frac{-y}{(x^2 + y^2)} \quad , \\ \epsilon_{yy}^0 &= 0 \quad , \\ \epsilon_{yz}^0 &= \frac{b_2}{2\pi} \frac{x}{(x^2 + y^2)} \quad , \\ \epsilon_{zz}^0 &= 0 \quad . \end{aligned} \quad (145)$$

The divergence of the strain tensor vanishes. The stress tensor followed by means of Hooke's law

$$\begin{aligned}
\sigma^{xx} &= 0 \quad , \\
\sigma^{xy} &= 0 \quad , \\
\sigma^{xz} &= -\frac{b_2}{\pi} \frac{E}{4(\nu+1)} \frac{y}{x^2+y^2} \quad , \\
\sigma^{yy} &= 0 \quad , \\
\sigma^{yz} &= \frac{b_2}{\pi} \frac{E}{4(\nu+1)} \frac{x}{x^2+y^2} \quad , \\
\sigma^{zz} &= 0 \quad .
\end{aligned} \tag{146}$$

The stress tensor is divergence-free. The z-component of the divergence of the stress tensor vanishes according to

$$\sigma^{z1}_{,1} = -\sigma^{z2}_{,2} = \frac{b_3}{\pi} \frac{E}{(2(\nu-1)(x^2+y^2)^2)} \frac{xy}{(x^2+y^2)^2} \quad . \tag{147}$$

In cylindrical coordinates the stress tensor writes

$$\begin{aligned}
\sigma^{rr} &= 0 \quad , \\
\sigma^{r\varphi} &= 0 \quad , \\
\sigma^{rz} &= 0 \quad , \\
\sigma^{\varphi\varphi} &= 0 \quad , \\
\sigma^{\varphi z} &= \frac{b_3}{\pi} \frac{E}{4(\nu+1)} \frac{1}{r} \quad , \\
\sigma^{zz} &= 0 \quad .
\end{aligned} \tag{148}$$

Diagonalisation yields the principal stresses

$$\begin{aligned}
\dot{\sigma}^{11} &= \frac{b_3}{4\pi} \frac{E}{(\nu+1)} \frac{1}{\sqrt{x^2+y^2}} \quad , \\
\dot{\sigma}^{22} &= -\frac{b_3}{4\pi} \frac{E}{(\nu+1)} \frac{1}{\sqrt{x^2+y^2}} \quad , \\
\dot{\sigma}^{33} &= 0 \quad .
\end{aligned} \tag{149}$$

The stress vector field, related to the normal vector pointing into the center of the cylinder, vanishes. We approximate for reasons of simplicity the normal vector field related to the top respectively the bottom of the cylinder as parallel to the z-axis. This can be done in the linear and elastic case, which is only useful for small dislocations. We get the stress vector field

$$\begin{aligned}
f_x &= -\frac{b_3}{4\pi} \frac{E}{(\nu+1)} \frac{y}{x^2+y^2} \quad , \\
f_y &= \frac{b_3}{4\pi} \frac{E}{(\nu+1)} \frac{x}{x^2+y^2} \quad , \\
f_z &= 0 \quad .
\end{aligned} \tag{150}$$

This is plotted in fig. 3.2 for  $b_3 = 0.1\pi$  [length].

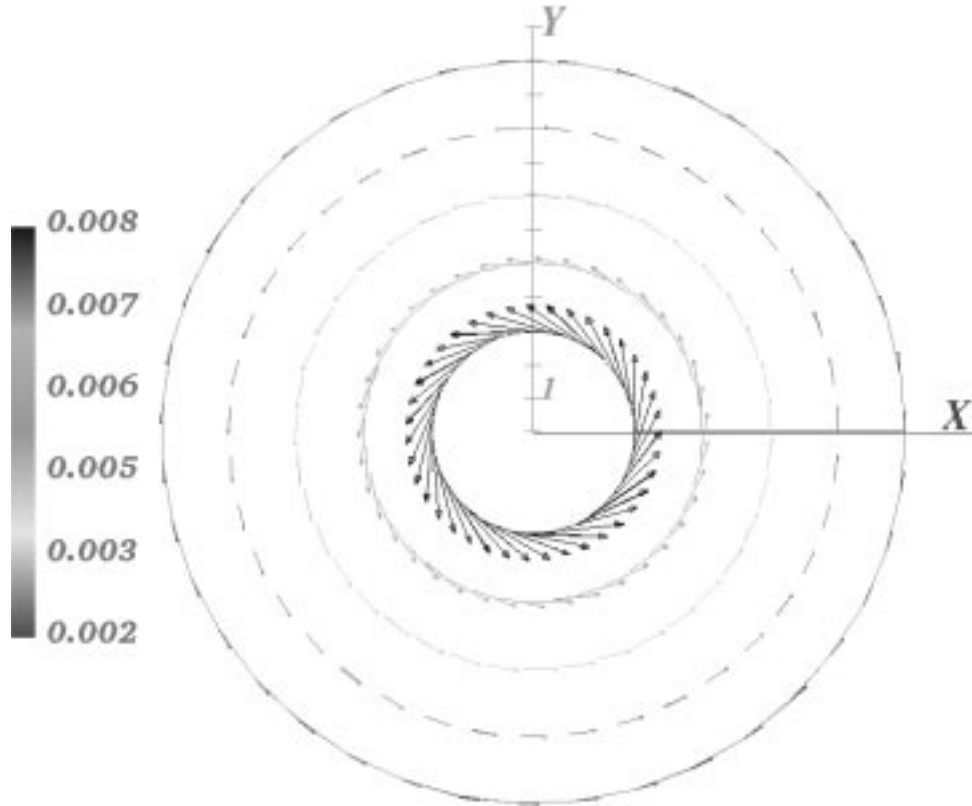


**Fig. 3.2.** Stress vector field around a screw dislocation in a crystal with  $b_3 = 0.1\pi$  [length]

The amount of the stress vector,

$$|\vec{f}| = \frac{b_3}{4\pi} \frac{E}{\nu + 1} \frac{1}{r} \quad , \quad (151)$$

is similar to  $1/r$ , and about ten times stronger than the related amount of the stress vector of the x- or the y-edge dislocation. It gets singular for very small radii ( $r \rightarrow 0$ ) and vanishes for large outer radii ( $r \rightarrow \infty$ ). The displacement field presented can be interpreted as analogous to a crystal defect.

The stress vector field is, as the figure 3.2 shows, everywhere orthogonal to the radial normal vector field ( $\vec{n} = (-x, -y, 0)$ ). This can easily be proved by the vanishing scalar product,  $\vec{f} \cdot \vec{n} = 0$ . The presented screw dislocation can therefore also be looked at as analogous to a tubular cylinder. This is one more hint for the special role of this dislocation.

The intensity distribution of the transmitted plane polarized light is depicted in fig 3.3. It rotates with  $\beta$  around the longitudinal axis of the cylinder and computes to

$$I = -I_0^2 \sin^2 \left( \frac{b_3}{4\pi} \frac{1}{\nu + 1} \frac{1}{\sqrt{x^2 + y^2}} \right) \times \left( \left( y \cos(\beta) - x \sin(\beta) \right)^2 - 2(x^2 + y^2) \right) \left( y \cos(\beta) - x \sin(\beta) \right)^2 \quad . \quad (152)$$

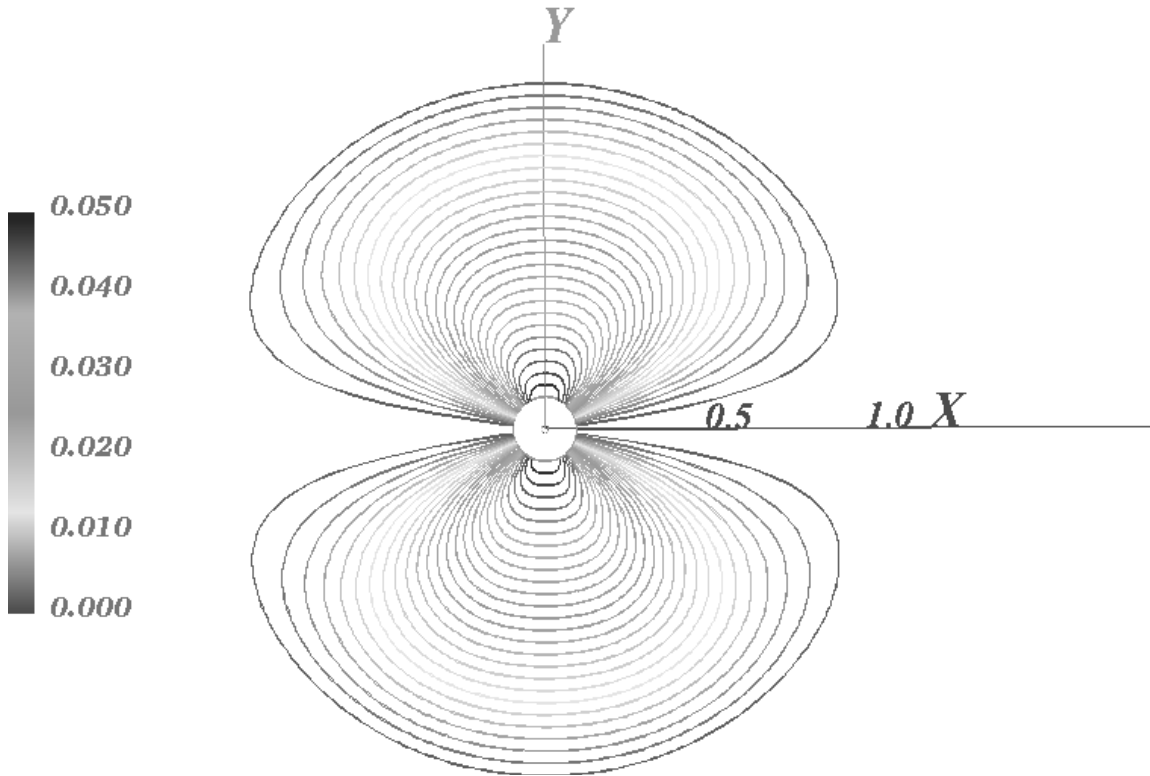


Fig. 3.3a.

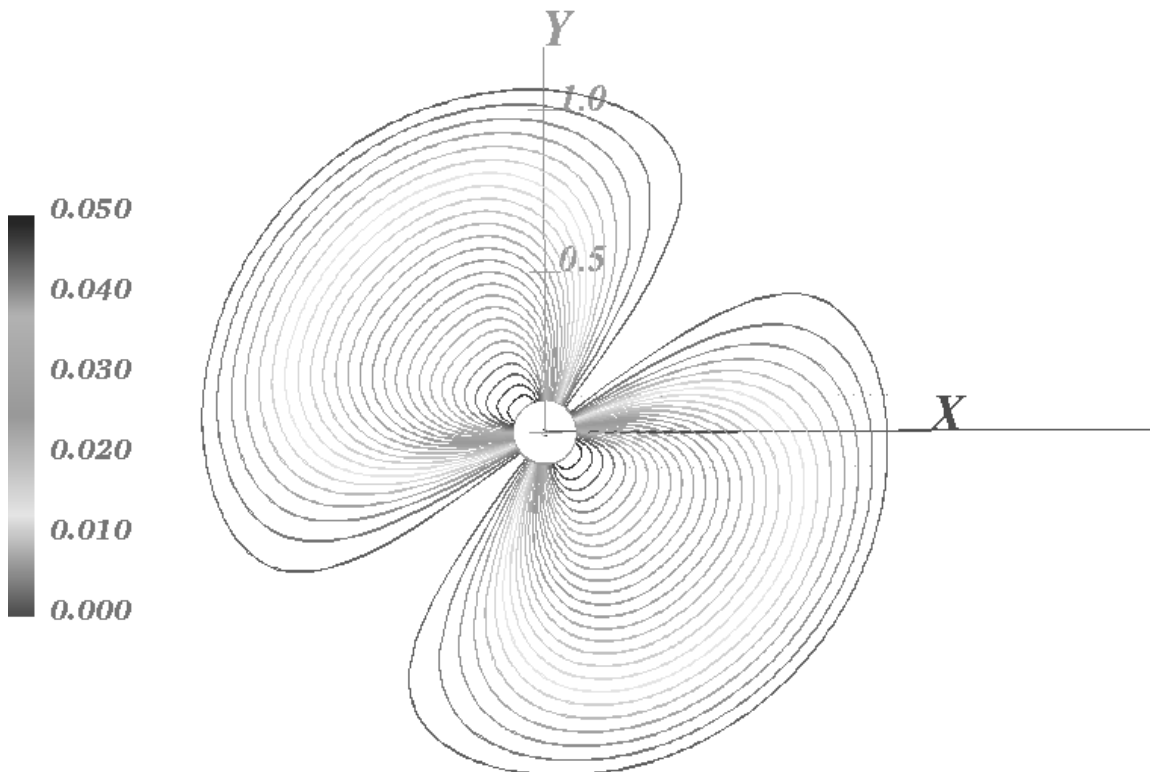


Fig. 3.3b.

**Fig. 3.3.** Isolines of the intensity of plane polarized light for double refraction fields due to the stress field around an screw dislocation for a)  $\beta = 0$ , and b)  $\beta = \pi/4$ ,  $b_3 = 0.1\pi$  [length]



For circular polarized light the intensity distribution of the transmitted light is given by

$$I = I_0^2 \sin^2 \left( \frac{b_3}{4\pi(\nu+1)} \frac{1}{\sqrt{x^2 + y^2}} \right) . \quad (153)$$

This is shown in fig. 3.4.

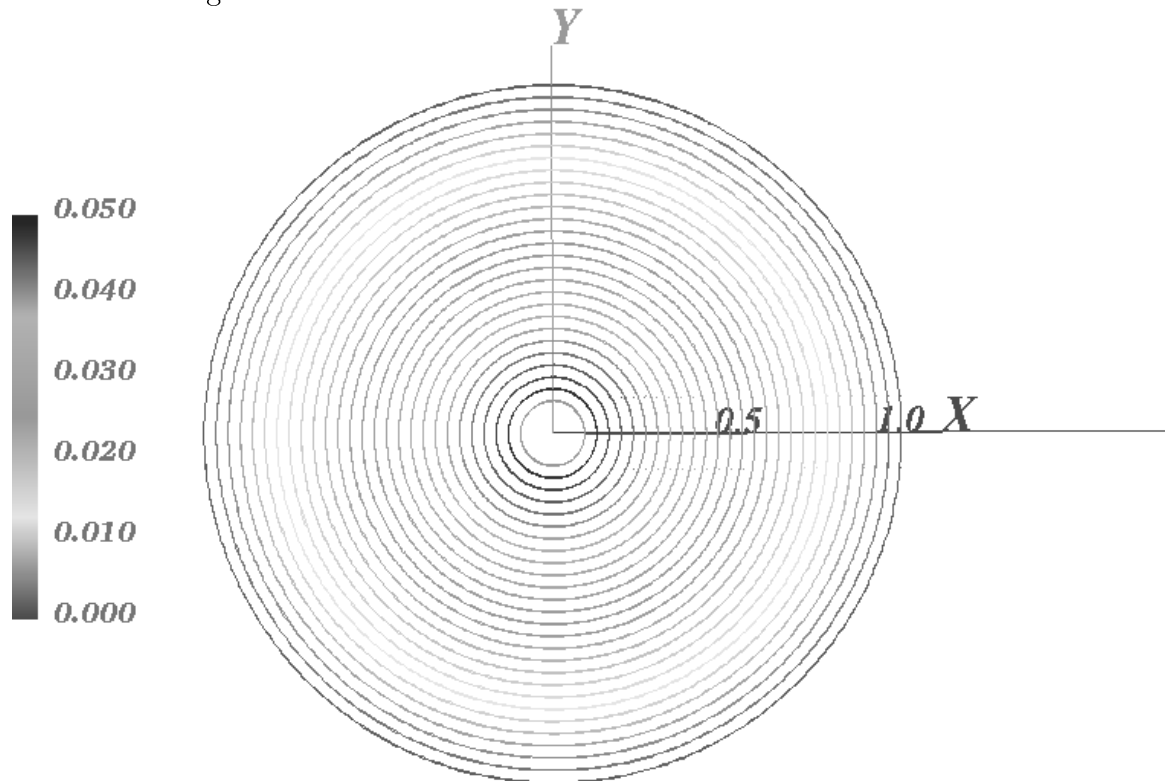


**Fig. 3.4.** Isolines of the intensity of circular polarized light (in units of  $I_0^2$ ) for double refraction fields due to the stress field around a screw dislocation in a crystal with  $b_3 = 0.1\pi$  [length]

The intensity is maximal at the inner radius and gets more and more less till the outer radius. We would get the same image, if we rotate the figures 3.3 around the z-axis, or if we depict the isolines of the specific energy for changing the shape of the origin body,

$$\tilde{U}_F = \frac{b_3^2}{16\pi^2} \frac{E}{(\nu+1)} \frac{1}{(x^2 + y^2)} . \quad (154)$$

The intensity distribution of circular polarized light is again approximately proportional to  $\tilde{U}_F$  (see e.g. section 1 chapter 3.2). The isolines of the amount of the stress vector shows approximately an analogous course. This time the minimum of the amount of the stress vector coincides with the minimum of the considered specific energy.



## 6 The x-twist disclination

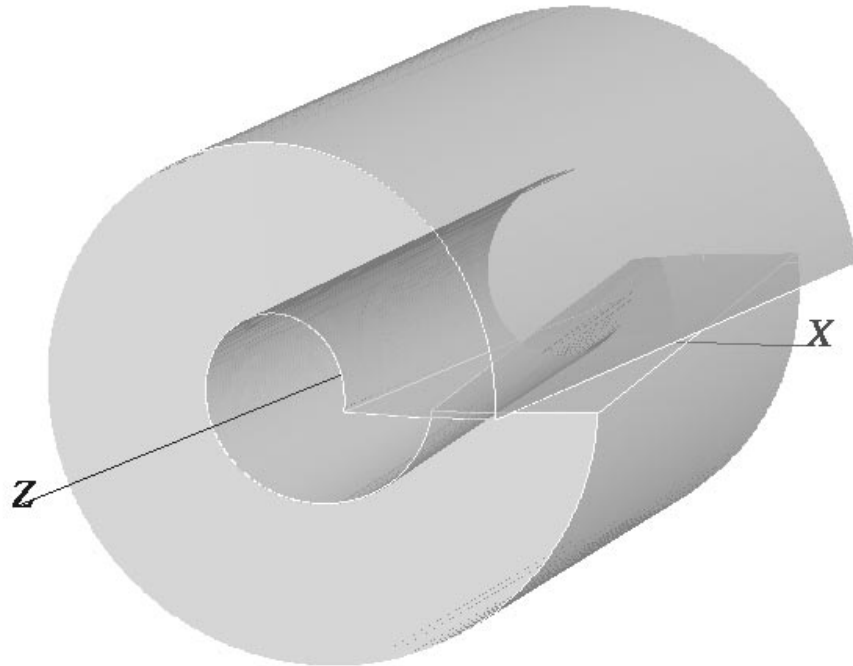


**Fig. 4.1.** The x-twist disclination

In the case of the x-twist disclination is one part of the cutoff cylinder rotated around an axis parallel to the y-axis in x-direction. We get this disclination, if we multiply the initial displacement field of the x-edge dislocation with  $z$ . Therefore we choose this name for the presented disclination. It is also the reason for the similar structure of the calculated tensors and vector fields of the x-edge dislocation and the x-twist disclination.

The initial displacement field, which characterizes the disclination and fulfills the St. Venant conditions is given by

$$\begin{aligned} u_x^0 &= \frac{\Omega_1}{2\pi} z \arctan\left(\frac{y}{x}\right) \quad , \\ u_y^0 &= 0 \quad , \\ u_z^0 &= 0 \quad . \end{aligned} \tag{155}$$

This is shown in fig. 4.1. The dimensionless constant  $\Omega_1$  depict the cutoff volume element. The displacement vector  $\vec{u}$  has to undergo a certain finite increment after passage around any closed contour  $s(t)$  that encircles the disclination line, analogous to the edge-dislocations. This condition writes here

$$\oint u_k ds_k = \oint u_k(s_k(t)) \frac{\partial s_k(t)}{\partial t} dt = \Omega_1 z \quad , \tag{156}$$

if we parameterize the contour with  $t$ .

We choose again

$$\vec{s}(t) = \left( \cos t, \sin t, 0 \right) \quad , \tag{31}$$

so the integral (156) along the contour-line  $\vec{s}(t)$  has the components

$$\begin{aligned} \oint u_x \frac{\partial s_x}{\partial t} dt &= \frac{\Omega_1}{2\pi} \left( t \cos(t) - \sin(t) \right) z \Big|_0^{2\pi} = \Omega_1 z \quad , \\ \oint u_y \frac{\partial s_y}{\partial t} dt &= 0 \quad , \\ \oint u_z \frac{\partial s_z}{\partial t} dt &= 0 \quad . \end{aligned} \tag{157}$$

The strain tensor of the initial displacement field turns out to be

$$\begin{aligned} \mathbf{e}_{xx}^0 &= -\frac{\Omega_1}{2\pi} \frac{yz}{(x^2 + y^2)} \quad , \\ \mathbf{e}_{xy}^0 &= \frac{\Omega_1}{4\pi} \frac{xz}{(x^2 + y^2)} \quad , \\ \mathbf{e}_{xz}^0 &= \frac{\Omega_1}{4\pi} \arctan\left(\frac{y}{x}\right) \quad , \\ \mathbf{e}_{yy}^0 &= 0 \quad , \\ \mathbf{e}_{yz}^0 &= 0 \quad , \\ \mathbf{e}_{zz}^0 &= 0 \quad , \end{aligned} \tag{158}$$

and as the divergence vector field of the strain tensor we find

$$\begin{aligned} \mathbf{e}_{xj}^0{}_{,j} &= \frac{\Omega_1}{2\pi} \frac{xyz}{(x^2 + y^2)^2} \quad , \\ \mathbf{e}_{yj}^0{}_{,j} &= -\frac{\Omega_1}{4\pi} \frac{(x^2 - y^2)z}{(x^2 + y^2)^2} \quad , \\ \mathbf{e}_{zj}^0{}_{,j} &= -\frac{\Omega_1}{4\pi} \frac{y}{(x^2 + y^2)} \quad . \end{aligned} \tag{159}$$

The divergence vector field of the stress tensor is again given by:

$$\boldsymbol{\sigma}^0{}_{ij}{}_{,j} = \frac{E}{(1 + \nu)(1 - 2\nu)} \mathbf{e}^0{}_{ij}{}_{,j} \quad . \tag{160}$$

The displacement field (155) has no divergence-free stress tensor. It needs to be extended by an additional vector field  $\overset{1}{\vec{u}}$ . This can be calculated with our ansatz (21). We find that for the x- and the y-component of the divergence of the stress tensor the partial differential equation (28) is again solved by the function

$$\overset{1}{\mathcal{W}} = x^2 + y^2 \quad , \tag{37}$$

and the constant

$$\overset{1}{w} = -\frac{1}{(4\nu - 3)} \quad . \tag{38}$$

They lead to the additional vector field

$$\begin{aligned} {}^1u_x &= -\frac{\Omega_1}{4\pi} \frac{1}{(4\nu-3)} \frac{xyz}{x^2+y^2} \quad , \\ {}^1u_y &= \frac{\Omega_1}{2\pi} \frac{1}{(4\nu-3)} \frac{(x^2-y^2)z}{x^2+y^2} \quad , \\ {}^1u_z &= \frac{\Omega_1}{4\pi} \frac{1}{(4\nu-3)} y \quad . \end{aligned} \tag{161}$$

Its addition to the initial displacement (155) derives

$$\begin{aligned} {}^{0+1}u_x &= \frac{\Omega_1}{4\pi} \left( z \arctan\left(\frac{y}{x}\right) - \frac{1}{(4\nu-3)} \frac{xyz}{x^2+y^2} \right) \quad , \\ {}^{0+1}u_y &= \frac{\Omega_1}{2\pi} \frac{1}{(4\nu-3)} \frac{(x^2-y^2)z}{x^2+y^2} \quad , \\ {}^{0+1}u_z &= \frac{\Omega_1}{4\pi} \frac{1}{(4\nu-3)} y \quad . \end{aligned} \tag{162}$$

The z-component of this displacement field has no influence on the divergence of the stress tensor. It enables us to modify the displacement field in z-direction. We find here the best solution in retrospect to the stress vector field if we deliver it. The x- and the y-component of the divergence of the belonging stress tensor vanishes, but the z-component is still unequal zero:

$$\sigma^{zj}_{\cdot j} = \frac{\Omega_1}{2\pi} \frac{E}{(4\nu-3)(\nu+1)} \frac{y}{x^2+y^2} \quad . \tag{163}$$

We are looking for an extension of the displacement field of equation (162), to compensate this divergence. It can be calculated by the known equilibrium conditions of eq.(12). We need here only an extension affecting the z-component of the divergence of the stress tensor, because the x- and the y-component are already zero. We can therefore reduce the equilibrium conditions to

$$\sum_j \left( \frac{1}{(1-2\nu)} \frac{\partial^2 u_j}{\partial x_3 \partial x_j} + \frac{\partial^2 u_z}{\partial x_j^2} \right) = -\frac{\Omega_1}{\pi} \frac{1}{(4\nu-3)} \frac{y}{(x^2+y^2)} \quad . \tag{164}$$

If we assume furthermore that the extensional vector field is independent of z, we get:

$$\sum_j \left( \frac{\partial^2 u_z}{\partial x_j^2} \right) = -\frac{\Omega_1}{\pi} \frac{1}{(4\nu-3)} \frac{y}{(x^2+y^2)} \quad . \tag{165}$$

This partial differential equation is easy to solve. One solution for the extensional vector field is

$$\begin{aligned} {}^e u_x &= 0 \quad , \\ {}^e u_y &= 0 \quad , \\ {}^e u_z &= \frac{\Omega_1}{2\pi} \frac{1}{4\nu-3} x \arctan\left(\frac{y}{x}\right) \quad . \end{aligned} \tag{166}$$

We want to remark, that this extensional vector field is proportional to the z-component of the radial normal vector field belonging to the envelope of the cylinder, which is deformed by the initial displacement field. May be this is helpful to solve other 3-dimensional problems. It is also an ingredient of the displacement field given by Volterra [20]. The summation of the initial, the additional and the extensional vector fields lead to a displacement field with a divergence-free stress tensor. As shown in the next section, the calculated displacement field fulfills approximately the boundary conditions of a crystal.

### 6.1 The x-twist disclination in a crystal

We take the initial displacement above  $\vec{u}^0$  (eq.(155)), add the calculated additional vector field  $\vec{u}^1$  of eq.(161) and the extensional vector field  $\vec{u}^e$  of eq.(166)

$$\vec{u}^c = \vec{u}^0 + \vec{u}^1 + \vec{u}^e \quad , \quad (167)$$

and assemble this way the realistic displacement field of the x-twist disclination in a crystal

$$\begin{aligned} u_x^c &= \frac{\Omega_1}{2\pi} z \left( \arctan\left(\frac{y}{x}\right) - \frac{1}{(4\nu-3)} \frac{xy}{x^2+y^2} \right) \quad , \\ u_y^c &= \frac{\Omega_1}{4\pi} \frac{1}{(4\nu-3)} \frac{(x^2-y^2)z}{x^2+y^2} \quad , \\ u_z^c &= \frac{\Omega_1}{2\pi} \frac{1}{(4\nu-3)} \left( x \arctan\left(\frac{y}{x}\right) \right) \quad . \end{aligned} \quad (168)$$

The integral (156) along the contour-line  $s(t)$  has the components

$$\begin{aligned} \oint u_x \frac{\partial s_x}{\partial t} dt &= \frac{\Omega_1}{6\pi} \left( 3(t \cos(t) - \sin(t)) + \frac{1}{(4\nu-3)} \sin^3(t) \right) z \Big|_0^{2\pi} = \Omega_1 z \quad , \\ \oint u_y \frac{\partial s_y}{\partial t} dt &= -\frac{\Omega_1}{12\pi} \frac{1}{(4\nu-3)} \left( 2 \sin^2(t) - 3 \right) \sin(t) z \Big|_0^{2\pi} = 0 \quad , \\ \oint u_z \frac{\partial s_z}{\partial t} dt &= 0 \quad , \end{aligned} \quad (169)$$

The strain tensor of this displacement field calculates to

$$\begin{aligned} \epsilon_{xx} &= -\frac{\Omega_1}{\pi} \frac{1}{(4\nu-3)} \frac{yz}{(x^2+y^2)^2} \left( 2\nu(x^2+y^2) - 2x^2 - y^2 \right) \quad , \\ \epsilon_{xy} &= \frac{\Omega_1}{\pi} \frac{1}{(4\nu-3)} \frac{xz}{(x^2+y^2)^2} \left( \nu(x^2+y^2) - x^2 \right) \quad , \\ \epsilon_{xz} &= \frac{\Omega_1}{2\pi} \frac{1}{(4\nu-3)} \left( (2\nu-1) \arctan\left(\frac{y}{x}\right) - \frac{xy}{(x^2+y^2)} \right) \quad , \\ \epsilon_{yy} &= -\frac{\Omega_1}{\pi} \frac{1}{(4\nu-3)} \frac{x^2 y z}{(x^2+y^2)^2} \quad , \\ \epsilon_{yz} &= \frac{\Omega_1}{8\pi} \frac{1}{(4\nu-3)} \frac{(3x^2-y^2)}{(x^2+y^2)} \quad , \\ \epsilon_{zz} &= 0 \quad , \end{aligned} \quad (170)$$

with the trace

$$\boldsymbol{\varepsilon}_k^k = -\frac{\Omega_1}{\pi} \frac{2\nu - 1}{(4\nu - 3)} \frac{yz}{x^2 + y^2} \quad , \quad (171)$$

and the divergence

$$\begin{aligned} \boldsymbol{\varepsilon}_{xj}^{,j} &= \frac{\Omega_1}{\pi} \frac{2\nu}{(4\nu - 3)} \frac{xyz}{(x^2 + y^2)^2} \quad , \\ \boldsymbol{\varepsilon}_{yj}^{,j} &= -\frac{\Omega_1}{\pi} \frac{\nu}{(4\nu - 3)} \frac{(x^2 - y^2)z}{(x^2 + y^2)^2} \quad , \\ \boldsymbol{\varepsilon}_{zj}^{,j} &= -\frac{\Omega_1}{\pi} \frac{\nu}{(4\nu - 3)} \frac{y}{(x^2 + y^2)} \quad . \end{aligned} \quad (172)$$

We find again the proportionality relation with the divergence of the strain tensor of the initial displacement field (159):

$$\boldsymbol{\varepsilon}_{xj}^{,j} = \frac{4\nu}{(4\nu - 3)} \mathbf{0}_{xj}^{,j} \quad . \quad (173)$$

We calculate the stress tensor by means of Hooke's law

$$\begin{aligned} \boldsymbol{\sigma}_{xx} &= -\frac{\Omega_1}{\pi} \frac{E}{(4\nu - 3)(\nu + 1)} \frac{yz}{(x^2 + y^2)^2} \left( \nu(x^2 + y^2) - 2x^2 - y^2 \right) \quad , \\ \boldsymbol{\sigma}_{xy} &= \frac{\Omega_1}{\pi} \frac{E}{(4\nu - 3)(\nu + 1)} \frac{xz}{(x^2 + y^2)^2} \left( \nu(x^2 + y^2) - x^2 \right) \quad , \\ \boldsymbol{\sigma}_{xz} &= \frac{\Omega_1}{2\pi} \frac{E}{(4\nu - 3)(\nu + 1)} \left( (2\nu - 1) \arctan\left(\frac{y}{x}\right) - \frac{xy}{(x^2 + y^2)} \right) \quad , \\ \boldsymbol{\sigma}_{yy} &= \frac{\Omega_1}{\pi} \frac{E}{(4\nu - 3)(\nu + 1)} \frac{yz}{(x^2 + y^2)^2} \left( \nu(x^2 + y^2) - x^2 \right) \quad , \\ \boldsymbol{\sigma}_{yz} &= \frac{\Omega_1}{2\pi} \frac{E}{(4\nu - 3)(\nu + 1)} \frac{(3x^2 - y^2)}{(x^2 + y^2)} \quad , \\ \boldsymbol{\sigma}_{zz} &= \frac{\Omega_1}{\pi} \frac{E\nu}{(4\nu - 3)(\nu + 1)} \frac{yz}{(x^2 + y^2)} \quad , \end{aligned} \quad (174)$$

with the trace

$$\boldsymbol{\sigma}_k^k = \frac{\Omega_1}{\pi} \frac{E}{(4\nu - 3)} \frac{yz}{x^2 + y^2} = -\frac{E}{(2\nu - 1)} \boldsymbol{\varepsilon}_k^k \quad . \quad (175)$$

The stress tensor is divergence-free. The x-component of the divergence of the stress tensor vanishes according to

$$\boldsymbol{\sigma}^{x1}_{,1} = -\boldsymbol{\sigma}^{x2}_{,2} = \frac{\Omega_1}{\pi} \frac{E}{(4\nu - 3)(\nu + 1)} \frac{2xyz \left( \nu(x^2 + y^2) - 2x^2 \right)}{(x^2 + y^2)^3} \quad , \quad (176)$$

the y-component according to

$$\boldsymbol{\sigma}^{y1}_{,1} = -\boldsymbol{\sigma}^{y2}_{,2} = -\frac{\Omega_1}{\pi} \frac{E}{(4\nu - 3)(\nu + 1)} \frac{\left( \nu(x^4 - y^4) + 3x^2y^2 - x^4 \right) z}{(x^2 + y^2)^3} \quad , \quad (177)$$

and the z-component according to

$$-\sigma^{z1}_{,1} = \sigma^{z2}_{,2} + \sigma^{z3}_{,3} \quad , \quad (178)$$

with

$$\begin{aligned} \sigma^{z1}_{,1} &= -\frac{\Omega_1}{\pi} \frac{E}{(4\nu-3)(\nu+1)} \frac{y(\nu(x^2+y^2)-x^2)}{(x^2+y^2)^2} \quad , \\ \sigma^{z2}_{,2} &= -\frac{\Omega_1}{\pi} \frac{E}{(4\nu-3)(\nu+1)} \frac{x^2 y}{(x^2+y^2)^2} \quad , \\ \sigma^{z3}_{,3} &= \frac{\Omega_1}{\pi} \frac{E\nu}{(4\nu-3)(\nu+1)} \frac{y}{(x^2+y^2)} \quad . \end{aligned} \quad (179)$$

The stress tensor writes in cylindrical coordinates

$$\begin{aligned} \sigma^{rr} &= \frac{\Omega_1}{\pi} \frac{E\nu}{(4\nu-3)(\nu+1)} \frac{\sin(\varphi)}{r} z \quad , \\ \sigma^{r\varphi} &= \frac{\Omega_1}{\pi} \frac{E(\nu-1)}{(4\nu-3)(\nu+1)} \frac{\cos(\varphi)}{r} z \quad , \\ \sigma^{rz} &= \frac{\Omega_1}{8\pi} \frac{E}{(4\nu-3)(\nu+1)} \left( 4(2\nu-1)\varphi \cos(\varphi) - \sin(\varphi) \right) \quad , \\ \sigma^{\varphi\varphi} &= -\frac{\Omega_1}{\pi} \frac{E(\nu-1)}{(4\nu-3)(\nu+1)} \frac{\sin(\varphi)}{r} z \quad , \\ \sigma^{\varphi z} &= -\frac{\Omega_1}{8\pi} \frac{E}{(4\nu-3)(\nu+1)} \left( 4(2\nu-1)\varphi \sin(\varphi) - 3 \cos(\varphi) \right) \quad , \\ \sigma^{zz} &= \frac{\Omega_1}{\pi} \frac{E\nu}{(4\nu-3)(\nu+1)} \frac{\sin(\varphi)}{r} z \quad . \end{aligned} \quad (180)$$

Next we will examine the sum of the stress vector fields belonging to the normal vector field of the envelope of the cylinder pointing into its center and to the normal vector field in the direction of the z-axis. We approximate in the case of the disclinations both stress vector fields by relating them to the origin undeformed body,

$$\begin{aligned} f_x &= \frac{\Omega_1}{2\pi} \frac{E}{(4\nu-3)(\nu+1)} \\ &\quad \times \left( (2\nu-1) \arctan\left(\frac{y}{x}\right) - \frac{xy}{(x^2+y^2)} - \frac{2xyz}{\sqrt{(x^2+y^2)}(x^2+y^2)} \right) \quad , \\ f_y &= -\frac{\Omega_1}{8\pi} \frac{E}{(4\nu-3)(\nu+1)} \left( \frac{8z(\nu(x^2+y^2)-x^2)}{\sqrt{(x^2+y^2)}(x^2+y^2)} - \frac{(3x^2-y^2)}{(x^2+y^2)} \right) \quad , \\ f_z &= -\frac{\Omega_1}{8\pi} \frac{E}{(4\nu-3)(\nu+1)} \frac{\sqrt{(x^2+y^2)}(4(2\nu-1)x \arctan(y/x) - y) - 8\nu yz}{(x^2+y^2)} \quad . \end{aligned} \quad (181)$$

This stress vector field depends on the z-position, because the twist disclination is a functions of z. With the approximation of a plane state of stress we neglect the z-component of this vector field, and visualize it in the figures 4.2.



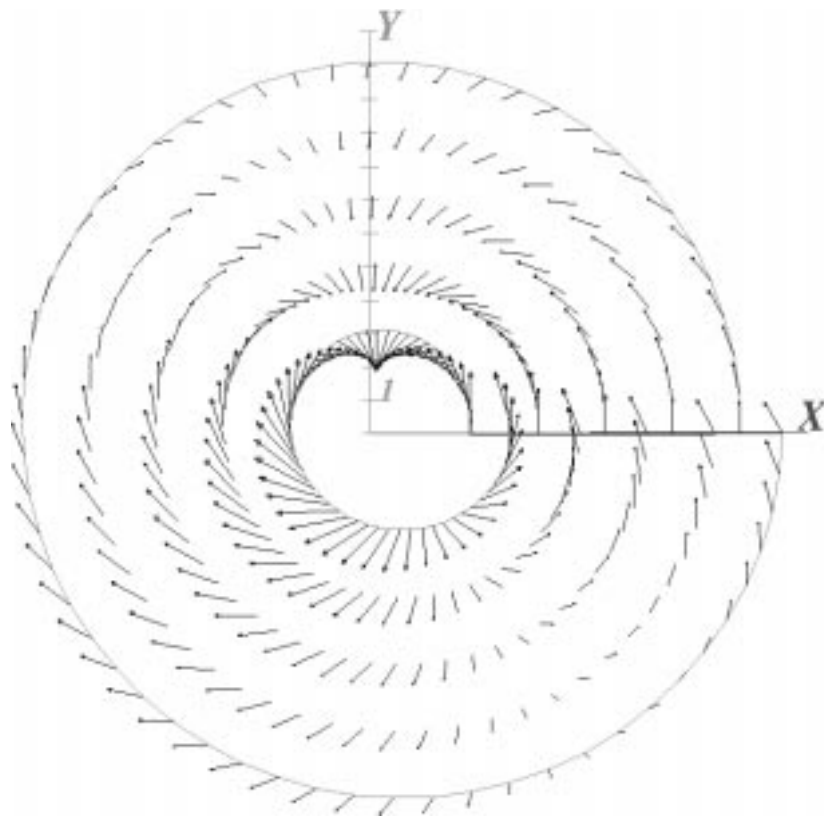


Fig. 4.2a. Stress vector field around an x-twist disclination in a crystal for  $\Omega_1 = 0.1\pi$  and  $z = 4$

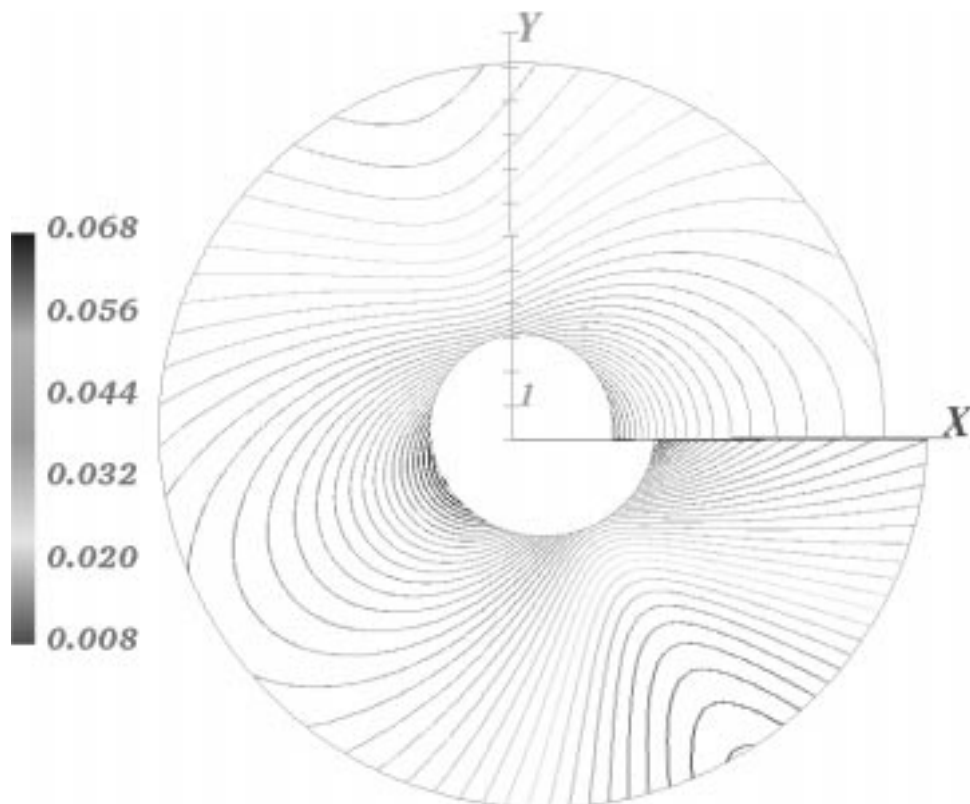


Fig. 4.2b. Isolines of the amount of the stress vector field around an x-twist disclination in a crystal for  $\Omega_1 = 0.1\pi$  and  $z = 4$

For convenience we examine the amount of this vector field. We depict especially the x- and the y-axis. The amount reads for  $\varphi = 0$

$$|\vec{f}| \Big|_{(\varphi=0)} = \frac{\Omega_1}{8\pi} \frac{E}{(4\nu - 3)(\nu + 1)} \frac{1}{r} \sqrt{9r^2 - 48(\nu - 1)rz + 64z^2(\nu - 1)^2} \quad , \quad (182)$$

and for  $\varphi = \pi/2$

$$|\vec{f}| \Big|_{(\varphi=\pi/2)} = \frac{\Omega_1}{8\pi} \frac{E}{(4\nu - 3)(\nu + 1)} \frac{1}{r} \sqrt{r^2 - 4(2\nu - 1)^2\pi^2r^2 + 16\nu z(4\nu z + r)} \quad . \quad (183)$$

Both rises for  $r \rightarrow 0$  and  $z \neq 0$  to infinity but reaches for  $r \rightarrow \infty$  a constant factor. If we make the inner radius small, we can neglect the stress vector at the outer radius in relation to the huge stresses in the center. We think that the displacement field presented can be interpreted as approximately analogous to a crystal defect.

The specific energy for changing the shape of the origin body calculates to

$$\begin{aligned} \tilde{U}_F = & \frac{\Omega_1^2}{192\pi^2} \frac{E}{(4\nu - 3)^2(\nu + 1)} \frac{1}{(x^2 + y^2)^2} \\ & \times \left( 48(2\nu - 1)^2(x^2 + y^2)^2 \arctan^2\left(\frac{y}{x}\right) \right. \\ & - 96xy(2\nu - 1)(x^2 + y^2) \arctan\left(\frac{y}{x}\right) \\ & + 64\nu^2z^2(3x^2 + 4y^2) - 128\nu z^2(3x^2 + 2y^2) \\ & \left. + 6x^2(5y^2 + 32z^2) + 27x^4 + 3y^4 + 64y^2z^2 \right) \quad , \quad (184) \end{aligned}$$

and is shown in fig. 4.3. The isolines of the amount of the stress vector field shows approximately an analogous course. The minimum of both agree nearly.

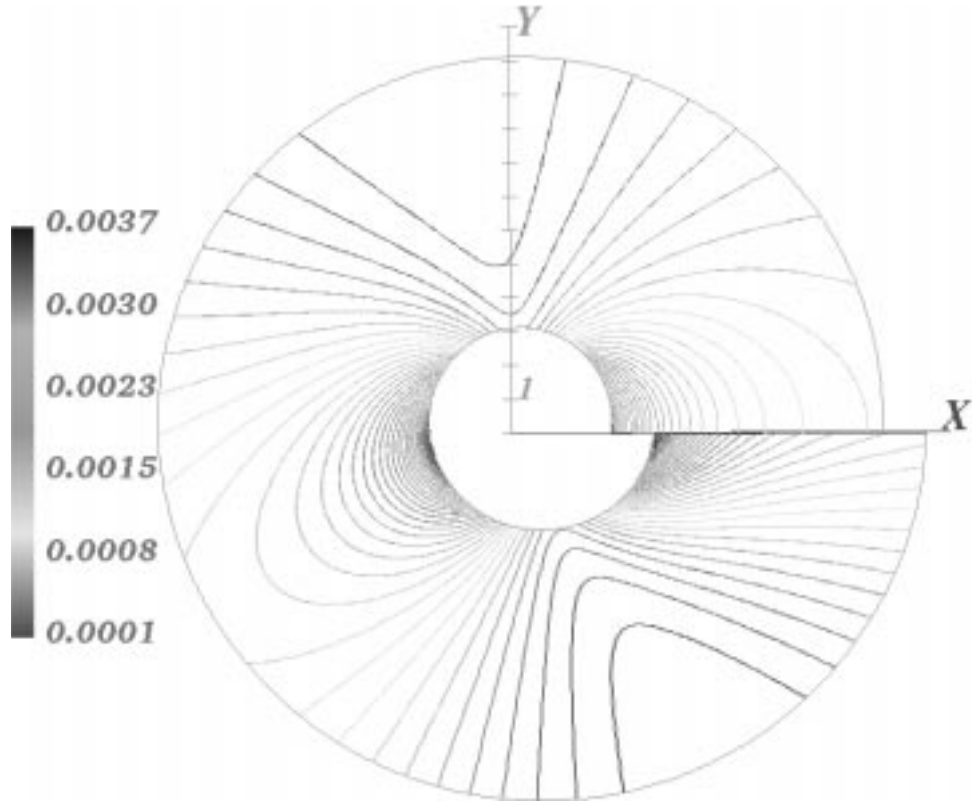


**Fig. 4.3.** Isolines [MPa] of the specific energy for changing the shape of the origin body with  $\Omega_1 = 0.1\pi$  and  $z = 4$

## 6.2 The x-twist disclination of a tubular cylinder

For a tubular cylinder the stress vector field has to vanish at the inner radius  $r_1$  and at the outer radius  $r_2$ . We proceed the disclinations analogous to a tubular cylinder the same way as before for the dislocations. We create an additional vector field based on the divergence of the strain tensor see section 3.2. Its addition to the realistic displacement in a crystal  $\vec{u}^c$  eq.(168) leads to the following ansatz for the displacement field of a x-twist disclination of a tubular cylinder

$$\begin{aligned}
 {}^t u_x &= \frac{\Omega_1}{2\pi} z \left( \arctan\left(\frac{y}{x}\right) - \frac{1}{(4\nu - 3)} \frac{xy}{(x^2 + y^2)} \left(1 - \frac{w^2}{(x^2 + y^2)}\right) \right) , \\
 {}^t u_y &= \frac{\Omega_1}{4\pi} \frac{1}{(4\nu - 3)} \frac{(x^2 - y^2)}{(x^2 + y^2)} z \left(1 - \frac{w^2}{(x^2 + y^2)}\right) , \\
 {}^t u_z &= \frac{\Omega_1}{2\pi} \frac{1}{(4\nu - 3)} x \arctan\left(\frac{y}{x}\right) .
 \end{aligned} \tag{185}$$

The integral (156) along the contour-line  $\vec{s}(t)$  of equation (31) has the components

$$\begin{aligned} \oint u_x \frac{\partial s_x}{\partial t} dt &= \frac{\Omega_1}{6\pi} \frac{1}{(4\nu - 3)} \left( 3(4\nu - 3) (t \cos(t) - \sin(t)) - (\overset{2}{w} - 1) \sin^3(t) \right) z \Big|_0^{2\pi} \\ &= \Omega_1 z \quad , \\ \oint u_y \frac{\partial s_y}{\partial t} dt &= \frac{\Omega_1}{12\pi} \frac{1}{(4\nu - 3)} (\overset{2}{w} - 1) (2 \sin^2(t) - 3) \sin(t) z \Big|_0^{2\pi} = 0 \quad , \\ \oint u_z \frac{\partial s_z}{\partial t} dt &= 0 \quad . \end{aligned} \tag{186}$$

They are independent of  $\overset{2}{w}$ . The passage around the closed contour-line  $\vec{s}(t)$  leads for every constant  $\overset{2}{w}$  to the increment  $\Omega_1 z$ .

We determine the constant  $\overset{2}{w}$  again with retrospect to the  $\sigma^{rr}$  component of the stress tensor. It writes in cylindrical coordinates

$$\begin{aligned} \sigma^{rr} &= \frac{\Omega_1}{2\pi} \frac{E}{(4\nu - 3)(\nu + 1)} z (2\nu r^2 - \overset{2}{w}) \frac{\sin(\varphi)}{r^3} \quad , \\ \sigma^{r\varphi} &= \frac{\Omega_1}{2\pi} \frac{E}{(4\nu - 3)(\nu + 1)} z \left( 2(\nu - 1)r^2 + \overset{2}{w} \right) \frac{\cos(\varphi)}{r^3} \quad , \\ \sigma^{rz} &= \frac{\Omega_1}{8\pi} \frac{E}{(4\nu - 3)(\nu + 1)} \left( 4(2\nu - 1)\varphi \cos(\varphi) + \left( \frac{\overset{2}{w}}{r^2} - 1 \right) \sin(\varphi) \right) \quad , \\ \sigma^{\varphi\varphi} &= -\frac{\Omega_1}{2\pi} \frac{E}{(4\nu - 3)(\nu + 1)} z \left( 2(\nu - 1)r^2 - \overset{2}{w} \right) \frac{\sin(\varphi)}{r^3} \quad , \\ \sigma^{\varphi z} &= -\frac{\Omega_1}{8\pi} \frac{E}{(4\nu - 3)(\nu + 1)} \left( 4(2\nu - 1)\varphi \sin(\varphi) - 3 \cos(\varphi) + \frac{\overset{2}{w}}{r^2} \cos(\varphi) \right) \quad , \\ \sigma^{zz} &= \frac{\Omega_1}{\pi} \frac{E\nu}{(4\nu - 3)(\nu + 1)} z \frac{\sin(\varphi)}{r} \quad . \end{aligned} \tag{187}$$

It is not possible to choose the constant  $\overset{2}{w}$  in a way that all radial components of the stress tensor  $\sigma^{rr}$ ,  $\sigma^{r\varphi}$  and  $\sigma^{rz}$  disappear. This is the reason why we get only an approximately stress vector field at the inner and at the outer radius of the cylinder. We take again

$$\overset{2}{w} = 2\nu r_1^2 \quad , \tag{188}$$

so  $\sigma^{rr}$  becomes zero for  $r = r_1$  and the displacement field of the x-twist disclination of a tubular cylinder writes

$$\begin{aligned} \overset{t}{u}_x &= \frac{\Omega_1}{2\pi} z \left( \arctan\left(\frac{y}{x}\right) - \frac{1}{(4\nu - 3)} \frac{xy}{(x^2 + y^2)} \left( 1 - \frac{2\nu r_1^2}{(x^2 + y^2)} \right) \right) \quad , \\ \overset{t}{u}_y &= \frac{\Omega_1}{4\pi} \frac{1}{(4\nu - 3)} \frac{x^2 - y^2}{(x^2 + y^2)} z \left( 1 - \frac{2\nu r_1^2}{(x^2 + y^2)} \right) \quad , \\ \overset{t}{u}_z &= \frac{\Omega_1}{2\pi} \frac{1}{(4\nu - 3)} x \arctan\left(\frac{y}{x}\right) \quad . \end{aligned} \tag{189}$$

The belonging strain tensor

$$\begin{aligned}
\epsilon_{xx} &= -\frac{\Omega_1}{\pi} \frac{1}{(4\nu-3)} \frac{yz}{(x^2+y^2)^3} \left( \nu \left( r_1^2(3x^2-y^2) + 2(x^2+y^2)^2 \right) - 2x^4 - 3x^2y^2 - y^4 \right) , \\
\epsilon_{xy} &= \frac{\Omega_1}{\pi} \frac{1}{(4\nu-3)} \frac{xz}{(x^2+y^2)^3} \left( \nu \left( r_1^2(x^2-3y^2) + (x^2+y^2)^2 \right) - x^4 - x^2y^2 \right) , \\
\epsilon_{xz} &= \frac{\Omega_1}{4\pi} \frac{1}{(4\nu-3)} \left( 2(2\nu-1) \arctan\left(\frac{y}{x}\right) + \frac{xy}{x^2+y^2} \left( \frac{2\nu r_1^2}{x^2+y^2} - 2 \right) \right) , \\
\epsilon_{yy} &= \frac{\Omega_1}{\pi} \frac{1}{(4\nu-3)} \frac{yz}{(x^2+y^2)^3} \left( \nu r_1^2(3x^2-y^2) - x^4 - x^2y^2 \right) , \\
\epsilon_{yz} &= -\frac{\Omega_1}{8\pi} \frac{1}{(4\nu-3)} \frac{1}{(x^2+y^2)^2} \left( 2\nu r_1^2 - (x^2+y^2)(x^2-y^2) - 2x^2(x^2+y^2) \right) , \\
\epsilon_{zz} &= 0 ,
\end{aligned} \tag{190}$$

has the same trace as in the case analogous to a crystal (eq.(171) ) and its divergence is the same as in eq.(172).

The stress tensor follows by means of Hooke's law

$$\begin{aligned}
\sigma^{xx} &= -\frac{\Omega_1}{\pi} \frac{E}{(4\nu-3)(\nu+1)} \frac{yz}{(x^2+y^2)^3} \\
&\quad \times \left( \nu \left( r_1^2(3x^2-y^2) + (x^2+y^2)^2 \right) - 2x^4 - 3x^2y^2 - y^4 \right) , \\
\sigma^{xy} &= \frac{\Omega_1}{\pi} \frac{E}{(4\nu-3)(\nu+1)} \frac{xz}{(x^2+y^2)^3} \\
&\quad \times \left( \nu \left( r_1^2(x^2-3y^2) + (x^2+y^2)^2 \right) - x^4 - x^2y^2 \right) , \\
\sigma^{xz} &= \frac{\Omega_1}{4\pi} \frac{E}{(4\nu-3)(\nu+1)} \left( (4\nu-3) \arctan\left(\frac{y}{x}\right) + \frac{xy}{(x^2+y^2)} \left( \frac{2\nu r_1^2}{(x^2+y^2)} - 2 \right) \right) , \\
\sigma^{yy} &= \frac{\Omega_1}{\pi} \frac{E}{(4\nu-3)(\nu+1)} \frac{yz}{(x^2+y^2)^3} \\
&\quad \times \left( \nu \left( r_1^2(3x^2-y^2) + (x^2+y^2)^2 \right) - x^4 - x^2y^2 \right) , \\
\sigma^{yz} &= -\frac{\Omega_1}{8\pi} \frac{E}{(4\nu-3)(\nu+1)} \frac{1}{(x^2+y^2)^2} \\
&\quad \times \left( \left( 2\nu r_1^2 - (x^2+y^2) \right) (x^2-y^2) - 2x^2(x^2+y^2) \right) , \\
\sigma^{zz} &= \frac{\Omega_1}{\pi} \frac{E\nu}{(4\nu-3)(\nu+1)} \frac{yz}{(x^2+y^2)} .
\end{aligned} \tag{191}$$

Its trace is again the same as in the case of the displacement analogous to a crystal (eq. (175)).

The stress tensor is divergence-free. The x-component of the divergence of the stress

tensor vanishes according to

$$\begin{aligned}\sigma^{x^1}_{,1} &= -\sigma^{x^2}_{,2} \\ &= \frac{\Omega_1}{\pi} \frac{2E}{(4\nu-3)(\nu+1)} \frac{xyz}{(x^2+y^2)^4} \\ &\quad \times \left( \nu \left( 6r_1^2(x^2-y^2) + (x^2+y^2)^2 \right) - 2x^4 - 2x^2y^2 \right) ,\end{aligned}\tag{192}$$

the y-component according to

$$\begin{aligned}\sigma^{y^1}_{,1} &= -\sigma^{y^2}_{,2} \\ &= -\frac{\Omega_1}{\pi} \frac{E}{(4\nu-3)(\nu+1)} \frac{z}{(x^2+y^2)^4} \\ &\quad \times \left( \nu \left( 3r_1^2(x^4-6x^2y^2+y^4) + x^6 + x^4y^2 - x^2y^4 - y^6 \right) - x^6 + 2x^4y^2 + 3x^2y^4 \right) ,\end{aligned}\tag{193}$$

and the z-component according to

$$-\sigma^{z^1}_{,1} = \sigma^{z^2}_{,2} + \sigma^{z^3}_{,3} ,$$

with

$$\begin{aligned}\sigma^{z^1}_{,1} &= -\frac{\Omega_1}{2\pi} \frac{E}{(4\nu-3)(\nu+1)} \frac{y}{(x^2+y^2)^3} \left( \nu \left( r_1^2(3x^2-y^2) + 2(x^2+y^2)^2 \right) - 2x^4 - 2x^2y^2 \right) , \\ \sigma^{z^2}_{,2} &= \frac{\Omega_1}{2\pi} \frac{E}{(4\nu-3)(\nu+1)} \frac{y}{(x^2+y^2)^3} \left( \nu r_1^2(3x^2-y^2) - 2x^4 - 2x^2y^2 \right) , \\ \sigma^{z^3}_{,1} &= \frac{\Omega_1}{\pi} \frac{E\nu}{(4\nu-3)(\nu+1)} \frac{y}{(x^2+y^2)} .\end{aligned}\tag{194}$$

The stress tensor of the x-twist disclination of a tubular cylinder reads in cylindrical coordinates

$$\begin{aligned}\sigma^{rr} &= -\frac{\Omega_1}{\pi} \frac{E\nu}{(4\nu-3)(\nu+1)} z \left( r_1^2 - r^2 \right) \frac{\sin(\varphi)}{r^3} , \\ \sigma^{r\varphi} &= \frac{\Omega_1}{\pi} \frac{E}{(4\nu-3)(\nu+1)} z \left( \nu r_1^2 + (\nu-1)r^2 \right) \frac{\cos(\varphi)}{r^3} , \\ \sigma^{rz} &= \frac{\Omega_1}{8\pi} \frac{E}{(4\nu-3)(\nu+1)} \left( 4(2\nu-1)\varphi \cos(\varphi) + \left( \frac{2\nu r_1^2}{r^2} - 1 \right) \sin(\varphi) \right) , \\ \sigma^{\varphi\varphi} &= \frac{\Omega_1}{\pi} \frac{E}{(4\nu-3)(\nu+1)} z \left( \nu r_1^2 - (\nu-1)r^2 \right) \frac{\sin(\varphi)}{r^3} , \\ \sigma^{\varphi z} &= -\frac{\Omega_1}{8\pi} \frac{E}{(4\nu-3)(\nu+1)} \left( 4(2\nu-1)\varphi \sin(\varphi) + \left( \frac{2\nu r_1^2}{r^2} - 3 \right) \cos(\varphi) \right) , \\ \sigma^{zz} &= \frac{\Omega_1}{\pi} \frac{E\nu}{(4\nu-3)(\nu+1)} z \frac{\sin(\varphi)}{r} .\end{aligned}\tag{195}$$

We found the following sum of the stress vector fields belonging to the approximated normal vector fields of the undeformed cylinder

$$\begin{aligned}
f_x &= \frac{\Omega_1}{4\pi} \frac{E}{(4\nu - 3)(\nu + 1)} \left( (4\nu - 2) \arctan\left(\frac{y}{x}\right) + \frac{xy}{(x^2 + y^2)} \left( \frac{2\nu r_1^2}{(x^2 + y^2)} - 2 \right) \right. \\
&\quad \left. + \frac{4xyz}{\sqrt{x^2 + y^2}(x^2 + y^2)^2} (2\nu r_1^2 - (x^2 + y^2)) \right) \\
f_y &= -\frac{\Omega_1}{8\pi} \frac{E}{(4\nu - 3)(\nu + 1)} \\
&\quad \times \left( \frac{8z}{\sqrt{(x^2 + y^2)}(x^2 + y^2)} \left[ \nu \left( (x^2 - y^2)r_1^2 + (x^2 + y^2)^2 \right) - x^4 - x^2 y^2 \right] \right. \\
&\quad \left. + \frac{1}{(x^2 + y^2)} \left( \left( \frac{2\nu r_1^2}{(x^2 + y^2)} - 1 \right) - 2x^2(x^2 + y^2) \right) \right) , \\
f_z &= -\frac{\Omega_1}{8\pi} \frac{E}{(4\nu - 3)(\nu + 1)} \frac{1}{\sqrt{(x^2 + y^2)}(x^2 + y^2)} \\
&\quad \left( 4(2\nu - 1)x(x^2 + y^2) \arctan\left(\frac{y}{x}\right) - 8\nu yz \sqrt{(x^2 + y^2)} + y(2\nu r_1^2 - (x^2 + y^2)) \right) .
\end{aligned} \tag{196}$$

We neglect again the z-component of this vector field. The resulting vectors are plotted in fig. 4.4a, the isolines of the amount of the stress vector are depicted in fig. 4.4b. To get more information about the amount of the stress vector field we depict the angle  $\varphi = 0$ :

$$\begin{aligned}
|\vec{f}| \Big|_{(\varphi=0)} &= \frac{\Omega_1}{8\pi} \frac{E\nu}{(4\nu - 3)(\nu + 1)} \frac{1}{r^2} \left( 16 \left( \nu(r_1^2 + r^2) - r^2 \right) zr(2\nu r_1^2 - 3r^2) \right. \\
&\quad \left. + 4\nu^2 \left( r_1^4(r^2 + 16z^2) + 32r_1^2 r^2 z^2 + 16r^4 z^2 \right) \right. \\
&\quad \left. - 4\nu r^2 \left( r_1^2(3r^2 + 32z^2) + 32r^2 z^2 \right) + 9r^6 + 64r^4 z^2 \right)^{1/2} .
\end{aligned} \tag{197}$$

This leads for  $r \rightarrow \infty$  and even for  $r = r_1$  to a constant depending on z. If we examine the angular  $\varphi = \pi/2$ , the amount leads for  $r \rightarrow \infty$  again to a constant which depends on z. For  $r = r_1$  we obtain the constant

$$|\vec{f}| \Big|_{(r=r_1)(\varphi=\pi/2)} = \frac{\Omega_1}{8\pi} \frac{E}{(4\nu - 3)(\nu + 1)} \sqrt{4(2\nu - 1)^2 \pi^2 + 4\nu^2 - 4\nu + 1} . \tag{198}$$

The amount of the stress vector (fig 4.4b) shows some similarities to the x-edge dislocation of a tubular cylinder (Fig 1.5b, page 28). We think that with regard to the done approximations the displacement field presented (eq.(189)) may be interpreted as approximately analogous to a tubular cylinder, if we neglect the area around the slip plane.

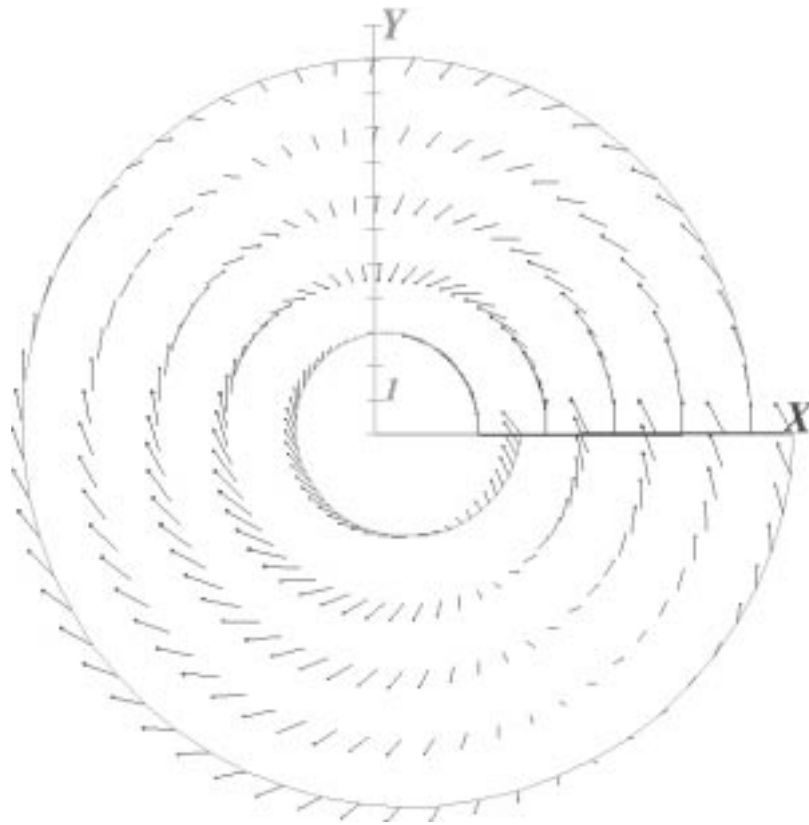


Fig. 4.4a. Stress vector field of a tubular cylinder for  $\Omega_1 = 0.1\pi$  and  $z = 4$

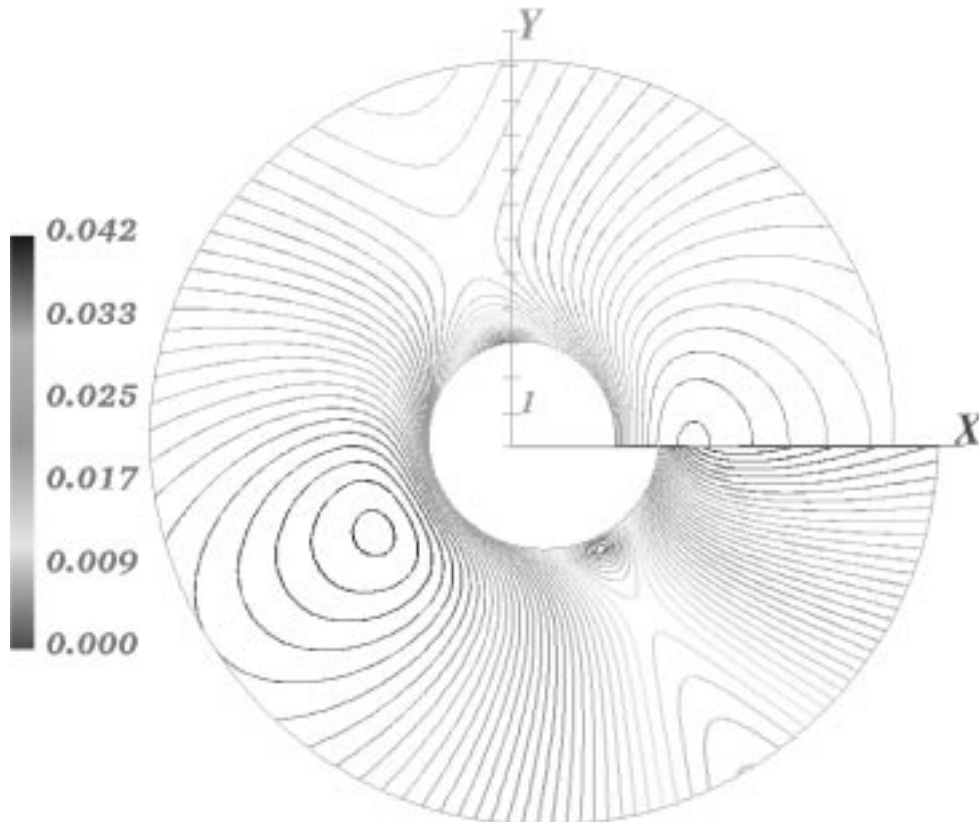


Fig. 4.4b. Isolines of the amount of the stress vector field of a tubular cylinder for  $z = 4$



The specific energy for changing the shape of the origin body calculates to

$$\begin{aligned}
\tilde{U}_F = & -\frac{\Omega_1^2}{192\pi^2} \frac{E}{(4\nu-3)^2(\nu+1)} \frac{1}{(x^2+y^2)^3} \\
& \times \left( 4\nu \left[ 3r_1^2 \left( 4x^2(y^2+8z^2) + 3x^4 + y^4 - 16y^2z^2 \right) + 16z^2 \left( 6x^4 + 10x^2y^2 + 4y^4 \right) \right] \right. \\
& - 4\nu^2 \left[ 3r_1^4(x^2+y^2+16z^2) + 16z^2 \left( 6r_1^2(x^2-y^2) + 3x^4 + 7x^2y^2 + 4y^4 \right) \right] \\
& - 96xy(2\nu-1)(x^2+y^2) \arctan\left(\frac{y}{x}\right)(\nu r_1^2 - (x^2+y^2)) \\
& - 48x^2y^2(2\nu-1)^2(x^2+y^2)^3 \arctan^2\left(\frac{y}{x}\right) - (33y^2 + 256z^2)x^2y^2 \\
& \left. - 3x^4(19y^2 + 64z^2) - 27x^6 - 3y^6 - 64y^4z^2 \right) . \tag{199}
\end{aligned}$$

This is shown in fig 4.6. The amount of the stress vector field shows more or less an analogous course.

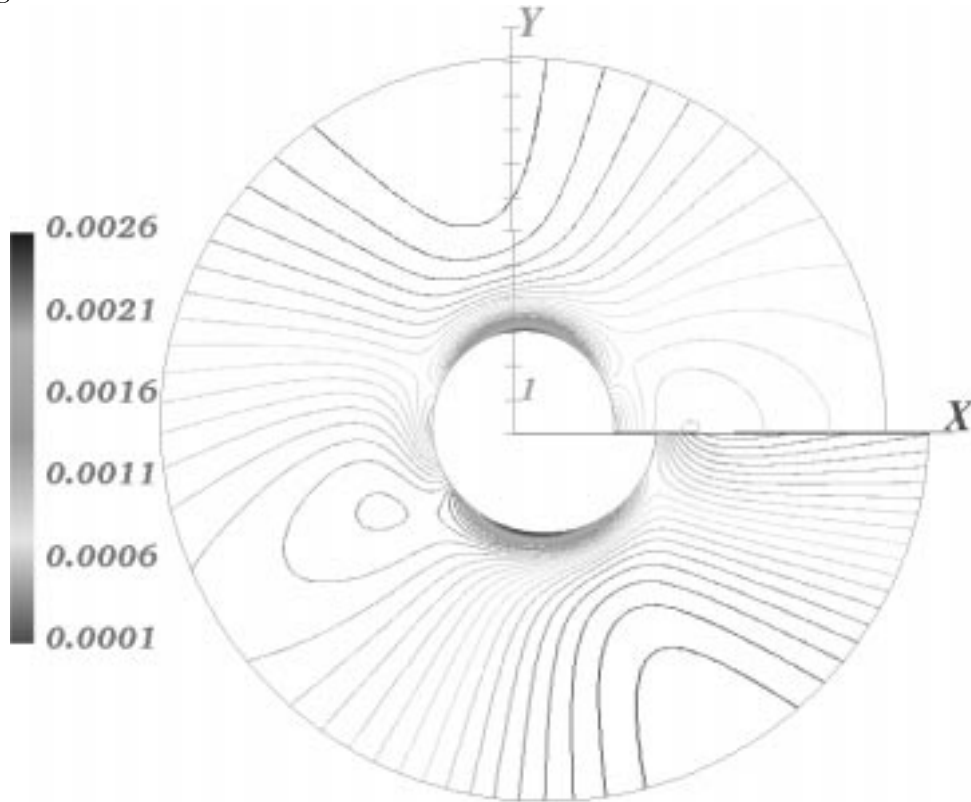


**Fig.4.5.** Isolines [MPa] of the specific energy for changing the shape of the origin body with  $\Omega_1 = 0.1\pi$



## 7 The y-twist disclination

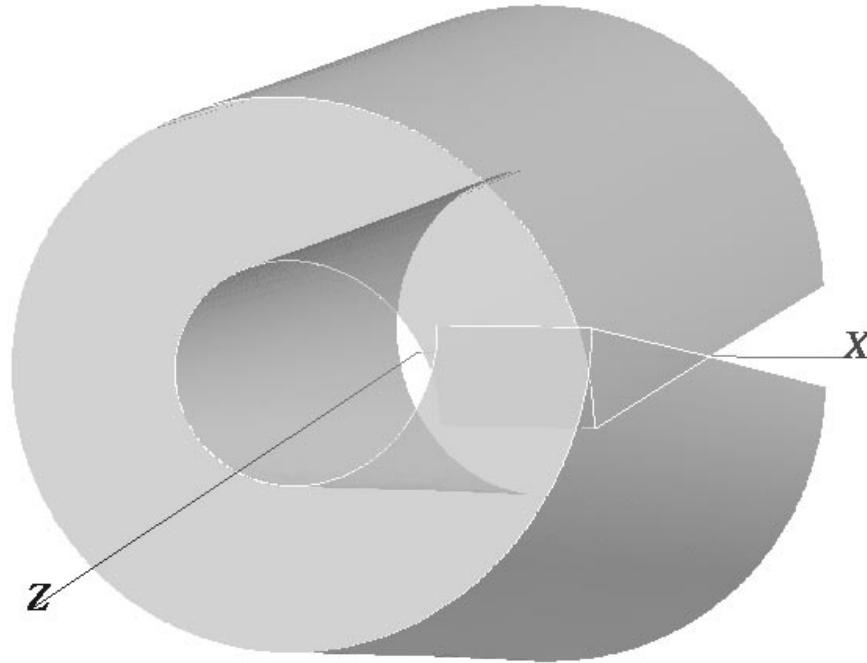


**Fig. 5.1.** The y-twist disclination

In the case of the y-twist disclination is one part of the cutoff cylinder rotated around the x-axis in y-direction. We get this disclination, if we multiply the initial displacement field of the y-edge dislocation with  $z$ . Therefore we choose this name of the presented disclination. Furthermore this is the reason for the analogous structures of the calculated tensors and vector fields with them of the y-edge dislocation. The initial displacement field, which characterizes the disclination and fulfills the St. Venant conditions is given by

$$\begin{aligned} u_x^0 &= 0 \quad , \\ u_y^0 &= \frac{\Omega_2}{2\pi} z \arctan\left(\frac{y}{x}\right) \quad , \\ u_z^0 &= 0 \quad . \end{aligned} \tag{200}$$

The dimensionless constant  $\Omega_2$  depicts the cutoff volume element. The y-twist disclination is shown in fig. 5.1.

The displacement vector  $\vec{u}$  has to undergo a certain finite increment after passage around any closed contour  $s(t)$  that encircles the disclination line. This condition writes here

$$\oint u_k ds_k = \oint u_k(s_k(t)) \frac{\partial s_k(t)}{\partial t} dt = \Omega_2 z \quad , \tag{201}$$

if we parameterize the contour with  $t$ .

The components of this integral calculates with the contour-line  $\vec{s}(t)$  of equation (31) to

$$\begin{aligned} \oint u_x \frac{\partial s_x}{\partial t} dt &= 0 \quad , \\ \oint u_y \frac{\partial s_y}{\partial t} dt &= \frac{\Omega_2}{2\pi} \left( t \sin(t) + \cos(t) \right) z \Big|_{-\pi/2}^{3\pi/2} = \Omega_2 z \quad , \\ \oint u_z \frac{\partial s_z}{\partial t} dt &= 0 \quad . \end{aligned} \tag{202}$$

The strain tensor of the initial displacement field turns out to be

$$\begin{aligned} \mathbf{e}_{xx}^0 &= 0 \quad , \\ \mathbf{e}_{xy}^0 &= -\frac{\Omega_2}{4\pi} \frac{yz}{(x^2 + y^2)} \quad , \\ \mathbf{e}_{xz}^0 &= 0 \quad , \\ \mathbf{e}_{yy}^0 &= \frac{\Omega_2}{2\pi} \frac{xz}{(x^2 + y^2)} \quad , \\ \mathbf{e}_{yz}^0 &= -\frac{\Omega_2}{4\pi} \arctan\left(\frac{y}{x}\right) \quad , \\ \mathbf{e}_{zz}^0 &= 0 \quad . \end{aligned} \tag{203}$$

As the divergence vector field of the strain tensor we have

$$\begin{aligned} \mathbf{e}_{xj}^0{}_{,j} &= -\frac{\Omega_2}{4\pi} \frac{(x^2 - y^2)z}{(x^2 + y^2)^2} \quad , \\ \mathbf{e}_{yj}^0{}_{,j} &= -\frac{\Omega_2}{2\pi} \frac{xyz}{(x^2 + y^2)^2} \quad , \\ \mathbf{e}_{zj}^0{}_{,j} &= \frac{\Omega_2}{4\pi} \frac{x}{(x^2 + y^2)} \quad . \end{aligned} \tag{204}$$

The divergence vector field of the stress tensor is again given by

$$\boldsymbol{\sigma}^0{}_{,j}{}^{ij} = \frac{E}{(1 + \nu)(1 - 2\nu)} \mathbf{e}_{ij}^0{}_{,j} \quad . \tag{205}$$

The displacement field (200) has no divergence-free stress tensor. It needs to be extended by an additional vector field  $\overset{1}{u}$ . We find that for the x- and the y-component of the divergence of the stress tensor the partial differential equation (28) is again solved by the function

$$\overset{1}{W} = x^2 + y^2 \quad , \tag{37}$$

and the constant

$$\overset{1}{w} = -\frac{1}{4\nu - 3} \quad , \tag{38}$$

leading to the additional vector field

$$\begin{aligned} u_x^1 &= \frac{\Omega_2}{4\pi} \frac{1}{(4\nu - 3)} \frac{(x^2 - y^2)z}{x^2 + y^2} \quad , \\ u_y^1 &= \frac{\Omega_2}{2\pi} \frac{1}{(4\nu - 3)} \frac{xyz}{x^2 + y^2} \quad , \\ u_z^1 &= -\frac{\Omega_2}{4\pi} \frac{1}{(4\nu - 3)} x \quad . \end{aligned} \quad (206)$$

The z-component of this displacement field has no influence on the divergence of the stress tensor. We deliver it again and obtain

$$\begin{aligned} u_x^{0+1} &= \frac{\Omega_2}{4\pi} \frac{1}{(4\nu - 3)} \frac{(x^2 - y^2)z}{x^2 + y^2} \quad , \\ u_y^{0+1} &= \frac{\Omega_2}{2\pi} \left( z \arctan\left(\frac{y}{x}\right) + \frac{1}{(4\nu - 3)} \frac{xyz}{x^2 + y^2} \right) \quad , \\ u_z^{0+1} &= 0 \quad . \end{aligned} \quad (207)$$

Like in the case of the x-twist disclination vanishes the x- and the y-component of the divergence of the stress tensor, but the z-component is still unequal zero:

$$\sigma_{,j}^{zj} = -\frac{\Omega_2}{2\pi} \frac{E}{(4\nu - 3)(\nu + 1)} \frac{x}{x^2 + y^2} \quad . \quad (208)$$

The extension of the displacement field of equation (207), which may compensate this divergence, can be calculated by the known equilibrium conditions of eq.(12). They reduce here to:

$$\sum_j \left( \frac{\partial^2 u_z}{\partial x_j^2} \right) = \frac{\Omega_2}{\pi} \frac{1}{(4\nu - 3)} \frac{x}{(x^2 + y^2)} \quad . \quad (209)$$

This partial differential equation is solved by

$$\begin{aligned} u_x^e &= 0 \quad , \\ u_y^e &= 0 \quad , \\ u_z^e &= \frac{\Omega_2}{2\pi} \frac{1}{(4\nu - 3)} y \arctan\left(\frac{y}{x}\right) \quad . \end{aligned} \quad (210)$$

We remark again, that this extensional vector field is proportional to the z-component of the radial normal vector field belonging to the envelope of the cylinder, that is deformed by the initial displacement field. Similar to the x-twist disclination it is an ingredient of the displacement field given by Volterra [20]. The summation of the initial, the additional and the extensional vector fields leads to a displacement field with a divergence-free stress tensor. As shown in the next section, the calculated displacement field fulfills approximately the boundary conditions of a crystal.

### 7.1 The y-twist disclination in a crystal

We take the initial displacement above  $\vec{u}^0$  (eq.(200)), add the calculated additional vector field  $\vec{u}^1$  of eq.(206) and the extensional vector field  $\vec{u}^e$  of eq.(210),

$$\vec{u}^c = \vec{u}^0 + \vec{u}^1 + \vec{u}^e \quad , \quad (211)$$

and derive this way the realistic displacement vector field, which may describe approximately a y-twist disclination in a crystal

$$\begin{aligned} \dot{u}_x^c &= \frac{\Omega_2}{4\pi} \frac{1}{(4\nu - 3)} \frac{(x^2 - y^2)z}{x^2 + y^2} \quad , \\ \dot{u}_y^c &= \frac{\Omega_2}{2\pi} z \left( \arctan\left(\frac{y}{x}\right) + \frac{1}{(4\nu - 3)} \frac{xy}{x^2 + y^2} \right) \quad , \\ \dot{u}_z^c &= \frac{\Omega_2}{2\pi} \frac{1}{4\nu - 3} y \arctan\left(\frac{y}{x}\right) \quad . \end{aligned} \quad (212)$$

The integral along the contour-line  $\vec{s}'(t)$  of eq.(31) has the components

$$\begin{aligned} \oint u_x \frac{\partial s_x}{\partial t} dt &= - \frac{\Omega_2}{12\pi} \frac{1}{(4\nu - 3)} \left( (2 \sin^2(t) + 1) \cos(t) - 1 \right) z \Big|_{-\pi/2}^{3\pi/2} = 0 \quad , \\ \oint u_y \frac{\partial s_y}{\partial t} dt &= \frac{\Omega_2}{6\pi} \frac{1}{(4\nu - 3)} \left( 3(4\nu - 3)t \sin(t) + \sin^2(t) \cos(t) \right. \\ &\quad \left. + (12\nu - 10) \cos(t) + 1 \right) z \Big|_{-\pi/2}^{3\pi/2} = \Omega_2 z \quad , \\ \oint u_z \frac{\partial s_z}{\partial t} dt &= 0 \quad . \end{aligned} \quad (213)$$

The strain tensor of this displacement field calculates to

$$\begin{aligned} \epsilon_{xx} &= \frac{\Omega_2}{\pi} \frac{1}{(4\nu - 3)} \frac{xy^2z}{(x^2 + y^2)^2} \quad , \\ \epsilon_{xy} &= - \frac{\Omega_2}{\pi} \frac{1}{(4\nu - 3)} \frac{yz}{(x^2 + y^2)^2} \left( \nu(x^2 + y^2) - y^2 \right) \quad , \\ \epsilon_{xz} &= \frac{\Omega_2}{8\pi} \frac{1}{(4\nu - 3)} \frac{(x^2 - 3y^2)}{(x^2 + y^2)} \quad , \\ \epsilon_{yy} &= \frac{\Omega_2}{\pi} \frac{1}{(4\nu - 3)} \frac{xz}{(x^2 + y^2)^2} \left( 2\nu(x^2 + y^2) - x^2 - 2y^2 \right) \quad , \\ \epsilon_{yz} &= \frac{\Omega_2}{2\pi} \frac{1}{(4\nu - 3)} \left( (2\nu - 1) \arctan\left(\frac{y}{x}\right) + \frac{xy}{(x^2 + y^2)} \right) \quad , \\ \epsilon_{zz} &= 0 \quad . \end{aligned} \quad (214)$$

with the trace

$$\epsilon_k^k = \frac{\Omega_2}{\pi} \frac{2\nu - 1}{(4\nu - 3)} \frac{xz}{x^2 + y^2} \quad . \quad (215)$$

Its divergence is given by

$$\begin{aligned}\boldsymbol{\varepsilon}_{xj}{}^{,j} &= -\frac{\Omega_2}{\pi} \frac{\nu}{(4\nu-3)} \frac{(x^2-y^2)z}{(x^2+y^2)^2} \quad , \\ \boldsymbol{\varepsilon}_{yj}{}^{,j} &= -\frac{\Omega_2}{\pi} \frac{2\nu}{(4\nu-3)} \frac{xyz}{(x^2+y^2)^2} \quad , \\ \boldsymbol{\varepsilon}_{zj}{}^{,j} &= \frac{\Omega_2}{\pi} \frac{\nu}{(4\nu-3)} \frac{x}{(x^2+y^2)} \quad .\end{aligned}\tag{216}$$

We find again the proportionality relation with the divergence of the strain tensor of the initial displacement field of eq. (204)

$$\boldsymbol{\varepsilon}_{xj}{}^{,j} = \frac{4\nu}{(4\nu-3)} \mathbf{0}_{xj}{}^{,j} \quad .\tag{217}$$

We calculate the stress tensor by means of Hooke's law

$$\begin{aligned}\boldsymbol{\sigma}_{xx} &= -\frac{\Omega_2}{\pi} \frac{E}{(4\nu-3)(\nu+1)} \frac{(\nu(x^2+y^2)-y^2)xz}{(x^2+y^2)^2} \quad , \\ \boldsymbol{\sigma}_{xy} &= -\frac{\Omega_2}{\pi} \frac{E}{(4\nu-3)(\nu+1)} \frac{yz}{(x^2+y^2)^2} (\nu(x^2+y^2)-y^2) \quad , \\ \boldsymbol{\sigma}_{xz} &= \frac{\Omega_2}{8\pi} \frac{E}{(4\nu-3)(\nu+1)} \frac{(x^2-3y^2)}{(x^2+y^2)} \quad , \\ \boldsymbol{\sigma}_{yy} &= \frac{\Omega_2}{\pi} \frac{E}{(4\nu-3)(\nu+1)} \frac{xz}{(x^2+y^2)^2} (\nu(x^2+y^2)-x^2-2y^2) \quad , \\ \boldsymbol{\sigma}_{yz} &= \frac{\Omega_2}{2\pi} \frac{E}{(4\nu-3)(\nu+1)} \left( (2\nu-1) \arctan\left(\frac{y}{x}\right) + \frac{xy}{(x^2+y^2)} \right) \quad , \\ \boldsymbol{\sigma}_{zz} &= -\frac{\Omega_2}{\pi} \frac{E\nu}{(4\nu-3)(\nu+1)} \frac{xz}{(x^2+y^2)} \quad ,\end{aligned}\tag{218}$$

with the trace

$$\boldsymbol{\sigma}_k{}^k = -\frac{\Omega_2}{\pi} \frac{E}{(4\nu-3)} \frac{xz}{x^2+y^2} = -\frac{E}{(2\nu-1)} \boldsymbol{\varepsilon}_k{}^k \quad .\tag{219}$$

The stress tensor is divergence-free. The x-component of the divergence of the stress tensor vanishes according to

$$\boldsymbol{\sigma}^{x1}{}_{,1} = -\boldsymbol{\sigma}^{x2}{}_{,2} = \frac{\Omega_2}{\pi} \frac{E}{(4\nu-3)(\nu+1)} \frac{(\nu(x^4-y^4)-3x^2y^2+y^4)z}{(x^2+y^2)^3} \quad ,\tag{220}$$

the y-component according to

$$\boldsymbol{\sigma}^{y1}{}_{,1} = -\boldsymbol{\sigma}^{y2}{}_{,2} = \frac{\Omega_2}{\pi} \frac{E}{(4\nu-3)(\nu+1)} \frac{2xyz(\nu(x^2+y^2)-2y^2)}{(x^2+y^2)^3} \quad ,\tag{221}$$

and the z-component according to

$$-\boldsymbol{\sigma}^{z1}{}_{,1} = \boldsymbol{\sigma}^{z2}{}_{,2} + \boldsymbol{\sigma}^{z3}{}_{,3} \quad ,\tag{222}$$

with

$$\begin{aligned}
\sigma^{z1}{}_{,1} &= \frac{\Omega_2}{\pi} \frac{E}{(4\nu-3)(\nu+1)} \frac{xy^2}{(x^2+y^2)^2} \quad , \\
\sigma^{z2}{}_{,2} &= \frac{\Omega_2}{\pi} \frac{E}{(4\nu-3)(\nu+1)} \frac{x(\nu(x^2+y^2)-y^2)}{(x^2+y^2)^2} \quad , \\
\sigma^{z3}{}_{,1} &= -\frac{\Omega_2}{\pi} \frac{E\nu}{(4\nu-3)(\nu+1)} \frac{x}{(x^2+y^2)} \quad .
\end{aligned} \tag{223}$$

In cylindrical coordinates the stress tensor writes

$$\begin{aligned}
\sigma^{rr} &= -\frac{\Omega_2}{\pi} \frac{E\nu}{(4\nu-3)(\nu+1)} \frac{\cos(\varphi)}{r} z \quad , \\
\sigma^{r\varphi} &= \frac{\Omega_2}{\pi} \frac{E(\nu-1)}{(4\nu-3)(\nu+1)} \frac{\sin(\varphi)}{r} z \quad , \\
\sigma^{rz} &= \frac{\Omega_2}{8\pi} \frac{E}{(4\nu-3)(\nu+1)} \left( 4(2\nu-1)\varphi \sin(\varphi) + \cos(\varphi) \right) \quad , \\
\sigma^{\varphi\varphi} &= \frac{\Omega_2}{\pi} \frac{E(\nu-1)}{(4\nu-3)(\nu+1)} \frac{\cos(\varphi)}{r} z \quad , \\
\sigma^{\varphi z} &= \frac{\Omega_2}{8\pi} \frac{E}{(4\nu-3)(\nu+1)} \left( 4(2\nu-1)\varphi \cos(\varphi) + 3 \sin(\varphi) \right) \quad , \\
\sigma^{zz} &= -\frac{\Omega_2}{\pi} \frac{E\nu}{(4\nu-3)(\nu+1)} \frac{\cos(\varphi)}{r} z \quad .
\end{aligned} \tag{224}$$

Next we will examine the sum of the stress vector fields belonging to the normal vector field of the envelope of the cylinder, and to the normal vector field in the direction of the z-axis. We approximate for reasons of simplicity both stress vector fields by relating them to the origin undeformed body. The resulting stress vector field turns out to

$$\begin{aligned}
f_x &= \frac{\Omega_2}{8\pi} \frac{E}{(4\nu-3)(\nu+1)} \frac{8z(\nu(x^2+y^2)-y^2) - \sqrt{(x^2+y^2)}(x^2-3y^2)}{\sqrt{(x^2+y^2)}(x^2+y^2)} \quad , \\
f_y &= \frac{\Omega_2}{2\pi} \frac{E}{(4\nu-3)(\nu+1)} \frac{\sqrt{(x^2+y^2)}\left((2\nu-1)(x^2+y^2) \arctan(y/x) + xy\right) + 2xyz}{\sqrt{(x^2+y^2)}(x^2+y^2)} \quad , \\
f_z &= -\frac{\Omega_2}{8\pi} \frac{E}{(4\nu-3)(\nu+1)} \frac{\sqrt{(x^2+y^2)}\left(4(2\nu-1)y \arctan(y/x) + x\right) + 8\nu xz}{(x^2+y^2)} \quad .
\end{aligned} \tag{225}$$

With the approximation of a plane state of stress we neglect the z-component of the stress vector. The resulting vector field of the x-y-plane is plotted in fig. 5.2a, the isolines of the amount of the stress vector can be inspected in fig 5.2b.



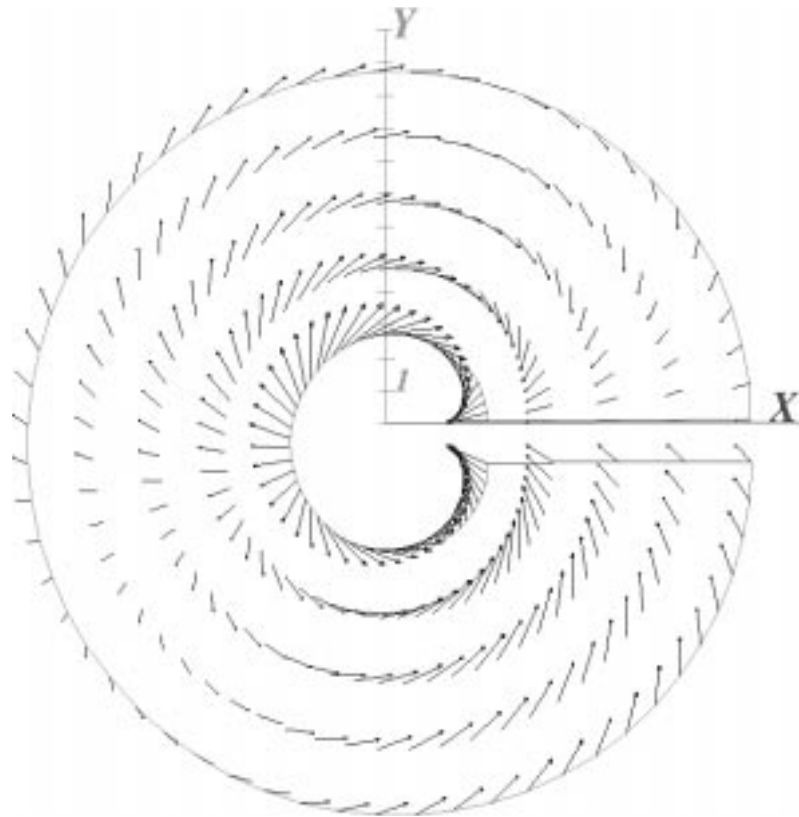


**Fig. 5.2a.** Stress vector field around an  $y$ -twist disclination in a crystal for  $\Omega_2 = 0.1\pi$  and  $z = 4$

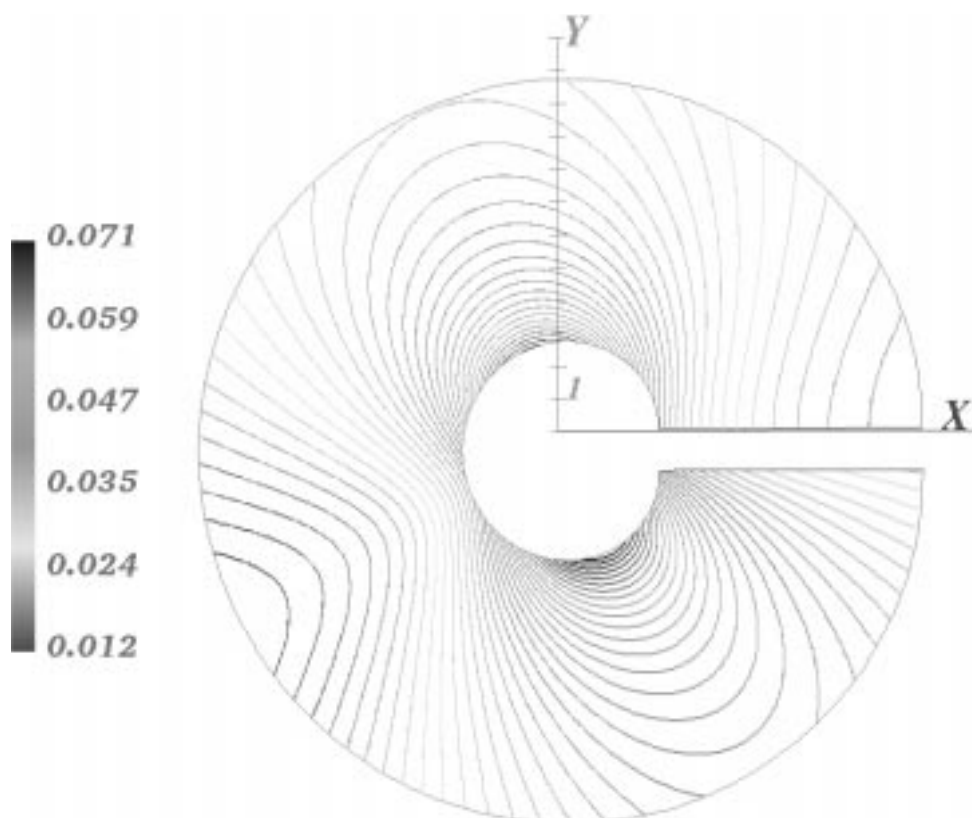


**Fig. 5.2b.** Isolines [MPa] of the amount of the stress vector field around an  $y$ -twist disclination in a crystal for  $z = 4$

We depict for an detailed examination of the stress vector field the x-axis and the y-axis. The amount of the stress vector field above reads at the x-axis

$$|\vec{f}| \Big|_{(\varphi=0)} = \frac{\Omega_2}{8\pi} \frac{E}{(4\nu-3)(\nu+1)} \frac{8\nu z + r}{r} \quad . \quad (226)$$

It rises for  $r \rightarrow 0$  and  $z \neq 0$  to infinity and leads for  $r \rightarrow \infty$  to a factor depending on  $z$ . The same behavior shows the amount at the y-axis:

$$|\vec{f}| \Big|_{(\varphi=\pi/2)} = \frac{\Omega_2}{8\pi} \frac{E}{(4\nu-3)(\nu+1)} \frac{1}{r} \sqrt{9r^2 + 4(2\nu-1)^2\pi^2 r^2 - 48(\nu-1)rz - 64z^2(\nu^2 - (2\nu-1))} \quad . \quad (227)$$

If we make the inner radius small enough, we can neglect the stress vector at the outer radius in relation to the huge stresses in the center. We think, that the displacement field presented can be interpreted as approximately analogous to a crystal defect.

The specific energy for changing the shape of the origin body calculates to

$$\begin{aligned} \tilde{U}_F = & \frac{\Omega_2^2}{192\pi^2} \frac{E}{(4\nu-3)^2(\nu+1)} \frac{1}{(x^2+y^2)^2} \\ & \times \left( 48(2\nu-1)(x^2+y^2) \arctan\left(\frac{y}{x}\right) \left( (2\nu-1)(x^2+y^2) \arctan\left(\frac{y}{x}\right) + 2xy \right) \right. \\ & \quad + 64\nu^2(4x^2+3y^2)z^2 - 128\nu(2x^2+3y^2)z^2 \\ & \quad \left. + 2x^2(15y^2+32z^2) + 3x^4 + 27y^4 + 192y^2z^2 \right) \quad , \quad (228) \end{aligned}$$

and is plotted in fig. 5.3.

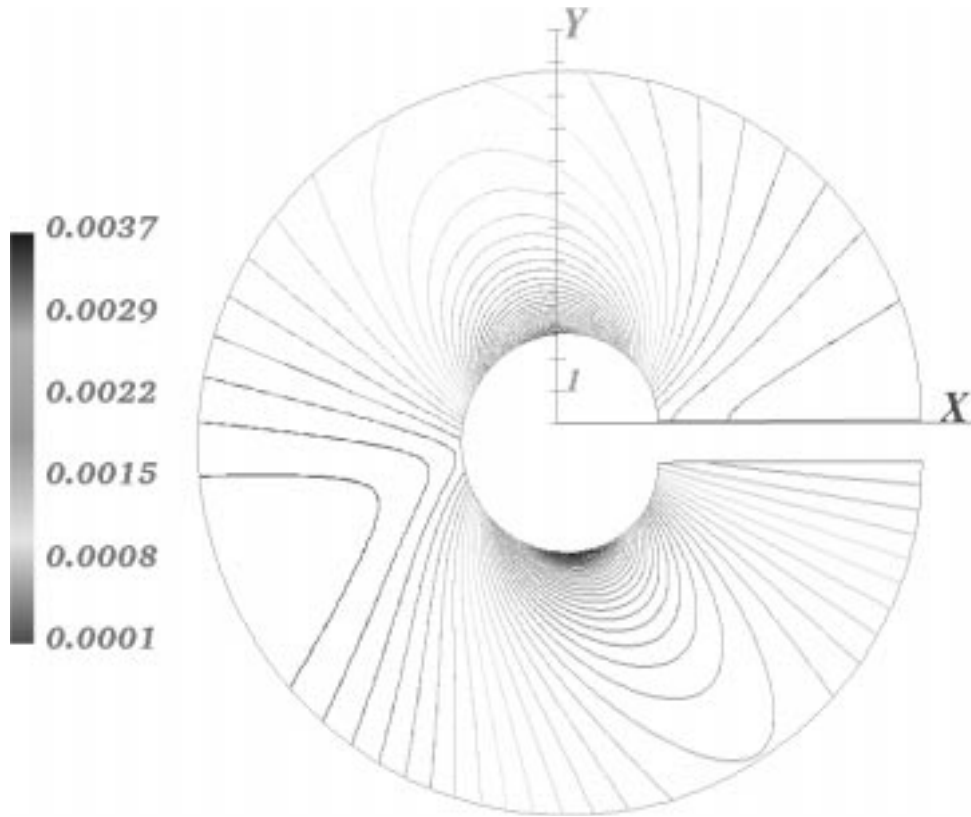


**Fig.5.3.** Isolines [MPa] of the specific energy for changing the shape of the origin body with  $\Omega_2 = 0.1\pi$  for  $z = 4$

The isolines of the amount of the stress vector field shows again approximately the same course.

## 7.2 The y-twist disclination of a tubular cylinder

The stress vector field of a tubular cylinder has to vanish at the inner radius  $r_1$  and at the outer radius  $r_2$ . Like done before in section 3.2 or in section 6.2 we add an additional vector field to the realistic displacement in a crystal  $\vec{u}^c$  eq.(212). This leads to the following ansatz for the displacement field of a y-twist disclination of a tubular cylinder

$$\begin{aligned}
 {}^t u_x &= \frac{\Omega_2}{4\pi} \frac{1}{(4\nu - 3)} \frac{(x^2 - y^2)z}{(x^2 + y^2)} \left(1 - \frac{w}{(x^2 + y^2)}\right) \quad , \\
 {}^t u_y &= \frac{\Omega_2}{2\pi} z \left( \arctan\left(\frac{y}{x}\right) + \frac{1}{(4\nu - 3)} \frac{xy}{(x^2 + y^2)} \left(1 - \frac{w}{(x^2 + y^2)}\right) \right) \quad , \\
 {}^t u_z &= \frac{\Omega_2}{2\pi} \frac{1}{(4\nu - 3)} y \arctan\left(\frac{y}{x}\right) \quad .
 \end{aligned} \tag{229}$$

The integral (201) along the contour-line  $\vec{s}(t)$  of eq.(31) has here the components

$$\begin{aligned} \oint u_x \frac{\partial s_x}{\partial t} dt &= \frac{\Omega_2}{12\pi} \frac{1}{(4\nu - 3)} (\overset{2}{w} - 1) \left( (2 \sin^2(t) + 1) \cos(t) - 1 \right) z \Big|_{-\pi/2}^{3\pi/2} = 0 \quad , \\ \oint u_y \frac{\partial s_y}{\partial t} dt &= \frac{\Omega_2}{6\pi} \frac{1}{(4\nu - 3)} \left( 3(4\nu - 3)t \sin(t) - (\overset{2}{w} - 1) \sin^2(t) \cos(t) \right. \\ &\quad \left. + \cos(t)(\overset{2}{w} + 12\nu - 10) - \overset{2}{w} + 1 \right) z \Big|_{-\pi/2}^{3\pi/2} = \Omega_2 z \quad , \\ \oint u_z \frac{\partial s_z}{\partial t} dt &= 0 \quad . \end{aligned} \tag{230}$$

They are independent of  $\overset{2}{w}$ . The passage around the closed contour-line leads for every constant  $\overset{2}{w}$  to the increment  $\Omega_2 z$ .

We determine the constant  $\overset{2}{w}$  again in retrospect to the  $\sigma^{rr}$ -component of the stress tensor in cylindrical coordinates

$$\begin{aligned} \sigma^{rr} &= \frac{\Omega_2}{2\pi} \frac{E}{(4\nu - 3)(\nu + 1)} z \left( \overset{2}{w} - 2\nu r^2 \right) \frac{\cos(\varphi)}{r^3} \quad , \\ \sigma^{r\varphi} &= \frac{\Omega_2}{2\pi} \frac{E}{(4\nu - 3)(\nu + 1)} z \left( \overset{2}{w} + 2(\nu - 1)r^2 \right) \frac{\sin(\varphi)}{r^3} \quad , \\ \sigma^{rz} &= \frac{\Omega_2}{8\pi} \frac{E}{(4\nu - 3)(\nu + 1)} \left( 4(2\nu - 1)\varphi \sin(\varphi) - \left( \frac{\overset{2}{w}}{r^2} - 1 \right) \cos(\varphi) \right) \quad , \\ \sigma^{\varphi\varphi} &= -\frac{\Omega_2}{2\pi} \frac{E}{(4\nu - 3)(\nu + 1)} z \left( \overset{2}{w} - 2(\nu - 1)r^2 \right) \frac{\cos(\varphi)}{r^3} \quad , \\ \sigma^{\varphi z} &= \frac{\Omega_2}{8\pi} \frac{E}{(4\nu - 3)(\nu + 1)} \left( 4(2\nu - 1)\varphi \cos(\varphi) - \left( \frac{\overset{2}{w}}{r^2} - 3 \right) \sin(\varphi) \right) \quad , \\ \sigma^{zz} &= -\frac{\Omega_2}{\pi} \frac{E\nu}{(4\nu - 3)(\nu + 1)} z \frac{\cos(\varphi)}{r} \quad . \end{aligned} \tag{231}$$

It is not possible to choose  $\overset{2}{w}$  in a way that all radial components of the stress tensor  $\sigma^{rr}$ ,  $\sigma^{r\varphi}$  and  $\sigma^{rz}$  disappear. This is the reason why we get only an approximately vanishing stress vector field at the inner and at the outer radius of the cylinder. We choose again

$$\overset{2}{w} = 2\nu r_1^2 \quad , \tag{232}$$

so  $\sigma^{rr}$  becomes zero for  $r = r_1$  and the displacement field of the y-twist disclination of a tubular cylinder writes

$$\begin{aligned} u_x &= \frac{\Omega_2}{4\pi} \frac{1}{(4\nu - 3)} \frac{x^2 - y^2}{(x^2 + y^2)} z \left( 1 - \frac{2\nu r_1^2}{(x^2 + y^2)} \right) \quad , \\ u_y &= \frac{\Omega_2}{2\pi} z \left( \arctan\left(\frac{y}{x}\right) + \frac{1}{(4\nu - 3)} \frac{xy}{(x^2 + y^2)} \left( 1 - \frac{2\nu r_1^2}{(x^2 + y^2)} \right) \right) \quad , \\ u_z &= \frac{\Omega_2}{2\pi} \frac{1}{(4\nu - 3)} y \arctan\left(\frac{y}{x}\right) \quad . \end{aligned} \tag{233}$$

The belonging strain tensor

$$\begin{aligned}
\epsilon_{xx} &= \frac{\Omega_2}{\pi} \frac{xz}{(4\nu - 3)} \frac{1}{(x^2 + y^2)^3} \left( \nu r_1^2 (x^2 - 3y^2) + x^2 y^2 + y^4 \right) , \\
\epsilon_{xy} &= \frac{\Omega_2}{\pi} \frac{yz}{(4\nu - 3)} \frac{1}{(x^2 + y^2)^3} \left( \nu \left( r_1^2 (3x^2 - y^2) - (x^2 + y^2)^2 \right) + x^2 y^2 + y^4 \right) , \\
\epsilon_{xz} &= -\frac{\Omega_2}{8\pi} \frac{1}{(4\nu - 3)} \frac{1}{(x^2 + y^2)^2} \left( (2\nu r_1^2 - (x^2 + y^2)(x^2 - y^2) + 2y^2(x^2 + y^2)) \right) , \\
\epsilon_{yy} &= -\frac{\Omega_2}{\pi} \frac{1}{(4\nu - 3)} \frac{xz}{(x^2 + y^2)^3} \\
&\quad \times \left( \nu \left( r_1^2 (x^2 - 3y^2) - 2(x^2 + y^2)^2 \right) + x^4 + 3x^2 y^2 + 2y^4 \right) , \\
\epsilon_{yz} &= \frac{\Omega_2}{4\pi} \frac{1}{(4\nu - 3)} \left( (4\nu - 2) \arctan\left(\frac{y}{x}\right) - \frac{xy}{(x^2 + y^2)} \left( \frac{2\nu r_1^2}{(x^2 + y^2)} - 2 \right) \right) , \\
\epsilon_{zz} &= 0 ,
\end{aligned} \tag{234}$$

has the same trace as in the case analogous to a crystal (eq.(215) ) and its divergence is the same as in eq.(216).

The stress tensor follows by means of Hooke's law

$$\begin{aligned}
\sigma^{xx} &= \frac{\Omega_2}{\pi} \frac{E}{(4\nu - 3)(\nu + 1)} \frac{xz}{(x^2 + y^2)^3} \left( \nu \left( r_1^2 (x^2 - 3y^2) - (x^2 + y^2)^2 \right) + x^2 y^2 + y^4 \right) , \\
\sigma^{xy} &= \frac{\Omega_2}{\pi} \frac{E}{(4\nu - 3)(\nu + 1)} \frac{yz}{(x^2 + y^2)^3} \left( \nu \left( r_1^2 (3x^2 - y^2) - (x^2 + y^2)^2 \right) + x^2 y^2 + y^4 \right) , \\
\sigma^{xz} &= -\frac{\Omega_2}{8\pi} \frac{E}{(4\nu - 3)(\nu + 1)} \frac{1}{(x^2 + y^2)^2} \left( \left( \frac{2\nu r_1^2}{(x^2 + y^2)} - 1 \right) (x^2 - y^2) + 2y^2 \right) , \\
\sigma^{yy} &= -\frac{\Omega_2}{\pi} \frac{E}{(4\nu - 3)(\nu + 1)} \frac{xz}{(x^2 + y^2)^3} \\
&\quad \times \left( \nu \left( r_1^2 (x^2 - 3y^2) - (x^2 + y^2)^2 \right) + x^4 + 3x^2 y^2 + 2y^4 \right) , \\
\sigma^{yz} &= \frac{\Omega_2}{4\pi} \frac{E}{(4\nu - 3)(\nu + 1)} \left( (4\nu - 2) \arctan\left(\frac{y}{x}\right) - \frac{xy}{(x^2 + y^2)} \left( \frac{2\nu r_1^2}{(x^2 + y^2)} - 2 \right) \right) , \\
\sigma^{zz} &= -\frac{\Omega_2}{\pi} \frac{E\nu}{(4\nu - 3)(\nu + 1)} \frac{xz}{(x^2 + y^2)} .
\end{aligned} \tag{235}$$

Its trace is again the same as in the case of the displacement analogous to a crystal (eq.(219)). The stress tensor is divergence-free. The  $x$ -component of the divergence of the

stress tensor vanishes according to

$$\begin{aligned} \sigma^{x^1}_{,1} = -\sigma^{x^2}_{,2} &= -\frac{\Omega_2}{\pi} \frac{E}{(4\nu-3)(\nu+1)} \frac{z}{(x^2+y^2)^4} \\ &\times \left( \nu \left( 3r_1^2(x^4 - 6x^2y^2 + y^4) - x^6 - x^4y^2 + x^2y^4 + y^6 \right) \right. \\ &\quad \left. + 3x^4y^2 + 2x^2y^4 - y^6 \right) , \end{aligned} \quad (236)$$

the y-component according to

$$\begin{aligned} \sigma^{y^1}_{,1} = -\sigma^{y^2}_{,2} &= -\frac{\Omega_2}{\pi} \frac{2E}{(4\nu-3)(\nu+1)} \frac{xyz}{(x^2+y^2)^4} \\ &\times \left( \nu \left( 6r_1^2(x^2 - y^2) - (x^2 + y^2)^2 \right) + 2x^2y^2 + 2y^4 \right) , \end{aligned} \quad (237)$$

and the z-component according to

$$\sigma^{z^1}_{,1} + \sigma^{z^2}_{,2} = -\sigma^{z^3}_{,3} , \quad (238)$$

with

$$\begin{aligned} \sigma^{z^1}_{,1} &= \frac{\Omega_2}{2\pi} \frac{E}{(4\nu-3)(\nu+1)} \frac{x}{(x^2+y^2)^3} \left( \nu r_1^2(x^2 - 3y^2) + 2x^2y^2 + 2y^4 \right) , \\ \sigma^{z^2}_{,2} &= -\frac{\Omega_2}{2\pi} \frac{E}{(4\nu-3)(\nu+1)} \frac{x}{(x^2+y^2)^3} \\ &\times \left( \nu \left( r_1^2(x^2 - 3y^2) - 2(x^2 + y^2)^2 \right) + 2x^2y^2 + 2y^4 \right) , \\ \sigma^{z^3}_{,1} &= -\frac{\Omega_2}{\pi} \frac{E\nu}{(4\nu-3)(\nu+1)} \frac{x}{(x^2+y^2)} . \end{aligned} \quad (239)$$

In cylindrical coordinates the stress tensor of the y-twist disclination of a tubular cylinder reads

$$\begin{aligned} \sigma^{rr} &= \frac{\Omega_2}{\pi} \frac{E\nu}{(4\nu-3)(\nu+1)} z \left( r_1^2 - r^2 \right) \frac{\cos(\varphi)}{r^3} , \\ \sigma^{r\varphi} &= \frac{\Omega_2}{\pi} \frac{E}{(4\nu-3)(\nu+1)} z \left( \nu r_1^2 + (\nu-1)r^2 \right) \frac{\sin(\varphi)}{r^3} , \\ \sigma^{rz} &= \frac{\Omega_2}{8\pi} \frac{E}{(4\nu-3)(\nu+1)} \left( 4(2\nu-1)\varphi \sin(\varphi) - \left( \frac{2\nu r_1^2}{r^2} - 1 \right) \cos(\varphi) \right) , \\ \sigma^{\varphi\varphi} &= -\frac{\Omega_2}{\pi} \frac{E}{(4\nu-3)(\nu+1)} z \left( \nu r_1^2 - (\nu-1)r^2 \right) \frac{\cos(\varphi)}{r^3} , \\ \sigma^{\varphi z} &= \frac{\Omega_2}{8\pi} \frac{E}{(4\nu-3)(\nu+1)} \left( 4(2\nu-1)\varphi \cos(\varphi) - \left( \frac{2\nu r_1^2}{r^2} - 3 \right) \sin(\varphi) \right) , \\ \sigma^{zz} &= -\frac{\Omega_2}{\pi} \frac{E\nu}{(4\nu-3)(\nu+1)} z \frac{\cos(\varphi)}{r} . \end{aligned} \quad (240)$$

We found the following sum of the stress vector fields belonging to the normal vector fields of the undeformed cylinder

$$\begin{aligned}
f_x &= -\frac{\Omega_2}{8\pi} \frac{E}{(4\nu-3)(\nu+1)} \frac{1}{(x^2+y^2)} \left( \left( \frac{2\nu r_1^2}{(x^2+y^2)} - 1 \right) (x^2 - y^2) + 2y^2 \right. \\
&\quad \left. + \frac{8z}{\sqrt{(x^2+y^2)}(x^2+y^2)} \left[ \nu \left( (x^2 - y^2)r_1^2 - (x^2 + y^2)^2 \right) + x^2 y^2 + y^4 \right] \right) \\
f_y &= \frac{\Omega_2}{4\pi} \frac{E}{(4\nu-3)(\nu+1)} \left( 2(2\nu-1) \arctan(y/x) - \frac{xy}{(x^2+y^2)} \left( \frac{2\nu r_1^2}{(x^2+y^2)} - 2 \right) \right. \\
&\quad \left. - \frac{4xyz}{\sqrt{(x^2+y^2)}} \left( \frac{2\nu r_1^2}{(x^2+y^2)} - 1 \right) \right) , \\
f_z &= -\frac{\Omega_2}{8\pi} \frac{E}{(4\nu-3)(\nu+1)} \left( 4(2\nu-1) \frac{y}{\sqrt{(x^2+y^2)}} \arctan(y/x) \right. \\
&\quad \left. + 8\nu \frac{xz}{(x^2+y^2)} - \frac{x}{\sqrt{(x^2+y^2)}} \left( \frac{2\nu r_1^2}{(x^2+y^2)} - 1 \right) \right) . \tag{241}
\end{aligned}$$

We neglect again the z-component of this vector field. The resulting vectors are plotted in fig. 5.4a and the isolines of the amount of the stress vector field are depicted in fig. 5.4b.

To get more information about the amount of the stress vector field we examine its behavior at the x-axis, where it reads

$$\begin{aligned}
|\vec{f}| \Big|_{(\varphi=0)} &= \frac{\Omega_2}{8\pi} \frac{E}{(4\nu-3)(\nu+1)} \frac{1}{r^3} \\
&\quad \left( r^6 + 4\nu^2 \left( r_1^4 (r^2 + 16z^2) - 16r^2 z^2 (2r_1^2 - r^2) \right) \right. \\
&\quad \left. + 16\nu r z (2\nu r_1^2 - r^2) (r_1^2 - r^2) - 4\nu r_1^2 r^4 \right)^{1/2} , \tag{242}
\end{aligned}$$

which becomes at the inner radius

$$|\vec{f}| \Big|_{(r=r_1)(\varphi=0)} = \frac{\Omega_2}{8\pi} \frac{E(2\nu-1)}{(4\nu-3)(\nu+1)} , \tag{243}$$

where it is constant. This amount leads for  $r \rightarrow \infty$  and even for  $r = r_1$  to a constant. The isolines of the amount of the stress vector field (fig 5.4b) shows some similarities to the y-edge dislocation (fig 2.5b, page 46). We think that, with regard to the done approximations, the displacement field presented (eq.(233)) may be interpreted as approximately analogous to a tubular cylinder, if we neglect the area around the slip plane.

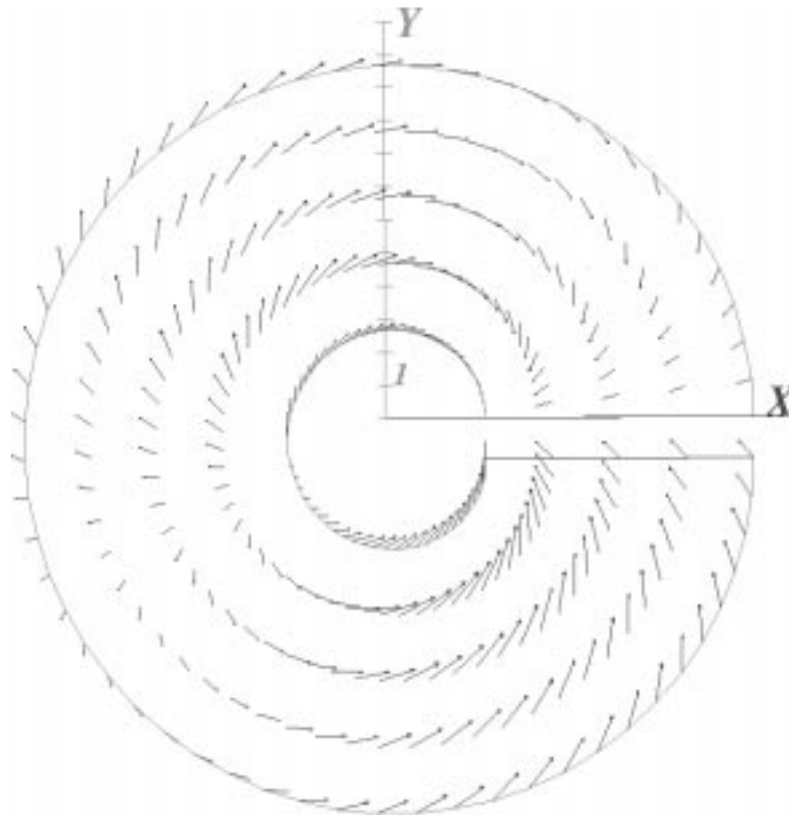


Fig. 5.4a. Stress vector field of a tubular cylinder for  $\Omega_2 = 0.1\pi$  and  $z = 4$

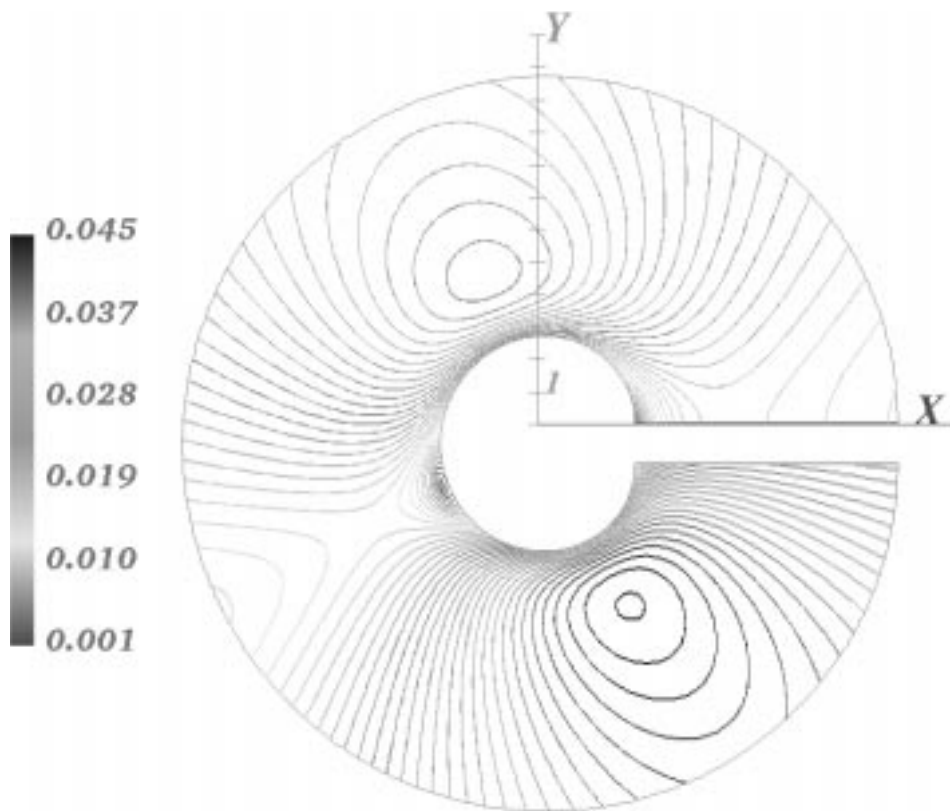


Fig. 5.4b. Isolines [MPa] of the amount of the stress vector field of a tubular cylinder for  $\Omega_2 = 0.1\pi$  and  $z = 4$



The specific energy for changing the shape of the origin body calculates to:

$$\begin{aligned} \tilde{U}_F = & -\frac{\Omega_2^2}{192\pi^2} \frac{2E}{(4\nu-3)^2(\nu+1)} \frac{1}{(x^2+y^2)^3} \\ & \times \left( 4\nu \left[ 3r_1^2 \left( x^4 + 4x^2(y^2 - 4z^2) + 3y^4 + 32y^2z^2 \right) + 16z^2 \left( 4x^4 + 10x^2y^2 + 6y^4 \right) \right] \right. \\ & - 4\nu^2 \left[ 3r_1^4 \left( x^2 + y^2 + 16z^2 \right) + 16z^2 \left( -6r_1^2(x^2 - y^2) + 4x^4 + 7x^2y^2 + 3y^4 \right) \right] \\ & - 48(2\nu-1)^2(x^2+y^2)^3 \arctan^2(y/x) \\ & + 96xy(2\nu-1)(x^2+y^2)(\nu r_1^2 - (x^2+y^2)) \arctan(y/x) \\ & \left. - x^2y^2(57y^2 + 256z^2) - x^4(33y^2 + 64z^2) - 3x^6 - 27y^6 - 192y^4z^2 \right) . \end{aligned} \quad (244)$$

This is shown in fig 5.5.

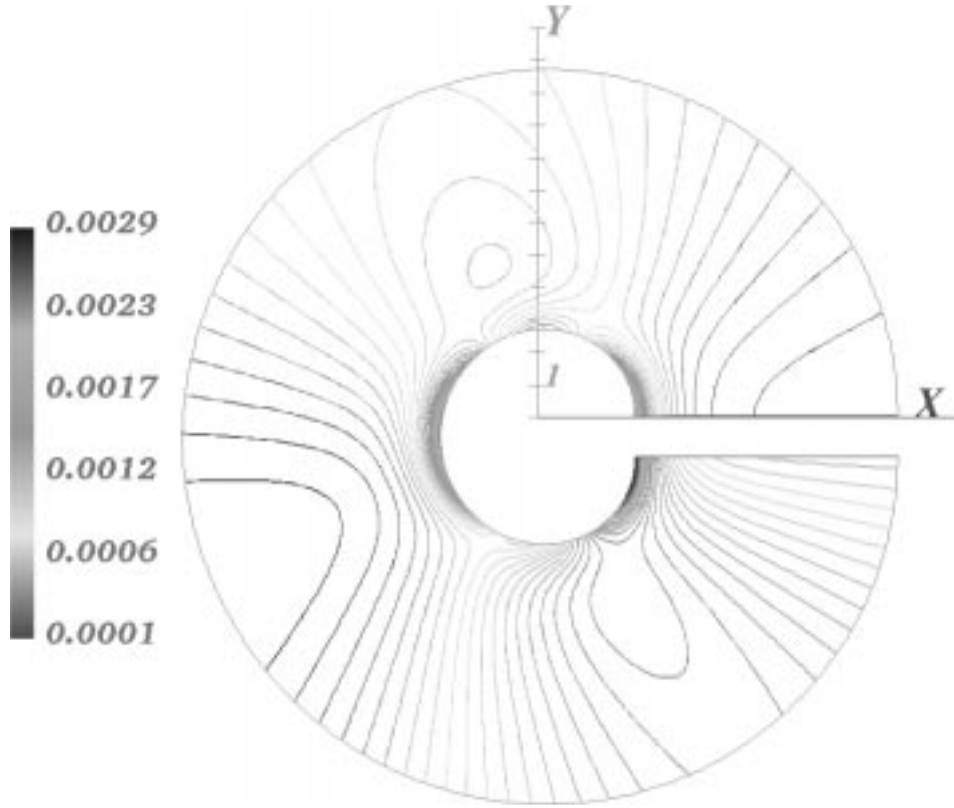


**Fig.5.5.** Isolines [MPa] of the specific energy for changing the shape of the origin body with  $\Omega_2 = 0.1\pi$  and  $z = 4$

The isolines of the amount of the stress vector shows again approximately an analogous course.



## 8 The wedge disclination

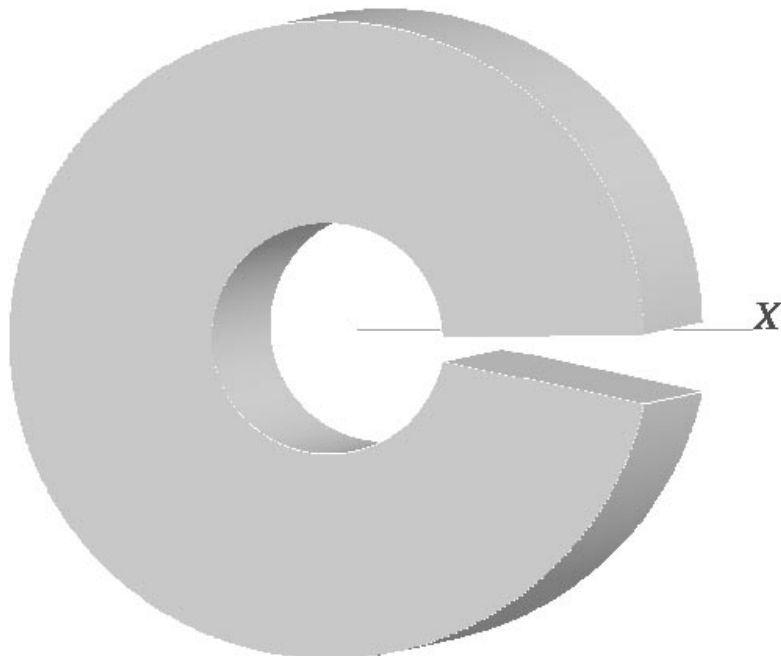


**Fig. 6.1.** The approximation of the wedge disclination

The removing or adding of a volume element with a constant angle is called a wedge disclination.

It is characterized by the following initial displacement field

$$\begin{aligned}
 {}^0u_x &= \sqrt{x^2 + y^2} \left( \cos \left( \arctan\left(\frac{y}{x}\right) \left(1 + \frac{\Omega_3}{2\pi}\right) \right) - x \right) , \\
 {}^0u_y &= \sqrt{x^2 + y^2} \left( \sin \left( \arctan\left(\frac{y}{x}\right) \left(1 + \frac{\Omega_3}{2\pi}\right) \right) - y \right) , \\
 {}^0u_z &= 0 .
 \end{aligned} \tag{245}$$

The dimensionless constant  $\Omega_3$  depicts the cutoff volume element. This displacement field doesn't fulfill the equilibrium conditions. We don't succeed in solving the differential equation (28) to calculate a displacement field with a divergence-free stress tensor. It is very hard to find a displacement which describes the problem and fulfills the equilibrium conditions. Therefore Volterra approximated the initial displacement field above and gave the following solution of a displacement field with a divergence-free stress tensor

$$\begin{aligned}
 {}^V u_x &= \frac{\Omega_3}{2\pi} \left( y \arctan\left(\frac{y}{x}\right) - x \frac{2\nu - 1}{4(\nu - 1)} \ln\left(\frac{x^2 + y^2}{R_0^2}\right) \right) , \\
 {}^V u_y &= \frac{\Omega_3}{2\pi} \left( -x \arctan\left(\frac{y}{x}\right) - y \frac{2\nu - 1}{4(\nu - 1)} \ln\left(\frac{x^2 + y^2}{R_0^2}\right) \right) , \\
 {}^V u_z &= 0 .
 \end{aligned} \tag{246}$$

This is show in fig. 6.1.

Like Kröner we notate explicit the constant  $R_0$  (with dimension of  $[\text{length}]^2$ ) to remark the consistency of the units of the equations. The presented displacement field of a plane state of strain is not realistic. It fulfills the equilibrium conditions, but the stress vector field increases from the center to its maximum at the outer radius. The approximation had to be modified to get an idea of the stresses in a crystal defect or in a tubular cylinder. We need two modifications for vanishing stress vectors at the envelopes of the cylinder. One for the inner and one for the outer radius. Our calculations of the additional displacement fields is again based on the the divergence vector of the strain tensor,

$$\begin{aligned} \mathbf{\epsilon}_{xj}^{V,j} &= -\frac{\Omega_3}{2\pi} \frac{x\nu}{(\nu-1)(x^2+y^2)} \quad , \\ \mathbf{\epsilon}_{yj}^{V,j} &= -\frac{\Omega_3}{2\pi} \frac{y\nu}{(\nu-1)(x^2+y^2)} \quad , \\ \mathbf{\epsilon}_{zj}^{V,j} &= 0 \quad . \end{aligned} \tag{247}$$

The stress tensor of Volterra's disclination is already divergence-free. The additional displacement field needs therefore to fulfill the differential equation (28) by itself. We make the same ansatz as in (eq. (69)):

$$u_i = w \mathcal{W} \mathbf{\epsilon}_{,m}^{V,im} \quad . \tag{248}$$

This displacement solves the differential equation (28) with

$$\mathcal{W} = 1 \quad , \tag{249}$$

or with the function

$$\mathcal{W} = x^2 + y^2 \quad , \tag{250}$$

and every dimensionless constant  $w$ . For a better overview we rename the first solution to:

$$\mathcal{V} = 1 \quad . \tag{251}$$

The ansatz for the additional displacement field turns with these functions to

$$u_i = \left( v \mathcal{V} + w \mathcal{W} \right) \mathbf{\epsilon}_{,m}^{V,im} = \left( v + w(x^2 + y^2) \right) \mathbf{\epsilon}_{,m}^{V,im} \quad . \tag{252}$$

We add this to Volterra's disclination  $u_i^V$  of eq.(246), and get the following ansatz for the *realistic* displacement field of the wedge disclination

$$\begin{aligned}
u_x &= \frac{\Omega_3}{2\pi} \left( y \arctan\left(\frac{y}{x}\right) - x \frac{2\nu - 1}{4(\nu - 1)} \ln\left(\frac{x^2 + y^2}{r_1^2}\right) \right. \\
&\quad \left. - \left( \frac{\overset{2}{v}}{(x^2 + y^2)} + \overset{2}{w} \right) \frac{\nu}{(\nu - 1)} x \right) , \\
u_y &= \frac{\Omega_3}{2\pi} \left( -x \arctan\left(\frac{y}{x}\right) - y \frac{2\nu - 1}{4(\nu - 1)} \ln\left(\frac{x^2 + y^2}{r_1^2}\right) \right. \\
&\quad \left. - \left( \frac{\overset{2}{v}}{(x^2 + y^2)} + \overset{2}{w} \right) \frac{\nu}{(\nu - 1)} y \right) , \\
u_z &= 0 \quad .
\end{aligned} \tag{253}$$

We've substituted the constant  $R_0$  by the inner radius  $r_1 > 0$ , which can be done for a tubular cylinder, if  $r_1$  is not too small to influence the displacement extremely. This ansatz is based on the displacement given by Volterra. In consistence with the uniqueness statements he got the same ansatz, but he calculated the constants another way. We do this, in the next sections, respectively to the stress vector field. In opposite to Volterra our stress vectors will vanish exactly at the cylinder envelopes.

We will show next, that the integral along the closed contour line

$$\vec{s}(t) = \left( \cos(t), \sin(t), 0 \right) \quad , \tag{31}$$

and the equilibrium conditions are independent of the constants  $\overset{2}{v}$  and  $\overset{2}{w}$ . For this purpose we examine first the components of the integral given by

$$\begin{aligned}
\oint u_1 \frac{\partial s_1}{\partial t} dt &= \frac{\Omega_3}{16\pi(\nu - 1)} \left( 2(\nu - 1)t \sin(t) \left( 2 \cos(t) - t \sin(t) \right) \right. \\
&\quad \left. + \left( \sin^2(t) - 1 \right) \left( (2\nu - 1) \ln\left(\frac{1}{r_1^2}\right) + 4\nu(\overset{2}{v} + \overset{2}{w}) + 2(\nu - 1)(t^2 - 1) \right) \right) \Big|_0^{2\pi} \\
&= -\frac{\Omega_3}{2} \pi \quad , \\
\oint u_2 \frac{\partial s_2}{\partial t} dt &= -\frac{\Omega_3}{16\pi(\nu - 1)} \left( 2(\nu - 1)t \left( (2 \cos(t) \sin(t)) - t \sin^2(t) + 2t \right) \right. \\
&\quad \left. + \left( \sin^2(t) - 1 \right) \left( (2\nu - 1) \ln\left(\frac{1}{r_1^2}\right) + 4\nu(\overset{2}{v} + \overset{2}{w}) + 2(\nu - 1)(t^2 - 1) \right) \right) \Big|_0^{2\pi} \\
&= -\frac{\Omega_3}{2} \pi \quad , \\
\oint u_3 \frac{\partial s_3}{\partial t} dt &= 0 \quad .
\end{aligned} \tag{254}$$

The stress tensor

$$\begin{aligned}
\sigma_{xx} &= \frac{\Omega_3}{2\pi} \frac{E}{4(\nu^2 - 1)(2\nu - 1)} \left( (2\nu - 1) \left( \ln \left( \frac{x^2 + y^2}{r_1} \right) + 4\nu \frac{x^2 - y^2}{(x^2 + y^2)^2} \right) \right. \\
&\quad \left. + 4\nu \frac{x^2}{r_1^2} + \frac{2\nu(x^2 + 3y^2)}{x^2 + y^2} - \frac{2x^4 + 6x^2y^2 + 4y^4}{(x^2 + y^2)^2} \right) , \\
\sigma_{xy} &= \frac{\Omega_3}{2\pi} \frac{E}{2(\nu^2 - 1)} \frac{xy(4\nu \frac{x^2}{r_1^2} - x^2 - y^2)}{(x^2 + y^2)^2} , \\
\sigma_{xz} &= 0 , \\
\sigma_{yy} &= \frac{\Omega_3}{2\pi} \frac{E}{4(\nu^2 - 1)(2\nu - 1)} \left( (2\nu - 1) \left( \ln \left( \frac{x^2 + y^2}{r_1} \right) - 4\nu \frac{x^2 - y^2}{(x^2 + y^2)^2} \right) \right. \\
&\quad \left. + 4\nu \frac{x^2}{r_1^2} + \frac{2\nu(3x^2 + y^2)}{x^2 + y^2} - \frac{4x^4 + 6x^2y^2 + 2y^4}{(x^2 + y^2)^2} \right) , \\
\sigma_{yz} &= 0 , \\
\sigma_{zz} &= \frac{\Omega_3}{2\pi} \frac{E\nu}{2(\nu^2 - 1)(2\nu - 1)} \left( (2\nu - 1) \ln \left( \frac{x^2 + y^2}{r_1} \right) + 4\nu \frac{x^2}{r_1^2} + 4\nu - 3 \right) , \quad (255)
\end{aligned}$$

is divergence-free. The x-component of the divergence of the stress tensor vanishes according to

$$\sigma^{x1}_{,1} = -\sigma^{x2}_{,2} = -\frac{\Omega_3}{2\pi} \frac{E}{2(\nu^2 - 1)} \frac{x}{(x^2 + y^2)^3} \left( 4\nu \frac{x^2}{r_1^2} (x^2 - 3y^2) - x^4 + y^4 \right) , \quad (256)$$

analogous vanishes the y-component according to

$$\sigma^{y1}_{,1} = -\sigma^{y2}_{,2} = -\frac{\Omega_3}{2\pi} \frac{E}{2(\nu^2 - 1)} \frac{y}{(x^2 + y^2)^3} \left( 4\nu \frac{x^2}{r_1^2} (3x^2 - y^2) - x^4 + y^4 \right) . \quad (257)$$

The stress tensor is divergence-free for every constants  $\frac{x^2}{r_1^2}$  and  $\frac{y^2}{r_1^2}$ .

## 8.1 The wedge disclination in a crystal

The stress vector field of a crystal had to increase continuously from zero at the outer radius  $r_2$  of the cylinder to its maximum at the inner radius  $r_1$ . Moreover the stresses had to rise to infinity for  $r_1 \rightarrow 0$ . In this section we calculate the displacement field of the wedge disclination in a crystal by determining the constant  $\frac{x^2}{r_1^2}$  for vanishing stress vectors. We neglect the stress vector field which belongs to the normal vector in z-direction and consists only of a z-component. The stress vector field belonging to the interior normal vector field of the cylinder computes to (cylindrical coordinates)

$$\begin{aligned}
f_r &= \frac{\Omega_3}{2\pi} \frac{E}{4(2\nu - 1)(\nu^2 - 1)} \frac{1}{r^2} \left( (2\nu - 1) \left( r^2 \ln \left( \frac{r^2}{r_1^2} \right) + 4\nu \frac{x^2}{r_1^2} \right) + 2(\nu - 1)r^2 + 4\nu \frac{x^2}{r_1^2} r^2 \right) , \\
f_\varphi &= 0 , \\
f_z &= 0 . \quad (258)
\end{aligned}$$

We find the whole stress vector field vanishing for

$$\overset{2}{w} = -\frac{(2\nu - 1)\left(r^2 \ln(r^2/r_1^2) + 4\nu\overset{2}{v}\right) + 2(\nu - 1)r^2}{4\nu r^2} . \quad (259)$$

This function can be modified in a way, that the stress vectors vanishes at the inner or the outer radius. We choose the outer radius  $r_2$ . For  $r = r_2$  the function  $\overset{2}{w}$  depends only on the outer and inner radii and on  $\overset{2}{v}$ :

$$\overset{2}{w} = -\frac{(2\nu - 1)\left(r_2^2 \ln(r_2^2/r_1^2) + 4\nu\overset{2}{v}\right) + 2(\nu - 1)r_2^2}{4\nu r_2^2} . \quad (260)$$

With this constant the regarded stress vector field writes in cylindrical coordinates

$$\begin{aligned} f_r &= \frac{\Omega_3}{2\pi} \frac{E}{4(2\nu - 1)(\nu^2 - 1)} \frac{1}{r^2 r_2^2} \left( (2\nu - 1)r^2 r_2^2 \left( \ln \frac{r_2^2}{r_1^2} - \ln \frac{r^2}{r_1^2} \right) + 4\nu\overset{2}{v}(r_2^2 - r^2) \right) , \\ f_\varphi &= 0 \quad , \\ f_z &= 0 \quad . \end{aligned} \quad (261)$$

If we choose

$$\overset{2}{v} = 0 \quad , \quad (262)$$

the conditions for a stress vector in a crystal are already accomplished,

$$\begin{aligned} f_r &= \frac{\Omega_3}{2\pi} \frac{E}{4(\nu^2 - 1)} \left( \ln \frac{r_2^2}{r_1^2} - \ln \frac{r^2}{r_1^2} \right) \quad , \\ f_\varphi &= 0 \quad , \\ f_z &= 0 \quad . \end{aligned} \quad (263)$$

The stresses go to infinity for  $r_1 \rightarrow 0$  and vanishes at the outer radius  $r_2$ . It is plotted in figure 6.2

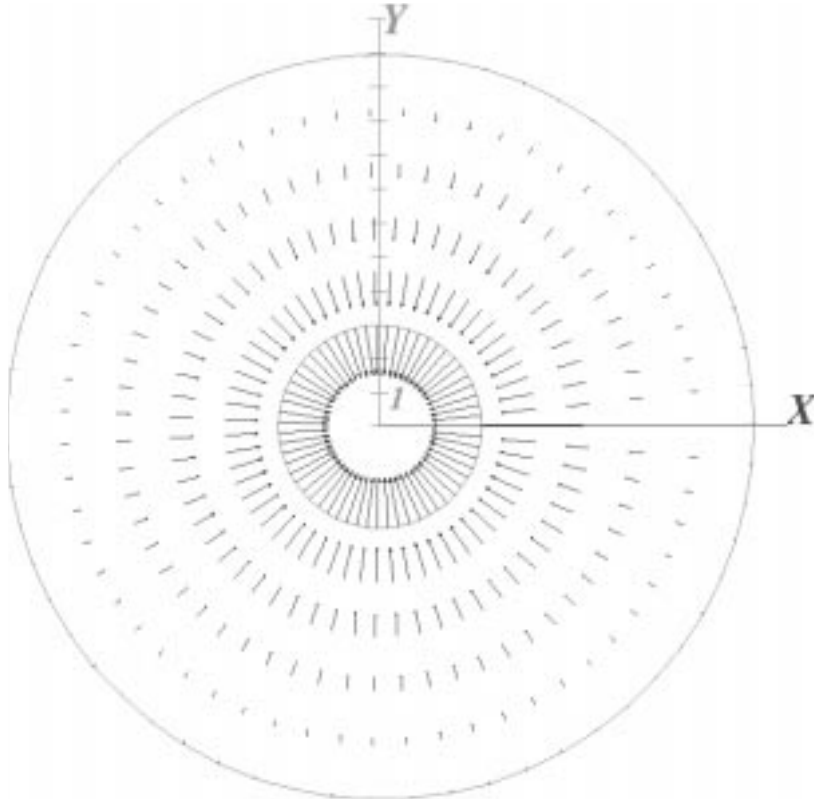


**Fig. 6.2.** Stress vector field around a wedge disclination in a crystal with  $\Omega_3 = 0.1\pi$

The maximum at the inner radius of the depicted amount lies in the range of 0.06 MPa. The realistic displacement field of an approximative wedge disclination in a crystal is now given by the displacement of eq. (253) with the constants from eq.(260) and eq.(262)

$$\begin{aligned} \overset{c}{u}_x &= \frac{\Omega_3}{2\pi} \left( y \arctan\left(\frac{y}{x}\right) + \frac{x}{2} + x \frac{(2\nu - 1)}{4(\nu - 1)} \left( \ln\left(\frac{r_2^2}{r_1^2}\right) - \ln\left(\frac{x^2 + y^2}{r_1^2}\right) \right) \right) , \\ \overset{c}{u}_y &= \frac{\Omega_3}{2\pi} \left( -x \arctan\left(\frac{y}{x}\right) + \frac{y}{2} + y \frac{(2\nu - 1)}{4(\nu - 1)} \left( \ln\left(\frac{r_2^2}{r_1^2}\right) - \ln\left(\frac{x^2 + y^2}{r_1^2}\right) \right) \right) , \\ \overset{c}{u}_z &= 0 . \end{aligned} \quad (264)$$

The strain tensor of this displacement calculates to

$$\begin{aligned} \epsilon_{xx} &= \frac{\Omega_3}{2\pi} \left( -\frac{y^2}{x^2 + y^2} + \frac{1}{2} + \frac{(2\nu - 1)}{4(\nu - 1)} \left( \frac{2x^2}{(x^2 + y^2)} + \ln\left(\frac{r_2^2}{r_1^2}\right) - \ln\left(\frac{x^2 + y^2}{r_1^2}\right) \right) \right) , \\ \epsilon_{xy} &= -\frac{\Omega_3}{2\pi} \frac{xy}{2(\nu - 1)(x^2 + y^2)} , \\ \epsilon_{xz} &= 0 , \\ \epsilon_{yy} &= \frac{\Omega_3}{2\pi} \left( -\frac{x^2}{x^2 + y^2} + \frac{1}{2} + \frac{(2\nu - 1)}{4(\nu - 1)} \left( \frac{2y^2}{(x^2 + y^2)} + \ln\left(\frac{r_2^2}{r_1^2}\right) - \ln\left(\frac{x^2 + y^2}{r_1^2}\right) \right) \right) , \\ \epsilon_{yz} &= 0 , \\ \epsilon_{zz} &= 0 . \end{aligned} \quad (265)$$



The stress tensor followed by Hooke's law

$$\begin{aligned}
\sigma_{xx} &= -\frac{\Omega_3}{2\pi} \frac{E}{4(\nu^2 - 1)} \left( \frac{2y^2}{(x^2 + y^2)} + \ln\left(\frac{r_2^2}{r_1^2}\right) - \ln\left(\frac{x^2 + y^2}{r_1^2}\right) \right) , \\
\sigma_{xy} &= -\frac{\Omega_3}{2\pi} \frac{E}{2(\nu^2 - 1)} \frac{xy}{(x^2 + y^2)} , \\
\sigma_{xz} &= 0 , \\
\sigma_{yy} &= -\frac{\Omega_3}{2\pi} \frac{E}{4(\nu^2 - 1)} \left( \frac{2x^2}{(x^2 + y^2)} + \ln\left(\frac{r_2^2}{r_1^2}\right) - \ln\left(\frac{x^2 + y^2}{r_1^2}\right) \right) , \\
\sigma_{yz} &= 0 , \\
\sigma_{zz} &= -\frac{\Omega_3}{2\pi} \frac{E\nu}{2(\nu^2 - 1)} \left( \ln\left(\frac{r_2^2}{r_1^2}\right) - \ln\left(\frac{x^2 + y^2}{r_1^2}\right) - 1 \right) .
\end{aligned} \tag{266}$$

It is divergence-free. The x-component of the divergence of the stress tensor vanishes according to

$$\sigma^{x1}_{,1} = -\sigma^{x2}_{,2} = \frac{\Omega_3}{2\pi} \frac{E}{2(\nu^2 - 1)} \frac{x(x^2 - y^2)}{(x^2 + y^2)^2} , \tag{267}$$

and the y-component according to

$$\sigma^{y1}_{,1} = -\sigma^{y2}_{,2} = \frac{\Omega_3}{2\pi} \frac{E}{2(\nu^2 - 1)} \frac{y(x^2 - y^2)}{(x^2 + y^2)^2} . \tag{268}$$

Diagonalisation yields the eigenvalues of the stress tensor

$$\begin{aligned}
\dot{\sigma}_{11} &= -\frac{\Omega_3}{2\pi} \frac{E}{4(\nu^2 - 1)} \left( \ln\left(\frac{r_2^2}{r_1^2}\right) - \ln\left(\frac{x^2 + y^2}{r_1^2}\right) - 2 \right) , \\
\dot{\sigma}_{22} &= -\frac{\Omega_3}{2\pi} \frac{E}{4(\nu^2 - 1)} \left( \ln\left(\frac{r_2^2}{r_1^2}\right) - \ln\left(\frac{x^2 + y^2}{r_1^2}\right) \right) , \\
\dot{\sigma}_{33} &= -\frac{\Omega_3}{2\pi} \frac{E\nu}{2(\nu^2 - 1)} \left( \ln\left(\frac{r_2^2}{r_1^2}\right) - \ln\left(\frac{x^2 + y^2}{r_1^2}\right) - 1 \right) .
\end{aligned} \tag{269}$$

The intensity distribution of the transmitted plane polarized light is given by

$$\begin{aligned}
I &= -\frac{4I_0^2}{(x^2 + y^2)^2} \left( -4(y \cos(\beta) - x \sin(\beta))^2 - (x^2 + y^2) \right) (y \cos(\beta) - x \sin(\beta))^2 \\
&\quad \times \sin^2 \left( \frac{\Omega_3}{16\pi} \frac{E}{(\nu^2 - 1)} 2\nu \left( \ln\left(\frac{r_2^2}{r_1^2}\right) - \ln\left(\frac{x^2 + y^2}{r_1^2}\right) - 1 \right) \ln\left(\frac{r_2^2}{r_1^2}\right) \right. \\
&\quad \left. + \ln\left(\frac{x^2 + y^2}{r_1^2}\right) + 2 \right) .
\end{aligned} \tag{270}$$

This is plotted in fig. 6.3.

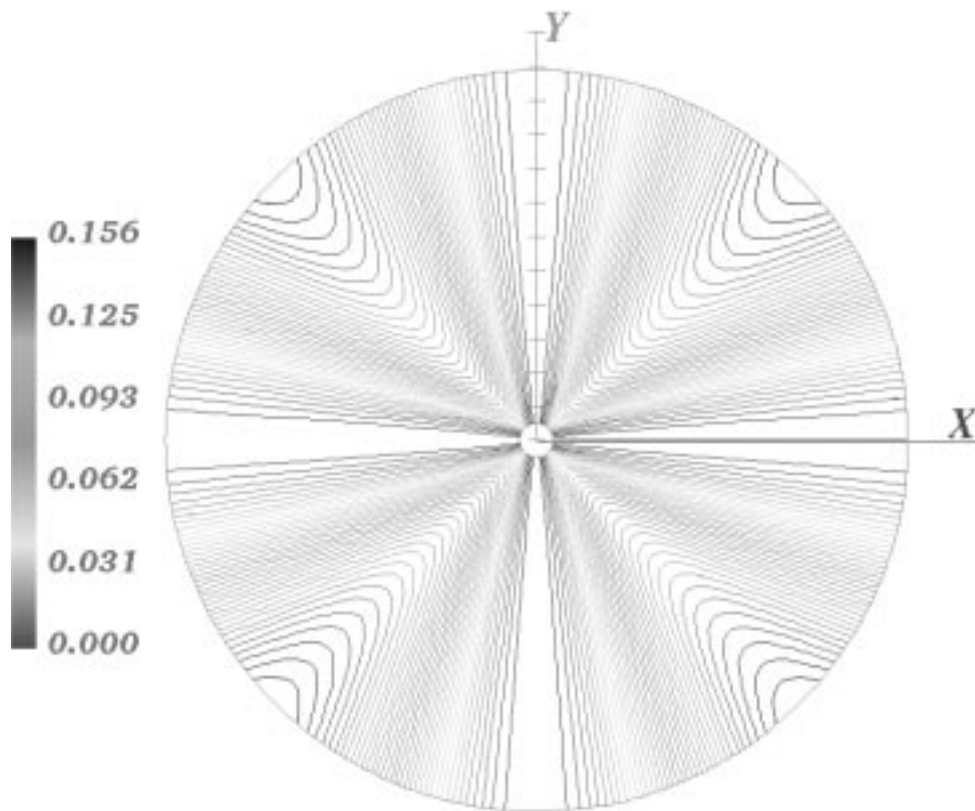


Fig. 6.3a.

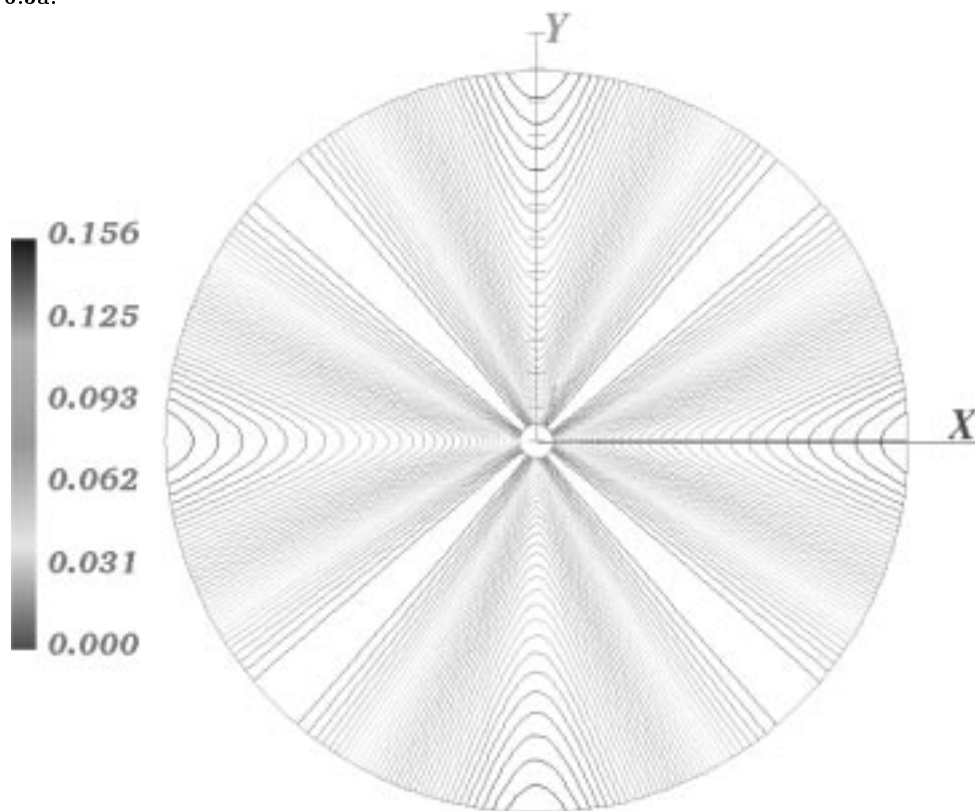


Fig. 6.3b.

**Fig. 6.3.** Intensity distribution  $[10^{-3}I_0^2]$  for double refraction fields caused by the stresses around a wedge disclination in a crystal with  $\Omega_3 = 0.1\pi$  for plane polarized light with a)  $\beta = 0$ , and b)  $\beta = \pi/4$ . See also colour plate V

The intensity distribution rotates with  $\beta$  around the longitudinal axis of the cylinder. The slip direction is the x-axis and the view is in z-direction.

The intensity of the transmitted circular polarized light is given by

$$I = I_0^2 \sin^2 \left( \frac{\Omega_3}{16\pi(\nu^2 - 1)} 2\nu \left( \ln \left( \frac{r_2^2}{r_1^2} \right) - \ln \left( \frac{x^2 + y^2}{r_1^2} \right) - 1 \right) - \ln \left( \frac{r_2^2}{r_1^2} \right) + \ln \left( \frac{x^2 + y^2}{r_1^2} \right) + 2 \right), \quad (271)$$

and is plotted in fig 6.4.

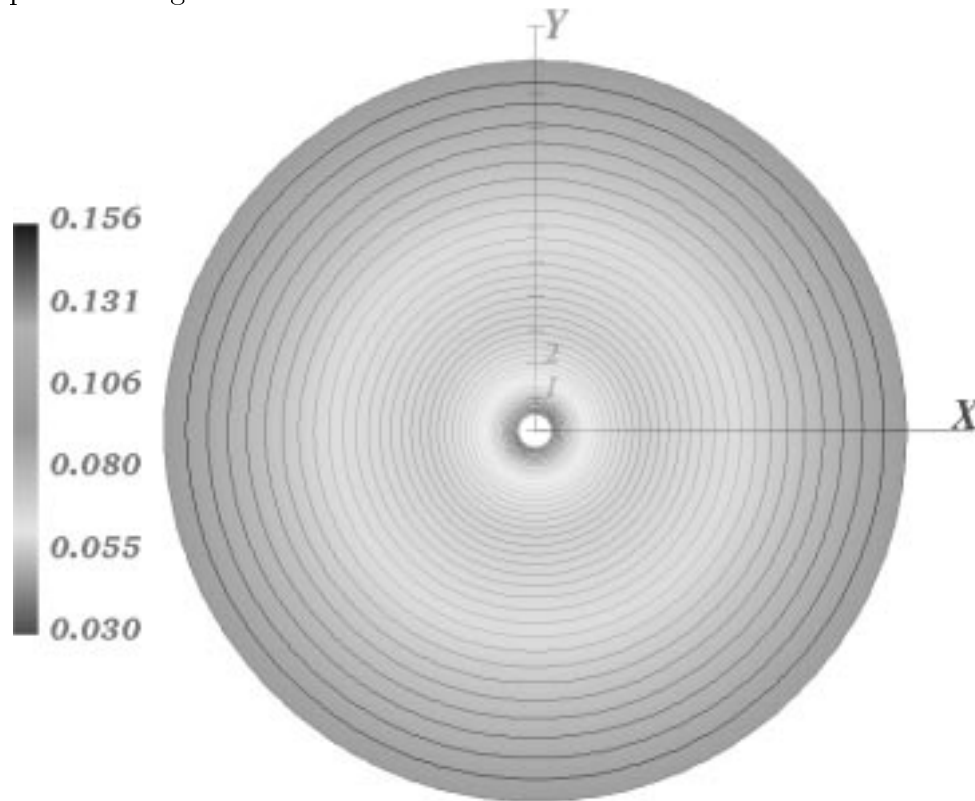


**Fig. 6.4.** Intensity distribution  $[10^{-3} I_0^2]$  for double refraction fields caused by the stresses around a wedge disclination in a crystal with  $\Omega_3 = 0.1\pi$  for circular polarized light

The inner radius is dark and light up at the outer envelope. We get nearly the same plot for the isolines of the negative amount of the stress vector field. The isolines of the

specific energy for changing the shape of the origin body

$$\begin{aligned}
 \tilde{U}_F = & -\frac{\Omega_3^2}{\pi^2} \frac{E}{192(\nu+1)(\nu-1)^2} \\
 & \times \left( 3(2\nu-1) \left( \ln^2 \left( \frac{r_2^2}{r_1^2} \right) + \ln^2 \left( \frac{x^2+y^2}{r_1^2} \right) + 2 \ln \left( \frac{x^2+y^2}{r_1^2} \right) \right) \right. \\
 & - 2(2\nu-1)(\nu+1) \left( \ln \left( \frac{r_2^2}{r_1^2} \right) - \ln \left( \frac{x^2+y^2}{r_1^2} \right) - 1 \right)^2 \\
 & \left. - 6(2\nu-1) + \ln \left( \frac{r_2^2}{r_1^2} \right) \left( \ln \left( \frac{x^2+y^2}{r_1^2} \right) + 1 \right) + 6(\nu-1) \right) , \quad (272)
 \end{aligned}$$

shows here another course, as can be seen in figure 6.5. It is maximal at the inner radius.

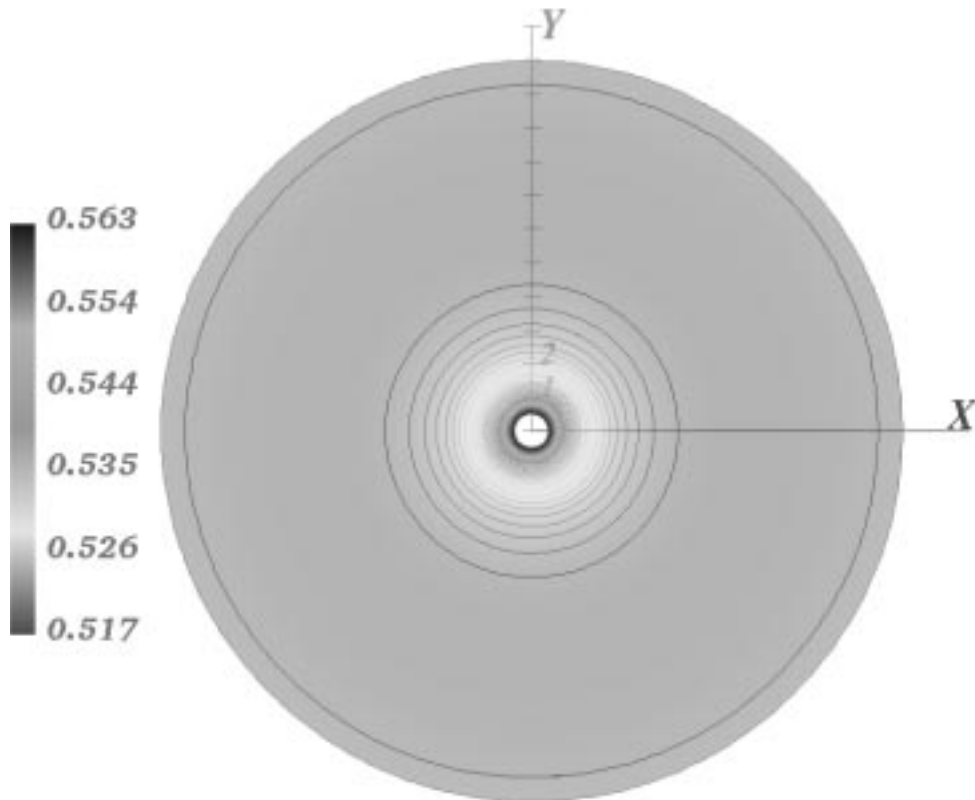


**Fig. 6.5.** Isolines [kPa] of the specific energy for changing the shape of the origin body around a wedge disclination in a crystal with  $\Omega_3 = 0.1\pi$ . See also colour plate VI

## 8.2 The wedge disclination of a tubular cylinder

The stress vector of a tubular cylinder had to vanish at the outer and the inner radius. The stress vector field of a wedge disclination is given by eq. (261), where the constant  $\overset{2}{v}$  is not determined yet. We get vanishing stress vectors at the inner radius  $r = r_1$  for

$$\overset{2}{v} = \frac{r_1^2 r_2^2}{4\nu(r_2^2 - r_1^2)} \ln\left(\frac{r_2^2}{r_1^2}\right) . \quad (273)$$

With this constant and with  $\overset{2}{w}$  from eq.(260) the stress vector field, which vanishes at the envelopes of the cylinder, is found to be (cylindrical coordinates)

$$\begin{aligned} f_r &= \frac{\Omega_3}{2\pi} \frac{E}{4(\nu^2 - 1)} \left( r^2 \ln\left(\frac{r^2}{r_1^2}\right) + r_2^2 \frac{(r^2 - r_1^2)}{r_1^2 - r_2^2} \ln\left(\frac{r_2^2}{r_1^2}\right) \right) , \\ f_\varphi &= 0 \quad , \\ f_z &= 0 \quad . \end{aligned} \quad (274)$$

This vector field is represented in fig. 6.6a. In fig. 6.6b we depict the amount.

We finally formulate with the displacement (253) and the constants (260) and (273), the realistic displacement field of an approximative wedge disclination of a tubular cylinder

$$\begin{aligned} \overset{t}{u}_x &= -\frac{\Omega_3}{2\pi} \left( -y \arctan\left(\frac{y}{x}\right) - x + x \frac{(2\nu - 1)}{4(\nu - 1)} \left( \ln\left(\frac{x^2 + y^2}{r_1^2}\right) + \frac{r_2^2}{(r_1^2 - r_2^2)} \ln\left(\frac{r_2^2}{r_1^2}\right) \right) \right. \\ &\quad \left. - \frac{1}{4(\nu - 1)} \frac{r_1^2 r_2^2}{(r_1^2 - r_2^2)(x^2 + y^2)} \right) , \\ \overset{t}{u}_y &= -\frac{\Omega_3}{2\pi} \left( x \arctan\left(\frac{y}{x}\right) - y + y \frac{(2\nu - 1)}{4(\nu - 1)} \left( \ln\left(\frac{x^2 + y^2}{r_1^2}\right) + \frac{r_2^2}{(r_1^2 - r_2^2)} \ln\left(\frac{r_2^2}{r_1^2}\right) \right) \right. \\ &\quad \left. - \frac{1}{4(\nu - 1)} \frac{r_1^2 r_2^2}{(r_1^2 - r_2^2)(x^2 + y^2)} \right) , \\ \overset{t}{u}_z &= 0 \quad . \end{aligned} \quad (275)$$

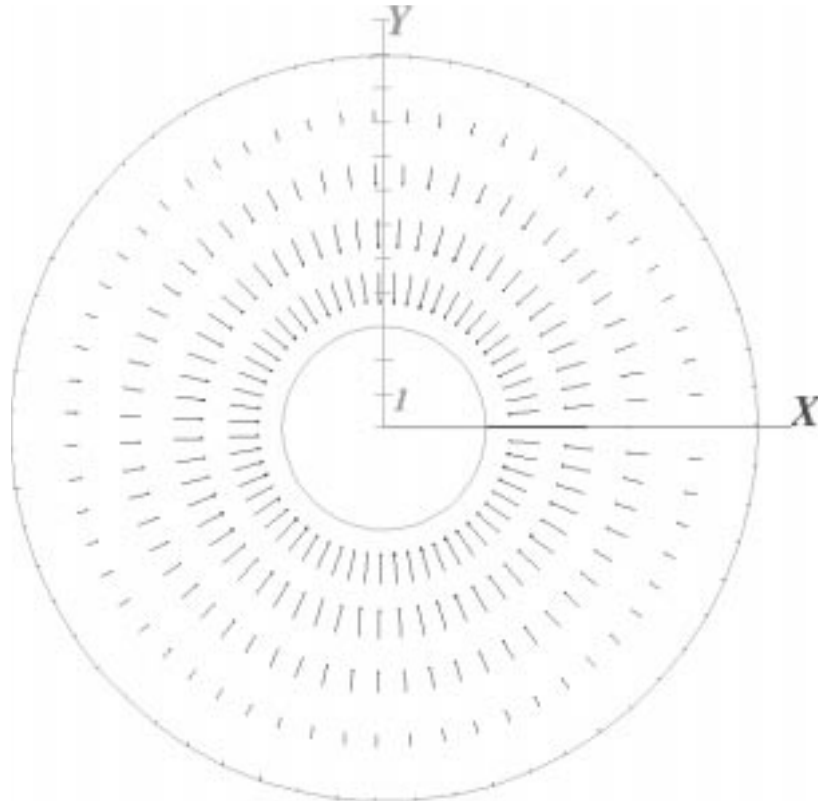


Fig. 6.6a. Stress vector field of the wedge disclination of a tubular cylinder with  $\Omega_3 = 0.1\pi$

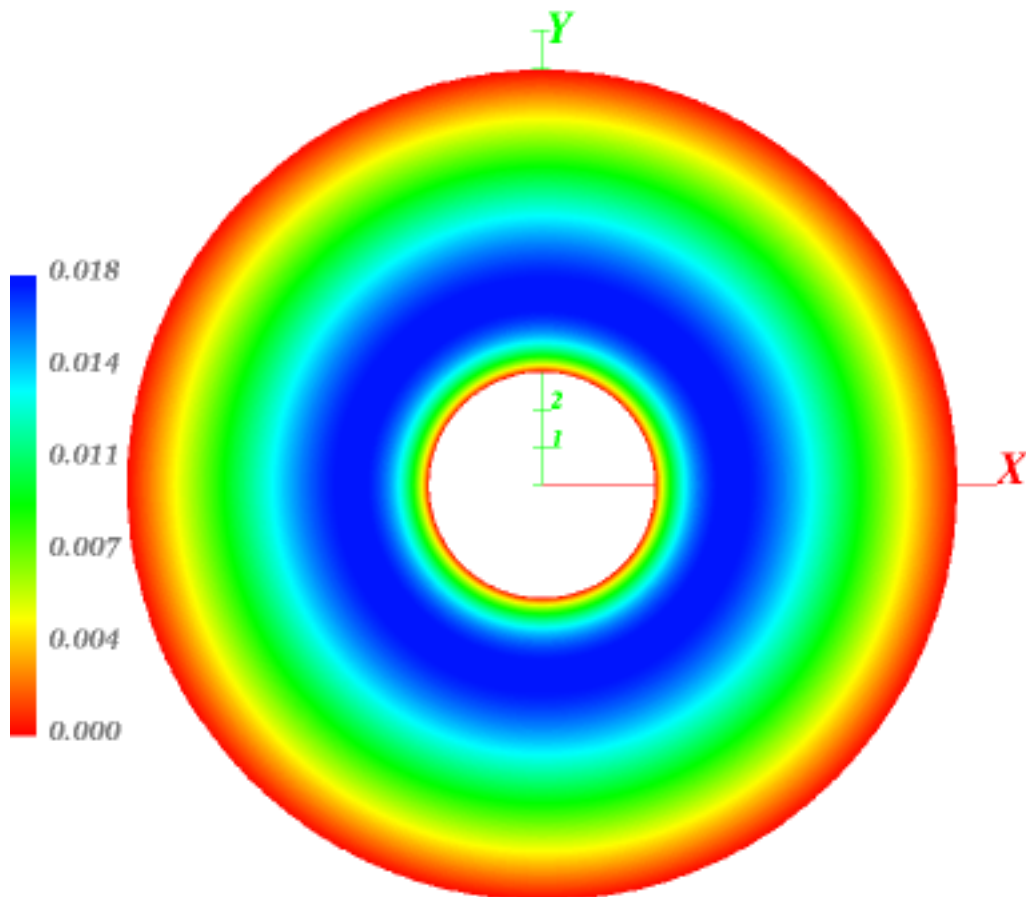


Fig. 6.6b. Isolines [MPa] of the amount of the stress vector field. See also colour plate VII

The strain tensor of this displacement calculates to

$$\begin{aligned}
\boldsymbol{\varepsilon}_{xx} &= -\frac{\Omega_3}{2\pi} \left( \frac{y^2}{x^2 + y^2} - \frac{1}{2} + \frac{2\nu - 1}{4(\nu - 1)} \left( \frac{2x^2}{x^2 + y^2} + \ln \left( \frac{x^2 + y^2}{r_1^2} \right) \right) \right. \\
&\quad \left. + \frac{\ln(r_2^2/r_1^2)}{4(\nu - 1)(r_1^2 - r_2^2)} \left( (2\nu - 1)(r_1^2 - 1) + r_1^2 r_2^2 \frac{x^2 - y^2}{x^2 + y^2} \right) \right) , \\
\boldsymbol{\varepsilon}_{xy} &= -\frac{\Omega_3}{2\pi} xy \left( \frac{1}{2(\nu - 1)(x^2 + y^2)} + \frac{r_1^2 r_2^2 \ln(r_2^2/r_1^2)}{2(\nu - 1)(x^2 + y^2)^2 (r_1^2 - r_2^2)} \right) , \\
\boldsymbol{\varepsilon}_{xz} &= 0 , \\
\boldsymbol{\varepsilon}_{yy} &= -\frac{\Omega_3}{2\pi} \left( \frac{x^2}{x^2 + y^2} - \frac{1}{2} + \frac{2\nu - 1}{4(\nu - 1)} \left( \frac{-2y^2}{x^2 + y^2} + \ln \left( \frac{x^2 + y^2}{r_1^2} \right) \right) \right. \\
&\quad \left. + \frac{\ln(r_2^2/r_1^2)}{4(\nu - 1)(r_1^2 - r_2^2)} \left( (2\nu - 1)(r_1^2 - 1) + r_1^2 r_2^2 \frac{x^2 - y^2}{x^2 + y^2} \right) \right) , \\
\boldsymbol{\varepsilon}_{yz} &= 0 , \\
\boldsymbol{\varepsilon}_{zz} &= 0 .
\end{aligned} \tag{276}$$

The stress tensor followed by Hooke's law

$$\begin{aligned}
\boldsymbol{\sigma}_{xx} &= \frac{\Omega_3}{2\pi} \frac{E}{4(\nu^2 - 1)} \left( \frac{r_2^2}{(r_1^2 - r_2^2)} \left( 1 - \frac{(x^2 - y^2)r_1^2}{(x^2 + y^2)^2} \right) \ln \left( \frac{r_2^2}{r_1^2} \right) \right. \\
&\quad \left. + \frac{1}{(x^2 + y^2)} \left( \ln \left( \frac{x^2 + y^2}{r_1^2} \right) + \frac{2y^2}{(x^2 + y^2)} \right) \right) , \\
\boldsymbol{\sigma}_{xy} &= -\frac{\Omega_3}{2\pi} \frac{E}{4(\nu^2 - 1)} \left( \frac{xy}{(x^2 + y^2)} \left( 1 + \frac{r_1^2 r_2^2}{(r_1^2 - r_2^2)(x^2 + y^2)} \ln \left( \frac{r_2^2}{r_1^2} \right) \right) \right) , \\
\boldsymbol{\sigma}_{xz} &= 0 , \\
\boldsymbol{\sigma}_{yy} &= \frac{\Omega_3}{2\pi} \frac{E}{4(\nu^2 - 1)} \left( \frac{r_2^2}{(r_1^2 - r_2^2)} \left( 1 + \frac{(x^2 - y^2)r_1^2}{(x^2 + y^2)^2} \right) \ln \left( \frac{r_2^2}{r_1^2} \right) \right. \\
&\quad \left. + \frac{1}{(x^2 + y^2)} \left( \ln \left( \frac{x^2 + y^2}{r_1^2} \right) + \frac{2x^2}{(x^2 + y^2)} \right) \right) , \\
\boldsymbol{\sigma}_{yz} &= 0 , \\
\boldsymbol{\sigma}_{zz} &= \frac{\Omega_3}{2\pi} \frac{E\nu}{4(\nu^2 - 1)} \left( \ln \left( \frac{x^2 + y^2}{r_1^2} \right) + \frac{r_2^2}{(r_1^2 - r_2^2)} \ln \left( \frac{r_2^2}{r_1^2} \right) + 1 \right) .
\end{aligned} \tag{277}$$

It is divergence-free. The x-component of the divergence of the stress tensor vanishes according to

$$\begin{aligned}
\boldsymbol{\sigma}_{,1}^{x1} = -\boldsymbol{\sigma}_{,2}^{x2} &= \frac{\Omega_3}{2\pi} \frac{E}{2(\nu^2 - 1)} \frac{x}{(x^2 + y^2)^3} \\
&\quad \times \left( (x^2 + y^2)(x^2 - y^2) + \frac{r_1^2 r_2^2 (x^2 - 3y^2) \ln(r_2^2/r_1^2)}{r_1^2 - r_2^2} \right) ,
\end{aligned} \tag{278}$$

and the y-component according to

$$\begin{aligned} \sigma^{y^1}_{,1} = -\sigma^{y^2}_{,2} &= \frac{\Omega_3}{2\pi} \frac{E}{2(\nu^2 - 1)} \frac{y}{(x^2 + y^2)^3} \\ &\times \left( (x^2 + y^2)(x^2 - y^2) + \frac{r_1^2 r_2^2 (x^2 - 3y^2) \ln(r_2^2/r_1^2)}{r_1^2 - r_2^2} \right) . \end{aligned} \quad (279)$$

Diagonalisation yields the eigenvalues of the stress tensor

$$\begin{aligned} \dot{\sigma}_{11} &= \frac{\Omega_3}{2\pi} \frac{E}{4(\nu^2 - 1)} \left( 2 + \ln\left(\frac{x^2 + y^2}{r_1^2}\right) + \frac{r_2^2 (r_1^2 + (x^2 + y^2))}{(r_1^2 - r_2^2)(x^2 + y^2)} \ln\left(\frac{r_2^2}{r_1^2}\right) \right) , \\ \dot{\sigma}_{22} &= -\frac{\Omega_3}{2\pi} \frac{E}{4(\nu^2 - 1)} \left( \ln\left(\frac{x^2 + y^2}{r_1^2}\right) + \frac{r_2^2 (r_1^2 - (x^2 + y^2))}{(r_1^2 - r_2^2)(x^2 + y^2)} \ln\left(\frac{r_2^2}{r_1^2}\right) \right) , \\ \dot{\sigma}_{33} &= \frac{\Omega_3}{2\pi} \frac{E\nu}{2(\nu^2 - 1)} \left( 1 + \ln\left(\frac{x^2 + y^2}{r_1^2}\right) + \frac{r_2^2}{(r_1^2 - r_2^2)} \ln\left(\frac{x^2 + y^2}{r_1^2}\right) \right) . \end{aligned} \quad (280)$$

The intensity distribution of the transmitted plane polarized light computes to

$$\begin{aligned} I &= -\frac{4I_0^2}{(x^2 + y^2)^2} \left( (x \cos(\beta) + y \sin(\beta))^2 - (x^2 + y^2) \right) \\ &\times (x \cos(\beta) + y \sin(\beta))^2 \\ &\times \sin^2 \left( \frac{\Omega_3}{8\pi} \frac{E}{\nu^2 - 1} \left( 1 + \ln\left(\frac{r_2^2}{r_1^2}\right) \frac{r_1^2 r_2^2}{(r_1^2 - r_2^2)} \frac{1}{(x^2 + y^2)} \right) \right) . \end{aligned} \quad (281)$$

This is plotted in fig. 6.7.



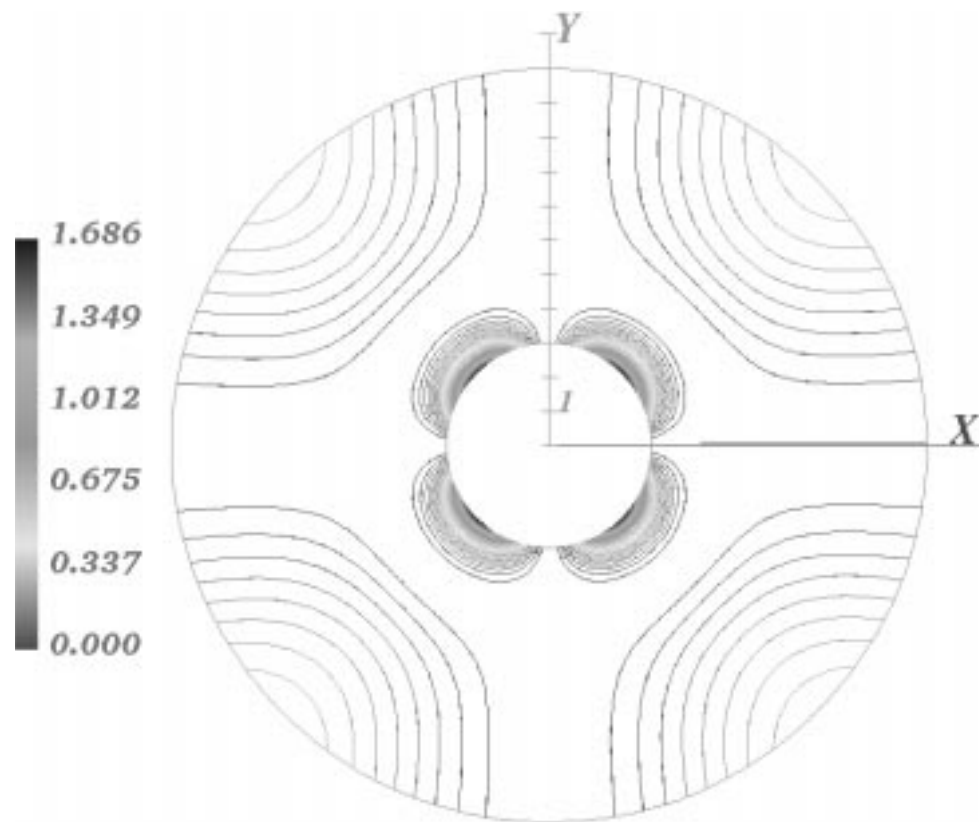


Fig. 6.7a.

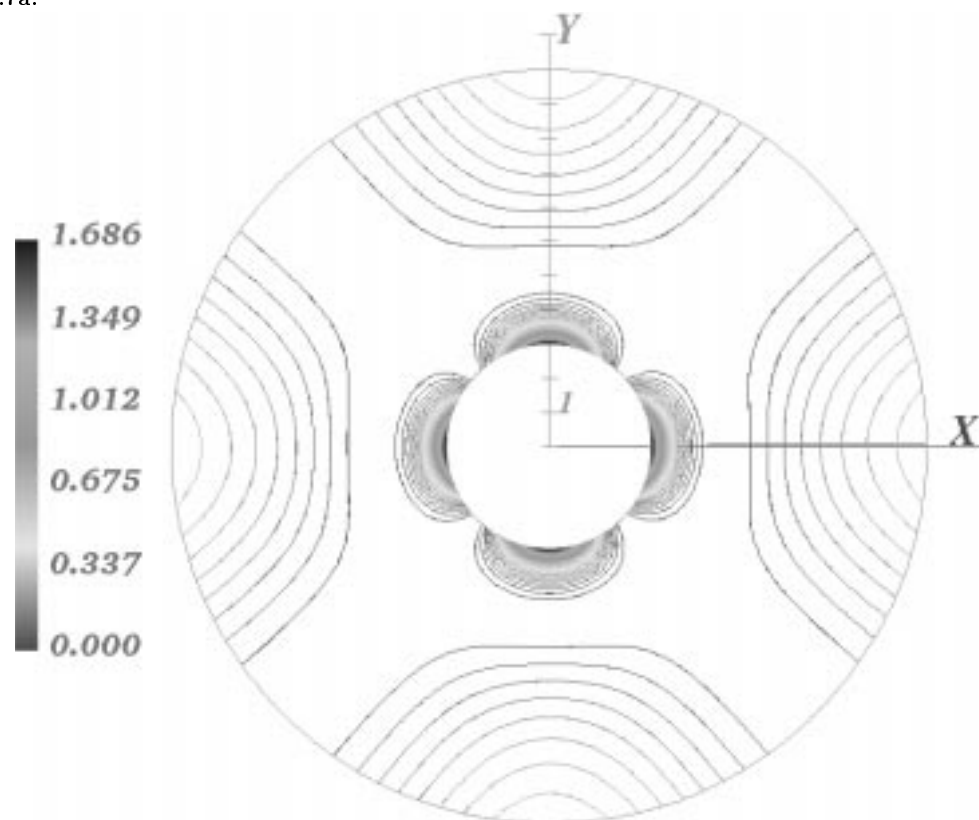


Fig. 6.7b.

**Fig. 6.7.** Isolines  $[10^{-3}I_0^2]$  of the intensity distribution for double refraction fields caused by the stresses of a wedge disclined cylinder with  $\Omega_3 = 0.1\pi$  for plane polarized light with a)  $\beta = 0$  and b)  $\beta = \pi/4$ . See also colour plate VIII.

The shape of this fringe pattern rotates with the angular  $\beta$  between the polarizer and the analyzer. This indicates the expected rotational symmetric of the wedge disclination. The equivalence with the photo shown by Volterra [21], [22] is obvious. The intensity of the transmitted circular polarized light is given by

$$I = I_0^2 \sin^2 \left( \frac{\Omega_3}{8\pi} \frac{1}{\nu^2 - 1} \left( 1 + \ln \left( \frac{r_2^2}{r_1^2} \right) \frac{r_1^2 r_2^2}{(r_1^2 - r_2^2)} \frac{1}{(x^2 + y^2)} \right) \right) . \quad (282)$$

This can be seen in fig. 6.8, which coincide with fig. 6.7 rotated around the z-axis of the cylinder. The maximum lies at the inner radius, it follows a dark ring, that lights up towards the outer radius.

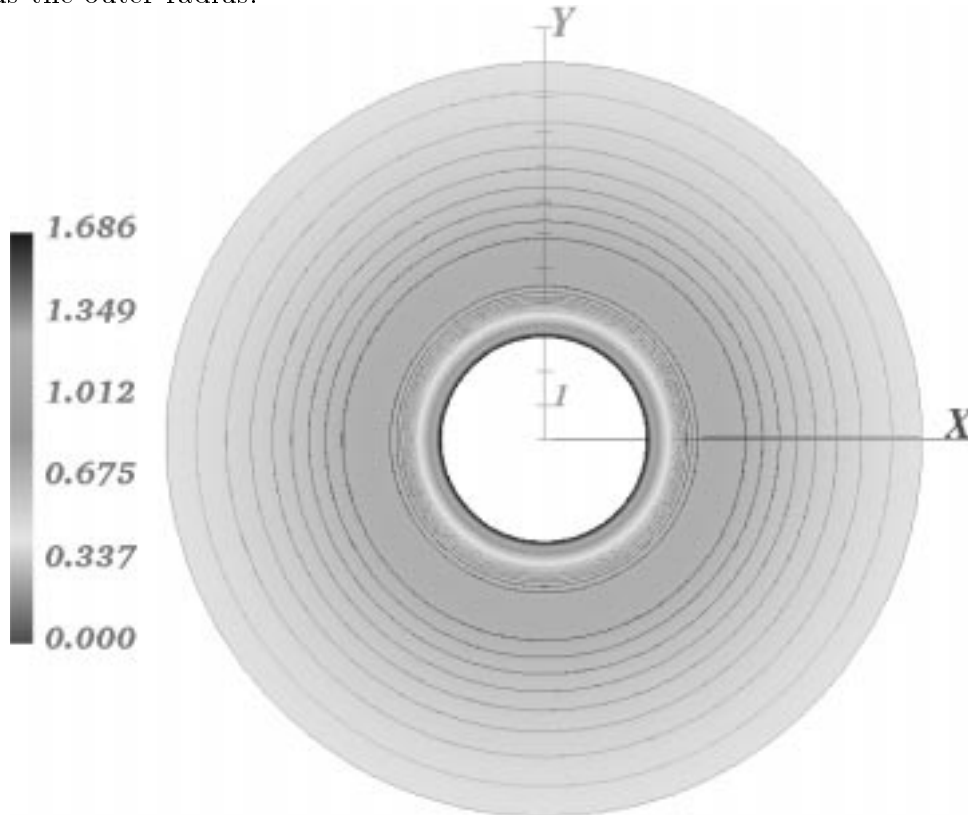


**Fig. 6.8.** Isolines of the Intensity distribution [ $10^{-3} I_0^2$ ] of circular polarized light for double refraction fields caused by the stresses of a wedge disclined cylinder

We get nearly the identical plot for the specific energy for changing the shape of the origin body. We do not notate the specific energy, because of its huge expression. The course of the isolines of the amount of the stress vector is similar (see fig 6.6b), the minima of the specific energy coincide with the maxima of the amount of the stress vector field.

## 9 Conclusions

### 9.1 Summary

We looked for a displacement which may describe the entire deformation of a body due to a defect. We introduced an effective algorithm to derive such a *realistic* displacement field  $\vec{u}^r$ . It corresponds to a strain tensor that fulfills the St. Venant compatibility conditions, a stress tensor that is a divergence-free and possesses vanishing stress vectors at the surface of the body.

The algorithm can be divided into two parts. The first part derives a displacement field with a divergence free stress tensor, the second part extends this to different boundary conditions. As examples we choose the Volterra defects in an isotropic elastic body. The algorithm is based on a modification of the displacement field by means of the divergence of the strain tensor. We started with an initial displacement field  $\vec{u}^0$ , to characterize the defect. Then we looked for an *additional* displacement field  $\vec{u}^1$  which leads together with  $\vec{u}^0$  to a displacement field with a divergence-free stress tensor,

$$\vec{u}^{(0+1)} := \vec{u}^0 + \vec{u}^1 . \quad (283)$$

Next we took the divergence of the strain tensor of the *initial* displacement  $\varepsilon_{ij}^0$  and made the following ansatz (21) for the *additional* displacement:

$$u_i^1 = w \mathcal{W} \varepsilon_{ij}^0 .$$

The function  $\mathcal{W}$  and the constant  $w$  were determined by the three linear second order partial differential equations (28). In the case of the Volterra defects, except the wedge disclination, we found

$$w \mathcal{W} = \frac{x^2 + y^2}{4\nu - 3} [\text{length}]^2 . \quad (284)$$

The consideration of the dimensional arguments helped to obtain this solution. In the case of the edge-dislocations are the calculated displacement fields  $\vec{u}^{(0+1)}$  already the *realistic* displacements corresponding to a crystal. The displacement fields we get this way for the twist disclinations had to be modified with the help of the known equilibrium equations. The wedge disclination is mathematically much more complicated as the other defects. We found no solution for the partial differential equations (28).

The second part of our algorithm is independent of the first part. It consists of a boundary problem for a displacement field with a divergence-free stress tensor. We worked out with its help the *realistic* displacement field for a tubular cylinder with approximately vanishing stress vectors at the envelope. We required for this purpose a second *additional* displacement field  $\vec{u}^2$ . As an ansatz we used the divergence vector field of the new strain tensor  $\varepsilon_{ij}^{(0+1)}$  of the displacement  $\vec{u}^{(0+1)}$  with a divergence-free stress tensor:

$$u_i^2 = \left( \vec{v}^2 + \vec{w}^2 \mathcal{W} \right) \varepsilon_{ij}^{(0+1)} . \quad (285)$$

We found in all six cases a proportional relation between the divergences of the strain tensor of the initial displacement and the divergence of the strain tensor of the new displacement ( $\boldsymbol{\varepsilon}_{ij}^0 \propto \boldsymbol{\varepsilon}_{ij}^{(0+1)}$ ). Therefore we can change the ansatz as above to

$$u_k = \left( \overset{2}{v}\mathcal{V} + \overset{2}{w}\mathcal{W} \right) \boldsymbol{\varepsilon}_{ij}^0 \quad , \quad (286)$$

where the functions  $\overset{2}{\mathcal{V}}$  and  $\overset{2}{\mathcal{W}}$  were again determined by the differential equation (28). The constant  $\overset{2}{w}$  and  $\overset{2}{v}$  enabled us to fit our calculations for two boundary condition. In all the considered cases, except the wedge disclination, we don't need the constant  $\overset{2}{v}$ , because the modification of the initial displacement field (see eq. (283)) leads already to a realistic displacement analogous to a crystal. This is not the fact for the wedge disclination, where we need the second constant to get a displacement field analogous to a tubular cylinder.

The combination of the *additional* vector fields  $\overset{1}{\vec{u}} + \overset{2}{\vec{u}}$  may be interpreted physically as the elastic deformation of the body caused by the *initial* displacement, i.e., the defect. The kernel of our algorithm, the divergence of the strain tensor, can be considered as the characteristic part of this *reactive* deformation. In this sense is our approach to get a divergence-free stress tensor physically motivated, beside the mathematically motivated known algorithm. We think that the *reactive* deformation may be helpful for any numerical and analytical calculations in elasticity theory, especially if the other algorithm fails. Respective the similarity of the solved differential equations it may be also useful for physics with related mathematics.

We demonstrated for the dislocations and the wedge disclination of a tubular cylinder the similarity between the intensity distribution of circular polarized light and the specific energy for changing the shape of the origin body. We remarked moreover the approximately analogous course of the isolines of the amount of the stress vector field. This does not always mean an analogous distribution of the amount of the isolines.

We showed in all the considered cases that the divergence of the stress tensor of the initial displacement field is proportional to the divergence of the belonging strain tensor.

## 9.2 The new Volterra defects

Our algorithm allows to calculate for all six Volterra defects the realistic displacement fields which are approximately analogous to a crystal or to a tubular cylinder. In our cases (except the wedge disclination) there is no extra parameter necessary to get a displacement field with the correct dimensions. For the edge dislocations we got solutions analogous to a crystal and a tubular cylinder, that coincides with earlier calculations. The computed fringe patterns were shown to be similar to the known photographs ([21], [22], [33], [34], [35], [36]). The twist disclinations were an example, how our algorithm matches together with the known equilibrium conditions in 3-dimensions. For the wedge disclination analogous to a tubular cylinder our computed fringe pattern is similar to the photo presented by Volterra [21], [22].

Here we present the summary of the resulting displacement fields. We start with the

initial displacement fields given by

$$\begin{aligned} u_x^0 &= \frac{1}{2\pi} \left( (b_1 + \Omega_1 z + \Omega_3 y) \arctan\left(\frac{y}{x}\right) \right) , \\ u_y^0 &= \frac{1}{2\pi} \left( (b_2 + \Omega_2 z - \Omega_3 x) \arctan\left(\frac{y}{x}\right) \right) , \\ u_z^0 &= \frac{1}{2\pi} b_3 \arctan\left(\frac{y}{x}\right) . \end{aligned} \quad (287)$$

The corresponding *realistic* displacement fields with a divergence free stress tensor writes (without the wedge disclination)

$$\begin{aligned} u_x^r &= \frac{1}{2\pi} \left( \left( (b_1 + \Omega_1 z) \arctan\left(\frac{y}{x}\right) \right. \right. \\ &\quad \left. \left. - \frac{1 - \overset{2}{w}}{(4\nu - 3)(x^2 + y^2)} \left( (b_1 + \Omega_1 z)xy - (b_2 + \Omega_2 z) \frac{(x^2 - y^2)}{2} \right) \right) \right) , \\ u_y^r &= \frac{1}{2\pi} \left( \left( (b_2 + \Omega_2 z) \arctan\left(\frac{y}{x}\right) \right. \right. \\ &\quad \left. \left. + \frac{1 - \overset{2}{w}}{(4\nu - 3)(x^2 + y^2)} \left( (b_2 + \Omega_2 z)xy + (b_1 + \Omega_1 z) \frac{(x^2 - y^2)}{2} \right) \right) \right) , \\ u_z^r &= \frac{1}{2\pi} \left( (b_3 + \Omega_1 x + \Omega_2 y) \arctan\left(\frac{y}{x}\right) \right) . \end{aligned} \quad (288)$$

For  $\overset{2}{w} = 0$  they may be interpreted as approximately analogous to a crystal, and for  $\overset{2}{w} = 2\nu r_1^2$  as analogous to a tubular cylinder with the inner radius  $r_1$ .

Our solution for the approximative wedge disclination is based on the displacement field given by Volterra [20] and reads (see eq.(253))

$$\begin{aligned} u_x &= \frac{\Omega_3}{2\pi} \left( y \arctan\left(\frac{y}{x}\right) - x \frac{2\nu - 1}{4(\nu - 1)} \ln\left(\frac{x^2 + y^2}{r_1^2}\right) \right. \\ &\quad \left. - \left( \frac{\overset{2}{v}}{(x^2 + y^2)} + \overset{2}{w} \right) \frac{\nu}{(\nu - 1)} x \right) , \\ u_y &= \frac{\Omega_3}{2\pi} \left( -x \arctan\left(\frac{y}{x}\right) - y \frac{2\nu - 1}{4(\nu - 1)} \ln\left(\frac{x^2 + y^2}{r_1^2}\right) \right. \\ &\quad \left. - \left( \frac{\overset{2}{v}}{(x^2 + y^2)} + \overset{2}{w} \right) \frac{\nu}{(\nu - 1)} y \right) , \\ u_z &= 0 . \end{aligned} \quad (289)$$

Volterra got the same ansatz, but he calculated the constants another way. Our modification leads for  $\overset{2}{v} = 0$ , and for

$$\overset{2}{w} = - \frac{(2\nu - 1) \left( r_2^2 \ln(r_2^2/r_1^2) + 4\nu\overset{2}{v} \right) + 2(\nu - 1)r_2^2}{4\nu r_2^2} , \quad (260)$$

to a displacement field, which can be interpreted as analogous to a crystal.

We get the displacement field corresponding to a tubular cylinder if we change the constant  $\frac{2}{v}$  to

$$\frac{2}{v} = \frac{r_1^2 r_2^2}{4\nu(r_2^2 - r_1^2)} \ln(r_2^2/r_1^2) \quad . \quad (273)$$

### **Acknowledgments**

The author thanks F.W. Hehl for critically reading the manuscript and important advises, Ralph Metzler, Uwe Münch, Frank Gronwald and Roland Puntigam for helpful discussions, and the “Graduiertenkolleg Scientific Computing Köln St.-Augustin” for support.

## References

- [1] **G. Galilei**, Discorsi e Dimostrazioni matematiche, Leiden (1638).
- [2] **L.D. Landau** and **E.M. Lifschitz**, Lehrbuch der Physik **7**, Elastizitätstheorie, Akademie Verlag Berlin (1965).
- [3] **A.E.H. Love**, A Treatise on the Mathematical Theory of Elasticity, 4th. edition, Dover Publications, New York (1944).
- [4] **E. Orowan** Zur Kristallplastizität, Z. Phys. **89** (1934) 605-659.
- [5] **M. Polanyi** Über eine Art Gitterströmung, die einen Kristall plastisch machen könnte, Z. Phys. **89** (1934) 660-664.
- [6] **G.I. Taylor** The mechanism of plastic deformation of crystals, Proc. roy. Soc. London Ser. A, **145** (1943) 362-415.
- [7] **E. Kröner**, Kontinuumstheorie der Versetzungen und Eigenspannungen, Springer Verlag Berlin (1958).
- [8] **H. Kleinert**, Gauge Fields in Condensed Matter, vol. II. World Scientific, Singapore (1989).
- [9] **M. Kléman**, Dislocation in Solids, Vol. 5, ed. F.R.N. Nabarro North-Holland, Amsterdam, (1980)
- [10] **Y. Bouligand**, Physique des Défauts, eds R. Balian, M. Kléman and J.P. Poirier, North-Holland, Amsterdam, (1981)
- [11] **M. Kléman**, Points, Lines and Walls Wiley, New York, (1983)
- [12] **F.R.N. Nabarro**, Physics of Strength and Plasticity, ed. A.S. Argon MIT Press, Cambridge, Ma, (1969) p. 97
- [13] **J.F. Nye**, Proc. Roy. A 387 (1983) 105
- [14] **B.J. Galperin**, Physique des Défauts, eds R. Balian, M. Kléman and J.P. Poirier, North-Holland, Amsterdam, (1981) p. 813.
- [15] **T.-W. Chou** and **H.J. Malasky**, J. Geophys. Res. B 84 (1974) 6083.
- [16] **K. Anthony**, **U. Essmann**, **A. Seeger** and **H. Träuble**, Mechanics of Generalized Continua, ed. E. Kröner Springer, Berlin (1968) p. 355.
- [17] **M.M. Salomaa** and **G.E. Volovik** Rev. Mod. Phys. 59 (1987) 533.
- [18] **K.P. Tod**. Conical singularities and torsion, Class. Quantum Grav. **11** (1994) 1331-1339 .
- [19] **R.A. Puntigam** and **H.H. Soleng**, Volterra Distorsions, Spinning Strings, and Cosmic Defects, submitted to Class. Quantum Grav. (1996).

- [20] **V. Volterra**, Sur l'équilibre des corps élastiques multiplément connexe, Ann. Ec. Norm. Sup. **24** (3) (1907) 401-515 .
- [21] **V. Volterra**, Drei Vorlesungen über neuere Fortschritte der mathematischen Physik, B.G.Teubner Berlin (1914).
- [22] **V. Volterra** and **E. Volterra** , Sur les distorsions des corps élastiques, Gauthier-Villars Paris (1960).
- [23] **R. deWit**, Theory of Disclinations 3: Continuous and Discrete Disclinations in Isotropic Elasticity, Journal of Research, National Bureau of Standards **77A** No. 3 (1973) 359-368 .
- [24] **R. deWit**, Theory of Disclinations 4: Straight Disclinations, Journal of Research, National Bureau of Standards **77A**, No. 5 (1973) 608-658 .
- [25] **J.Friedel**, Dislocations. Pergamon Press 1964
- [26] **F.R.N. Nabarro**, Theory of Crystal Dislocations Clarendon Press, Oxford, (1967).
- [27] **F.C. Frank**, Dic. Farad. Soc. 25 (1958) 19.
- [28] **A.E. Romanov** and **V.I. Vladimirov**, Disclinations in Crystalline Solids, Dislocation in Solids North-Holland Publishing Company ed. by F.N.R. Nabarro **9** (1992) 191-402 .
- [29] **J.S. Koehler**, On the Dislocation Theory of Plastic Deformation. Phys. Rev. **60** (1941) 397-410 .
- [30] **G. Leibfried** und **K. Lücke**, Über das Spannungsfeld einer Versetzung, Zeitschrift für Physik **126** (1949) 450-464.
- [31] **P.W. Berg** and **J.L. McGregor**, Elementary Partial Differential Equations, Department of Mathematics, Stanford University, Holden-Day, Inc. San Francisco (1966).
- [32] **F. Mises**, Differentialgleichungen **2A**, Viewegdruck Braunschweig (1935).
- [33] **R. Bullough**, Birefringence Caused by Edge Dislocation in Silicon, Phys. Rev. **110** (1958) 620-624 .
- [34] **W.L. Bond** and **J. Andrus**, Photographs of the Stress field around Edge Dislocations, Phys. Rev. **101** (1956) 111 .
- [35] **V.I. Nikitenko** and **L. M. Dedukh**, Application of the Photoelasticity Method to the Investigation of Stresses around individual Dislocations and their Influence on Crystal Properties, Phys. stat. sol. (A) **3** (1970) 383-392 .
- [36] **A.M. Kosevich**, Crystal Dislocation and the Theory of Elasticity, Dislocation in Solids, North-Holland Publishing Company ed. by F.R.N. Nabarro **1** (1979) 33-141 .



- [37] **I.S. Sokolnikoff**, *Mathematical Theory of Elasticity*, McGraw-Hill New York (1956).
- [38] **E. Klingbeil**, *Tensorrechnung für Ingenieure*, B.I. Wissenschaftsverlag, Hochschultaschenbuch Band 197, Mannheim (1989).
- [39] **H. Eschenauer**, *Elastizitätstheorie*, Band 1, B.I. Wissenschaftsverlag, Zürich (1981).
- [40] **J.W. Steeds** and **J.R. Willis** *Dislocation in Anisotropic Media*, *Dislocation in Solids*, North-Holland Publishing Company ed. by F.R.N. Nabarro **1** (1979) 141-164 .
- [41] **G. Green**, *Transactions of the Cambridge Philosophical Society*, **7** (1839) 121 .
- [42] **D. Bovet**, *The Continuous Theory of Dislocations in Elastostatics and Elastodynamics*, *SM Archives*, Vol. 4, Issue 1, Sijthoff & Noordhoff International Publishers Alphen aan den Rijn, Netherlands (1979).
- [43] **J. and J. Weertman**, *Elementary Dislocation theory*, Oxford University Press (1992).
- [44] **S. Flügge**, *Handbuch der Physik*, **6**, *Elastizität und Plastizität*, Springer Verlag Berlin (1958).
- [45] **F.R.N. Nabarro**, ed., *Dislocation in Solids*, vols. 1-9 North-Holland, Amsterdam, (1979-1992).

For more literature see e.g. [7] or [45].



## A The divergence of the stress tensor

In this appendix we will prove for the x-edge dislocation, that the function  $\overset{1}{\mathcal{W}}$  of eq.(37) solves, together with the constant  $\overset{1}{w}$  of eq.(38), the differential equations (36). For this purpose we will explicitly calculate the x- and the y-component of the divergence of the stress tensor.

The x-component of the divergence of the stress tensor is given by

$$\sigma^{xj}_{,j} = \sigma^{xx}_{,x} + \sigma^{xy}_{,y} + \sigma^{xz}_{,z} \quad , \quad (290)$$

that reads with the generalized Hooke's law from eq.(7)

$$\sigma^{xj}_{,j} = \frac{E}{(1+\nu)} \left( \frac{1}{(1-2\nu)} \left[ (1-\nu)\epsilon_{xx} + \nu(\epsilon_{yy} + \epsilon_{zz}) \right]_{,x} + \epsilon_{xy,y} + \epsilon_{xz,z} \right) \quad . \quad (291)$$

It follows with the strain tensors of eq.(23) and eq.(26),

$$\begin{aligned} \sigma^{xj}_{,j} = & \frac{E}{(1+\nu)} \left( \frac{1}{(1-2\nu)} \left[ (1-\nu) \left( \overset{0}{\epsilon}_{xx} + \overset{1}{w} \left( \overset{1}{\mathcal{W}} \overset{0}{\epsilon}_{xm,m} \right)_{,x} \right) \right. \right. \\ & \left. \left. + \nu \left( \overset{0}{\epsilon}_{yy} + \overset{1}{w} \left( \overset{1}{\mathcal{W}} \overset{0}{\epsilon}_{ym,m} \right)_{,y} + \overset{0}{\epsilon}_{zz} + \overset{1}{w} \left( \overset{1}{\mathcal{W}} \overset{0}{\epsilon}_{zm,m} \right)_{,z} \right) \right]_{,x} \right. \\ & \left. + \left[ \overset{0}{\epsilon}_{12} + \frac{\overset{1}{w}}{2} \left( \left( \overset{1}{\mathcal{W}} \overset{0}{\epsilon}_{ym,m} \right)_{,x} + \left( \overset{1}{\mathcal{W}} \overset{0}{\epsilon}_{xm,m} \right)_{,y} \right) \right]_{,y} \right. \\ & \left. + \left[ \overset{0}{\epsilon}_{xz} + \frac{\overset{1}{w}}{2} \left( \left( \overset{1}{\mathcal{W}} \overset{0}{\epsilon}_{zm,m} \right)_{,x} + \left( \overset{1}{\mathcal{W}} \overset{0}{\epsilon}_{xm,m} \right)_{,z} \right) \right]_{,z} \right) \quad . \quad (292) \end{aligned}$$

This can be written as

$$\begin{aligned} (1-2\nu)\sigma^{xj}_{,j} = & \frac{E}{1+\nu} \left( \overset{1}{w} \left[ (1-\nu) \left( \overset{1}{\mathcal{W}} \overset{0}{\epsilon}_{xm,m} \right)_{,x,x} \right. \right. \\ & \left. \left. + \left( \frac{1}{2} - \nu \right) \left( \left( \overset{1}{\mathcal{W}} \overset{0}{\epsilon}_{xm,m} \right)_{,y,y} + \left( \overset{1}{\mathcal{W}} \overset{0}{\epsilon}_{xm,m} \right)_{,z,z} \right) \right. \right. \\ & \left. \left. + \frac{1}{2} \left( \left( \overset{1}{\mathcal{W}} \overset{0}{\epsilon}_{ym,m} \right)_{,x,y} + \left( \overset{1}{\mathcal{W}} \overset{0}{\epsilon}_{zm,m} \right)_{,x,z} \right) \right] \right. \\ & \left. + (1-\nu) \overset{0}{\epsilon}_{xx,x} + (1-2\nu) \left( \overset{0}{\epsilon}_{xy,y} + \overset{0}{\epsilon}_{xz,z} \right) + \nu \left( \overset{0}{\epsilon}_{yy,x} + \overset{0}{\epsilon}_{zz,x} \right) \right) \quad . \quad (293) \end{aligned}$$

We insert the strain tensor (33) and its divergence (34). The x-component of the divergence of the stress tensor vanishes, if the following partial differential equation with

variable coefficients (36) is fulfilled:

$$\begin{aligned} & \overset{1}{w} \left[ (1 - \nu) \left( \overset{1}{\mathcal{W}} \frac{xy}{(x^2 + y^2)^2} \right)_{,x,x} \right. \\ & + \left. \left( \frac{1}{2} - \nu \right) \left( \left( \overset{1}{\mathcal{W}} \frac{xy}{(x^2 + y^2)^2} \right)_{,y,y} + \left( \overset{1}{\mathcal{W}} \frac{xy}{(x^2 + y^2)^2} \right)_{,z,z} \right) \right. \\ & \left. - \frac{1}{2} \left( \overset{1}{\mathcal{W}} \frac{x^2 - y^2}{2(x^2 + y^2)^2} \right)_{,x,y} \right] + \frac{xy}{(x^2 + y^2)^2} = 0 \quad . \end{aligned} \quad (294)$$

If we choose (eq.(37))

$$\overset{1}{\mathcal{W}} = x^2 + y^2 \quad ,$$

and (eq.(38))

$$\overset{1}{w} = -\frac{1}{(4\nu - 3)} \quad ,$$

this reads

$$\begin{aligned} & -\frac{1}{(4\nu - 3)} \left[ (1 - \nu) \right. \\ & \times \left( \left( \frac{xy}{(x^2 + y^2)^2} \right)_{,x,x} + \left( \frac{1}{2} - \nu \right) \left( \frac{xy}{(x^2 + y^2)^2} \right)_{,y,y} + \left( \frac{xy}{(x^2 + y^2)^2} \right)_{,z,z} \right. \\ & \left. - \frac{1}{2} \frac{x^2 - y^2}{2(x^2 + y^2)^2} \right]_{,x,y} + \frac{xy}{(x^2 + y^2)^2} = 0 \quad , \end{aligned} \quad (295)$$

and turns finally out to

$$-\frac{2}{(4\nu - 3)} \left[ (1 - \nu)(x^2 - 3y^2) + \left( \frac{1}{2} - \nu \right)(-3x^2 + y^2) - (x^2 - y^2) \right] + (x^2 + y^2) = 0 \quad .$$

The y-component of the stress tensor vanishes if

$$\begin{aligned} & \overset{1}{w} \left[ (1 - \nu) \left( \overset{1}{\mathcal{W}} \overset{0}{\boldsymbol{\varepsilon}}_{ym}^0 \right)_{,y,y}^m + \left( \frac{1}{2} - \nu \right) \left( \left( \overset{1}{\mathcal{W}} \overset{0}{\boldsymbol{\varepsilon}}_{ym}^0 \right)_{,x,x} + \left( \overset{1}{\mathcal{W}} \overset{0}{\boldsymbol{\varepsilon}}_{ym}^0 \right)_{,z,z} \right) \right. \\ & \left. + \frac{1}{2} \left( \left( \overset{1}{\mathcal{W}} \overset{0}{\boldsymbol{\varepsilon}}_{xm}^0 \right)_{,x,y} + \left( \overset{1}{\mathcal{W}} \overset{0}{\boldsymbol{\varepsilon}}_{zm}^0 \right)_{,y,z} \right) \right] \\ & + (1 - \nu) \overset{0}{\boldsymbol{\varepsilon}}_{yy}^0 \overset{y}{y} + (1 - 2\nu) \left( \overset{0}{\boldsymbol{\varepsilon}}_{xy}^0 \overset{x}{x} + \overset{0}{\boldsymbol{\varepsilon}}_{yz}^0 \overset{z}{z} \right) + \nu \left( \overset{0}{\boldsymbol{\varepsilon}}_{xx}^0 \overset{y}{y} + \overset{0}{\boldsymbol{\varepsilon}}_{zz}^0 \overset{y}{y} \right) = 0 \quad . \end{aligned} \quad (296)$$

With eq.(37) and eq.(38), the strain tensor (33), and its divergence (34) we achieve

$$\begin{aligned} & \frac{1}{(4\nu - 3)} \left[ - (1 - \nu) \left( \frac{x^2 - y^2}{2(x^2 + y^2)^2} \right)_{,y,y} + \left( \frac{1}{2} - \nu \right) \left( \frac{x^2 - y^2}{2(x^2 + y^2)^2} \right)_{,x,x} \right. \\ & \left. - \frac{1}{4} \left( \frac{xy}{(x^2 + y^2)^2} \right)_{,x,y} \right] \\ & + (1 - 2\nu) \left( \frac{x}{2(x^2 + y^2)^2} \right)_{,x} - \nu \left( \frac{y}{(x^2 + y^2)^2} \right)_{,y} = 0 \quad , \end{aligned} \quad (297)$$

which reads explicitly

$$\frac{1}{(4\nu - 3)} \left[ (1 - \nu)2x^2(-x^2 + 3y^2) + \left(\frac{1}{2} - \nu\right)2y^2(-3x^2 + y^2) - \frac{1}{2}(-x^4 + 6x^2y^2 - y^4) \right] - \frac{1}{2}(x^2 - y^2)(x^2 + y^2) = 0 \quad . \quad (298)$$

The function  $\mathcal{W}^1$  chosen in eq.(37) and the constant  $w^1$  in eq.(38) are one solution of the differential equation (28).

## B Reduce-Programm für die Elastizitätstheorie

Hier wird das zur Erstellung dieser Arbeit erzeugte Reduce-Programm vorgestellt, mit welchem die charakteristischen Größen der linearen Elastizitätstheorie berechnet werden können. Als Beispiel dient die X-Stufenversetzung nach Volterra. Aufgrund der Analogie der Berechnung der Tensorgrößen werden diese nur einfach angeführt.

```

clear uu,vv,ww,phi,ra,lis,sigma,ela,c1,ew,x,y,z,za$
clear le,ke,tvr11,tvr12,tvr21,tvr22,ny,my,lamda,energy,gg,hh;
clear ii,jj,nu,c1,c2,c3,equi,uv,xv,ver,tsp,g,atan(y/x)$
array equi(3),n(3),divt(3),divtn1(3),uv(3),xv(3)$
      %Verzerrungstensor
clear x11,x12,x13,x21,x22,x23,x31,x32,x33,ew,ew1,ew2,ew3,ewk$
clear ev1,ev2,ev3,ev11,ev12,ev13,ev21,ev22,ev23,ev31,ev32,ev33$
clear lis,lew,multi,n31,n32,n33,n11,n12,n13,vminor,vdminor;
clear ma3,mew3,u3,vdet,vddet,vspur,vdspur,tspurneu1,mino1,mino2,mino3,dia3;
matrix ma3(3,3),u3(3,3),un3(3,3),dia3(3,3),ver(3,3),g(3,3)$
matrix mew3(3,3),mino1(2,2),mino2(2,2),mino3(2,2);
      %Spannungstensor:
clear tspur,tdspur,tdet,tddet,tminor,tdminor,tmi1,tmi2,tmi3;
matrix tsp(3,3),tma3(3,3),ut(3,3),utn(3,3),tdia(3,3),ttm(3,3)$
matrix tm(3,3),tmew3(3,3),tmi1(2,2),tmi2(2,2),tmi3(2,2)$
clear energy,energy2,energy2a,r,r1,r2,phi,inten,intencirc,intensi;
clear fla1,fla2,fla3,pv,pu,xn,yn,zn,xn2,yn2,zn2,divuneu1;
clear uu1,uu2,uu3,vv1,vv2,pfn1,pfn2,pfn3,pfnr,sv1,sv2,s,sv31;
clear betap,gammap,deltap,thetap,pol11,pol12,pol13,bpol,bev1,bev2;
clear intenn,intenb,betapb,gammapb,polb1,polb2,polb3,bpolb,konst;
clear fxnk,fynk,fznk,frnz,fphinz,fznz,uvenery,ufenergy;
      load_package avector;
vec uuu,fla,no,norm,ve1,ve2,ve3,no2,norm2,ka1,ka2,ka3$
clearrules;
clear x,y,z,r,phi;
      load_package gentran;
gentranlang!* := 'C;
on mcd; on gcd;
on factor; on echo; on nat;
      %Selbstdefinition der Logarythmusableitung:
for all x let df(log10(x),x)=(1/(x*log(10)));
let{(sin(~f)**2)+(cos(~f)**2)=>1};
      %Eingabe der Deformationen:
%In Zylinderkoordinaten gilt:
%xv(1):=ra;%xv(2):=phi;%xv(3):=za;
%In kartesischen Koordinaten gilt:
xv(1):=x; xv(2):=y; xv(3):=z;

clear lamda,my,nu;
%Versetzungen speziell nach Weertmann .36; Trafo zwischen lambda, my und E,nu
uu:=(b/(2*pi))*(atan(y/x)+((lamda+my)/(lamda+2*my))*((x*y)/(x*x+y*y)));
vv:=(b/(2*pi))*(-my/(2*(lamda+2*my))*log((x*x+y*y))
+((lamda+my)/(lamda+2*my))*((y*y)/(x*x+y*y)));
ww:=0;

%Transformationsformeln WEERTMANN --> LANDAU (Kleinert .761)
my:=ela/(2*(1+sigma));
lamda:=ela*sigma/((1+sigma)*(1-2*sigma));
%nu:=sigma;
sigma:=nu;

```

```

%ela:=my*(3*lamda+2*my)/(lamda+my);
%sigma:=lamda/(2*(lamda+my));

%Uberpr"ufung der "Gleichgewichtbedinungen" (Landau .20)
%biharmonische Gleichung
clear ii,jj,equi;
array equi(3);
uv(1):=uu; uv(2):=vv; uv(3):=ww;
for ii:=1:3 do equi(ii):=(for jj:=1:3 sum ((1/(1-2*nu))*
df(df(uv(jj),xv(ii)),xv(jj))+df(df(uv(ii),xv(jj)),xv(jj))));
equi(1);equi(2);equi(3);

%Bestimmung der Divergenz des Verzerrungsvektorfeldes vec uuu:
uuu:=avec(uu,vv,ww);
divu:=div(uuu);
%curl(uuu);

%Berechnung bzgl. des Weges s(t)=(cos(t), sin(t),0) (Feldmann .315)
%mit :ds(t)/dt=(-sin(t), cos(t),0)
clear oint1,oint2,x,y;
x:=cos(t); y:=sin(t);
oint1:=int((uv(1)*(-1)*sin(t)),t); oint2:=int((uv(2)*cos(t)),t);
clear x,y;

%Berechnung des Verzerrungstensors nach Lifschitz:
ver(1,1):=(df(uv(1),xv(1))); ver(2,2):=(df(uv(2),xv(2)));
ver(3,3):=(df(uv(3),xv(3))); ver(1,2):=0.5*((df(uv(1),xv(2))+df(uv(2),xv(1))));
ver(1,3):=0.5*((df(uv(1),xv(3))+df(uv(3),xv(1))));
ver(2,3):=0.5*((df(uv(2),xv(3))+df(uv(3),xv(2))));
ver(2,1):=ver(1,2); ver(3,2):=ver(2,3); ver(3,1):=ver(1,3);
ver(2,1):=ver(1,2); ver(3,1):=ver(1,3); ver(3,2):=ver(2,3);

%Berechnung der ST. Venant Komponenten;
stven1123:=df((-df(ver(2,3),xv(1))+df(ver(3,1),xv(2))
+df(ver(1,2),xv(3))),xv(1))-df(df(ver(1,1),xv(2)),xv(3));
stven2231:=df((df(ver(2,3),xv(1))-df(ver(3,1),xv(2))
+df(ver(1,2),xv(3))),xv(2))-df(df(ver(2,2),xv(3)),xv(1));
stven3312:=df((df(ver(2,3),xv(1))+df(ver(3,1),xv(2))
-df(ver(1,2),xv(3))),xv(3))-df(df(ver(3,3),xv(1)),xv(2));
stven1212:=df(df(ver(1,1),xv(2)),xv(2))+df(df(ver(2,2),xv(1)),xv(1))
-2*df(df(ver(1,2),xv(1)),xv(2));
stven2323:=df(df(ver(2,2),xv(3)),xv(3))+df(df(ver(3,3),xv(2)),xv(2))
-2*df(df(ver(2,3),xv(2)),xv(3));
stven1313:=df(df(ver(3,3),xv(1)),xv(1))+df(df(ver(1,1),xv(3)),xv(3))
-2*df(df(ver(3,1),xv(3)),xv(1));
%Summe der Saint Venant Gleichungen:
sstven:=stven1123+stven2231+stven3312+stven1212+stven2323+stven1313;

%Berechnung der Divergenz des Verzerungstensors
%Reducefile volt/reduce/div.rei
%TENSORDIVERGENZ kovariant Ableitung!!!! (Schaum Tensoranalysis .186)
%F"ur symmetrische Matrize gilt: A=AT (A transponiert), EW sind reell
%Kartesische Koordinaten ausgedr"uckt in den neuen Koordinaten n_i :
xv(1):=x$ xv(2):=y$ xv(3):=z$
%neue allgemeine Koordinaten n_i :
n(1):=x; n(2):=y; n(3):=z;

```

```

%Berechnung der metrischen Koeffizienten g_ij= (dr/du_i)*(dr/du_j)
g(1,1):= ((df(xv(1),n(1)))*(df(xv(1),n(1)))+(df(xv(2),n(1)))
*(df(xv(2),n(1)))+(df(xv(3),n(1)))*(df(xv(3),n(1)))));
for ii:=1:3 do for jj:=1:3 do (g(ii,jj):= (for kk:=1:3 sum
(df(xv(kk),n(ii))*df(xv(kk),n(jj)))) );
g(1,1);g(1,2);g(1,3);g(2,1);g(2,2);g(2,3);g(3,1);g(3,2);g(3,3);
%Berechnung der einzelnen Komponenten der Divergenz (Wheeler .82):
for jj:=1:3 do <<divv(jj):= for ii:=1:3 sum (1/sqrt(det(g))
*df((sqrt(det(g))*ver(jj,ii)),xv(ii)))>>;
divv(1);divv(2);divv(3);%Divergenz des alten Verzerrungstensors

%Diagonalisierung des Verzerrungstensors:
%BESTIMMUNG DER EIGENVEKTOREN:Hier mit frei gew"ahltem x11=x21=x33=1 !!!
%F"ur symmetrische Matrize gilt: A=AT (A transponiert), EW sind reell
%Die Komponenten des diagonalisierten Tensors sind die Eigenwerte
%Bestimmung der Eigenwerte der Matrix ver:
on mcd; on gcd;
ma3:=ver$
mew3:=ver$
for ll:=1:3 do mew3(ll,ll):=ma3(ll,ll)-ew$
%L"osen der charakteristischen Gleichung
lew:=solve(det(mew3),ew);
multi:=multiplicities!*;
%Eigenwerte des Verzerrungstensors
ew1:=rhs(first(lew)); ew2:=rhs(second(lew)); ew3:=rhs(third(lew));
vew1:=ew1; vew2:=ew2; vew3:=ew3;

%Bestimmung der Eigenvektoren der Matrix ver:
%Festlegung der evtl. frei w"ahlbaren Komponente der Eigenvektoren:
% z.B x11:=1$ dann mu/3 die Variable x11 aber aus dem Gleichungssystem
%der EW entfernt werden...)
%Je nach frei gew"ahltem Faktor (zB. x11) sind die evij zu bestimmen
%Achtung manchmal kann die Wahl des frei gew"ahlten Faktors die
%L"osbarkeit beeintr"achtigen - dann ANDEREN FAKTOR FREI W"AHLEN !!!!!
%ACHTUNG DURCH DIE FESTE VORGABE z.B x11:=1 wird der Nenner von x12
%in den Z"ahler von x11 geschrieben !!!!!!!!!!!!!!!!!!!!!!!!!!!!!!!!!!!!!!!
x11:=1$ %frei gew"ahlt
ev1:=solve({(ma3(1,1)-ew1)*x11+ma3(1,2)*x12+ma3(1,3)*x13,
ma3(2,1)*x11+(ma3(2,2)-ew1)*x12+ma3(2,3)*x13,
ma3(3,1)*x11+ma3(3,2)*x12+(ma3(3,3)-ew1)*x13}, {x12,x13})$
ev11:=1; ev12:=rhs(first(first(ev1))); ev13:=rhs(second(first(ev1)));

x21:=1$
ev2:=solve({(ma3(1,1)-ew2)*x21+ma3(1,2)*x22+ma3(1,3)*x23,
ma3(2,1)*x21+(ma3(2,2)-ew2)*x22+ma3(2,3)*x23,
ma3(3,1)*x21+ma3(3,2)*x22+(ma3(3,3)-ew2)*x23}, {x22,x23})$
ev21:=x21; ev22:=rhs(first(first(ev2))); ev23:=rhs(second(first(ev2)));

x33:=1$
ev3:=solve({(ma3(1,1)-ew3)*x31+ma3(1,2)*x32+ma3(1,3)*x33,
ma3(2,1)*x31+(ma3(2,2)-ew3)*x32+ma3(2,3)*x33,
ma3(3,1)*x31+ma3(3,2)*x32+(ma3(3,3)-ew3)*x33}, {x31,x32})$
ev31:=rhs(first(first(ev3))); ev32:=rhs(second(first(ev3))); ev33:=x33;

%Spur des Verzerrungstensors:
trace (ver);vspur:=ver(1,1)+ver(2,2)+ver(3,3);

```



```

%Determinante des Verzerrungstensors:
vdet:=det(ver);
%Summe der Minoren:
%Bestimmung der ersten Minoren zu den Spurelementen (Teichmann .42)
mino1(1,1):=ver(2,2); mino1(1,2):=ver(2,3);
mino1(2,1):=ver(3,2); mino1(2,2):=ver(3,3);
%Bestimmung der zweiten Minoren zu den Spurelementen
mino2(1,1):=ver(3,3); mino2(1,2):=ver(3,1);
mino2(2,1):=ver(1,3); mino2(2,2):=ver(1,1);
%Bestimmung der dritten Minoren zu den Spurelementen
mino3(1,1):=ver(1,1); mino3(1,2):=ver(1,2);
mino3(2,1):=ver(2,1); mino3(2,2):=ver(2,2);
%UNBEDINT RANG BEACHTEN SONST WERDEN DIE DETERMINANTEN FALSCH!!!!
%Ist der Rang der Matrix niedriger als der hier definierte, so ist die
%Determinante =0
det(mino1); det(mino2); det(mino3);
%Summe der Minoren des Verzerrungstensors
vminor:=det(mino1)+det(mino2)+det(mino3);

%Berechnung des Spannungstensors nach Lifschitz (.17):
tsp(1,1):=(ela/((1+sigma)*(1-2*sigma)))*((1-sigma)*ver(1,1)+sigma*(ver(2,2)+ver(3,3)));
tsp(2,2):=(ela/((1+sigma)*(1-2*sigma)))*((1-sigma)*ver(2,2)+sigma*(ver(1,1)+ver(3,3)));
tsp(3,3):=(ela/((1+sigma)*(1-2*sigma)))*((1-sigma)*ver(3,3)+sigma*(ver(1,1)+ver(2,2)));
tsp(1,2):=(ela/(1+sigma))*ver(1,2); tsp(1,3):=(ela/(1+sigma))*ver(1,3);
tsp(2,3):=(ela/(1+sigma))*ver(2,3);
tsp(2,1):=tsp(1,2)$tsp(3,1):=tsp(1,3)$tsp(3,2):=tsp(2,3)$

%Berechnung der Volumen"anderungsenergie uvenergy:
uvenergy:=1.0/6.0*(tspur*vspur);
%Berechnung der Form"anderungsenergie
ufenergy:=energy-uvenergy;

%Berechnung der Spannungsoptischen Aktivit"at
%Photoelasticity method, nach Bullough
clear x,y,ra,phi;
%betap:=Winkel zwische Polarisatorebene u. Versetzungsebene (KONSTANT)
%Eingabe der Polarisatorebene (wird durch betap bestimmt)
%und ist definiert von Polarisationssebene aus in Richtung
%der Versetzungsebene
%betap:=0;
pol11:=cos(betap);
pol12:=sin(betap);
pol13:=0;
bpol:=sqrt(pol11*pol11+pol12*pol12+pol13*pol13);

%Eingabe der Polarisatorebene (wird durch betap bestimmt)
betapb:=-pi/4; %betap=-45 Achtung beta geht als -beta in die Rechnung ein
%definiert von Polarisationssebene aus in Richtung
polb1:=cos(betapb); %Achtung beta geht als -beta in die Rechnung ein
polb2:=sin(betapb); %definiert von Polarisationssebene aus in Richtung
polb3:=0; %der Versetzungsebene
bpolb:=sqrt(polb1*polb1+polb2*polb2+polb3*polb3);
bev1:=sqrt(ev11*ev11+ev12*ev12+ev13*ev13);
gammab:=acos((ev11*pol11+ev12*pol12+ev13*pol13)/(bpol*bev1));
clear deltap;
deltap:=konst*(tew1-tew2);

```

```

inten:=intensi*intensi*sin(deltap/2)*sin(deltap/2)*sin(2*gammap)*sin(2*gammap);
%Cicular polarisiert:
intencirc:=intensi*intensi*sin(deltap/2)*sin(deltap/2);

%Bestimmung der Fl"achengleichung (kartesisch) zur Bestimmung der Normalen:
    fla1:=x+uu;fla2:=y+vv;fla3:=z+ww;
%Parametrisierung der Fl"achengleichung durch Zylinderkoordinaten
%zur Bestimmung der Fl"achennormalen:
clear x,y,ra,phi;
x:=ra*cos(phi); y:=ra*sin(phi);
fla:=avec(flal,fla2,fla3);
%Hier wird bestimmt, welcher Normalenvektor genommen wird:
%frho f"ur pv=phi, pu=z; fphi f"ur pv=rho pu=z; fz f"ur pv=rho=ra, pu=phi
pv:=phi;%pv:=ra;%pu:=phi;
pu:=z;
%Bestimmung des Normalenvektors (parametrisiert in Zylinderkoordinaten):
%Bestimmung der partiellen Ableitungen der Fl"achengleichung nach u,v:
pflau:=avec((df(flal,pu)),(df(flal2,pu)),(df(flal3,pu)));
pflav:=avec((df(flal,pv)),(df(flal2,pv)),(df(flal3,pv)));

clear x,y,ra,phi;
ra:=sqrt(x*x+y*y); phi:=atan(y/x);
no:=- (pflav cross pflau); %Kreuzprodukt
%Normierung des Normalenvektors vmod no; Betrag
norm:=no/vmod no$

%Berechnung der Komponenten des Spannungsvektors X_n, Y_n, Z_n der
% auf eine Fl"ache mit der Normalen "norm" wirkt (Muskhelishvili .8 .61f)
%Komponenten des Spannungstensors: tsp(1,1), tsp(1,2),...,tsp(3,3)
%Vorzeichen beachten (Sommerfeld 2 .59)
%Skalarprodukt des Spannungsvektors mit dem entsprechenden Normalenvektor
%Definition der kartesischen Einheitsvektoren
ve1:=avec(1,0,0)$ ve2:=avec(0,1,0)$ ve3:=avec(0,0,1)$
    %Bestimmung der Spannungsvektorkomponenten
xn:=tsp(1,1)*((norm dot ve1)/(vmod norm * vmod ve1))+tsp(1,2)*((norm dot ve2)
/(vmod norm * vmod ve2))+tsp(1,3)*((norm dot ve3)/(vmod norm * vmod ve3));
yn:=tsp(2,1)*((norm dot ve1)/(vmod norm * vmod ve1))+tsp(2,2)*((norm dot ve2)
/(vmod norm * vmod ve2))+tsp(2,3)*((norm dot ve3)/(vmod norm * vmod ve3));
zn:=tsp(3,1)*((norm dot ve1)/(vmod norm * vmod ve1))+tsp(3,2)*((norm dot ve2)
/(vmod norm * vmod ve2))+tsp(3,3)*((norm dot ve3)/(vmod norm * vmod ve3));
    %Spannungsvektor kartesisch:
fxnk:=xn; fynk:=yn; fznk:=zn;

%Trafo des Spannungsvektor in Zylinderkoordinaten
clear alphav,k,l,x,y,z,ra,phi,theta$
clear j,k,vnz1,vnz2,vnz3,va,vn,n,g,gkon,jf$
clear galtll,galthh,gneull,gneuhh;
matrix jf(3,3),gll(3,3),galtll(3,3),galthh(3,3),gneull(3,3),gneuhh(3,3);
array g(3),gkon(3),vn(3),n(3),va(3),xa(3),galt(3),gneu(3),xaz(3),nk(3)$
on echo;on nat;
    %Berechnung der Metriken:
%Berechnung der Metrik der alten Koordinaten:
%Eingabe der kartesischen Koordinaten nk(i) ausgedr"uckt in den
% alten Koordinaten:
%Kartesisch in kartesisch ausgerdr"uckt
nk(1):=x; nk(2):=y; nk(3):=z;

```

```

%Eingabe der alten Koordinaten
%Zylinder
xaz(1):=x; xaz(2):=y; xaz(3):=z;
%Berechnung der Metrik gll_ij:(Gro/3mann .266) f"ur Komponententrafo
for ii:=1:3 do for jj:=1:3 do (galtll(ii,jj):=for kk:=1:3 sum
(df(nk(kk),xaz(ii))*df(nk(kk),xaz(jj))));
%Berechnung der Metrik der neuen Koordinaten (hier Zylinder)
%Eingabe der kartesischen Koordinaten nk(i) ausgedr"uckt in den
% neuen Koordinaten:
nk(1):=ra*cos(phi); nk(2):=ra*sin(phi); nk(3):=z;
%Eingabe der neuen Koordinaten
%Zylinder
xa(1):=ra; xa(2):=phi; xa(3):=z;
%Berechnung der Metrik der neuen Koordinaten
%gneull_ij:(Gro/3mann .266) f"ur Komponententrafo
for ii:=1:3 do for jj:=1:3 do (gneull(ii,jj):=for kk:=1:3 sum
(df(nk(kk),xa(ii))*df(nk(kk),xa(jj))));
%KOVARIANZ !!!!!
%Eingabe der neuen Koordinaten ni in die transformiert werden soll:
%ZYLINDER:
n(1):=ra; n(2):=phi; n(3):=z;
%Angabe der alten Koordinaten xa ausgedr"uckt in den neuen Koordinaten ni:
%kovariant
%KARTESISCH-ZYLINDER:
xa(1):=ra*cos(phi); xa(2):=ra*sin(phi); xa(3):=z;

%Hier Eingabe des alten zu transformierenden Vektorfeldes
va(1):=xn; va(2):=yn; va(3):=zn;
%Berechnung der Komponenten des neuen Vektorfeldes vn:
%kovariant:
for j:=1:3 do <<vn(j):=for k:=1:3 sum (va(k)*sqrt(gneuhh(j,j))*
1/sqrt(galthh(k,k))*df(xa(k),n(j)))>>;
%Zylinder
x:=ra*cos(phi); y:=ra*sin(phi);
clear frnz, fphinz, fznz;
%Spannungsvektor in Zylinder koordinaten frnz, fphinz, fznz:
on nat;
frnz:=vn(1); fphinz:=vn(2); fznz:=vn(3);

%Berechnung des zweiten Spannungsvektors bzgl. der Zylinderdeckel (Z-Achse)
%Parametrisierung der Fl"achengleichung durch Zylinderkoordinaten
%zur Bestimmung der Fl"achennormalen:
clear x,y,ra,phi;
%ra:=sqrt(x*x+y*y); phi:=atan(y/x);
x:=ra*cos(phi); y:=ra*sin(phi);

%Hier wird bestimmt, welcher Normalenvektor genommen wird:
%frho f"ur pv=phi, pu=z; fphi f"ur pv=rho pu=z; fz f"ur pv=rho=ra, pu=phi
%pv:=phi;
pv:=ra;
pu:=phi;
%pu:=z;
%Bestimmung des Normalenvektors (parametrisiert in Zylinderkoordinaten):
%Bestimmung der partiellen Ableitungen der Fl"achengleichung nach u,v:
pflau:=avec((df(flal,pu)),(df(flal2,pu)),(df(flal3,pu)));
pflav:=avec((df(flal,pv)),(df(flal2,pv)),(df(flal3,pv)));

```

```

clear x,y,ra,phi;
ra:=sqrt(x*x+y*y);   phi:=atan(y/x);
%x:=ra*cos(phi);   y:=ra*sin(phi);
no2:=(pflav cross pflau); %Kreuzprodukt
no2(0):=0;   no2(1):=0;   no2(2):=1;
           %Normierung des Normalenvektors
%vmod no; %Betrag
norm2:=(no2)/vmod (no2)$
%Explizite Ausgabe der Komponenten des normierten Normalenvektors
norm2(0); norm2(1); norm2(2);

%Berechnung der Komponenten des Spannungsvektors X_n, Y_n, Z_n der
% auf eine Fl"ache mit der Normalen "norm" wirkt (Muskhelishvili .8 .61f)
%Komponenten des Spannungstensors: tsp(1,1), tsp(1,2),...,tsp(3,3)
%Vorzeichen beachten (Sommerfeld 2 .59)
%Skalarprodukt des Spannungsvektors mit dem entsprechenden Normalenvektor
%Bestimmung der Spannungsvektorkomponenten
xn2:=tsp(1,1)*((norm2 dot ve1)/(vmod norm2 * vmod ve1))
+tsp(1,2)*((norm2 dot ve2)/(vmod norm2 * vmod ve2))+tsp(1,3)
*((norm2 dot ve3)/(vmod norm2 * vmod ve3));
yn2:=tsp(2,1)*((norm2 dot ve1)/(vmod norm2 * vmod ve1))
+tsp(2,2)*((norm2 dot ve2)/(vmod norm2 * vmod ve2))+tsp(2,3)
*((norm2 dot ve3)/(vmod norm2 * vmod ve3));
zn2:=tsp(3,1)*((norm2 dot ve1)/(vmod norm2 * vmod ve1))
+tsp(3,2)*((norm2 dot ve2)/(vmod norm2 * vmod ve2))+tsp(3,3)
*((norm2 dot ve3)/(vmod norm2 * vmod ve3));
off echo; off nat;
clear x,y,ra,phi,atan(y/x);

           %Filebeschreibung hier f"ur C++-Programm:
atan(y/x):=phi;
gentranout "volt1c.Creo";
gentran u1 := eval(uv(1));gentran u2 := eval(uv(2));gentran u3 := eval(uv(3));
           %Divergenz des Deformationsvektorfeldes:
gentran divu := eval(divu);
           %Divergenz des alten Verzerrungstensors
gentran divv1 := eval(divv(1));gentran divv2 := eval(divv(2));
gentran divv3 := eval(divv(3));
           %Eigenwerte des Verzerrungstensors:
gentran ver11 := eval(vew1);gentran ver22 := eval(vew2);
gentran ver33 := eval(vew3);
           %Determinante
gentran vdet := eval(vdet);
           %Minore
gentran vminor := eval(vminor);
           %Divergenz
gentran divt1 := eval(divt(1));
gentran divt2 := eval(divt(2));
gentran divt3 := eval(divt(3));
           %Spannungstensor:
gentran tsp11 := eval(tsp(1,1));gentran tsp22 := eval(tsp(2,2));
gentran tsp33 := eval(tsp(3,3));gentran tsp12 := eval(tsp(1,2));
gentran tsp13 := eval(tsp(1,3));gentran tsp23 := eval(tsp(2,3));
           %Eigenwerte des Spannungstensors:

```

```

gentran ts11 := eval(ew1);gentran ts22 := eval(ew2);
gentran ts33 := eval(ew3);
    %Spannungstensor in Zylinderkoordinaten
gentran tspz11 := eval(neu(1,1));gentran tspz12 := eval(neu(1,2));
gentran tspz13 := eval(neu(1,3));gentran tspz22 := eval(neu(2,2));
gentran tspz33 := eval(neu(3,3));gentran tspz23 := eval(neu(2,3));
    %Eigenvektoren:
gentran ev11 := eval(ev11);gentran ev12 := eval(ev12);
gentran ev13 := eval(ev13);gentran ev21 := eval(ev21);
gentran ev22 := eval(ev22);gentran ev23 := eval(ev23);
gentran ev31 := eval(ev31);gentran ev32 := eval(ev32);
gentran ev33 := eval(ev33);
    %Determinante des Spannungstensors:
gentran tdet := eval(tdet);
    %Summe der Minoren des Spannungstensors
gentran tminor := eval(tminor);
    %Berechnung der freien Energiedichte:
gentran energy := eval(energy);
    %Optische Aktivit"at (lineart polarisiert betap =0)
gentran inten := eval(inten);
    %Optische Aktivit"at (lineart polarisiert betap =pi/4)
%gentran inten45:= eval(intenb);
    %Optische Aktivit"at (cicular polarisiert)
gentran intencirc := eval(intencirc);
    %Normalenvektor (nicht normiert)
gentran n11 := eval(no(0));gentran n12 := eval(no(1));
gentran n13 := eval(no(2));
    %Spannungsvektor (nicht normiert) kartesisch:
gentran f11 := eval(xn);gentran f12 := eval(yn);
gentran f13 := eval(zn);
    %Normalenvektor (normiert)
gentran no31 := eval(norm2(0));gentran no32 := eval(norm2(1));
gentran no33 := eval(norm2(2));
    %Spannungsvektor 2 (nicht normiert) kartesisch:
gentran f31 := eval(xn2);gentran f32 := eval(yn2);
gentran f33 := eval(zn2);
gentranshut "volt1c.Creo";
%Gentran User Manual .46
clear phi,atan(y/x),ra,x,y,ra,r1,phi;;
phi:=atan(y/x); ra:=sqrt(x*x+y*y);
on echo;on nat;

uv(1);uv(2);
%Filebeschreibung
on nat;
off echo;
clear uu,vv,ww;
on echo;
out "volt1c.reo";
%file:/volt/volt1/volt1zyl.rei - volt1.reo
    %Deformationsvektor
uv(1); uv(2); uv(3);
    %Gleichgewichtsbedingung (Divergenz des Spannungstensors)
equi(1); equi(2); equi(3);
    %Komponenten des Umlauflinienintegrals ueber u laengs (cos(t0, sin(t), 0):
    %ES sind noch die Grenzen von 0 bis 2\pi einzusetzen!!!!

```

```

oint1; oint2;
    %Divergenz des Deformationsvektorfeldes:
divu;
    %St. Venant:
stven1123+stven2231+stven3312+stven1212+stven2323+stven1313;
seps1123;seps2311;seps3121;seps1231;seps2231;
seps2312;seps3122;seps1232;seps3312;seps2313;seps3123;seps1233;seps1212;
seps1122;seps2211;seps2323;seps2233;seps3322;seps1313;seps3311;seps1133;
    %Divergenz des Verzerrungstensors
divv(1); divv(2); divv(3);
    %Komponenten der Divergenz des Verzerrungstensors (kartesisch!!)
ver111;ver122; ver133; ver211;ver222; ver233; ver311;ver322; ver333;
    %Verzerrungstensor
ver(1,1); ver(2,2); ver(3,3); ver(1,2); ver(1,3); ver(2,3);
    %Eigenwerte des Verzerrungstensors:
vew1; vew2; vew3;
    %Spur des Verzerrungstensors:
vspur;
    %Determinante des Verzerrungstensors:
vdet;
    %Summe der Minoren des Verzerrungstensors
vminor;
    %Divergenz des Spannungstensors
divt(1); divt(2); divt(3);
    %Komponenten der Divergenz des Spannungstensors (kartesisch!!)
tsp111;tsp122;tsp133; tsp211;tsp222;tsp233; tsp311;tsp322; tsp333;
    %Spannungstensor
tsp(1,1); tsp(2,2); tsp(3,3); tsp(1,3); tsp(2,3); tsp(2,1);
off echo$
clear phi,x,y,ra;
x:=ra*cos(phi);y:=ra*sin(phi);
on echo$
    %Komponenten d. Spannungstensors in Zylinderkoordinaten
neu(1,1);neu(1,2);neu(1,3);neu(2,2);neu(2,3);neu(3,3);
clear x,y,ra,r1,phi;
phi:=atan(y/x);
ra:=sqrt(x*x+y*y);
on echo$
    %Eigenwerte des Spannungstensors:
tew1;tew2;tew3;
    %Spur des Spannungstensors:
tspur;
    %Determinante des Spannungstensors:
tdet;
    %Summe der Minoren des Spannungstensors
tminor;
    %Berechnung der freien Energiedichte:
energy;
    %Berechnung der Volumen"anderungsenergie uvenergy:
%uvenergy:=1.0/6.0*(tspur*vspur);uvenergy;
    %Berechnung der Form"anderungsenergie
%ufenergy=energy-uvenergy;
ufenergy;
    %Eigenvektoren:
ev11;ev12;ev13; ev21;ev22;ev23; ev31;ev32;ev33;
    %Eigenvektoren des Spannungstensors (Probe):

```

```

%M"ussen in gleicher Reihenfolge sein wie oben, sonst umsortieren
%der EW n"otig
tev11;tev12;tev13; tev21;tev22;tev23; tev31;tev32;tev33;
    %Optische Aktivit"at (lineart polarisiert betap =0)
inten;
    %Optische Aktivit"at (lineart polarisiert betap =pi/4)
intenb;
    %N"aherung f"ur kleine deltap
intenn;
    %Optische Aktivit"at (cicular polarisiert)
intencirc;
    %Normalenvektor (nicht normiert)
no(0); no(1); no(2);
off echo$
clear x,y,ra,phi;
x:=ra*cos(phi); y:=ra*sin(*phi);
on echo$
    %Spannungsvektor (nicht normiert) ZYLINDERKOORDINATEN:
frnz;fphinz;fzonz;
    %Betrag des Spannungsvektors
bsp;
    %Betrag des Spannungsvektors phi:=0;
bsp0;
    %Betrag des Spannungsvektors phi:=pi/2;
bsp12;
clear x,y,ra,phi;
ra:=sqrt(x*x+y*y); phi:=atan(y/x);
on echo$
    %Spannungsvektor kartesisch (nicht normiert):
fxnk; fynk; fznk;
    %Normalenvektor2 (normiert)
norm2(0); norm2(1); norm2(2);
    %Spannungsvektor (nicht normiert) kartesisch:
xn2; yn2; zn2;
shut "volt1c.reo";
end;

```

## C C++-Programm zur Visualisierung

Hier wird die gekürzte Version eines C++-Programms vorgestellt, welches die Visualisierung der gemäß Volterra verformten Zylinder ermöglicht. Die erzeugten Daten werden hier automatisch in einen File geschrieben, der von dem „Advanced Visualization System“ verstanden wird.

```
//C++-Programm volt/volt11/volterra/      zu Volterra .447
//Datum 4.12.95
//letzte "Anderung: 4.3.96
//F"ur AVS-Header-File /volt/volt11/volterra/avs/11.fld,
// Netzwerk 11.net
//Berechnung eines Zylinderelements nach Volterra ORIGINAL
//Berechnung in kartesischen Koordinaten
//Compilieren durch CC -o volt v1c.C -lm ("-lm" fuer Mathe-Bibliothek)
//Programmaufruf dann durch "volt"
#include <stdio.h>
#include <math.h>
#include <iostream.h>
#include <fstream.h>
//ifstream eindp;
int printf(); //Deklaration von printf
//main(int argc, char *argv[ ])
main ()
{
    //Beginn des main-Programms
    //File *eindp, *fopen();
    char ch,cin;
        //Rundungsfehler --> INTEGER-TYPEN vermeiden !!
double l,k,r1,r2,mtaz,mraz,mphiz,mzaz,tver,phiver,zver,rver,phivero;
double taz,raz,phiz,zaz,veclen,stride;
double x0,x1,x2,x3,x,y,z,rs;
double ta,phi,Phi,za,pi,xe,ye,no11,no12,no13,b,no21,no22,no23,no31,no32,no33;
double ra,rad2,tspur;
double alpha,alphap,inten,inten1,inten2,intencirc,beta,alphav,betav,Phio,gamma,rho;
double lv,mv,nv,pv,qv,rv,ke,le,sigma,ela,eaz;
double n11,n12,n13,n21,n22,n23,n31,n32,n33,f11,f12,f13,f21,f22,f23,f31,f32,f33;
double fb1,fb2,fb3,fspur,fa11,fa12,fa13,fa21,fa22,fa23,fa31,fa32,fa33,energy;
double det,invsu,minspur,maxspur,mindet,maxdet,mininvsu,maxinvsu,minenergy,maxenergy;
double minfb1,maxfb1,minfb2,maxfb2,minfb3,maxfb3;
double bspur,bdet,binvsu,divf1,bdivf1,vspur,bvspur,intensi;
double f11no,f12no,f13no,fs1,fs2,fs3;
double pfn,pfnr11,pfnr12,pfnr13,pfnr21,pfnr22,pfnr23;
double dpfnr11,dpfnr12,dpfnr13,dpfnr21,dpfnr22,dpfnr23;
double bpfnr1,bpfnr2,bdpfnr1,bdpfnr2;
double energy2,ny,nu;
::::::::::::::::::::::::::::::::::::::::::::::::::::::::::::::::::::::::::::::::::
//Bestimmung einzelner Arrays
float energysum[100][300][7];
float xf1[100][300][7];
float xf2[100][300][7];
float xf3[100][300][7];

//Bestimmung der Ausgabefiles
ofstream *ausno = new ofstream("11no.Cout", ios::out);
ofstream *aus = new ofstream("11.Cout", ios::out);
ofstream *ausf1 = new ofstream("11.fld", ios::out);
ofstream *aus1 = new ofstream("111.fld", ios::out);
```



```

ofstream *aus2 = new ofstream("112.fld", ios::out);
ofstream *aus3 = new ofstream("113.fld", ios::out);
ofstream *aus11 = new ofstream("111.Cout", ios::out);
ofstream *aus22 = new ofstream("112.Cout", ios::out);
ofstream *aus33 = new ofstream("113.Cout", ios::out);

*aus<<"Avs-Datenfile /volt/volt11/volterra/vneu/11.Cout/n"; //Erste Zeile im AVS-Datenfile
pi=3.141592654;

//Festlegung der Zylinder Parameter
//Radius ra, Winkel Phi, Z-Achse za

        /* Bestimmung der Darstellung des "Zylinders" */

mraz=0.12; //0.12!      /*(mraz):=Anzahl der dargestellten Kreise (radial)*/
r1=0.001;
//Vermeidung der Singularitat des Spannungstensors (r=0) r1<0.001 wird Unsinn
r2=mraz;              //Zur Berechnung des Spannungstensors
rs=0.1; //0.01       //Schrittvariable
rver=1;              /*Anzahl der Versetzungen in r-Richtung*/
                    rho=rver/(6.283185307);

mphiz=520;
//mphiz=60; /* Anzahl der Gitterpl"atze l"angs des Radius (Letzter */
            /* ( mphiz)!!!! :=Gitterpl"atze pro Kreisfl"ache */
            /* Erster Gitterplatz = Letzter Gitterplatz */
            /* (mphiz-1) =Anzahl der dargestellten Kreissegmente mit */
            /*Winkel Phi=2*pi/(mphiz-1)*/

phiver=0; /*phiver:= Anzahl der Gitterpl"atze,die herausgeschnitten werden*/
            /* entspricht der Anzahl der herausgenommenen Kreissegmente */

mzaz=14; /*mzaz):=Anzahl der Gitterpl"atze in z-Richtung*/

zver=0; /*zver= Z0 Anzahl d. Gitterpl"atze um die in z-Richtung */
            /*versetzt wird*/

            /*Durchlaufen der einzelnen Koordinatenlinien*/
/*Zuerst z-Achse, da sonst Querverbindungen in der Darstellung*/
dim3=0;
for (zaz=-mzaz; zaz<=(mzaz); zaz=zaz+1 ) //Faktor 8 zur Streckung des Bildes
{
    za=zaz;
//if (zaz>=0.0){za=0.0;}
//    za=-7*mzaz;
    dim3=dim3+1; //Dim ist eine Laufvariable des AVS
    fdim3=dim3-1;
//Ausgabe des aktuellen Programmstandes
    printf("z-Koordinatenstelle %i von %i\n", (int)zaz, (int) (27*(mzaz)));
//    cout<<"z-Koordinatenstelle " <<zaz <<"von"<<dim3 <<"
dim2=0;
    for (phiz=0; phiz<=(mphiz-phiver-1); phiz=(phiz+1))
// (mphiz-phiver-1) (-1) damit obige Anzahl der Gitterpl"atze stimmt !
    {
        phi=(phiz*(6.283185307/(mphiz-1)));
// wird hier das (-1) weggelassen, so fehlt die letzte Verbindung -

```

```

    //- zum vollst"andigen Kreis*/
dim2=dim2+1;
dim1=0;
    //rs=2.0;
//Wird die Schritt variable rs ge"andert,
// so mu/3 diese auch im field file ge"andert werden!! (hier automatisch)
//da dim-ensionsangabe in for-Schleife
    for (raz=r1; raz<=mraz; raz=(raz+rs))
        {
            ra=raz;
            if (ra==0) ra=0.0001;
            dim1=dim1+1;

rad2=ra*cos(phi)*ra*cos(phi)+ra*sin(phi)*ra*sin(phi); /* Radius-Quadrat */

            /*Berechnung der Komponenten des Spannungstensors*/
//Materialkonstanten
sigma=0.45;
ela=1.0;
b=1;

//Trafo in Zylinderkoordinaten
x=ra*cos(phi);
y=ra*sin(phi);
z=za;

//Hier werden die mit Reduce berechneten Groessen eingegeben
u1=((4.0*nu-3.0)*(x*x+y*y)*phi-(x*y)*b)/(2.0*(4.0*nu-3.0)*(x*x+y*y)*pi);
u2=((x+y)*(x-y)*b)/(4.0*(4.0*nu-3.0)*(x*x+y*y)*pi);
u3=0.0;

u11=-(x*y)*b/(2.0*(4.0*nu-3.0)*(x*x+y*y)*pi);
u12=u2;
u13=0;
divu=-((2.0*nu-1.0)*b*y)/((4.0*nu-3.0)*(x*x+y*y)*pi);
divv1=(2.0*b*nu*x*y)/((4.0*nu-3.0)*((x*x+y*y)*(x*x+y*y))*pi);
divv2=-((x+y)*(x-y)*b*nu)/((4.0*nu-3.0)*((x*x+y*y)*(x*x+y*y))*pi);
divv3=0.0;
::::::::::::::::::::::::::::::::::::::::::::::::::::::::::::::::::::::::::::::::::
//Darstellung: Grundkoerper (unverformt) + Verformung ui
x1=x+u1;
x2=y+u2;
x3=z+u3;

tspur=(ts11+ts22+ts33);
bspur=sqrt(tspur*tspur);
vspur=ver11+ver22+ver33;
bvspur=sqrt(vspur*vspur);

//Berechnung der Gesamtenergie:
//Wichtung der einzelnen Summanden der Gesamtenergie
energysumw[dim1][dim2][dim3]=energyw;
energysum[dim1][dim2][dim3]=energy;
xf1[dim1][dim2][dim3]=x1;
xf2[dim1][dim2][dim3]=x2;
xf3[dim1][dim2][dim3]=x3;

```

```

//Zur Untersuchung eventueller Gemeinsamkeiten
//wurden die einzelnen charakteristischen Komponenten
//(Normalenvektor, Spannungsvektor, Spuren, Divergenzvektoren ..)
//verschiedenen mathematischen Formalismen unterworfen

//Eigenvektoren zum Spannungs- Verzerrungstensor
//(normiert und multipliziert
// mit der entsprechenden Komponente des Verzerrungstensors):

bev1=sqrt(ev11*ev11+ev12*ev12+ev13*ev13);
vev11=ver11*ev11/bev1;
vev12=ver11*ev12/bev1;
vev13=ver11*ev13/bev1;
::::::::::::::::::::::::::::::::::::::::::::::::::::::::::::::::::
//Projektion von f-rho auf n-rho:
pfnr11=(f11*no11+f12*no12+f13*no13)*no11;
pfnr12=(f11*no11+f12*no12+f13*no13)*no12;
pfnr13=(f11*no11+f12*no12+f13*no13)*no13;
::::::::::::::::::::::::::::::::::::::::::::::::::::::::::::::::::
//Je nach Bedarf Wahlm\ "oglichkeit verschiedener Datenausgaben
//Tensoren + Invarianten
//*aus <<10*x1<< " <<10*x2<< " <<x3<< " <<tspur<< " <<bpfnr<<
"<<fb1<< " <<ts11+ts22<< " <<ts22<< " <<ts33<< " <<uenergy<< " <<ufenergy<<
" <<energy<< " <<tdet*tdet<< " <<inten*944<< " <<tdet<< " <<inten<< " ;

//Deformations- und Divergenz und Spannungsvektoren:
*aus <<100*x1<< " <<100*x2<< " <<x3<< " <<ufenergy<< " <<uenergy<<
"<<pfnc<< " <<100*f11<< " <<100*f12<< " <<100*f13<< " <<0<<
"<<sqrt((divv1*divv1+divv2*divv2+divv3*divv3))<< " <<energy<< " <<inten1<<
"<<inten2<< " <<intencirc<< " <<sqrt((f11*f11+f12*f12+f13*f13))<< " ;
//Projektionen
//*aus <<50*x1<< " <<50*x2<< " <<x3<< " <<bpfnr<< " <<fb1<< " <<pfu<<
" <<puf<< " <<puev<< " <<pfev<< " <<tdet<< " <<bpev1nr+bpev2nr<< " <<divt2<<
" <<100*f11<< " <<100*f12<< " <<100*f13<< " <<inten<< " ;
::::::::::::::::::::::::::::::::::::::::::::::::::::::::::::::::::
}
}
}

energyges=0;
energygesw=0;
//Berechnung der Gesamtenergie:
//Hier wird in einem extra Durchlauf eine Annaeherung an die
//Gesamtenergie vorgenommen.
for (fz=1; fz<(dim3); fz=(fz+1))
{

for (fphi=1; fphi<(dim2-2); fphi=(fphi+1))
{
for (fr=1; fr<(dim1); fr=(fr+1))
{
energyges=energyges+0.25*(energysum[fr][fphi][fz]+energysum[fr+1][fphi][fz]
+energysum[fr][fphi+1][fz]+energysum[fr][fphi][fz+1])
*(0.5*(sqrt((xf1[fr+1][fphi][fz]-xf1[fr][fphi][fz])
*(xf1[fr+1][fphi][fz]-xf1[fr][fphi][fz]))+

```

```

sqrt((xf1[fr+1][fphi+1][fz]-xf1[fr][fphi+1][fz])
*(xf1[fr+1][fphi+1][fz]-xf1[fr][fphi+1][fz]))
::::::::::::::::::::::::::::::::::::::::::::::::::::::::::::::::::
//Interaktive Ausgabe der Energie nach der Rechnung
/cout<<"Energie"<<energygesw[][dim2-1][fdim3]<<"
xf1="<<xf1[dim1-1][dim2-1][fdim3]<<" xf2="<<xf2[dim1-1][dim2-1][fdim3]<<"
xf3="<<xf3[dim1-1][dim2-1][fdim3]<<" \n";
//Klammern beenden die for-Scleifen der Energieberechnung
}
}
}
/* Bestimmung der Anzahl der Punkte pro Koordinatenlinie f"ur AVS-field-file*/
//dim1=(mraz-rver-r1)/rs; //rs kommt von der Streckung (raz=raz+rs)!
dim1=dim1;
//dim2=mphiz-phiver;
dim2=dim2;
dim3=dim3;
//dim3=(2*mzaz)-zver; //bleibt unver"andert bei Streckung !
veclen=13;
stride=veclen+3;

                /*Erzeugung des AVS-Field-Files volt1.fld */
*ausfl <<"# AVS field file jw/volt/volt1/1.fld
(mit AVS mu/3 jeder field-file beginnen !)\n#(User .2-7ff)\n#\n";
*ausfl <<"ndim=3";
*ausfl<<"      # Dimension des Feldes (Berechneter Raum)\n\n";
*ausfl<<"dim1="<<dim1<<"      # Dimension der 1.Koordinate coord1 - \n";
*ausfl<<"dim2="<<dim2<<"      # - Anzahl der Punkte je Koordinatenlinie\n";
*ausfl<<"dim3="<<dim3<<"\n";
*ausfl<<"      # (dim1*dim2*dim3 = Anzahl der Punkte insgesamt)\n";
*ausfl<<"nspace=3
      #Anzahl der physikalischen Koordinaten (physikalischer Raum)\n";
*ausfl<<"veclen="<<veclen<<"
      #Anzahl der jedem Koordinatenpunkt zugeordneten Elemente\n
      #d.h. den \"Variablen\" zB.Temperatur,Druck,Spannungsfeld..\n\n
      #(dim1*dim2*dim3*veclen = Gesantanzahl der Datenpunkte)\n\n";
*ausfl<<"data=float #Daten-typ (byte, integer, float, double)\n";

*ausfl<<"field=irregular
      # Feldtyp (uniform, rectilinear, irregular (User .2-8ff))\n \n";

*ausfl<<"# Angabe der Datenfiles der Koordinatenpunkte      \n";

*ausfl<<"coord 1 file=/home/jw/volt/volt1/1l.Cout
      filetype=ascii skip=1 offset=0 stride="<<stride<<"\n";
*ausfl<<"coord 2 file=/home/jw/volt/volt1/1l.Cout
      filetype=ascii skip=1 offset=1 stride="<<stride<<"\n";
*ausfl<<"coord 3 file=/home/jw/volt/volt1/1l.Cout
      filetype=ascii skip=1 offset=2 stride="<<stride<<"\n";

*ausfl<<"
# Angabe der Datenfiles der unter veclen=.. angegeben Variablen \n";
*ausfl<<"variable 1 file=/home/jw/volt/volt1/1l.Cout
      filetype=ascii skip=1 offset=3 stride="<<stride<<"\n";
*ausfl<<"variable 2 file=/home/jw/volt/volt1/1l.Cout
      filetype=ascii skip=1 offset=4 stride="<<stride<<"\n";

```

```

*ausfl<<"variable 3 file=/home/jw/volt/volt1/1l.Cout
  filetype=ascii skip=1 offset=5 stride="<<stride<<"\n";
*ausfl<<"variable 4 file=/home/jw/volt/volt1/1l.Cout
  filetype=ascii skip=1 offset=6 stride="<<stride<<"\n";
*ausfl<<"variable 5 file=/home/jw/volt/volt1/1l.Cout
  filetype=ascii skip=1 offset=7 stride="<<stride<<"\n";
*ausfl<<"variable 6 file=/home/jw/volt/volt1/1l.Cout
  filetype=ascii skip=1 offset=8 stride="<<stride<<"\n";
*ausfl<<"variable 7 file=/home/jw/volt/volt1/1l.Cout
  filetype=ascii skip=1 offset=9 stride="<<stride<<"\n";
*ausfl<<"variable 8 file=/home/jw/volt/volt1/1l.Cout
  filetype=ascii skip=1 offset=10 stride="<<stride<<"\n";
*ausfl<<"variable 9 file=/home/jw/volt/volt1/1l.Cout
  filetype=ascii skip=1 offset=11 stride="<<stride<<"\n";
*ausfl<<"variable 10 file=/home/jw/volt/volt1/1l.Cout
  filetype=ascii skip=1 offset=12 stride="<<stride<<"\n";
*ausfl<<"variable 11 file=/home/jw/volt/volt1/1l.Cout
  filetype=ascii skip=1 offset=13 stride="<<stride<<"\n";
*ausfl<<"variable 12 file=/home/jw/volt/volt1/1l.Cout
  filetype=ascii skip=1 offset=14 stride="<<stride<<"\n";
*ausfl<<"variable 13 file=/home/jw/volt/volt1/1l.Cout
  filetype=ascii skip=1 offset=15 stride="<<stride<<"\n";

*ausfl<<"# filetype= ascii, unformatted, binary \n# skip=k
Anzahl der Linien des Datenfilekopfes die uberlesen werden sollen\n#\n#
Datenzuordnungsparameter:\n# offset=m
Anzahl der Datenspalten die uberlesen werden sollen.\n#
stride=y Anzahl der Datenpunkte bis einschlie3lich des n\"achsten\n
# zu lesenden Datenpunktes (In der Regel Anzahl der Spalten).\n";

/* Bestimmung der Anzahl der Punkte pro Koordinatenlinie f"ur AVS-field-file*/
//dim1=mraz-rver-r1/rs;
//dim2=mpfiz-phiver;
dim3=dim3;
//dim3=(2*mzaz)-zver; //bleibt unver"andert bei Streckung !
veclen=0;
stride=veclen+3;
::::::::::::::::::::::::::::::::::::::::::::::::::::::::::::::::::::::::::
cout<<"Gesamtenergie energyges="<<energyges<<" \n
Gesamtenergie Weertmann eneregygesw="<<energygesw<<"\n
Gesamtenergie Volterra genenergyv="<<genenergyv<<"\n";

//Schlie3en der Datenfiles
delete aus;      delete ausfl;      delete aus1;      delete aus2;
delete aus3;      delete aus11;      delete aus22;      delete aus33;

```

## **Part II**

### **The Space around a Black Hole**



# Zusammenfassung

Im Folgenden wird eine neue Darstellung eines Zeitschnittes durch eine Raumzeit vorgestellt, die durch die Schwarzschild-Metrik beschrieben wird. Im weiteren Verlauf wird diese Schnittdarstellung mit dem Flammischen Paraboloid verglichen.

Die Schwarzschild-Metrik stellt eine exakte Lösung der Einsteinschen Vakuum-Feldgleichungen dar. Sie ermöglicht eine Beschreibung der Krümmung der (3+1)-dimensionalen Raum-Zeit in der Umgebung einer ruhenden Masse. Zur numerisch visuellen Darstellung der metrischen Struktur eines Raumes ist ein Koordinatensystem nötig. Der Ricci-Kalkül (Tensoranalysis) bietet sich demnach als geschickte Notation an.

Ein wesentliches Problem bei der Darstellung der Schwarzschild-Metrik oder anderer exakter Lösungen der Einsteinschen Feldgleichungen ist das Fehlen eines globalen Koordinatensystems. Ausgehend vom flachen Raum wird hier ein Koordinatensystem vorgestellt, daß für den Zeitschnitt  $t = 0$  zu einer Metrik führt, deren zeitliche und radiale Komponenten exakt mit denen der Schwarzschild-Metrik übereinstimmen. Der Bezug zum flachen Raum ermöglicht eine leicht verständliche und anschauliche Darstellung der Raumzeit. Der Unterschied der hier berechneten Metrik zur Schwarzschild-Metrik wird physikalisch interpretiert und mit dem Flammischen Paraboloid verglichen. Schließlich wird die bisherige Vorstellung vom Ablauf eines Fluges in ein schwarzes Loch erweitert.

Es werden geometrische Einheiten verwendet. Die Lichtgeschwindigkeit  $c$  und die Newtonsche Gravitationskonstante  $G$  werden zu normierten einheitsfreien Größen ( $c = 1, G = 1$ ). Hierdurch haben die Energie, die Masse, die Zeit und die Länge die gleiche Einheit:

$$\begin{aligned} [\text{Energie}] &= [\text{Masse}] = [\text{Zeit}] = [\text{Länge}] \\ E_{\text{Planck}} &= m_{\text{Planck}} = t_{\text{Planck}} = l_{\text{Planck}} = \sqrt{\hbar} \quad . \end{aligned}$$

## Contents

|          |  |            |
|----------|--|------------|
| <b>1</b> | <b>Introduction</b>                                      | <b>136</b> |
| <b>2</b> | <b>The Schwarzschild Metric</b>                          | <b>136</b> |
| 2.1      | The radial distance . . . . .                            | 137        |
| 2.2      | The proper time . . . . .                                | 138        |
| 2.3      | The coordinate transformation . . . . .                  | 139        |
| 2.4      | The line element . . . . .                               | 139        |
| <b>3</b> | <b>The Schwarzschild Metric and the Flamm Paraboloid</b> | <b>142</b> |
| <b>4</b> | <b>Conclusion</b>  | <b>146</b> |
|          | <b>References</b>  | <b>147</b> |



## 1 Introduction

The Schwarzschild metric is an exact solution of the Einstein vacuum field equations. It enables us to describe the curvature of the (3+1)-dimensional space-time around a mass at rest. One difficulty in visualizing the Schwarzschild metric or other exact solutions is the lack of a global coordinate system. The coordinate system presented leads to a metric, which coincides with the Schwarzschild metric in the radial and the time component. The difference will be physically explained.

We use the Ricci calculus, since the visualization of the metric structure requires a coordinate system.

Every symmetric covariant tensor of second rank e.g.  $\mathbf{g}_{ij}$  defines a metric. A manifold with a metric is termed a Riemannian manifold [1]. A metric is also called the line element, and is related to the tensor product of a holonomic vector frame  $dx^i$  by means of

$$ds^2 = \mathbf{g}_{ij} dx^i \otimes dx^j \quad , \quad (1)$$

where  $\mathbf{g}_{ij}$  are the holonomic components of the metric tensor. The metric can also be determined by the anholonomic coframe  $\vartheta^\alpha$ ,

$$ds^2 = \mathbf{O}_{\alpha\beta} \vartheta^\alpha \otimes \vartheta^\beta \quad , \quad (2)$$

with the local Minkowski-metric  $\mathbf{O}_{\alpha\beta}$ , i.e.,

$$\mathbf{O}_{\alpha\beta} = \begin{pmatrix} -1 & & & 0 \\ & 1 & & \\ & & 1 & \\ 0 & & & 1 \end{pmatrix} \quad \alpha, \beta = 0, 1, 2, 3 \quad . \quad (3)$$

For more details see [2].

## 2 The Schwarzschild Metric

The coframe 1-form of the Schwarzschild metric, is in terms of the Schwarzschild coordinates  $t$ ,  $r$ ,  $\theta$ ,  $\varphi$  and for the normalized light velocity  $c = 1$ , and the Newtonian gravitational constant  $G = 1$  given by

$$\begin{aligned} \vartheta^{\hat{0}} &= \vartheta^t = \sqrt{1 - \frac{2M}{r}} dt \quad , \\ \vartheta^{\hat{1}} &= \vartheta^r = \left(1 / \sqrt{1 - \frac{2M}{r}}\right) dr \quad , \\ \vartheta^{\hat{2}} &= \vartheta^\theta = r d\theta \quad , \\ \vartheta^{\hat{3}} &= \vartheta^\varphi = r \sin \theta d\varphi \quad . \end{aligned} \quad (4)$$

The circumflex  $\hat{\phantom{x}}$  stands over anholonomic indices. The curvature of the space-time is caused by the mass  $M$ . The time coordinate  $t$  is related to the proper time of a clock resting at infinity (Fließbach [4] page 153). The space coordinate  $r$  is characterized by

the property that the surfaces of the concentric spheres around the mass are given by  $4\pi r^2$ .

The Schwarzschild metric in terms of the Schwarzschild coordinates reads

$$\mathbf{g}_{ij} = \begin{pmatrix} -(1 - \frac{2M}{r}) & & & 0 \\ & 1/(1 - \frac{2M}{r}) & & \\ & & r^2 & \\ 0 & & & r^2 \sin^2 \theta \end{pmatrix} \quad i, j = 0, 1, 2, 3 \quad . \quad (5)$$

## 2.1 The radial distance

The Schwarzschild coordinates are orthogonal coordinates. The holonomic vector frame, i.e. the tangent vectors of the coordinate lines of the space-time, which is described by the Schwarzschild metric, for the angles  $\theta$  and  $\varphi$  is identical to the 3-dimensional polar coordinates. The radial and the time tangent vectors only agree in direction, but not in modulus. The Schwarzschild metric describes a (3+1)-dimensional space-time with spherical symmetry. Gravity is generating, in a way, an "extension" in radial direction. The radial distance  $L(r_k, r_{(k+1)})$  of two spheres with the radii  $r_k$  and  $r_{(k+1)}$ , respecting, and with  $r_{(k+1)} - r_k = 1$ , depends on the parameter  $k$ , and is no longer constant, as it is for the polar coordinates in a Minkowski space. The radial distance  $L(r_1, r_2)$  of two spheres with the radii  $r_1$  and  $r_2$  turns out to be (Stephani [5] page 198)

$$\begin{aligned} L(r_1, r_2) &= \int_{r_1}^{r_2} \vartheta^{\hat{r}} \\ &= \int_{r_1}^{r_2} \sqrt{g_{rr}} dr \\ &= \int_{r_1}^{r_2} 1/\sqrt{1 - \frac{2M}{r}} dr \\ &= \left( \sqrt{r(r-2M)} + 2M \ln \frac{\sqrt{r} + \sqrt{r-2M}}{\sqrt{2M}} \right) \Big|_{r_1}^{r_2} . \end{aligned} \quad (6)$$

We calculate this integral with help of the Computer Algebra system "Reduce". The lower boundary of this integral becomes zero if we choose for  $r_1$  the event horizon  $r_1 = 2M$ . The distance function  $L(r_1, r_2)$  describes, for  $r_1 = 2M$ , the radial distance of the  $\tilde{r}$ -sphere from the center,

$$\begin{aligned} \tilde{r} &:= L(r_1 = 2M, r_2) \\ &= \sqrt{r_2(r_2 - 2M)} + 2M \ln \frac{\sqrt{r_2} + \sqrt{r_2 - 2M}}{\sqrt{2M}} . \end{aligned} \quad (7)$$

This expression only depends on  $r_2$  and  $M$ . We rename  $r_2$  by  $r$  and write

$$\tilde{r} = \sqrt{r(r-2M)} + 2M \ln \frac{\sqrt{r} + \sqrt{r-2M}}{\sqrt{2M}} . \quad (8)$$

The radial coordinate  $\tilde{r}(r, M)$  indicates the distance, which a clock, resting at position  $r$ , seems to have to the mass  $M$ , for an observer who rests near infinity.

Figure II.1 shows in plot ① the distance function  $\tilde{r}(r, 1)$  of equation (8) for  $M = 1$ . Plot ② for the comparison shows the function  $\tilde{r} = r$ .

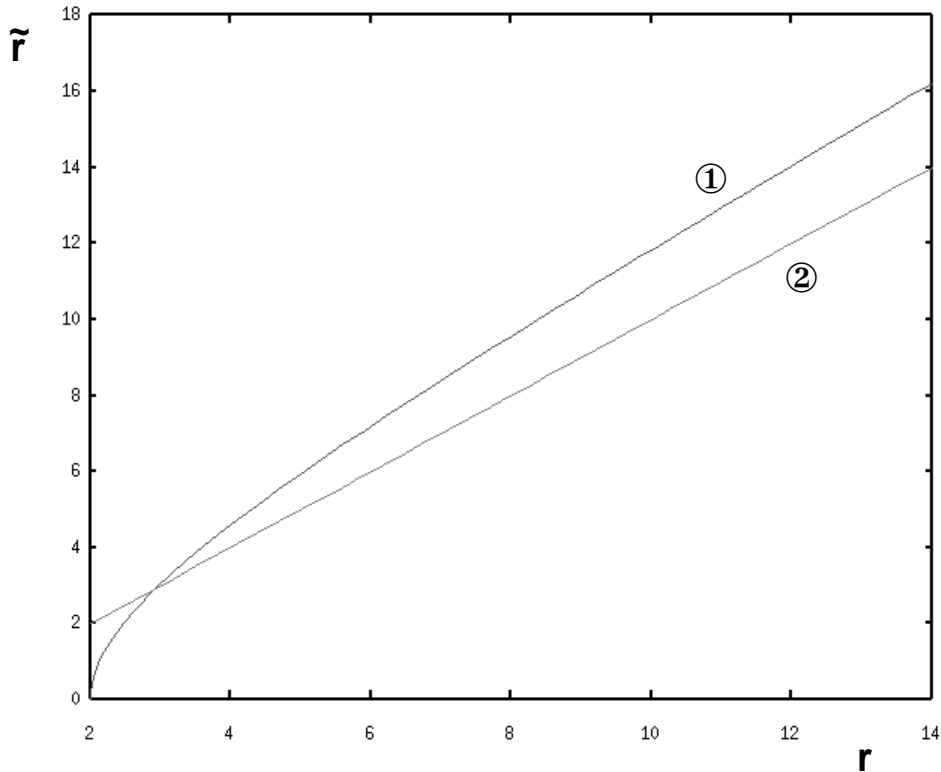


**Fig. II.1.** The distance function  $\tilde{r}$  for  $M = 1$ , and the function  $\tilde{r} = r$  (plot ②)

The sphere  $r = 2M$  turns obviously to the point  $\tilde{r} = 0$ . The event horizon is thus appearing in the center of the mass for an observer at nearly infinite distance. For it seems that the area  $r > 2M$  of the flat space as bijectively mapped on a regular, complete, continual and spherical symmetric space with  $\tilde{r} \in [0, \infty]$ . This space is deformed in radial direction.

## 2.2 The proper time

The connection of the space dependent proper time  $\tilde{t}(t, r, M)$  of a clock resting at position  $r$  and the proper time of a clock resting at infinity can be derived in an analogous way as above:

$$\begin{aligned}
 \tilde{t}(t, r, M) &:= \int_0^t \vartheta^i \\
 &= \int_0^t \sqrt{g_{tt}} dt \\
 &= \int_0^t \sqrt{\frac{r-2M}{r}} dt \\
 &= \sqrt{\frac{r-2M}{r}} t \quad .
 \end{aligned} \tag{9}$$

The time coordinate  $\tilde{t}(t, r, M)$  is the time difference, which is displayed by a clock that rests at the position  $r$  relative to an observer resting near infinity reading  $t$ .

The calculated extension of the radial distances of the coordinate lines and the time dilatation are related to an observer resting near infinity and hence to a flat space-time.

## 2.3 The coordinate transformation

With the help of equations (8) and (9), we transform the Schwarzschild coordinates  $t, r, \theta, \varphi$  like

$$\begin{aligned} t' &= \tilde{t} = \sqrt{\frac{r-2M}{r}}t \quad , \\ r' &= \tilde{r} = \sqrt{r(r-2M)} + 2M \ln \frac{\sqrt{r} + \sqrt{r-2M}}{\sqrt{2M}} \quad , \\ \theta' &= \theta \quad , \\ \varphi' &= \varphi \quad . \end{aligned} \tag{10}$$

The coordinate lines of this coordinates can be imagined as a static frame made of rigid bars, because  $r', \theta', \varphi'$  are independent of  $t$ .

## 2.4 The line element

The line element of the Minkowski space is with equations (1), (2), and (3), in Schwarzschild coordinates  $t, r, \theta, \varphi$  given by

$$ds^2 = -dt^2 + dr^2 + r^2 d\theta^2 + r^2 \sin^2 \theta d\varphi^2 \tag{11}$$

We can also write

$$ds^2 = -dt'^2 + dr'^2 + r'^2 d\theta'^2 + r'^2 \sin^2 \theta' d\varphi'^2 \quad , \tag{12}$$

because the line element is invariant respectively coordinate transformations.

The total differentials reads

$$dx'^j = \frac{\partial x'^j}{\partial x^k} dx^k \quad , \quad \text{or} \quad dx^k = \frac{\partial x^k}{\partial x'^j} dx'^j \quad . \tag{13}$$

This leads with  $x'^j = t', r', \theta', \varphi'$  for  $j = 0, 1, 2, 3$ , and with the introduced coordinate transformation to

$$\begin{aligned} dt' &= \frac{\partial t'}{\partial x^j} dx^j = \frac{\partial t'}{\partial t} dt + \frac{\partial t'}{\partial r} dr + \frac{\partial t'}{\partial \theta} d\theta + \frac{\partial t'}{\partial \varphi} d\varphi \\ &= \sqrt{\frac{r-2M}{r}} dt + \frac{Mt}{r^2} dr / \sqrt{1 - \frac{2M}{r}} \quad , \\ dr' &= \frac{\partial r'}{\partial x^j} dx^j = \frac{\partial r'}{\partial t} dt + \frac{\partial r'}{\partial r} dr + \frac{\partial r'}{\partial \theta} d\theta + \frac{\partial r'}{\partial \varphi} d\varphi = dr / \sqrt{1 - \frac{2M}{r}} \quad , \\ d\theta' &= d\theta \quad , \\ d\varphi' &= d\varphi \quad . \end{aligned} \tag{14}$$

The line element in Schwarzschild coordinates  $t, r, \theta, \varphi$  follows with equations (1), and (12)

$$\begin{aligned}
ds^2 = & - \left(1 - \frac{2M}{r}\right) dt^2 + \left(1 + \frac{M^2 t^2}{r^4}\right) dr^2 / \left(1 - \frac{2M}{r}\right) + \frac{2Mt}{r^2} dr dt \\
& + \left(\sqrt{r(r-2M)} + 2M \ln \frac{\sqrt{r} + \sqrt{r-2M}}{\sqrt{2M}}\right)^2 d\theta^2 \\
& + \left(\sqrt{r(r-2M)} + 2M \ln \frac{\sqrt{r} + \sqrt{r-2M}}{\sqrt{2M}}\right)^2 \sin^2 \theta d\varphi^2 \quad . \quad (15)
\end{aligned}$$

We use  $\tilde{r}$  of equation (8) to shorten this expression

$$\begin{aligned}
ds^2 = & - \left(1 - \frac{2M}{r}\right) dt^2 + \left(1 + \frac{M^2 t^2}{r^4}\right) dr^2 / \left(1 - \frac{2M}{r}\right) + \frac{2Mt}{r^2} dr dt \\
& + \tilde{r}^2 d\theta^2 + \tilde{r}^2 \sin^2 \theta d\varphi^2 \quad . \quad (16)
\end{aligned}$$

The Riemann curvature tensor of this metric vanishes and it fulfills the Einstein vacuum field equations. This was checked with help of the Reduce programs given by F.W. Hehl et al. [3]. The coordinate transformation introduced leads with equations (1) to the following components of the metric tensor

$$\mathbf{g}_{ij} = \begin{pmatrix} -\left(1 - \frac{2M}{r}\right) & \frac{Mt}{r^2} & & 0 \\ \frac{Mt}{r^2} & \left(1 + \frac{M^2 t^2}{r^4}\right) / \left(1 - \frac{2M}{r}\right) & & \\ & & \tilde{r}^2 & \\ 0 & & & \tilde{r}^2 \sin^2 \theta \end{pmatrix} \quad . \quad (17)$$

For  $t = 0$  changes this tensor to the diagonal form

$$\mathbf{g}_{ij}^0 = \begin{pmatrix} -\left(1 - \frac{2M}{r}\right) & & & 0 \\ & 1 / \left(1 - \frac{2M}{r}\right) & & \\ & & \tilde{r}^2 & \\ 0 & & & \tilde{r}^2 \sin^2 \theta \end{pmatrix} \quad i, j = 0, 1, 2, 3 \quad . \quad (18)$$

This cut in time can be interpreted as a momentary "snapshot" of the space described by the coordinate system introduced. It is shown in figure II.2.1. The time component  $\mathbf{g}_{tt}^0$  and the radial component  $\mathbf{g}_{rr}^0$  are identical with those of the Schwarzschild metric. The  $\mathbf{g}_{\theta\theta}^0$  and the  $\mathbf{g}_{\varphi\varphi}^0$ -component of the metric plotted are different. The distances along a path in radial direction are the same as for the Schwarzschild metric, but not the distances along a sphere with  $r = \text{const.}$ . It is at this time only possible to point out a diametrically line with  $\varphi = \text{const.}$  as analogous to the Schwarzschild metric.

A plot of the metric above can be seen in fig. II.2.1 for  $\theta = \frac{\pi}{2}$ ,  $2 \leq r \leq 14$ , and  $M = 1$ . It shows the distance function  $\tilde{r}(r, M)$  analogous to fig. II.1. The center of the concentric circles corresponds to  $r = 2$ , ( $M = 1$ ). The first circle corresponds to  $r = 3$ , the second to  $r = 4$ , ..., the last to  $r = 14$ .

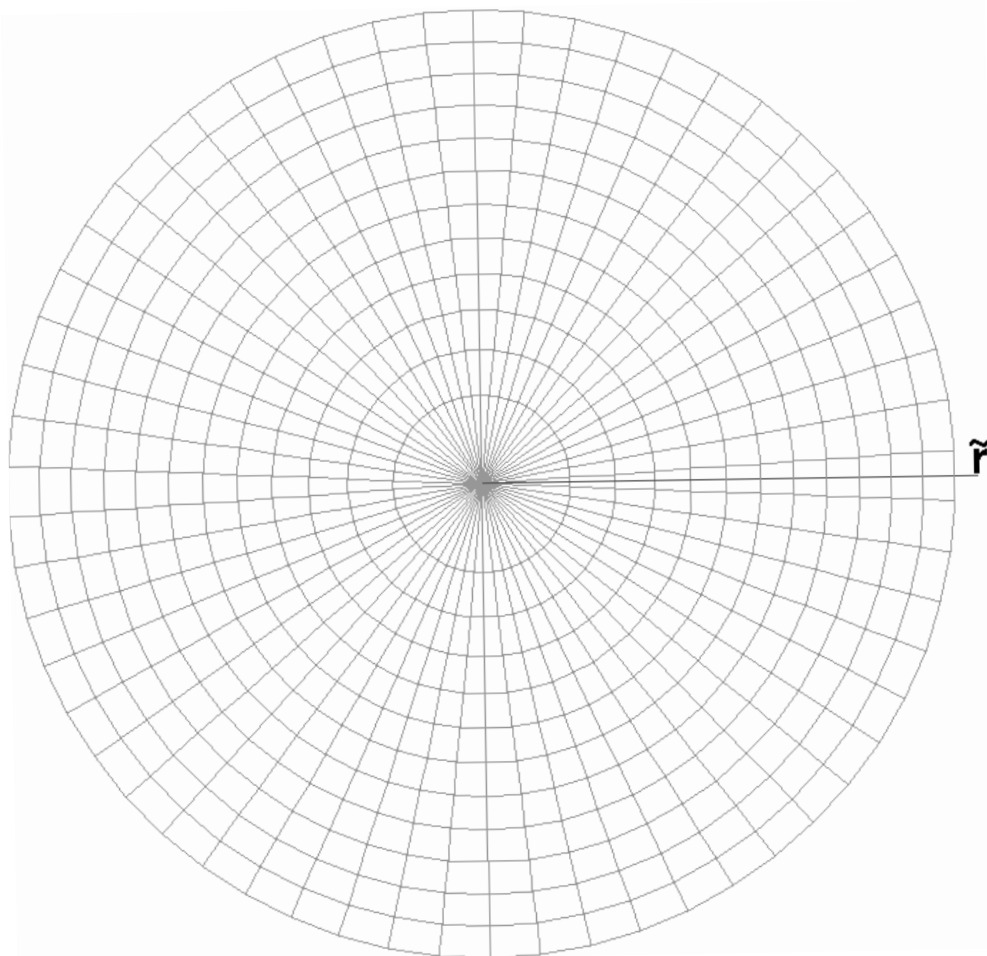


**Fig. II.2.1.** Static frame made of rigid bars around a Schwarzschild black hole with  $M = 1$ , related to an observer resting near infinity.  $\tilde{r}(r, M)$  is the distance function of equation (8)

The radial extension of the space depicted is evident. The spatial part of the coordinate transformation introduced describes the static frame made of rigid bars, that was already mentioned above. The difference between Schwarzschild coordinates and the coordinates above can be physically explained by the centrally directed gravitational attraction of the mass. Each movement in space is effected by this force. If a test mass is accelerated in the tangential direction, it is also radially guided. Einstein's geometrical interpretation of the gravitation takes this supplementary radial acceleration into consideration by the curvature of the space-time. If we consider only one moment in time, e.g.  $t = 0$ , this acceleration can be taken out of account. Thus a flat space-time may describe such a time cut. Figure II.2.1 shows a static frame made of rigid bars around a Schwarzschild black hole at the moment  $t = 0$ .

Fig. II.2.2 indicates the time  $\tilde{t}$  of equation (9), which is displayed to an observer who rests near infinity, while his watch shows him one unit of time ( $t = 1$ ).

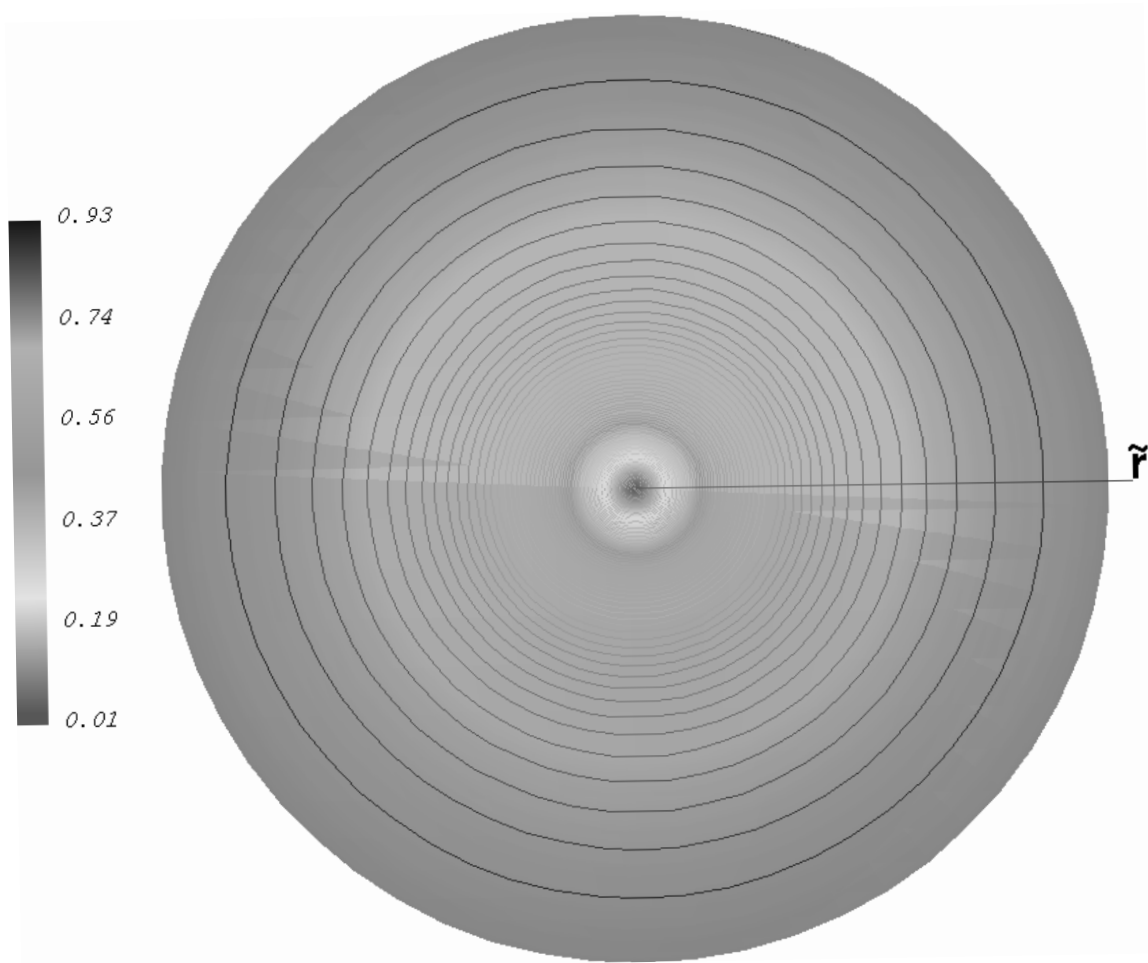


**Fig. II.2.2.** Isolines of the time function  $\tilde{t}(t, r, M)$  of equation (9) for  $t = 1$ , and  $M = 1$ . The time  $\tilde{t}$  indicates the time delay of a clock resting at  $r$  relative to an observer resting near infinity. See also colour plate IX

For the region depicted we have  $2 \leq r \leq 14$ , analogous to fig II.2.1.

### 3 The Schwarzschild Metric and the Flamm Paraboloid

Another presentation of the Schwarzschild metric is the Flamm paraboloid. The 2-dimensional ( $t = 0$ )- and ( $\theta = \frac{\pi}{2}$ )- plane of the Schwarzschild metric is embedded here in an 3-dimensional space via cylindrical coordinates. This mathematical trick allows an exact representation of the radial- and the  $\varphi$ -coordinate lines. The depicted surface is extended in the radial direction like in Schwarzschild coordinates and also along the  $\varphi$ -coordinate line. The figures II.3.1 show an paraboloid with the inner radius  $r_1 = 2M$ , an outer radius of  $r_2 = 14$  and the mass  $M = 1$ .

The top view in z-direction is considered in fig II.3.1a.

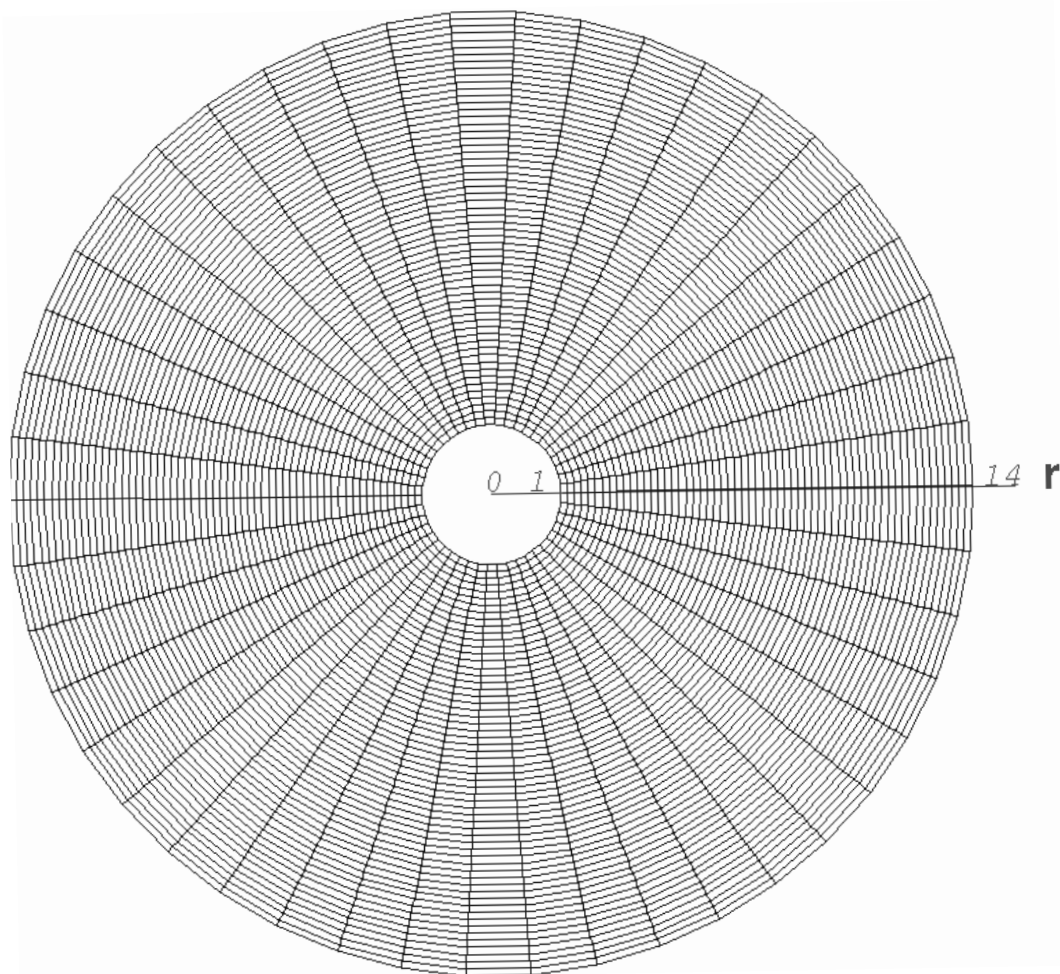


**Fig. II.3.1a.** Top view on the Flamm paraboloid with an inner radius  $r_1 = 2$ , an outer radius  $r_2 = 14$ , and  $M = 1$

The increment is five times smaller than in fig II.2.1. The course of the coordinate lines corresponds to the case of the polar coordinates. The next figures help to understand the difference between the Flamm paraboloid and the introduced presentation of the space around a black hole. Figure II.3.1b is the same figure as II.3.1a but viewed from the side. The parabolical structure is obvious. We would also get a paraboloid, if we rotated the radial distance function  $\tilde{r}$ , shown in plot ① of fig II.1, around the z-axis.

The surfaces  $t = 0$ , and  $\theta = \frac{\pi}{2}$  are depicted in figures II.2 and II.3. The association of both can be constructed by the diametrical cutting of the figure II.2.1, and spreading the produced "cake pieces" upon the Flamm paraboloid. The interspace corresponds to the curvature, which is caused by the gravitational force. The curvature indicates the change of the distances between the coordinate lines of the flat space compared with the Schwarzschild metric. The center of the figure introduced coincide with the event horizon of the Flamm paraboloid.

The figures II.3.2 (a,b) shows, similar as in figure II.2.2, the time function  $\tilde{t}(t, r, M)$  of equation (9) for  $t = 1$ , and  $M = 1$ , with reference to an observer resting near infinity.



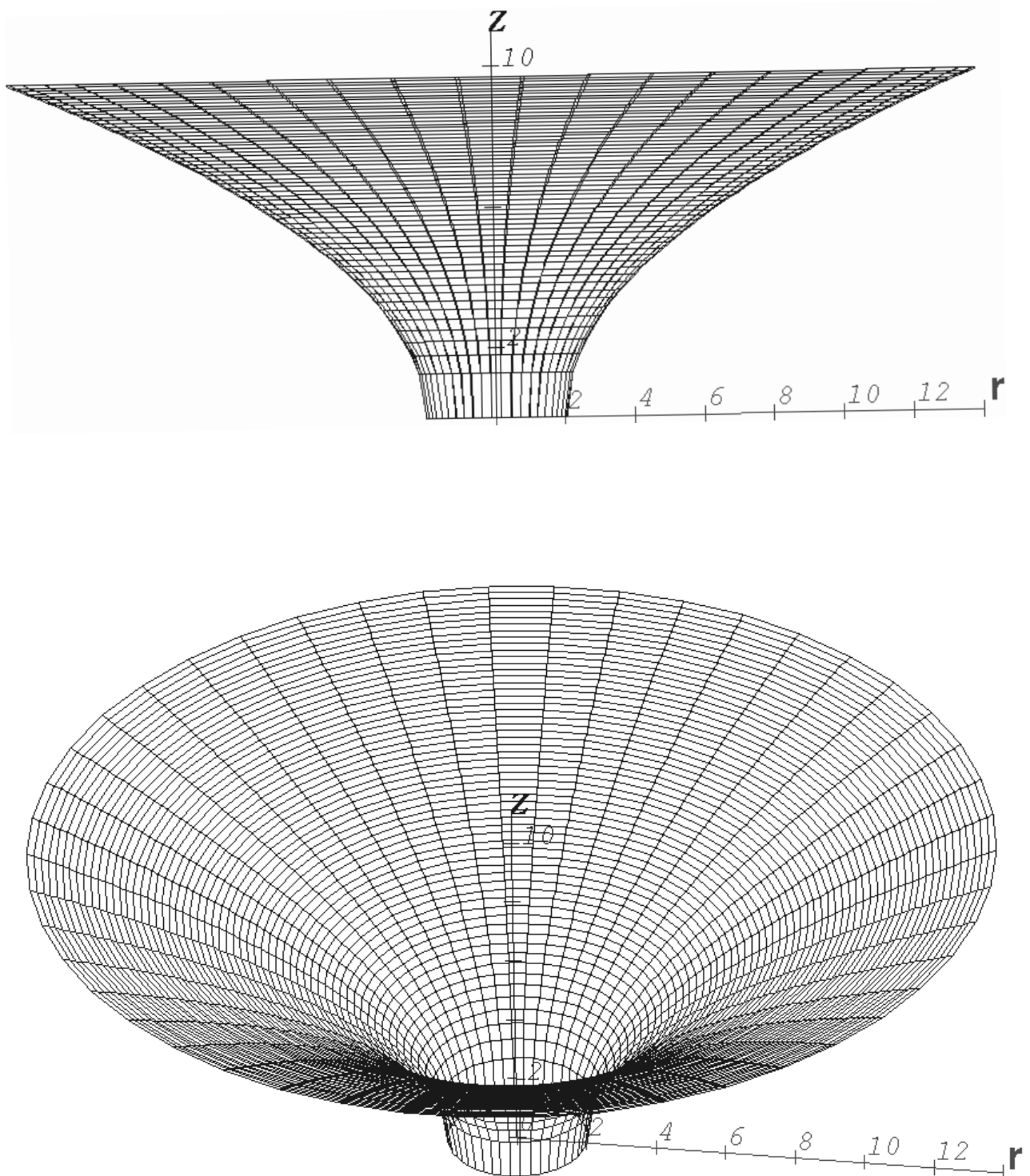


**Fig. II.3.1 b,c** Views on the Flamm paraboloid with an inner radius  $r_1 = 2$ , an outer radius  $r_2 = 14$ , and  $M = 1$

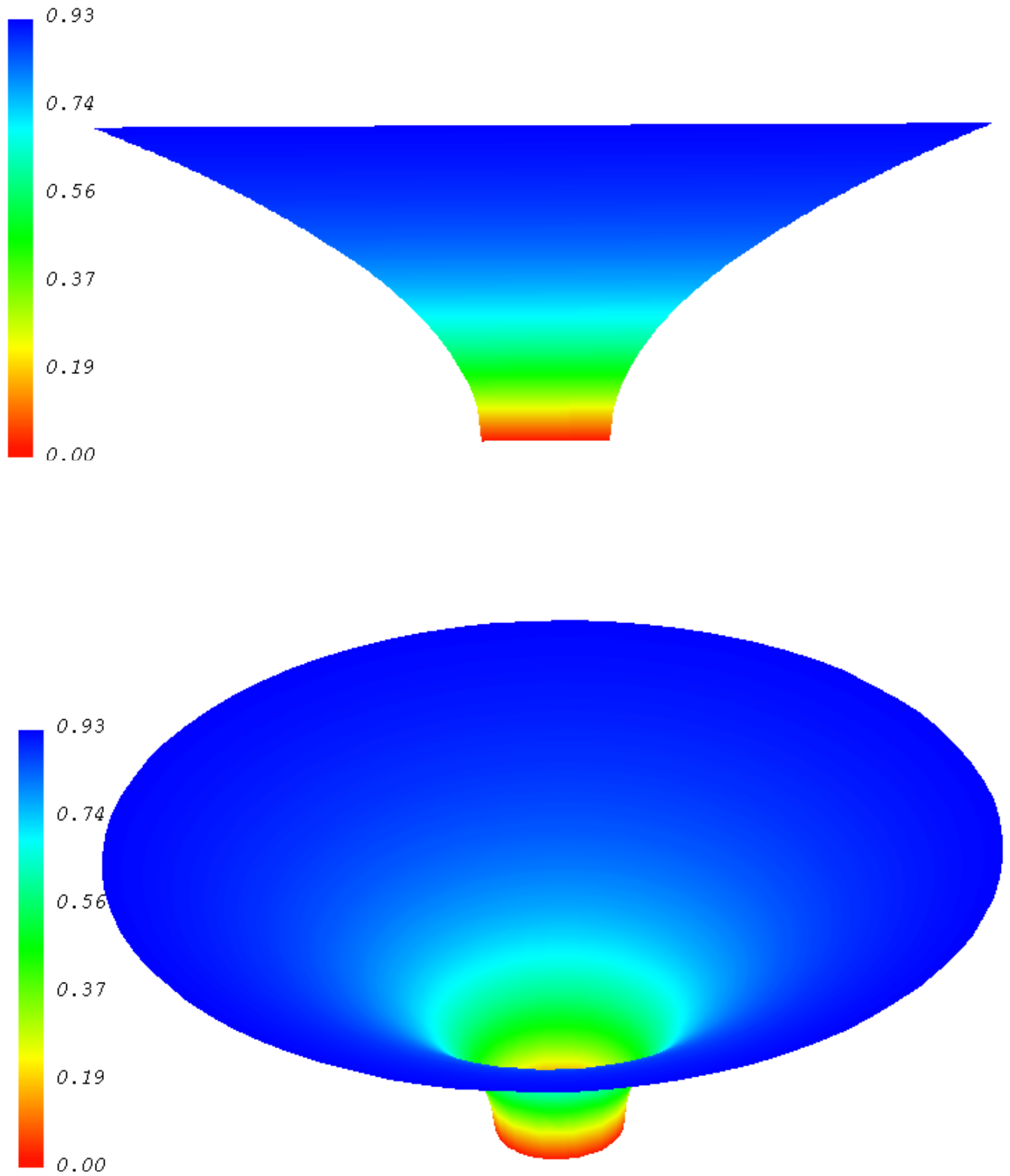


**Fig. II.3.2 a,b** The Flamm paraboloid in combination with the time function  $\bar{t}$  of equation (9). It indicates the time delay of a clock that rests at the position  $r$  relative to an observer resting near infinity. See also colour plate X

## 4 Conclusion

We considered the case of an observer resting near infinity. For him the event horizon  $r = 2M$  appears in the center  $\tilde{r} = 0$  of the space described by Schwarzschild coordinates. The event horizon is reduced to one point for this observer. For him everything seems scaled down. The actual imagination of a flight into a black hole (see e.g. J.-P. Luminet [8]) can be extended in a way, that the observer, who rests in a huge distance from the Schwarzschild radius, assumes a free falling astronaut already in the center, in the singularity, of the black hole, as the astronaut passes the event horizon. If the astronaut flies on the radial geodesic connecting the observer with the black hole, the observer gets nearly the same impression as if the astronaut flies on this geodesic towards infinity, because of the perspective reduction. The observer in this special case can hardly distinguish whether there is a black hole or not. The gravitational redshift will be the help for this purpose.

## References

- [1] **R. d’Inverno**, Einführung in die Relativitätstheorie, VCH Verlagsgesellschaft mbH, Weinheim (1995).
- [2] **F.W. Hehl, J. Dermott McCrea, E. W. Mielcke, Yuval Ne’eman**, Metric-affine gauge theory of gravity, Physics Reports **258** 1-171 (1995).
- [3] **F.W. Hehl, V. Winkelman, H. Meyer**, Reduce, zweite Aufl., Springer-Verlag Heidelberg (1992).
- [4] **T. Fließbach**, Allgemeine Relativitätstheorie, B.I. Wissenschaftsverlag, Mannheim (1990).
- [5] **H. Stephani**, Allgemeine Relativitätstheorie, Deutscher Verlag der Wissenschaften (1991).
- [6] **R.U. Sexl u. H.K. Urbantke**, Gravitation und Kosmologie, B.I. Wissenschaftsverlag, Zürich (1987).
- [7] **Max Born**, Die Relativitätstheorie Einsteins, Springer-Verlag, Berlin 1964.
- [8] **Jean-Pierre Luminet**, Schwarze Löcher, Vieweg Verlagsgesellschaft mbH, Braunschweig/Wiesbaden (1997).

## **Mit Dank an:**

Herrn Prof. F.W. Hehl für die Betreuung dieser Arbeit, die vielen wichtigen Ratschläge und das kritische Lesen des Manuskriptes.

Jan Budczies, Frank Gronwald, Horst Konzen, Ralph Metzler, Uwe Münch, Roland Puntigam, und an alle anderen Mitglieder des Instituts für Theoretische Physik, für die freundliche Atmosphäre, ergiebigen Diskussionen, aufmunternden Worte, und manche netten Abende.

Andreas Sindermann, für seine unerschöpfliche Hilfsbereitschaft und das Lösen aller Rechnerprobleme.

Volker Winkelmann, der besonders bei Visualisierungsproblemen mit Rat und Tat zur Seite stand.

Den "Graduiertenkolleg Scientific Computing Köln St.-Augustin" für die finanzielle und wissenschaftliche Förderung.

Meine Familie, für den Rückhalt und die Unterstützung.

Alle Freunde, für ihr Interesse und Verständnis. Manche Türen sollen der Physik wohl noch verschlossen bleiben.

## **Erklärung**

Ich versichere, daß ich die von mir vorgelegte Dissertation selbstständig und ohne unzulässige Hilfe angefertigt, die von mir benutzten Quellen und Hilfsmittel vollständig angegeben und die Stellen der Arbeit - einschließlich Tabellen, Karten und Abbildungen -, die anderen Werken im Wortlaut oder dem Sinn nach entnommen sind, in jedem Einzelfall als Entlehnung kenntlich gemacht habe; daß diese Dissertation noch keiner anderen Fakultät oder Universität zur Prüfung vorgelegt hat; daß sie - abgesehen von unten angegebener Teilpublikation - noch nicht veröffentlicht worden ist, sowie daß ich eine solche Veröffentlichung vor Abschluß des Promotionsverfahrens nicht vornehmen werde. Die Bestimmungen der Promotionsordnung sind mir bekannt. Die von mir vorgelegte Dissertation ist von Prof. Dr. F.W. Hehl betreut worden.

## **Teilpublikation:**

J.K.Weidmann, New Solution Algorithm for Volterra's Defects, phys. stat. sol. (b) **202**, 903 (1997).

## Lebenslauf

|                         |   |
|-------------------------|---|
| Name                    | Weidmann  |
| Vorname                 | Jürgen  |
| Anschrift               | Institut für Theoretische Physik<br>Universität Köln<br>50923 Köln  |
| E-Mail                  | jw@thp.uni-koeln.de   |
| Homepage                | <a href="http://www.thp.uni-koeln.de/~jw/">www.thp.uni-koeln.de/~jw/</a>  |
| Geburtsdatum            | 1. Juli 1965  |
| Geburtsort              | Sindelfingen  |
| Staatsangehörigkeit     | deutsche  |
| Familienstand           | ledig   |
| 1971 - 1975             | Grundschule Eichholz  |
| 1975 - 1984             | Gymnasium in den Pfarrwiesen<br>Abitur, Gesamtnote 1,9  |
| WS 1984 - SS 1985       | Universität Stuttgart (Physik)<br>vorgezogene Vordiplomprüfung im Nebenfach Chemie  |
| August 1985 - Dez. 1986 | Zivildienst in der Jugendbegegnungs- und bildungsstätte<br>„Kupferdächle“ in Pforzheim  |
| April 1987 - April 1993 | Philipps-Universität Marburg.<br>Vordiplom, Gesamtnote 2<br>Oberseminare in Theoretischer Ökologie (Systemphysik)<br>und in Biophysik (Neuronale Netze)<br>Diplom in Theoretischer Festkörperphysik mit dem Thema<br>„Exitonische Absorptionsspektren unter dem Einfluß eines<br>gepulsten elektrischen Feldes“, Gesamtnote 1 |
| Mai 1993 - Juni 1993    | BAT2/2-Stelle an der Fachbereichsbibliothek der<br>Physikalischen Institute Marburg   |
| Juli 1993 - Juni 1998   | Universität Köln<br>Bis Sommer 1995 Stipendiat des Graduiertenkollegs<br>„Scientific Computing Köln-St. Augustin“.  |